Technical Report No. III.

Analyses of the Effects of the USACE IHNC Lock Expansion Project East Bank Industrial Area Site Clearing Excavations on Development of the Breaches at the Lower 9th Ward During Hurricane Katrina

Technical Report to

Katrina Canal Breaches Consolidated Litigation

[Civil Action Number: 05-4182 "K" (2)]

United States District Court

Eastern District of Louisiana

Pertains to MR-GO, Robinson [No. 06-2268]

By

Dr. Robert Bea and Diego Cobos-Roa

Risk Assessment and Management Services

Moraga, California

July 11, 2008

SYNOPSIS

This report summarizes work performed for the Katrina Canal Breaches Consolidated Litigation [USDC, E.D. La. No. 05-4182 "K" (2) Pertains to MR-GO (Mississippi River – Gulf Outlet), Robinson (No. 06-2268)] related to analyses of the USACE Inner Harbor Navigation Canal (IHNC) Lock Expansion Project East Bank Industrial Area (EBIA) engineering and site clearing excavations conducted by the Washington Group International (WGI) for the USACE on development of the North Breach and South Breach at the Lower 9th Ward during hurricane Katrina.

This report is organized into 13 sections:

1) Executive summary of elements addressed, analytical approaches used, and findings regarding hydraulic effects and stability of the levee and floodwall sections that breached (failed) during hurricane Katrina.

2) Review of the available background on the physical aspects of the constructed flood protection structures and geology at the breach locations

3) Summary of available information pertaining to previous analyses of the breaches, the presence of drainage structures in the vicinity, and historic performance of flood protection structures in this area.

4) Analyses of background information on geometric characteristics of soil layers and deposits in the vicinity of the North and South Breaches (stratigraphic interpretations).

5) Summary of available information on the soils in the vicinity of the North and South Breaches.

6) Based on the available geologic and soil information, the properties of the soil materials at the North and South Breaches are described and quantified.

7) Available information on the hydraulic conductivity characteristics of marsh – swamp – peat – humus layers similar to those that underlie the area is summarized.

8) Analytical models are developed to characterize hydraulic conductivity (water flow and water pressure) effects at the North and South Breaches. Results from the parametric analyses to characterize these effects during hurricane Katrina are summarized. These analyses include a wide range in native soil, excavation, and backfill characteristics.

9) Analytical models are developed to characterize the stability characteristics of the levee – floodwall sections at the North and South Breaches during hurricane Katrina. The stability characteristics are summarized as the 'factors of safety' that express the ratio of the 'driving demands' from the destabilizing forces to the 'resisting capacities' – stabilizing forces - of the levee and floodwall sections. Results from the parametric analyses to characterize these effects during hurricane Katrina are summarized. These analyses include a wide range in native soil, excavation, and backfill characteristics.

10) Probabilistic analyses are performed to evaluate the effects of inherent (natural) uncertainties on the stability characteristics at the North and South Breaches. Results from these analyses result in characterizations of the probabilities of failure (lateral instability) at the North and South Breaches during the evolution of hurricane Katrina.

11) A summary of results and conclusions is presented.

12) References utilized during this work are summarized.

13) Appendices contain details on available soils information, statistical characterizations at the North and South Breaches, hydraulic conductivity functions, and results from Monte Carlo Simulations utilized in the probabilistic analyses.

SUMMARY

At the Lower 9th Ward, engineering and industrial site clearing activities performed by WGI for the USACE at the East Bank Industrial Area (EBIA) consisting of ground excavations to remove buried storage tanks and other debris outside the floodwall and levee were major contributors to the catastrophic breaches that developed at the Lower 9th Ward during hurricane Katrina. These EBIA USACE and WGI engineering and site clearing activities were associated with the USACE navigation lock expansion project (completed early 2005). Water that came in through these breaches not only devastated the Lower 9th Ward, but as well contributed to the catastrophic flooding of the St. Bernard Parish – Lower 9th Ward 'bowl'.

Results of analyses performed to determine the timing and causes of the levee and floodwall at the Lower 9th Ward, clearly demonstrate the adverse effects of excavations developed during the USACE IHNC Navigation Lock Expansion Project site clearing operations performed by WGI. These operations were completed just prior to hurricane Katrina (about May 2005). The locations of the breaches are directly correlated with the locations of these excavations. Both the sand backfilled, native soil backfilled and non-backfilled excavations provided ready and early access of the rising waters in the IHNC to communicate with the buried marsh and swamp layers that

underlie this entire area. These excavation activities were not conducted in accordance with USACE guidelines pertaining to excavations adjacent to flood protection structures (USACE 2005). The sheet piling used to support the floodwalls were not driven to a depth sufficient to cut-off water communication through these buried high hydraulic conductivity layers. The hydraulic flow and pressure effects were sufficient to initiate very early movements of the supporting levee and floodwalls – well before overtopping, opening up the vertical water-stop joints, and eventually developing complete breaching as the floodwalls were overtopped.

TABLE OF CONTENTS

Synopsis i

Summary iii

1. SUMMARY 1

1.1 Overview 1

1.2 Scope 4

1.3 Approaches and Methods 6

1.3.1 Hydraulic Conductivity – Seepage Analyses 6

1.3.2 Lateral Stability of levee and floodwall 7

1.3.3 Probabilistic Analyses 8

1.4 Findings 8

1.4.1 Hydraulic Conductivity Analyses 8

1.4.2 Lateral Stability Analyses 9

1.4.3 Probabilistic Analyses 11

2. PART I – BACKGROUND INFORMATION 11

2.1 Levee & Floodwall Cross Sections 11

2.2 Sheet Piles 15

2.3 Site Geology 15

3. PART II – BACKGROUND INFORMATION 18

3.1 Recorded Surge Hydrographs 18

3.2 USACE Navigation Lock Expansion EBIA Site Clearing Excavations 19

3.3 Design Cross Sections Compared With LiDAR Survey Cross Sections 27

3.4 Soil Stratigraphy and Analysis Sections by IPET and ILIT (2006) 28

3.5 Drainage Structures 31

3.6 Historic Breaches 32

4. STRATIGRAPHIC INTERPRETATIONS 40

4.1 North Breach Section and Failed Configuration 44

4.2 South Breach Section & Failed Configuration 47

5. IHNC SOILS DATA REVIEW 50

6. MATERIAL PROPERTIES 53

6.1 South Breach Section 53

6.2 North Breach Section 59
7. MARSH PERMEABILITY 65
8. SEEPAGE & Hydraulic Effects ANALYSES 72
8.1 Analytical Model Description 72
8.2 South Breach Section 74
8.2.1 Steady State 74
8.2.2 Transient Analyses 76
8.2.3 Effects of Excavations 84
8.3 North Breach 86
8.3.1 Steady State 86
8.3.2 Transient Models 87
8.3.3 Effects of Waterside Excavations 95
8.4 Summary of Results from Seepage Analyses 98
8.4.1 South Breach 98
8.4.2 North Breach 99
9. SLOPE STABILITY ANALYSES 100
9.1 Analytical Model Description 100
9.2 South Breach Results 101
9.3 North Breach Results 104
10. PROBABILILISTIC ANALYSES 108
10.1 Statistical Analysis of Undrained Shear Strengths for South Breach 108
10.2 Statistical Analysis of Undrained Shear Strengths for North Breach 111
10.3 Results of Probability of Failure Analyses 112
11. SUMMARY OF RESULTS AND CONCLUSIONS 119
12. REFERENCES 122
13. APPENDICES 125
13.1 Available soil boring and laboratory tests utilized in analyses 125
13.2 STATISTICAL CALCULATIONS OF SHEAR STRENGTH AND UNIT WEIGHT– SOUTH BREACH 138
13.3 STATISTICAL CALCULATIONS OF SHEAR STRENGTH AND UNIT WEIGHT – NORTH BREACH 144

13.4 HYDRAULIC CONDUCTIVITY FUNCTIONS USED FOR SEEPAGE ANALYSES (ALL SECTIONS) 148
13.4.1 CLAY MATERIALS 148
13.4.2 SANDS 149
13.4.3 MARSH, K: 1e-03 cm/s 150
13.4.4 MARSH, K: 1e-04 cm/s (under levee). 151
13.5 RESULTS FROM THE MONTE CARLO SIMULATIONS 152
13.5.1 SOUTH BREACH – EXCAVATION AT TOE OF LEVEE 152
13.5.2 NORTH BREACH – EXCAVATION AT TOE OF LEVEE 160

1. SUMMARY

1.1 Overview

The Inner Harbor Navigation Canal (IHNC) is located west of the Lower Ninth Ward, in Saint Bernard Parish. The levees and floodwalls along the east bank of the IHNC canal constitute part of the flood protection system that protects the western St. Bernard Parish.

During Hurricane Katrina in August 29, 2005, the storm surge from Gulf of Mexico and Lake Borgne, hydraulically connected to IHNC by the Gulf Intercoastal WaterWay (GIWW) / Mississippi River – Gulf Outlet (MR-GO) channel, raised the water levels in the IHNC and induced several catastrophic breaches along the IHNC (Figure 1-1). This report addresses the two breaches (identified herein as the North Breach and the South Breach) that developed adjacent to the Lower 9th Ward during hurricane Katrina.

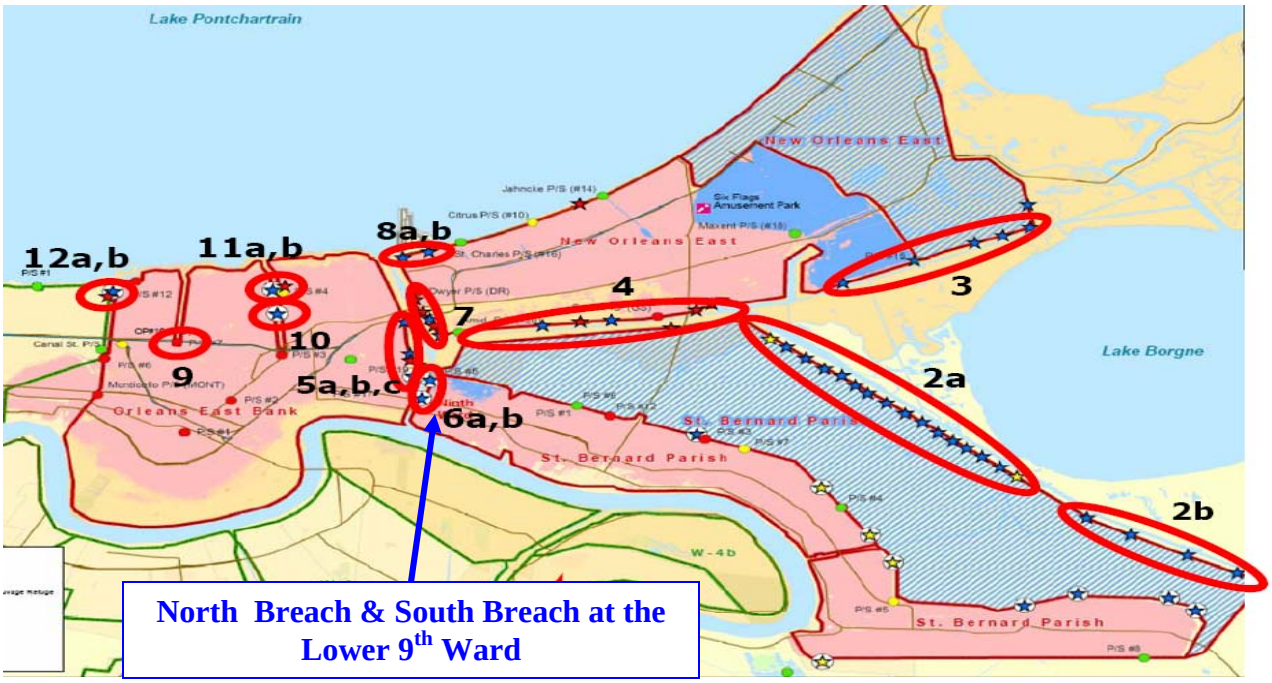


Figure 1-1. Summary of principal failures, breaches, and distress features with identification of the two breaches (6a, b) at the Lower 9th Ward adjacent to the IHNC (base map provided by USACE, ILIT 2006)

Figure 1-2 shows the location of the two breaches along the east bank of the IHNC. The longer South Breach was approximately 900 feet in length, located north of Claiborne Avenue. The shorter North Breach occurred close to Florida Avenue; this was approximately 250 feet long. Available information indicates the North Breach initiated before the wall was overtopped by the surge generated by hurricane Katrina, between 5:00 and 6:00am on August 29, 2005 (CDT. The available information indicates the South Breach fully developed after the surge overtopped the I-wall, between 7:00 am and 8:00 am on the same day.

Times of failures were determined from available eyewitnesses' accounts, "Stopped-clock" measurements, and recorded surge elevation – time data (hydrographs) along the IHNC (IPET 2007, ILIT 2006, Team Louisiana 2007).

This report integrates available background information on these locations and failures into advanced and comprehensive analytical models to address the hydraulic conductivity and levee – floodwall stability. The following data sources were utilized in construction of these analytical models:

- Original USACE Design Memoranda (DM)
- LIDAR surveys performed Pre (2000) and Post-Katrina
- Background documentation on the East Bank Industrial Area (EBIA) engineering and site clearing operations conducted by the Washington Group International (WGI) for the USACE IHNC Lock Expansion Project
- Post-Katrina forensic engineering investigations (IPET 2006; ILIT 2006; Team Louisiana 2007).

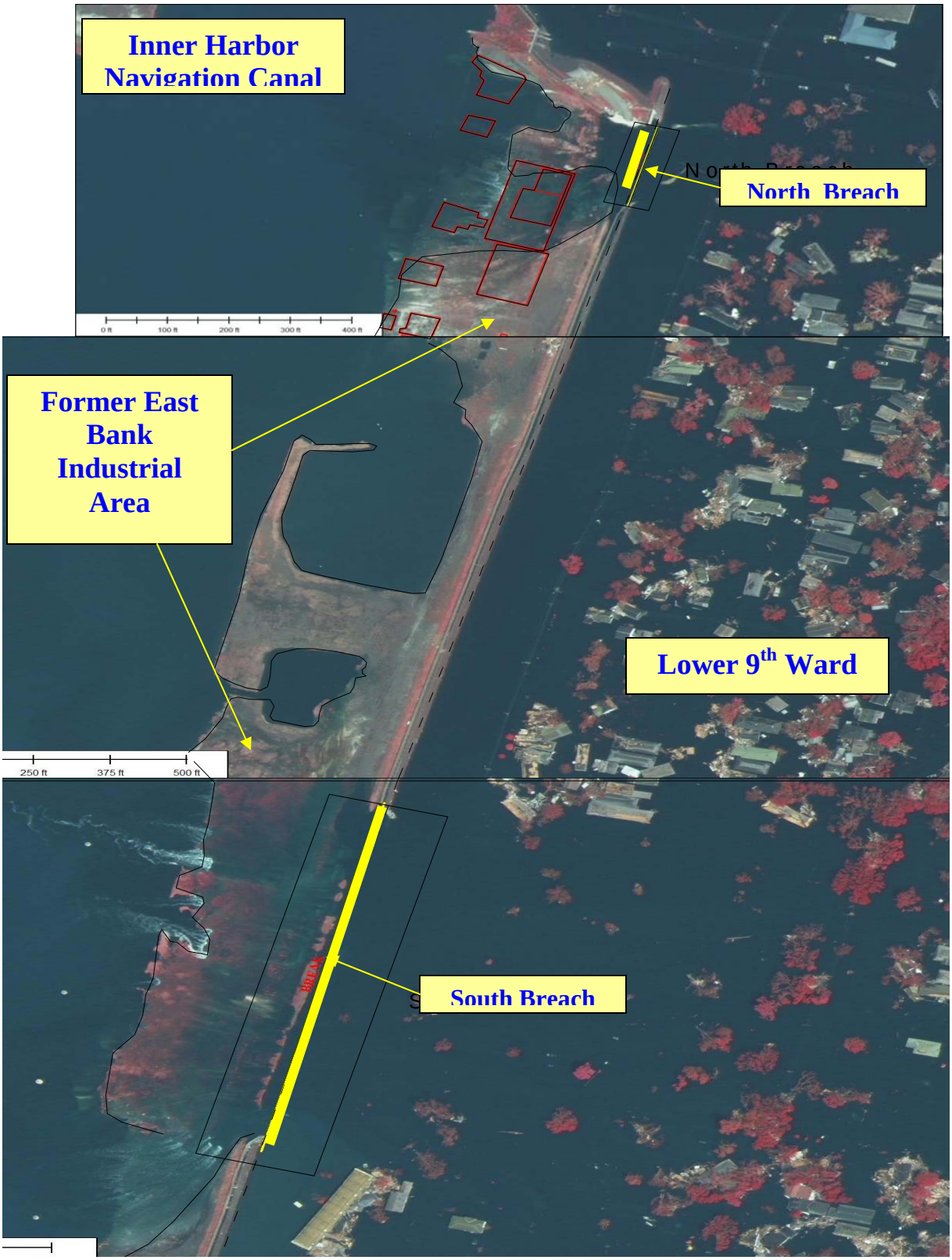


Figure 1-2. Aerial photographs showing the two breach sites on IHNC (NOAA 2005).

1.2 Scope

Parametric steady-state (fully developed conditions) and transient (time history development based) hydraulic conductivity (seepage) analyses were carried out to assess the influences of the buried Marsh (wetlands, swamp, peat, humus) deposit permeability values and relative permeability compared with the surrounding soils on the development of pore water pressures on the lateral stability of the levee and floodwall adjacent to the Lower 9th Ward during hurricane Katrina.

The impacts of uncertainties on hydraulic conductivity parameters were analyzed by performing parametric analyses considering a wide range of plausible values of permeabilities (water transmissibilities) for the Marsh deposits. The analyses showed that a near steady state of pore water pressures is developed on the soils underneath the levee when subject to the storm surge for the entire range of plausible permeability values. These saturated permeable soils are directly hydraulically connected to the water in the IHNC. This hydraulic connectivity is reflected in almost immediate and proportionate increases in water pressures as the water levels in the IHNC increase significantly. These pore water pressures result in significant hydraulic uplift forces that act to reduce the lateral resistance of the soil levee – floodwall system.

The effect of the canal-side excavations initiated by WGI in 1991 and completed in 2005 as part of the USACE Navigation Lock Expansion Project were evaluated in the seepage and stability analyses documented in this report by including approximate dimensions, depths, and locations of these “holes” in the seepage and stability analyses. These analyses clearly indicate these excavations unfavorably impacted the stability of the levees - floodwalls, as the sand-backfilled excavations produced increases in the hydraulic conductivity of the strata and associated uplift

forces acting on the soils supporting the levee and floodwalls . This, combined with the gap formed between the sheet piling and supporting soils on the waterside and the surge generated by hurricane Katrina rose in the IHNC, dramatically increased the lateral forces and simultaneously decreased the lateral resistance and associated factors of safety of potential failure planes along the Marsh deposits.

The analyses summarized in this report provide insights into the failure mechanisms that developed at the North Breach and South Breach along the east bank of IHNC, with special emphasis given to:

- **The excavated holes** backfilled with sand and native materials on the canal-side of the East bank of the IHNC – Lower Ninth Ward (EBIA), near the north and South Breaches. These holes were present near the canal-side levee toe –less than 100 feet from the levee – and in some cases as close as 40 feet.
- **Uncertainties** associated with soil shear strength parameters. The Marsh deposits underlying the levee are a highly variable material, difficult to sample, characterize and model. The high variability of shear strengths and unit weights, and limited test data increase the probability of failure for surfaces passing through this stratum.
- **Underseepage.** For **any** structure subject to transient water loads, it is important to perform hydraulic conductivity (seepage, pore water pressure) analyses to assess the development of pore water pressures on embankment and foundation soils. Common practice involves the assumption of a phreatic surface (imaginary water surface for the stability calculations. This has proven to be unconservative as calculated pore water

pressures on soft shallow deposits are often significantly larger than the hydrostatic pressures (depth multiplied by unit weight of water).

1.3 Approaches and Methods

1.3.1 Hydraulic Conductivity – Seepage Analyses

Hydraulic conductivity, seepage, and pore water pressure development was assessed by means of Finite Element Modeling. The software SEEP\W, part of the computer program package GEOSTUDIO was employed for the task of calculating hydraulic heads, pore water pressures and hydraulic gradients through the levee and embankment soils.

The approach consisted on reviewing the geological information, borings, topographic surveys and stratigraphic profiles by DM03 (USACE, 1966), IPET (2006) and ILIT (2006); in order to create a new and more complete geological, geotechnical and geometrical interpretation.

The most influential findings that deviated from the analyses from the available ILIT and IPET reports are:

- The location of the landside toe of the levee, as new information made available by IPET (Figure 14 "LIDAR data at toe of Levee", from Final Draft Analysis of Performance of the Inner Harbor Navigation Canal", 2006) showed that toe elevation for the South Breach was located between -4 and –5 feet (NAVD88)[1] , and on the vicinity of the North Breach the toe was located approximately 4ft lower (Elevation -7 feet to –8 feet). These very low landside toe elevations had a negative impact on slope stability.
- The presence of waterside excavations very close to the levee significantly and adversely impacted the seepage behavior of the levee - floodwall system.

After the geometry and stratigraphy were defined, material properties were assigned to each layer for the seepage and stability analyses. Shear resistance parameters were taken from the

[1] this vertical datum will be used on the entire document

ILIT (2006) report and compared with the "IPET MODEL" strengths. Both behavior models are similar, yet the main difference between the two reports lies in the characterization of the soft gray Clays underneath the Marsh deposits.

ILIT (2006) determined a history of consolidation and evidence of several desiccation (and therefore overconsolidation) stages based on their in situ Cone Penetrometer Tests (CPT) interpretation. The IPET model concluded that all Clays were normally consolidated; both IPET and ILIT assign a Stress-dependant behavior model to the clays (SHANSEP model).

Seepage analyses were conducted for steady-state (time independent) and transient (time dependent) hydraulic load conditions for a wide range of plausible permeabilities on the Marsh deposit. The seepage modeling in this report focuses in the influence of different permeability contrasts between the Marsh and surrounding soils and to assess its impact on the static stability of the system. The range of values assigned to the Marsh was based on in situ and laboratory experimental data documented in technical journal publications and encompassed permeabilities 4 orders of magnitude in difference.

1.3.2 Lateral Stability of levee and floodwall

The influence of the developed pore water pressures of a rising storm surge, and the distribution as a function of the relative permeabilities on lateral stability of the levee – floodwall was assessed by calculating Factors of Safety (FOS) using Limit Equilibrium Analyses (LEA). Plots of FOS versus storm elevation were used to summarize results of the analyses. The results show that the calculated FOS drop below unity at a water elevation of approximately +9 feet (NAVD88) for the North Breach, and +12 feet to +14 feet for the South Breach.

1.3.3 Probabilistic Analyses

The effects of uncertainties concerning soil shear strengths, unit weights and water surge elevations were assessed by calculating statistical parameters for all available laboratory data. Stability analyses were coupled with Monte-Carlo simulations and Probability of Failure (Pf), Mean Factor of Safety and Reliability Index were calculated based on the "expected values" and distributions of different parameters.

1.4 Findings

1.4.1 Hydraulic Conductivity Analyses

The hydraulic conductivity analyses show that pore water pressures develop quickly due to the presence of the waterside excavations and the development of a waterside water-filled gap between the sheet piles and the soil embankment. The presence of these "shortcuts" that connect the storm surge to the underlying Marsh deposits produced elevated pore water pressures on the soils beneath the toe of the levee.

Calculated pore water pressures and hydraulic gradients are within less than 30% of those computed for a hypothetical steady state at the water elevation at time of failure (El. +9-10 feet for the North Breach, and approximately +14 feet for the South Breach).

The influence of different permeability values assigned to the Marsh deposit was found to be a key factor on the hydraulic behavior of the system. The generation of hydraulic gradients that could potentially initiate uplift or blowout failures was found to be an important factor some two hours before the static Factor of Safety to slope stability dropped below 1.0. Gradients in excess

of 0.5 though fine-grained (clay) blanket layers started to develop as early as 5:00 am (Central Daylight Time, CDT)[2] on the North Breach, and 6:00 am on the South Breach.

The uplift pressure acting on the landside surficial layers could have contributed to softening of the materials near the toe of the levee and consequently the initiation of the translational movements evidenced for both breaches.

1.4.2 Lateral Stability Analyses

The models presented in this report consider the development of a crack (gap) between the waterside embankment and sheet-pile. The consequence of such feature results in the full hydrostatic pressure being applied on the sheet-pile, and furthermore, the full storm surge being fed directly beneath the levee embankment into the Marsh layer; connecting the storm surge to the soil layers beneath the toe. Non-circular failure surfaces were analyzed within the Marsh layer and underlying gray clay deposits. Slightly lower results were obtained for the potential failure surfaces located at shallower depths (through Marsh).

The slope stability results show that the hydrograph observations are matched by the calculated Factor of Safety at time of failure (FOS = 1.0), between elevations +9 feet and +10 feet for the North Breach; approximately at 6:00 am on August 29, 2005.

For the South Breach, the time of failure (FOS = 1.0) is indicated to be approximately 8:00 am, with a water elevation between +12 feet and +13 feet, on August 29, 2005.

[2] this time reference will be used throughout this text unless noted otherwise.

It is important to note that 'failure' of the levee – floodwall results from a series of 'progressive' failures. Visual observations and analytical results indicate that such failures develop from a series of local failures that are accumulated to result in the final global failure. In general, deformations are developed in the soils supporting the flood-wall – sheet pile system. When these deformations are large enough, the vertical 'water stop' joints in the concrete floodwalls can open and given that the water is high enough, water can begin to flow into the protected side. As the water continues to rise, the concrete floodwall and sheet pile system incline away from the rising water further opening the water stop joints. When these inclinations exceed those developing in the supporting soils, a gap on the water side between the sheet piling and the soils opens. This gap allows the water to intrude between the supporting soils and the sheet piling. This results in increasing the lateral water pressures acting directly against the floodwall – sheet piles, reduces the resisting soil forces due to a reduction in the part of the supporting levee that is resisting the forces exerted directly on the floodwall and sheet piling, and allows water access to conductive layers at and below the tips of the sheet piling. These water effects and forces act to develop greater deformations in the floodwall and levee. When the water reaches the top of the floodwall, the water will overtop the wall and rush down the backside of the floodwall – eroding the supporting soils. Due to physical removal of the supporting soils on the protected side, this scouring – erosion process can lead to further deformations of the floodwall and sheet piling. In the final stages of the failure, the driving water forces overwhelm the resisting forces of the floodwall – sheet piling – levee, and a breach is developed.

1.4.3 Probabilistic Analyses

The Monte-Carlo simulations performed for the slope stability analyses show that the calculated Probabilities of failure are in excess of 60 % when the storm surge rises above 10 feet on the South Breach, and above 12 feet for the South Breach. Soil units were grouped by material type and stress range (depth) for the statistical analyses.

Statistical parameters for unit weight and shear strength parameters of the gray high-plasticity clays are consistent with published literature, with coefficients of variations on the range of 20 % to 40 %. In the Marsh deposit, the heterogeneity, anisotropy and difficulty of testing is evidenced by coefficients of variations larger than 50%, and a significant lower number of tests performed in this unit.

2. PART I – BACKGROUND INFORMATION

2.1 Levee & Floodwall Cross Sections

The levees protecting the Lower Ninth Ward were relatively small clay embankments of slopes inclined 3 feet horizontal to 1 foot vertical (USACE DM 03, 1966). Design cross sections from the 1966 Design Memorandum show that in the proximity of the landside toe of the levee a drainage ditch known as the Jourdan Avenue Canal existed and was bottomed at elevation -10 feet to –12 feet (Figure 2-1a). Toe elevations along the landside (protected side) were approximately –4 feet. The landside canal was filled sometime in the 1990's (ILIT, 2006) with unknown materials.

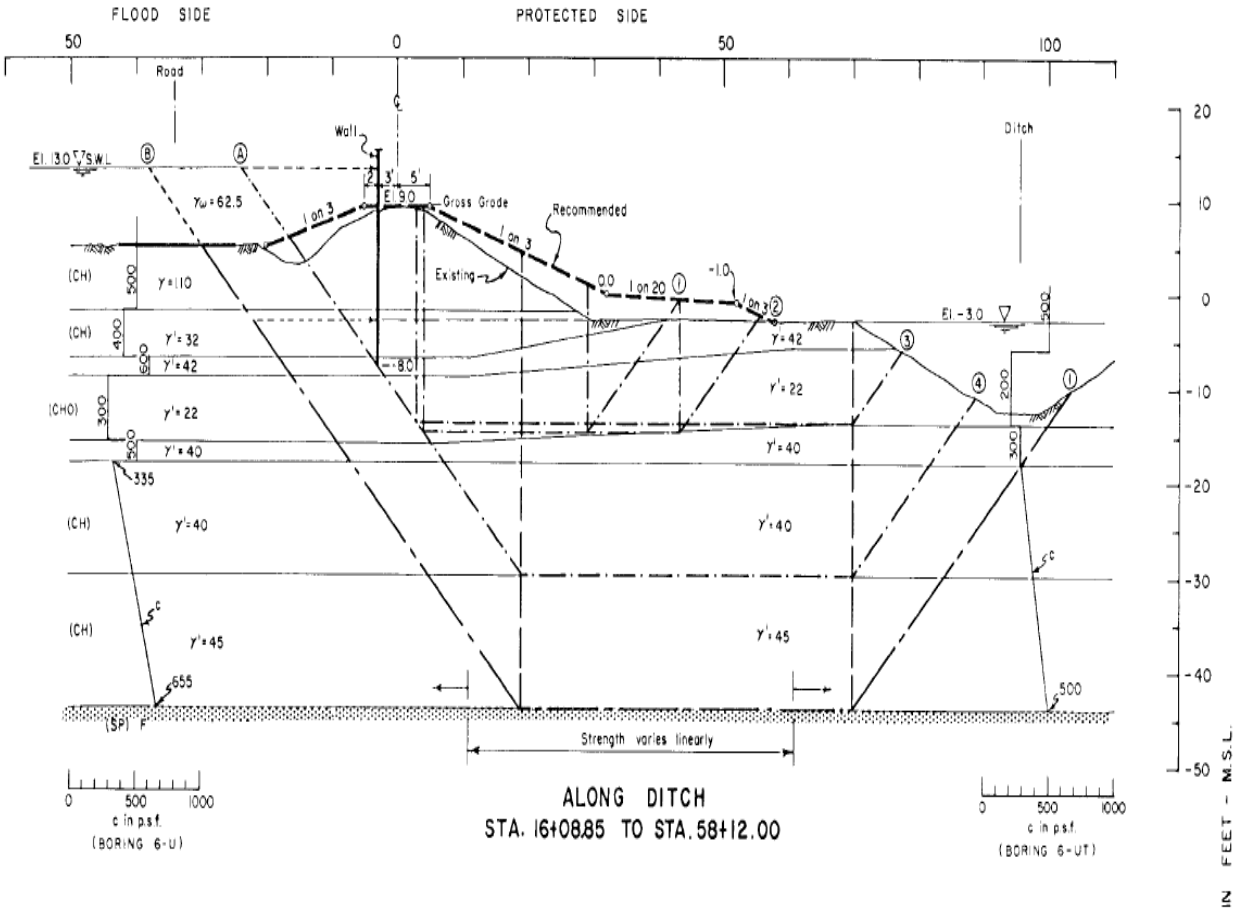


Figure 2-1a. Analysis cross section for the levee stretch south of Florida Avenue. This section was considered representative of the levees protecting the Lower Ninth Ward. Source: USACE DM 03 (1966).

Based on the design drawings (Figure 2-1b) the design sheet piles were topped at elevation +14.8 feet, and tipped at elevation –8 feet. Elevation survey data provided by IPET (2007) indicate that the top of the sheet pile supported I-wall was located at elevation +12 feet (NAVD88), and the sheet piles tipped at -10.5 feet. This was a 2.5 feet elevation difference between the design and pre-Katrina conditions.

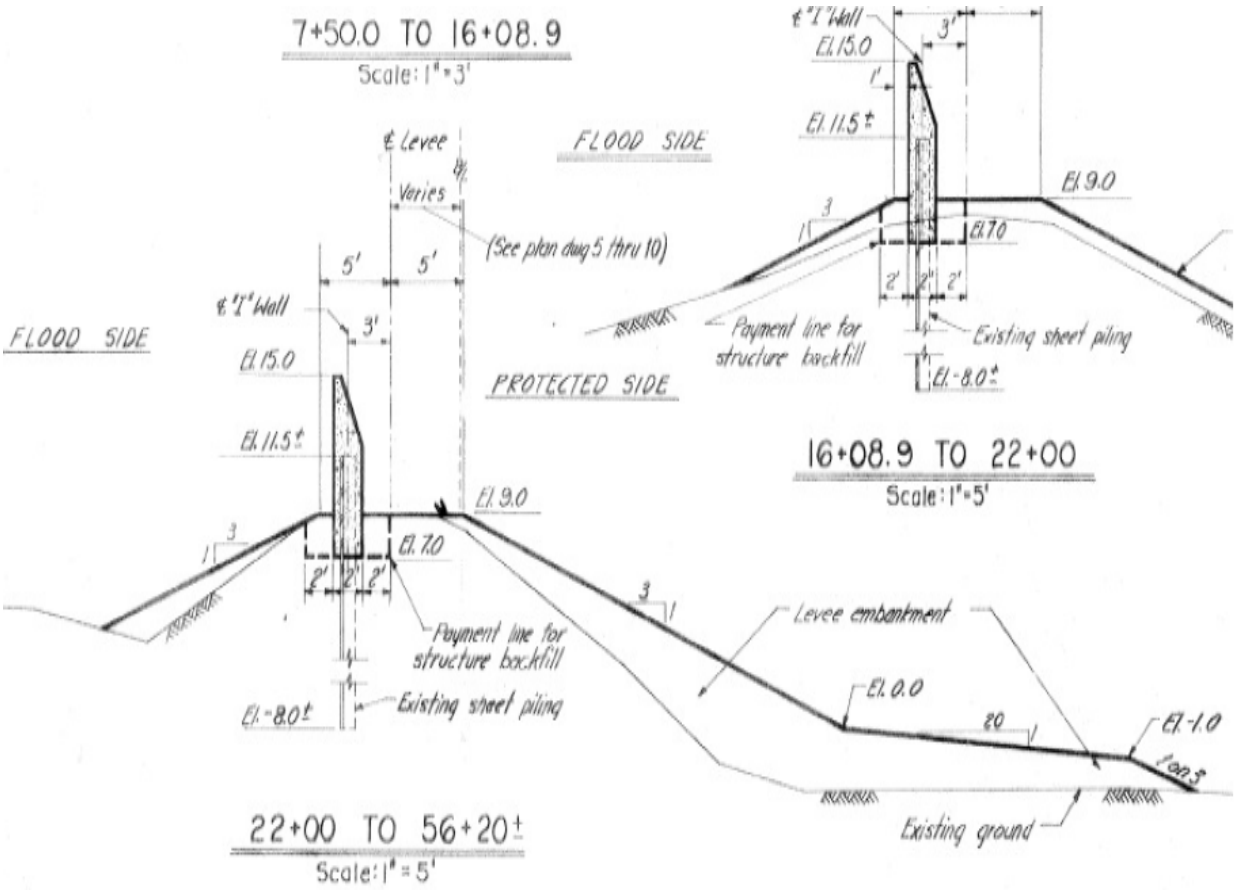


Figure 2-1b: I-wall as-built drawings for Lower 9th Ward south of Florida Avenue. Source: USACE DM 03 (1966).

Figure 2-2a shows the elevation difference between landside toe elevations from LIDAR surveys performed in 2000, showing an elevation difference of approximately 4 feet between the North Breach and South Breach. As shown in Figure 2-2b, There were substantial differences between the design levee profiles and those actually present.

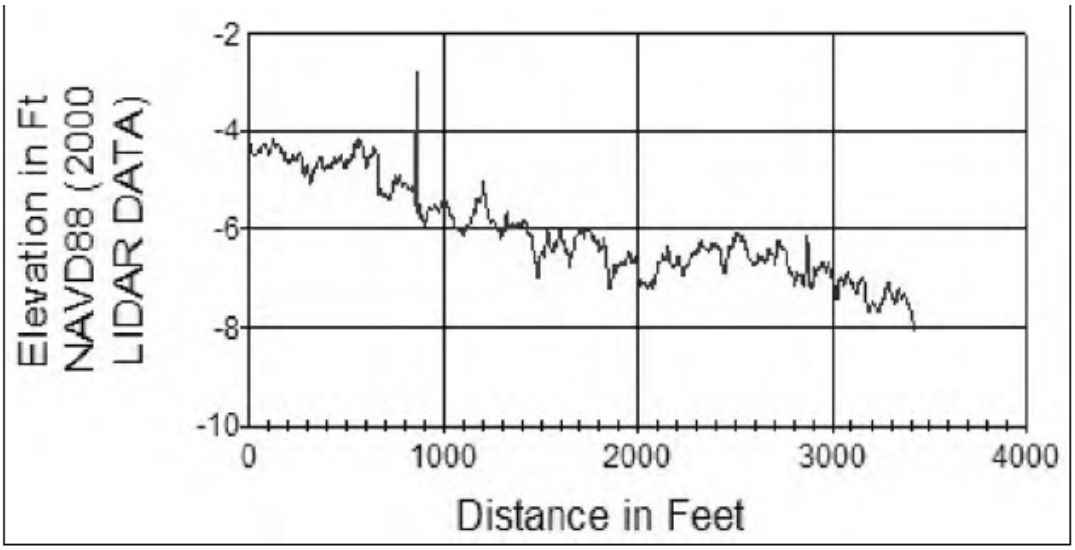


Figure 2-2a. LIDAR survey along landside toe. Source: IPET report (2006). Volume V, Appendices, page V-11-28.

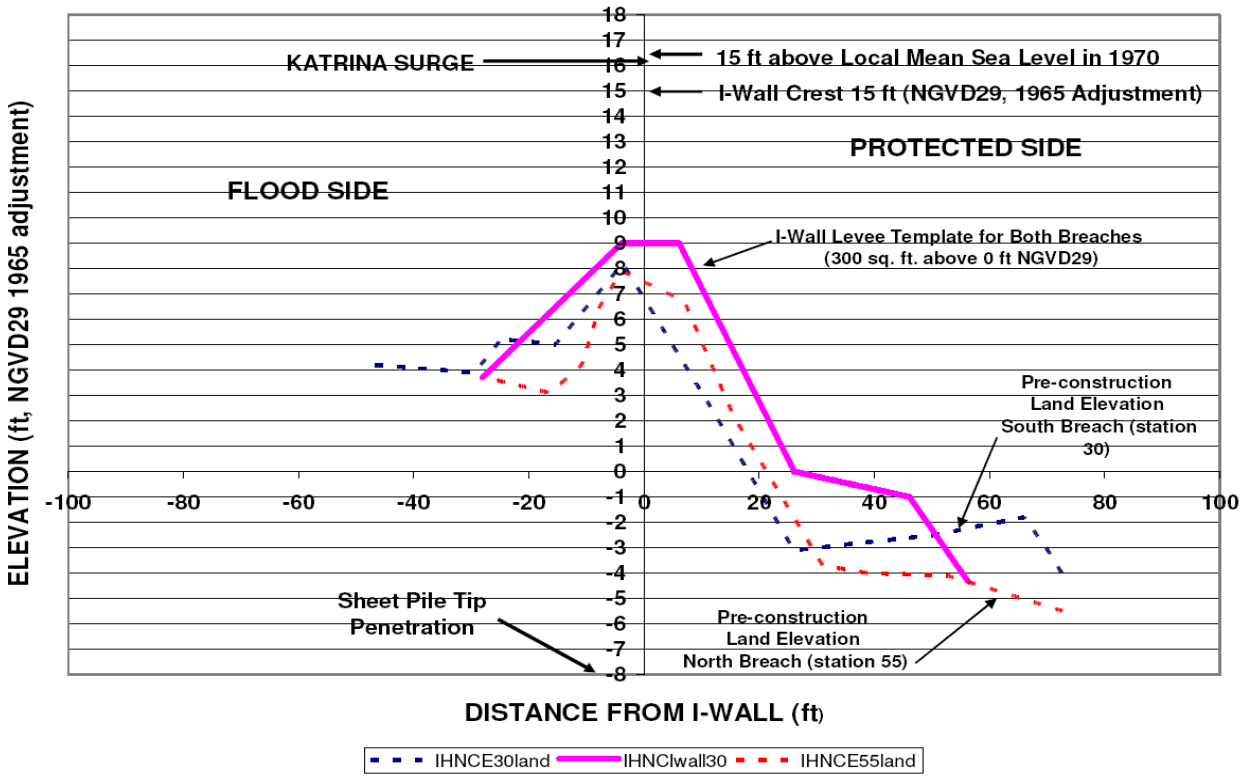


Figure 2-2b. Comparison of the as-built I-wall levee profile with pre-construction surveys at south and North Breaches. Source:Team Louisiana, 2007.

2.2 Sheet Piles

Based on the information provided in Figures 2-1a and 2-1b the design sheet piles were topped at elevation +14.8 feet, and tipped at elevation –8 feet. Cross sections by IPET (2006) indicate that the top of the sheet piles was located at elevation +12 feet, and tipped at -10.5 feet. This was a 2.5 foot difference between the designed cross sections and the pre-Katrina conditions.

2.3 Site Geology

The levee embankment is underlain by a thick irregular Marsh (Peat) deposit. According to the field evidence and analysis results from the ILIT investigation team, this layer had an important role on the shape and extents of both the North and South levee breaches.

A recently published report by Gagliano (2005) shows evidence of geological features in the vicinity of the Lower Ninth Ward area. In this report, the presence of the Lake Borgne fault, -a Growth fault- is evidenced by desiccation fissures and seepage zones oriented perpendicular to the levee alignment, and by a down-dropped block clearly shown in the boring logs performed for DM03 (USACE, 1966), where the marsh deposit shows a pronounced drop of about 15ft at the north end of the area, near the pump station (Figures 2-3a, 2-3b, 2-3c, and 2-3d).

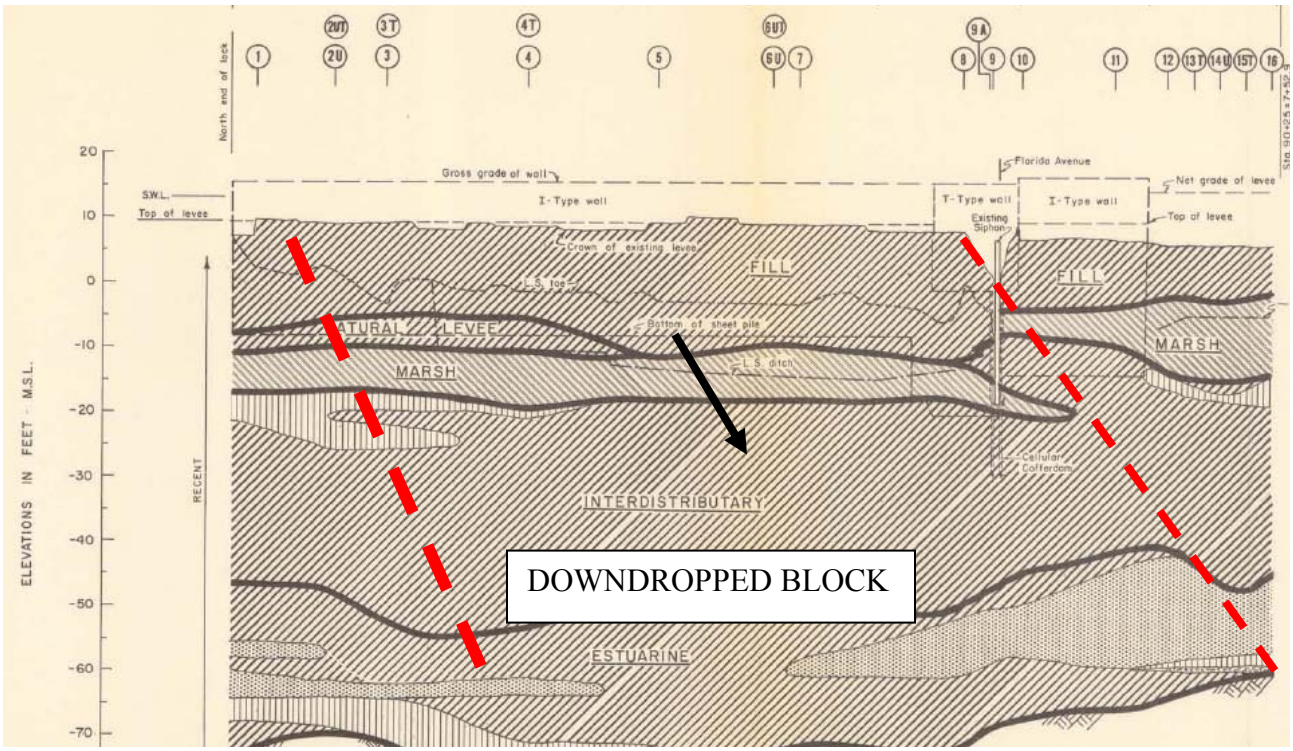


Figure 2-3a. Geologic profile showing discontinuity on the Marsh deposit near the north end of the area. Source: DM03 (USACE, 1966).

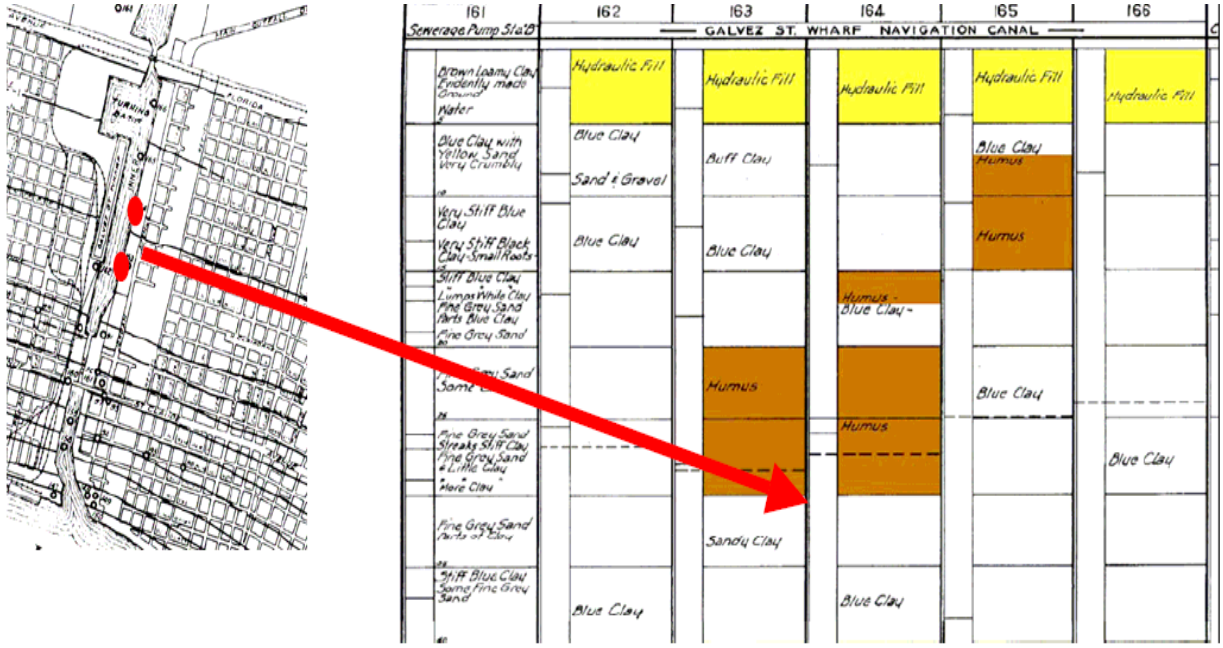


Figure 2-3b. Geologic profile showing discontinuity on the Marsh deposit near the north end of the area. Source: Rogers (2006).

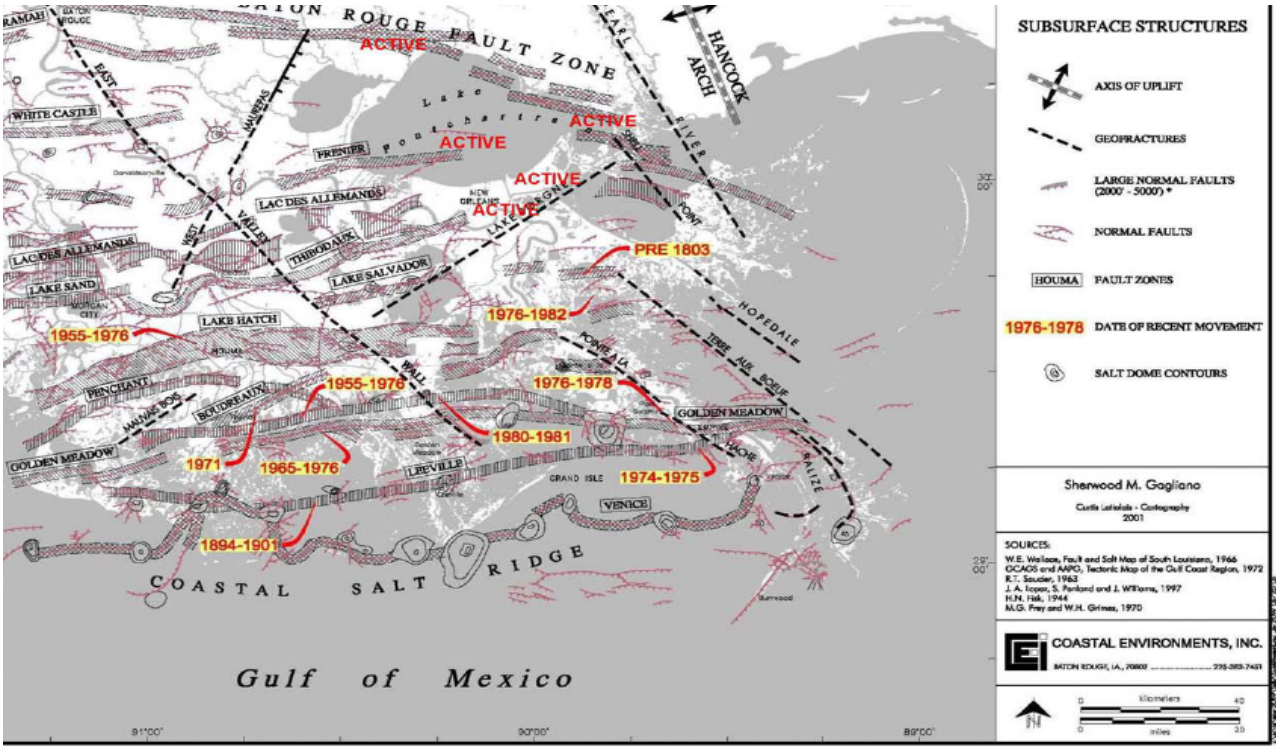


Figure 2-3c. Growth faulting in southeast Louisiana. Source: Gagliano 2005.

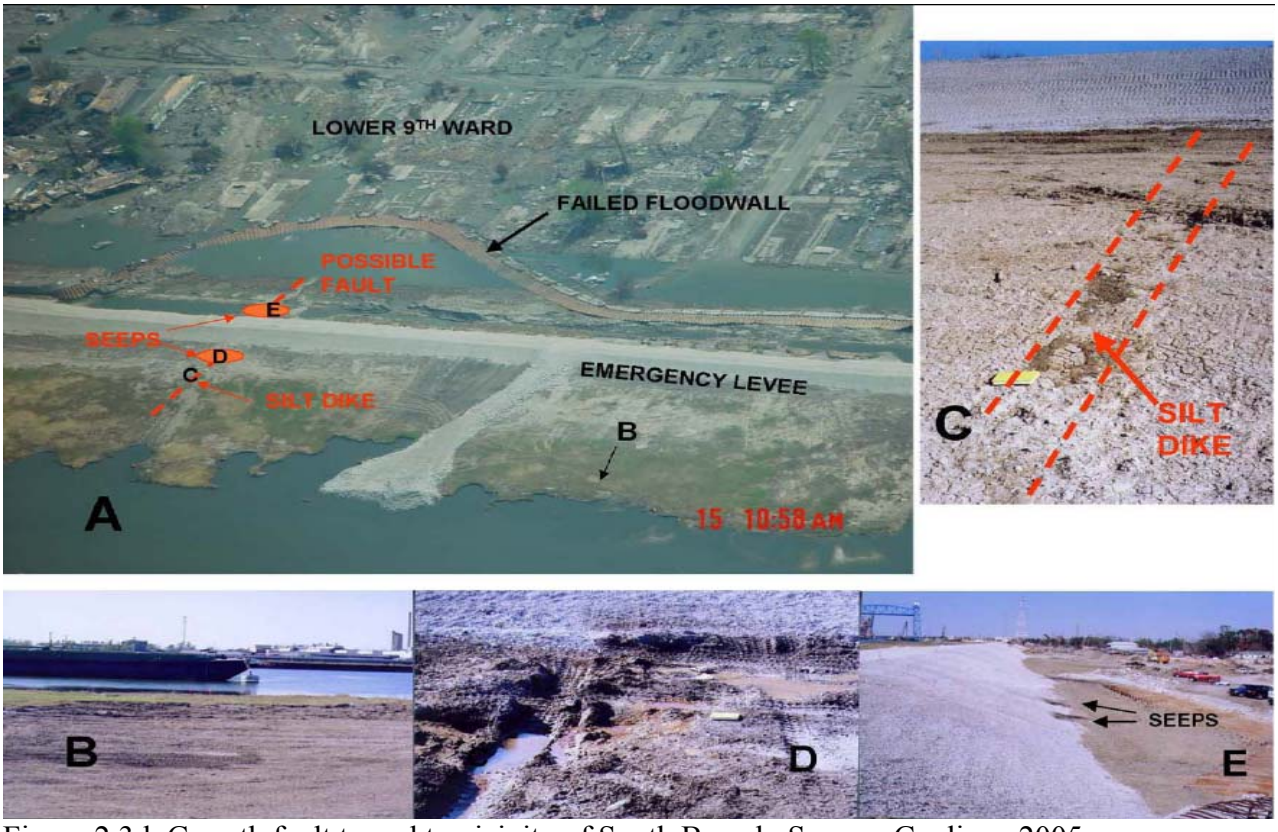


Figure 2.3d. Growth fault traced to vicinity of South Breach. Source: Gagliano 2005

The geologic interpretation shows a probable fault alignment in the vicinity of the South Breach, explaining fissures, preferential seepage paths and flow concentration beneath the levee embankment and sheet piling supporting the floodwall.

3. PART II – BACKGROUND INFORMATION

3.1 Recorded Surge Hydrographs

The hydrographs (surge elevation versus time plots) in Figure 3-1 shows measurements of water elevation in the vicinity of the IHNC. The hydrograph recorded at the IHNC Lock Staff Gage was used in the generation of the seepage analyses. The sudden decreases in recorded water elevations about 5:00 am shown for the hydrographs close to the I-10 IHNC overpass appear to have been associated with the breach at the intersection on the west side of the CSX railroad at the I-10 overpass (sandbags placed in gap left by missing – damaged flood gate blew out).

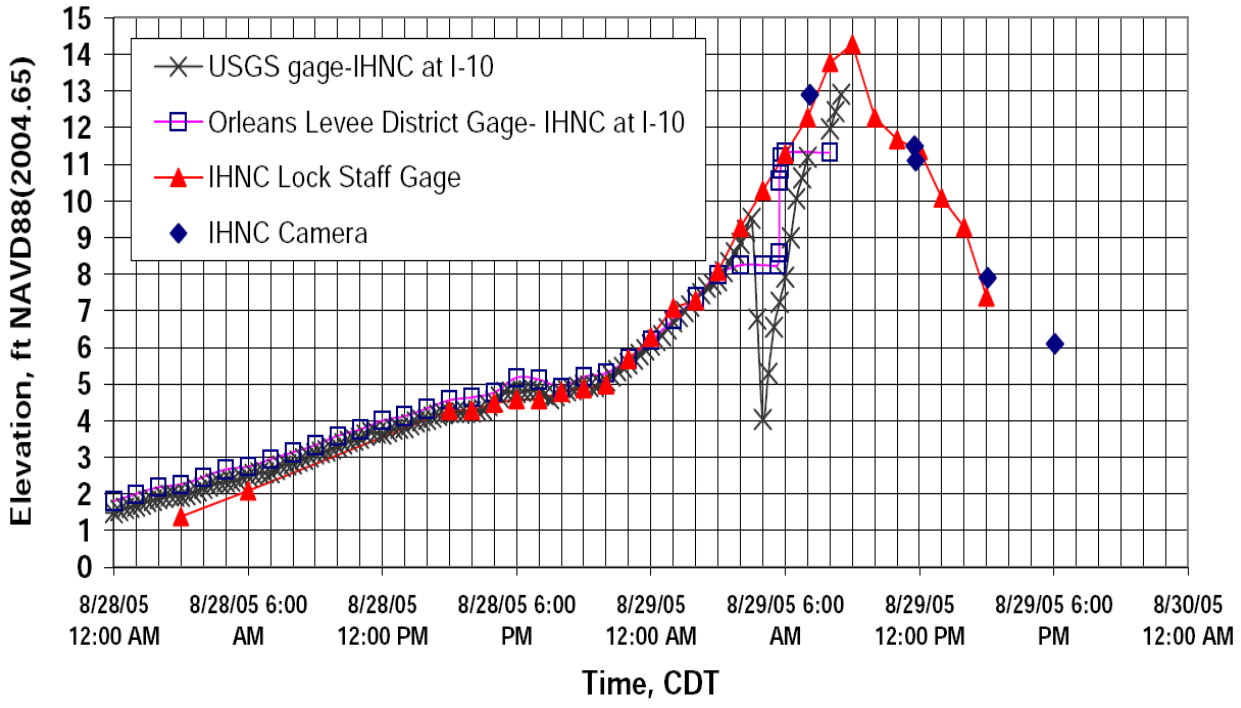


Figure 3-1. Hydrograph of the IHNC area. Source: IPET, 2006.

3.2 USACE Navigation Lock Expansion EBIA Site Clearing Excavations

Information regarding waterside excavations (WGI 2005) suggested that work near the area of the breaches placed permeable material down to elevations of approximately –25 feet, more than 10 feet deeper than the sheet pile tips; thus producing significantly shorter paths for the pore pressure pulse to reach beneath the embankment soils and levee toe, starting material saturation and softening potentially faster, as opposed to the subsoils being hydraulically charged from more than two hundred feet away (e.g. charged from the IHNC canal). Figures 3-2 through 3-4 show an evolution of the excavation along the IHNC waterside, and how alarmingly close the IHNC canal water was "moved" to the floodwall early in 2005. Figure 3-5 shows excavations located from 10 feet to 60 feet from the I-wall

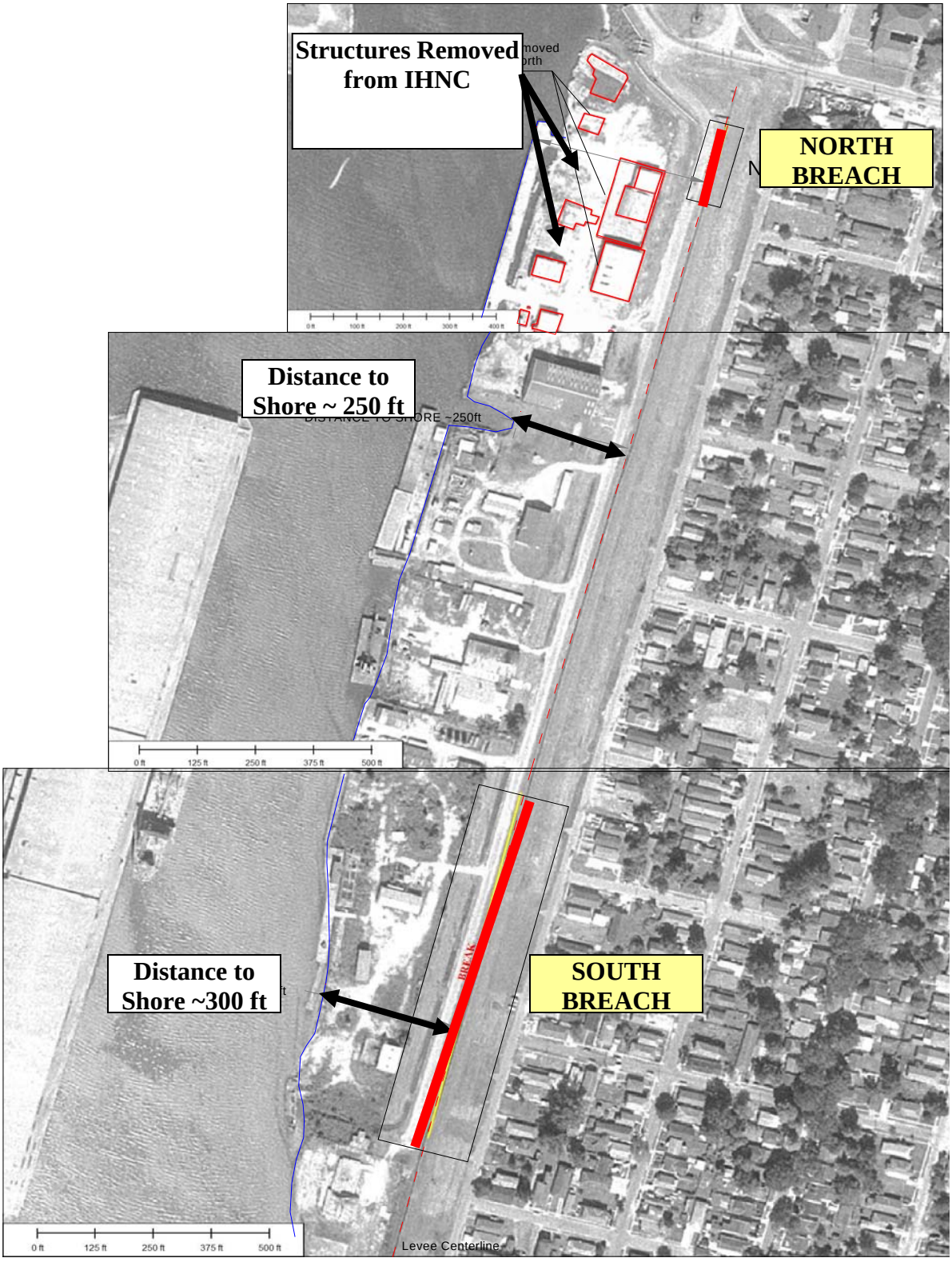


Figure 3-2. East bank of IHNC as of October 18, 1996.

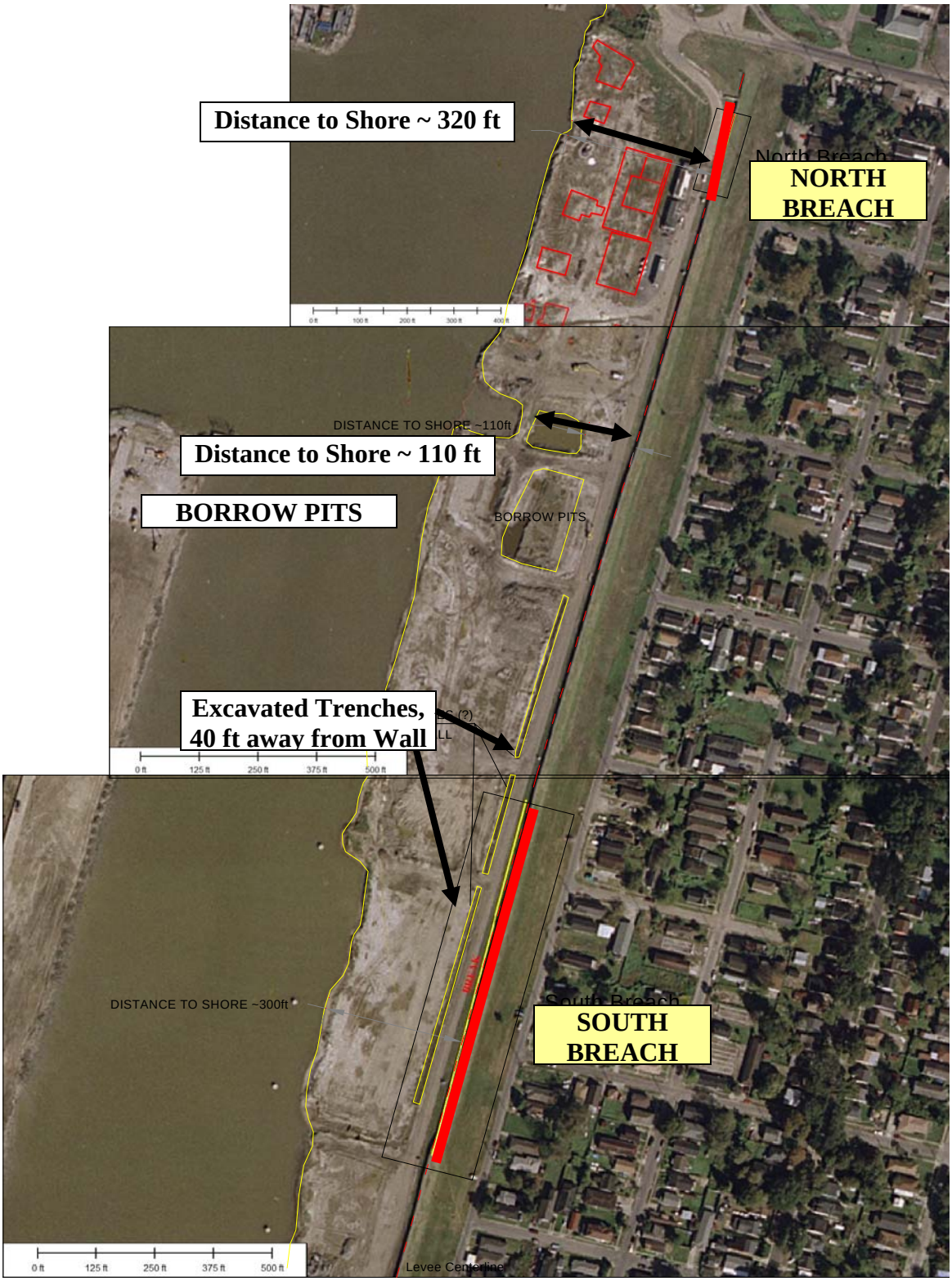


Figure 3-3. East bank of IHNC as of November 13, 2002.



Figure 3-4. East bank of IHNC as of April 13, 2005.



Figure 3-5. East bank of IHNC as of September 2, 2005.

The canal-side excavations took place in the late 1990s, as part of an expansion of the East Bank Industrial Area (EBIA). EBIA is precisely the area located between the levee and the IHNC canal, between Florida avenue and Claiborne avenue. The area was occupied by industrial facilities and used for storage of underground tanks that were eventually removed in 1991 (WGI, 2005). Figures 3-6 through 3-10 show some of the available information regarding tanks and other structures on the canal-side of the levees along IHNC.



Figure 3-6. Cofferdam excavation bottomed at elevation –23 feet (MSL).

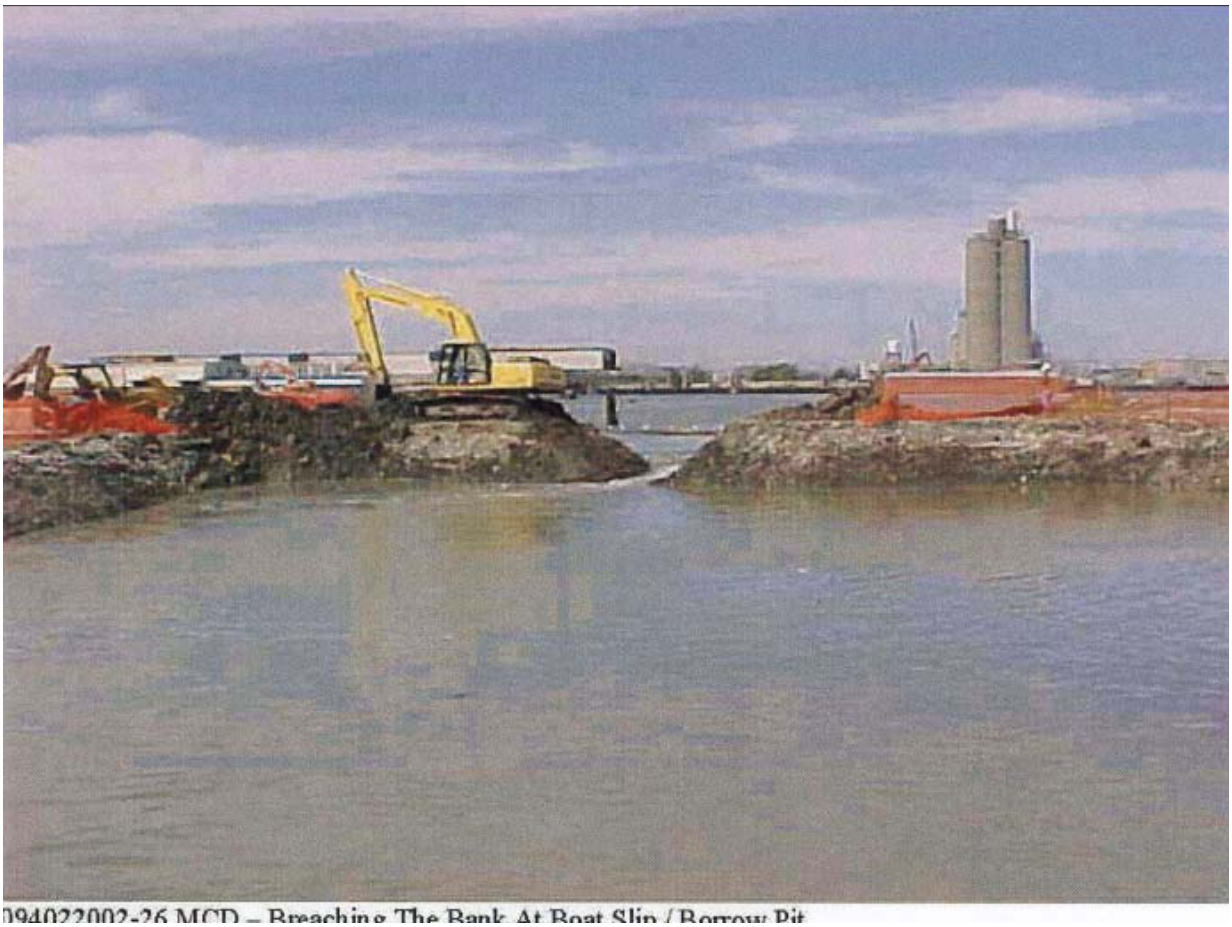


Figure 3-7. The banks of the excavation were breached so the water from the canal filled the hole. This brought the canal even closer to the floodwalls.



Figure 3-8. Backfill of cofferdam. Note the proximity to the I-wall (left side of machinery).



231021805-07 Placing imported sand backfill in Phase 2 ACM excavation east of Area 8 at Boland Marine

Figure 3-9. Coarse-grained backfill of excavations.

No precise dimensions or locations for the excavations could be obtained from information made available by the USACE and WGI. The analyses in this report include different plan dimensions, locations and depths for the excavations, analyzing the presence of the excavations located at the waterside toe of the levee, and 60 feet away from the levee toe.

3.3 Design Cross Sections Compared With LiDAR Survey Cross Sections

Comparison between the designed sections (DM03) and the Pre-Katrina configuration was achieved using LiDAR elevation surveys performed in 2000 and the cross sections in the design memorandum. The surface overlays shows that the pre-Katrina sections have approximately the desired design slope, but the levee crown width is substantially less than the design section. Figures 3-10 and 3-11 show the cross sections at the North Breach and South Breach, respectively.

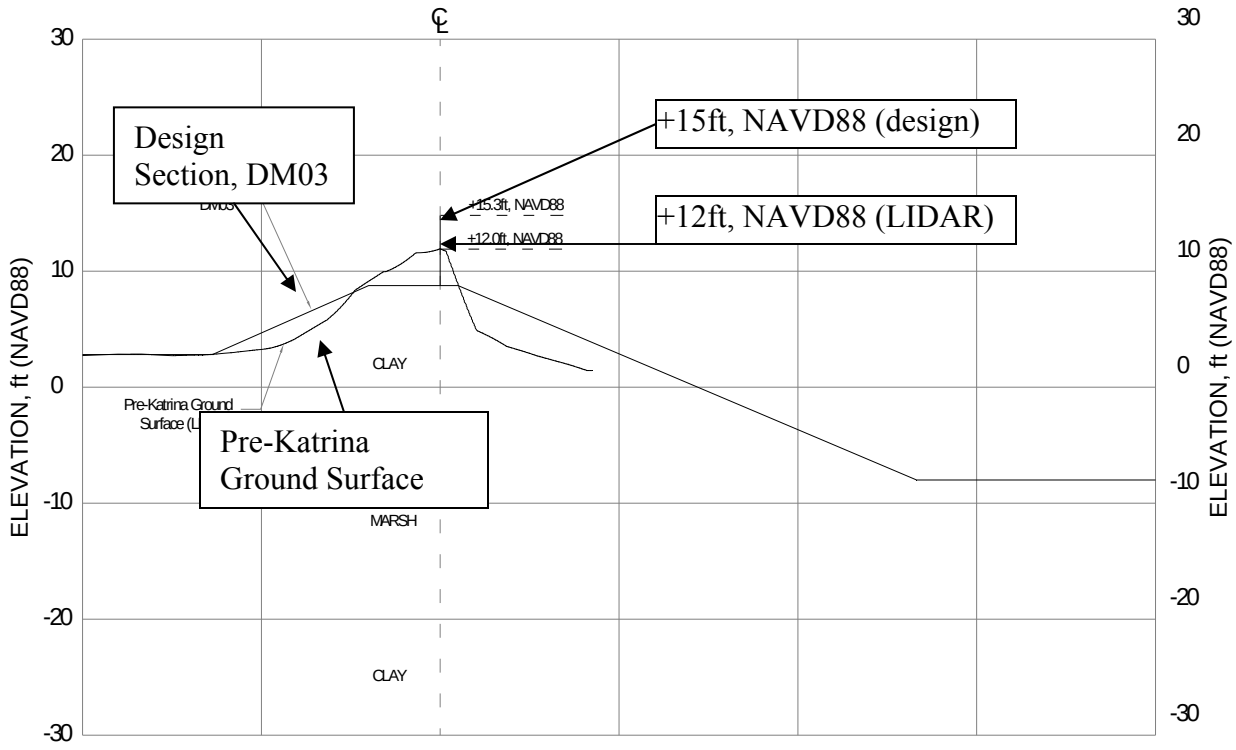


Figure 3-10. North Breach cross sections comparing design geometry from DM03 and pre-Katrina section from LiDAR survey performed in 2000.

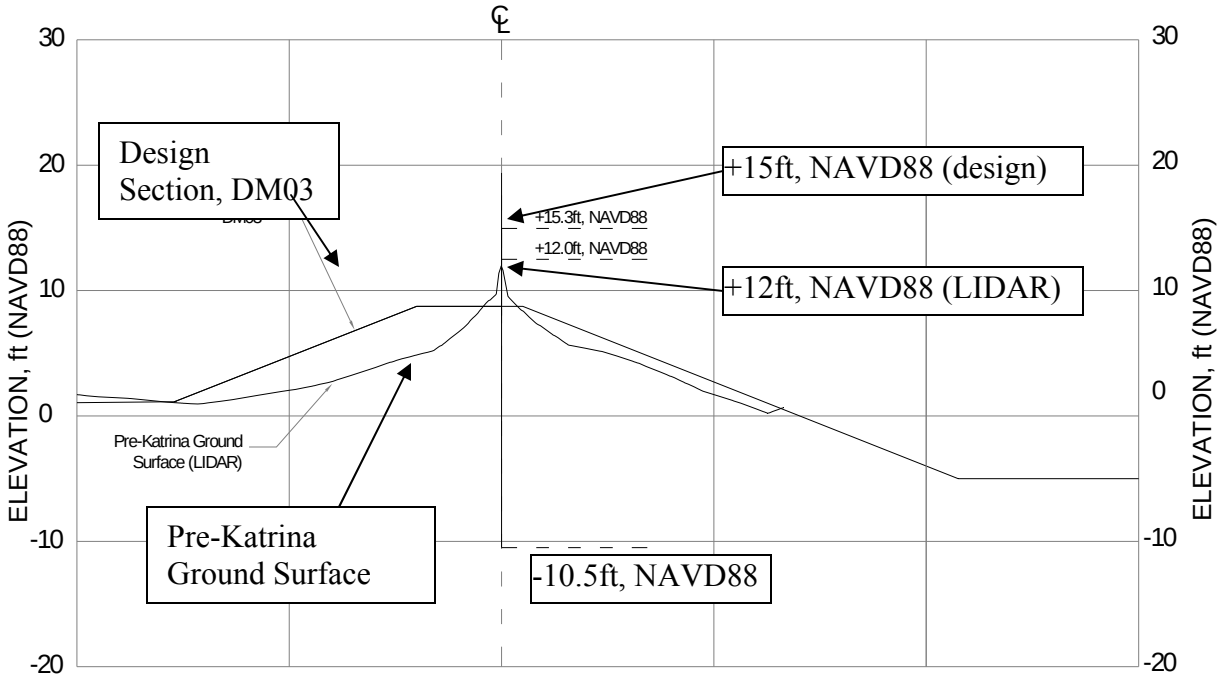


Figure 3-11. South Breach cross sections comparing design geometry from DM03 and pre-Katrina section from LIDAR survey performed in 2000.

3.4 Soil Stratigraphy and Analysis Sections by IPET and ILIT (2006)

Analyses performed by IPET (2006) and ILIT (2006) show some differences in interpretations of the available information. IPET shows that for the South Breach, a thick marsh deposit, divided in two "stages" based on index and strength properties. Under the marsh, a normally consolidated clay deposit is found extending to elevation –40 feet (Figure 3-12). ILIT considered a slightly different profile, with a thin clay layer found near the toe of the levee, underlain by the Marsh deposits, and in turn, the gray clays. Figures 3-12 and 3-13 show the profiles from ILIT and IPET, respetively. The main difference between the two cross sections is the presence of the thin clay layer beneath the levee embankment, which acts as a blanket against uplift pressures from the under-seepage flow. For both breaches, IPET considers the top of the I-wall to be at elevation +12.5 feet, and the sheet pile tip at elevation -10.5 feet. ILIT considered a

higher I-Wall, topped at +14 feet and sheet piles tipped at –8 feet, in accordance with the Design Memorandum.

For the North Breach, ILIT and IPET sections are similar, the principal difference lies on the thickness of the surficial clay layer beneath the levee embankment, which ultimately controls the hydraulic stability of the levee and foundation soils. Figures 3-14 and 3-15 show the sections from ILIT and IPET, respectively.

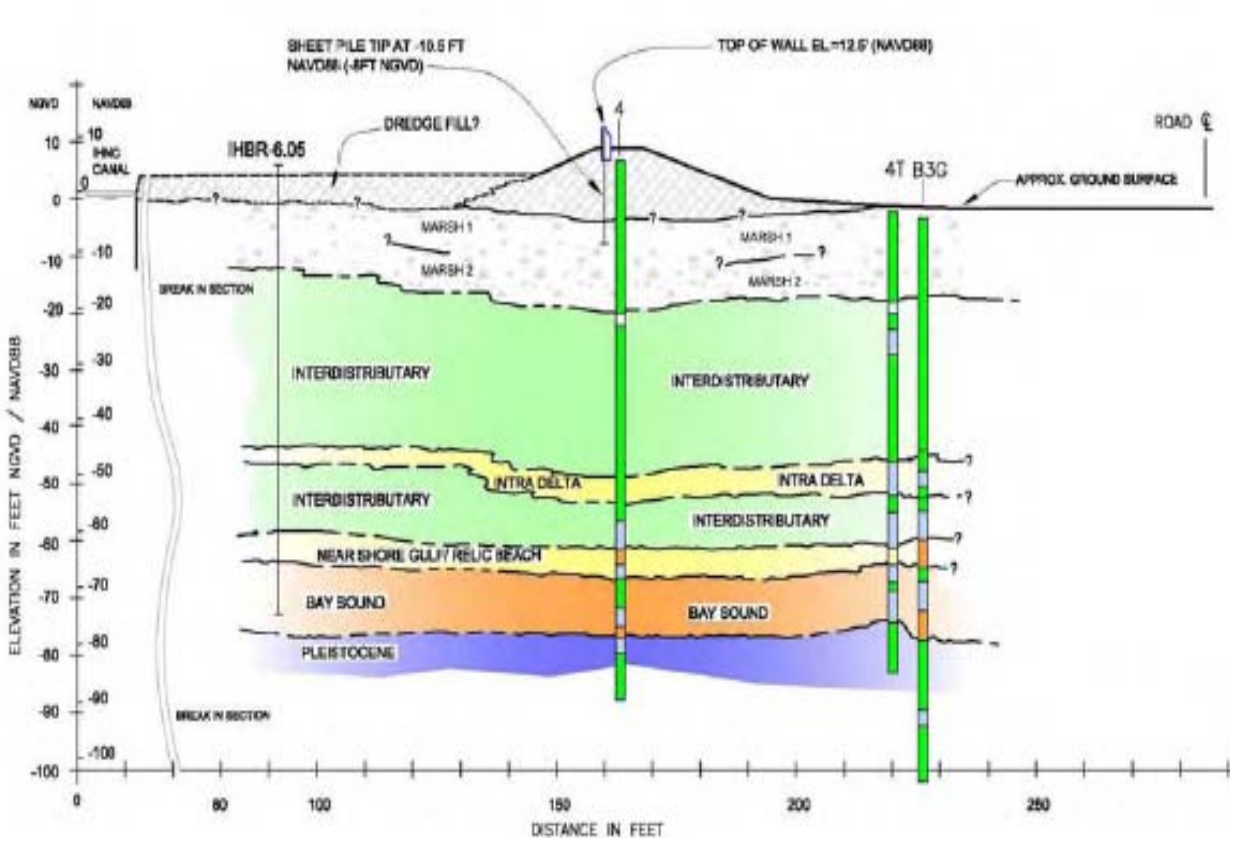


Figure 3-12. South section from ILIT (2006). Source: ILIT final report, Volume V, appendix 11.

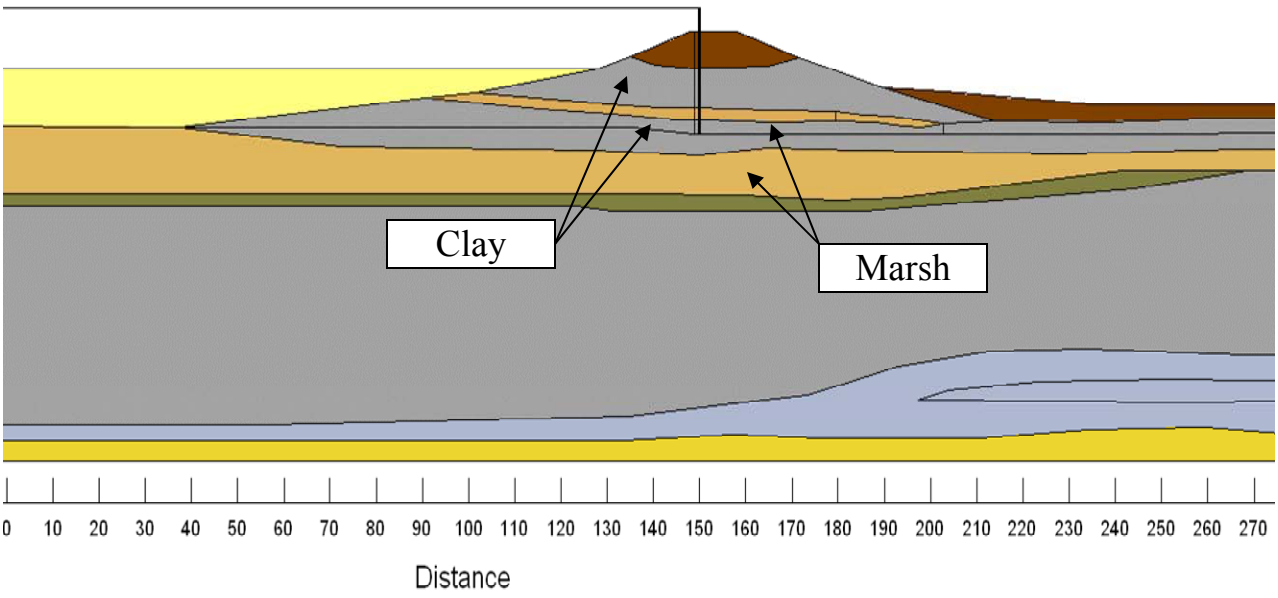


Figure 3-13. South section from IPET (2006). Source: IPET final report, Chapter 5.

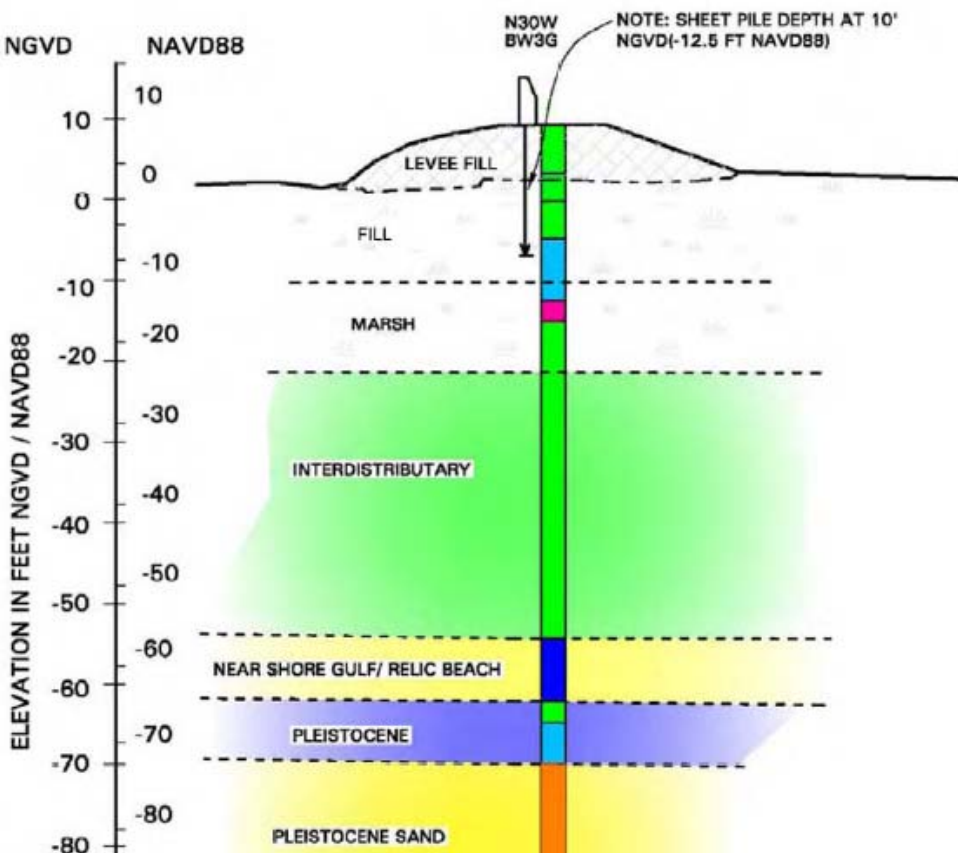


Figure 3-14. North Breach cross section from ILIT (2006). Source: LIT final report, Volume V, appendix 11.

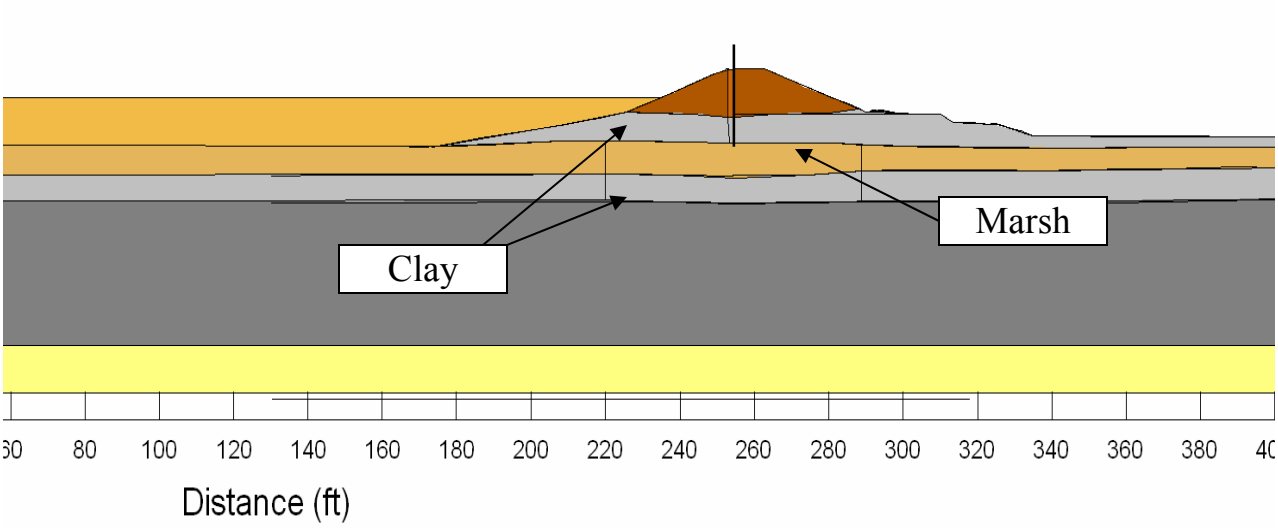


Figure 3-15. North Breach cross section from IPET (2006). Source: IPET final report, Volume V, appendix 11.

3.5 Drainage Structures

A drainage canal ran parallel to the levee and floodwall on the East bank of the IHNC at the Lower Ninth Ward. The Jourdan canal (shown in cross section in Figure 2-1) was backfilled sometime in the 1990's. Figure 3-16 shows a map of the drainage structures present on the New Orleans Flood Protection system as of 1992. The canal drained into a pump station located north of Florida Avenue, which could extract from 1751 to 3190 cubic feet per second of rain or floodwaters.

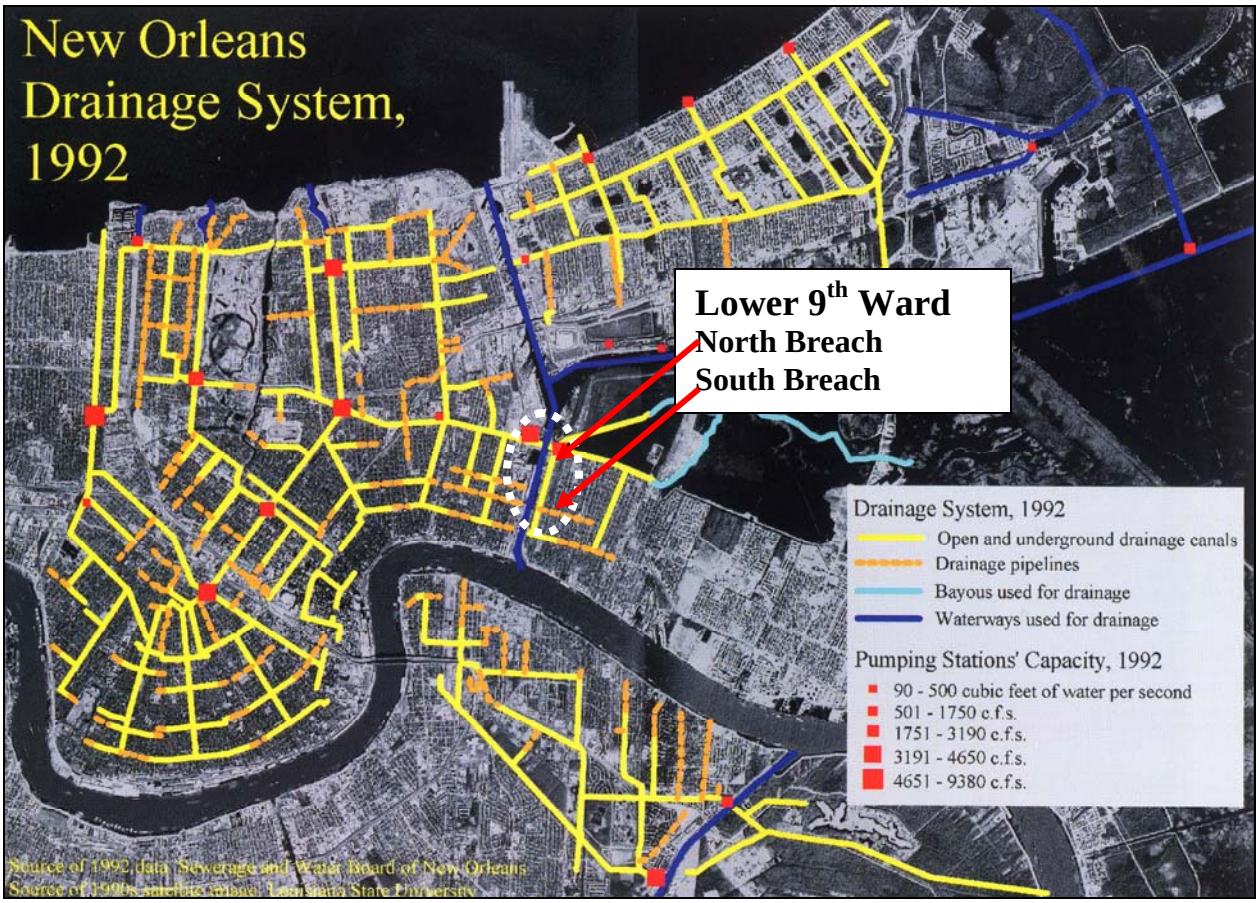


Figure 3-16. Principal elements of the pre-Katrina drainage system infrastructure as it existed in 1992. Source: ILIT 2006, Chapter 4.

3.6 Historic Breaches

Both sides of the IHNC experienced breaks and overtopping during Hurricane Betsy in September 1965. 6,560 homes and 40 businesses were flooded in water up to 7 feet deep on the west side of the IHNC (ILIT, 2006). The east side of the IHNC also failed, flooding the west end of St. Bernard's Parish. A map of the flood inundation of New Orleans caused by Hurricane Betsy in September 1965 is shown in Figure 3-17.

The IHNC was heightened using steel sheet piles and concrete I-walls in the 1980s and 1990s. On August 29, 2005 during Hurricane Katrina both sides of the IHNC were overtopped by the

storm surge converging on the IHNC from Lakes Borgne and Pontchartrain. Sustained overtopping flow undermined the landside toe of the I-walls, in places gouging down as much as 5+ feet below the crest of the earthen levee. In addition, there was ample physical evidence of underseepage at both the eastern IHNC breaches, in the form of linear sand boils (IPET 2007; ILIT 2006, Team Louisiana 2007).

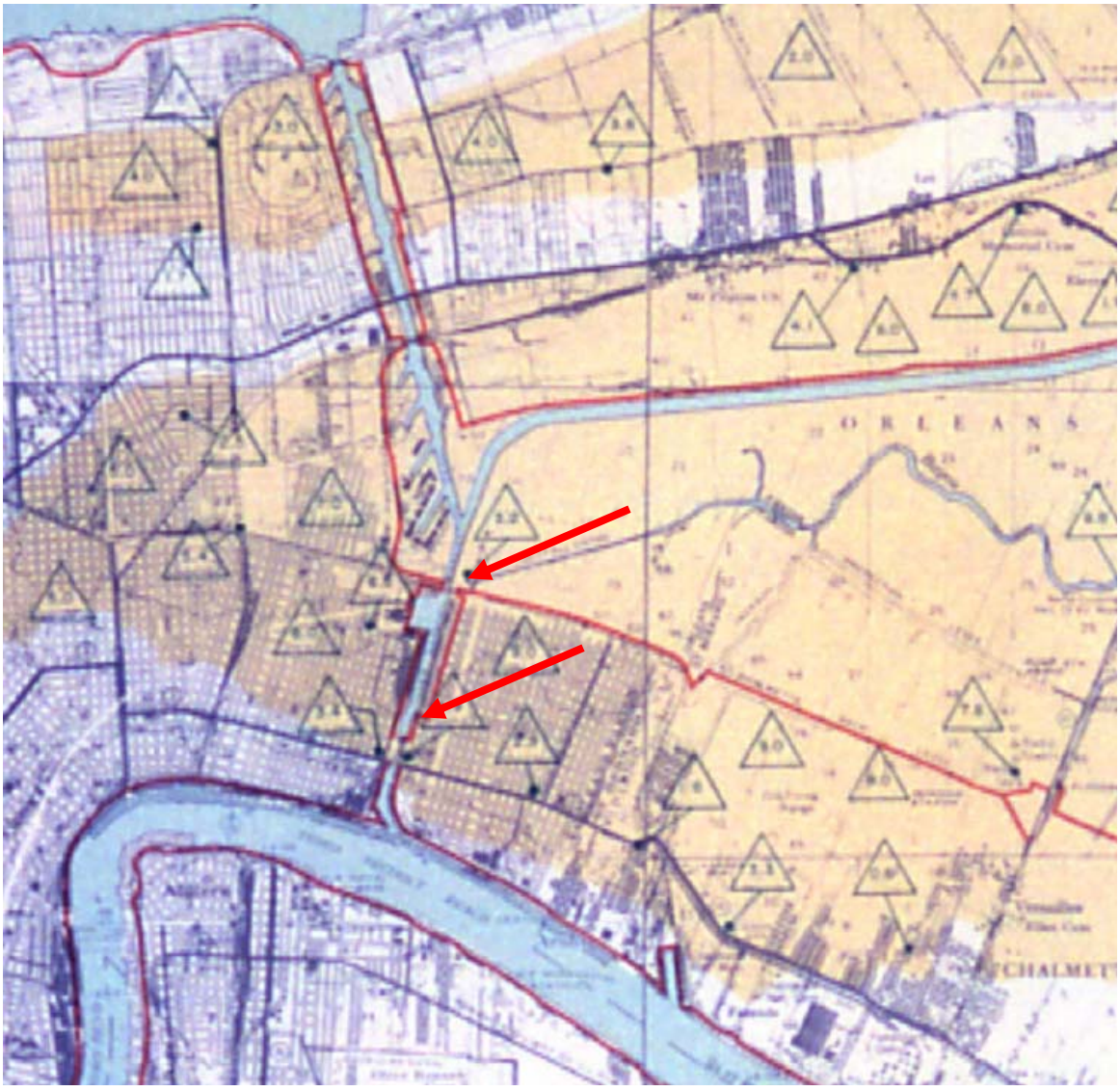


Figure 3-17. Portion of the flood inundation map from Hurricane Betsy in 1965, showing the areas on either side of the Inner Harbor Navigation Channel which were affected by overtopping, from storm surges on Lakes Borgne and Pontchartrain (from ILIT, Chapter 4, 2006).

3.7 Dwyer Road Canal Project

During the period 1999 through 2003, a drainage improvements project located approximately 3 miles north of the Lower 9th Ward at the IHNC intersection of Jourdan Road with Dwyer Road (Figure 3-18; Rosenberg 2008). This drainage improvements project provided important information concerning seepage and soil heaving associated with excavations into the same geologic sequence as present at the Lower 9th Ward.

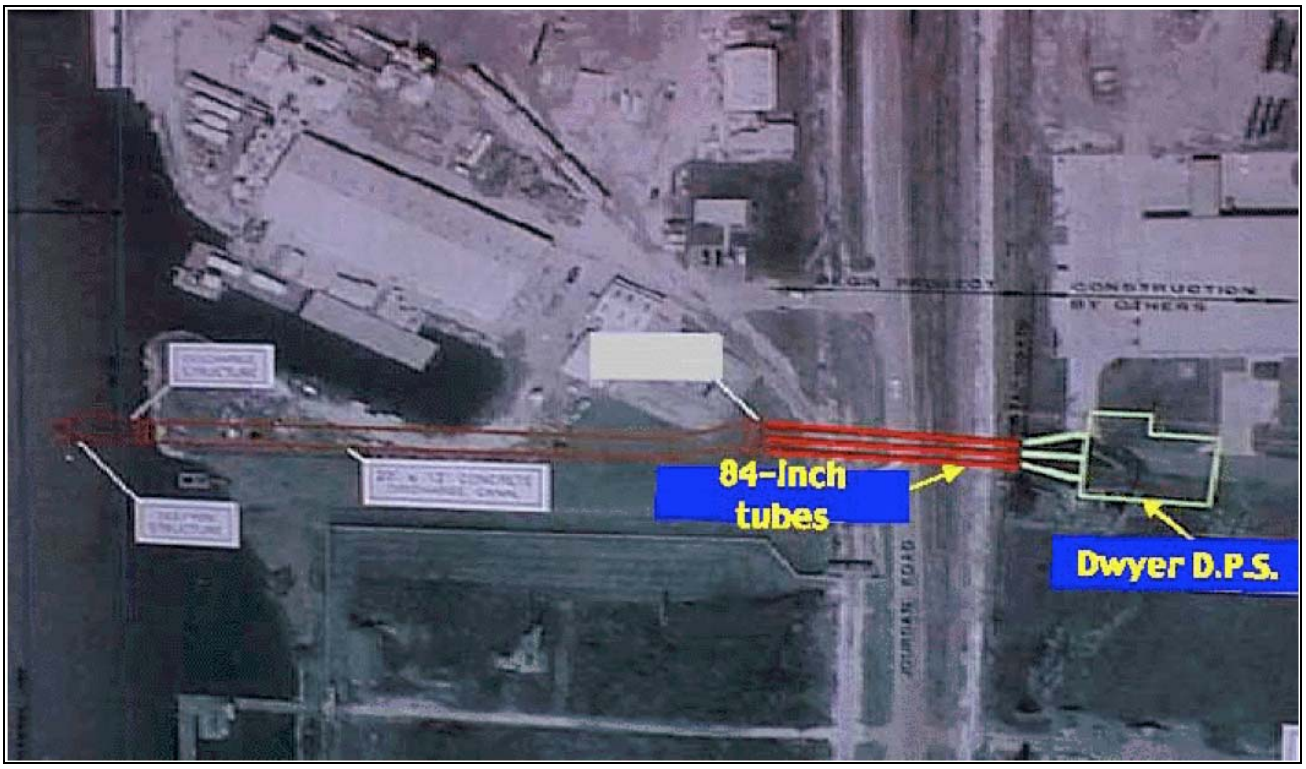


Figure 3-18. Site plan for the Dwyer Road drainage pumping station improvements (Rosenberg 2008).

The project was concerned with replacing the existing single 54-inch diameter discharge pipe with three 84-inch diameter steel tubes to carry drainage water from the pump station and into an underground concrete box canal 20 feet wide by 12 feet high leading into the IHNC. This routed the new discharge tubes under the existing floodwall system. All of these structures required extensive

braced excavations up to approximately 20 feet beneath the existing grade using a sheet pile Temporary Retraining System (TRS) and a wellpoint dewatering system (Figure 3-19).



Figure 3-19. Installation of pre-cast concrete outfall segments using a sheet pile TRS (Rosenberg 2008).

The project encountered many significant seepage and water control problems associated with organic layers (Swamp and Marsh layers buried under landfill) similar to those found at the Lower 9th Ward at identical elevations (-12 feet to –20 feet) (Figures 3-20 and 3-21). When the wellpoint drainage system pump would shut-down there was immediate influx of water into the excavation – indicating the high permeability of the soils exposed at the bottom of the excavations.



Figure 3-20. Exposed Swamp and Marsh layers at bottom of TRS (approximately –15 feet).



Figure 3-21. Close-up of tree roots and organic matter exposed by TRS excavation at approximately –14 feet.

Similar observations were developed when piles were pulled at the bottom of parts of the excavations (Figure 3-22). Holes left when the piles were pulled filled immediately with water. When attempts were made to fill these holes with a water – bentonite mix, there was almost immediate communication with holes left from other nearby pulled piles – up to 60 feet away from the hole being filled. It was obvious that these soils were highly water and water pressure conductive.



Figure 3-22. View of construction crew pulling concrete piles. Note the pile void (middle right) full of water.

The construction was also fraught with many instances of soil heaving – the soils would rise in the bottom of the excavations due to the pressure of the soils and water outside of the TRS. This indicated the relatively low shear strengths of the soils and their high mobility under pressure.



Figure 3-22. View of TRS after soil heaving into the bottom of the excavation required re-grading (bobcat loader at near top center of photograph is being used to remove material).

3.8 USACE Guidelines for Work Near Flood Control Projects

The work performed by WGI to clear the EBIA site of underground obstructions (WGI 2005) was under the direction and supervision of the USACE as part of their authorized IHNC Navigation Lock Expansion project (USACE 2001, 2002).

Guidelines were issued by the USACE for work proposed near or within a federally constructed flood control project (USACE 2005):

"The Corps of Engineers provides engineering review to ensure that any work within or near the flood control unit does not reduce the level of protection to assure the continued integrity of the flood control system."

"The critical area is generally considered the area from 300 feet riverward to 500 feet landward of a flood control project centerline. In some instances the critical area is extended beyond 500 feet if any impact on the flood control project can be considered."

Under the topic of Excavation and Backfill, these guidelines stipulate:

"General. Excavation and backfill in the critical area of a flood control project could have a direct impact on the stability of the flood control project. Improper excavation in the levee embankment or in the critical area can create unstable slopes and slope failures, which damage the levee embankment and weaken the flood protection structure. Additional damages to the levee embankment or flood protection structure can also be caused by underseepage conditions associated with piping and heave. This removal of material from the flood control structure foundation (piping) can ultimately produce collapse of a levee embankment or floodwall. All excavation and backfill activities within the critical area are to be reviewed and approved by the COE and the local sponsor before construction begins."

None of the WGI or USACE documentation reviewed indicated that such precautions regarding protection of the flood protection structures were taken. There was plentiful evidence that the primary concerns were focused on environmental protection due to the hazardous wastes known to be present at the EBIA and due to US Environmental Protection Agency requirements (USACE 2002). For additional details on this topic see the Technical Report (VII) by Bea and Storesund (2008).

4. STRATIGRAPHIC INTERPRETATIONS

After a detailed review of all available borings and results from in situ tests (e.g. Cone Penetrometer Test - CPT probes), the locations of explorations were geo-referenced using a (Geographic Information System (GIS) interface overlaying aerial photographs of the area. From the Pre and Post-Katrina LiDAR surveys and the DM03 ground elevations, a longitudinal profile was drawn, locating the borings and CPTs. To include the explorations into this report, the 1966 DM03 borings had to be scaled from the image versions of this report, as well as the laboratory testing results. The 2005 IPET borings available in the IPET website (www.ipet.wes.army.mil).

Figure 4-1 shows the complete longitudinal profile in a "profile/plan" format, containing a pre-Katrina aerial photograph, and below it, the borings and CPTs were placed as best as the available information on elevations allowed. Figures 4-2 and 4-3 are close-ups of the South Breach and the North Breach cross sections, respectively; the stratigraphic interpretation is shown, depicting the main soil units in the area as 1) Surficial Clays, 2) Marsh deposits, 3) Deeper "Gray" clays, and 4) Sands (relict beach deposits).

The stratigraphic interpretation clearly shows that the embankment fills that compose the levees are mainly composed by clays (CL, CH), and an irregular Marsh (peat) layer underlies the levee. The Marsh layer appears to be continuous along the entire IHNC east bank and it is thickest near the area surrounding the South Breach. Horizontal lines representing approximate elevations of I-wall crest, sheet pile tip, levee crest and levee toe are included in the longitudinal profile. From the longitudinal profile, two cross sections (perpendicular to the longitudinal alignment) were created. The first one is located in the area along the South Breach, and the second one in the North Breach. The borings in the vicinity of the section were located at their appropriate

elevations and another interpretation (more detailed) was performed at the particular section. These sections were chosen for the seepage and stability analyses.

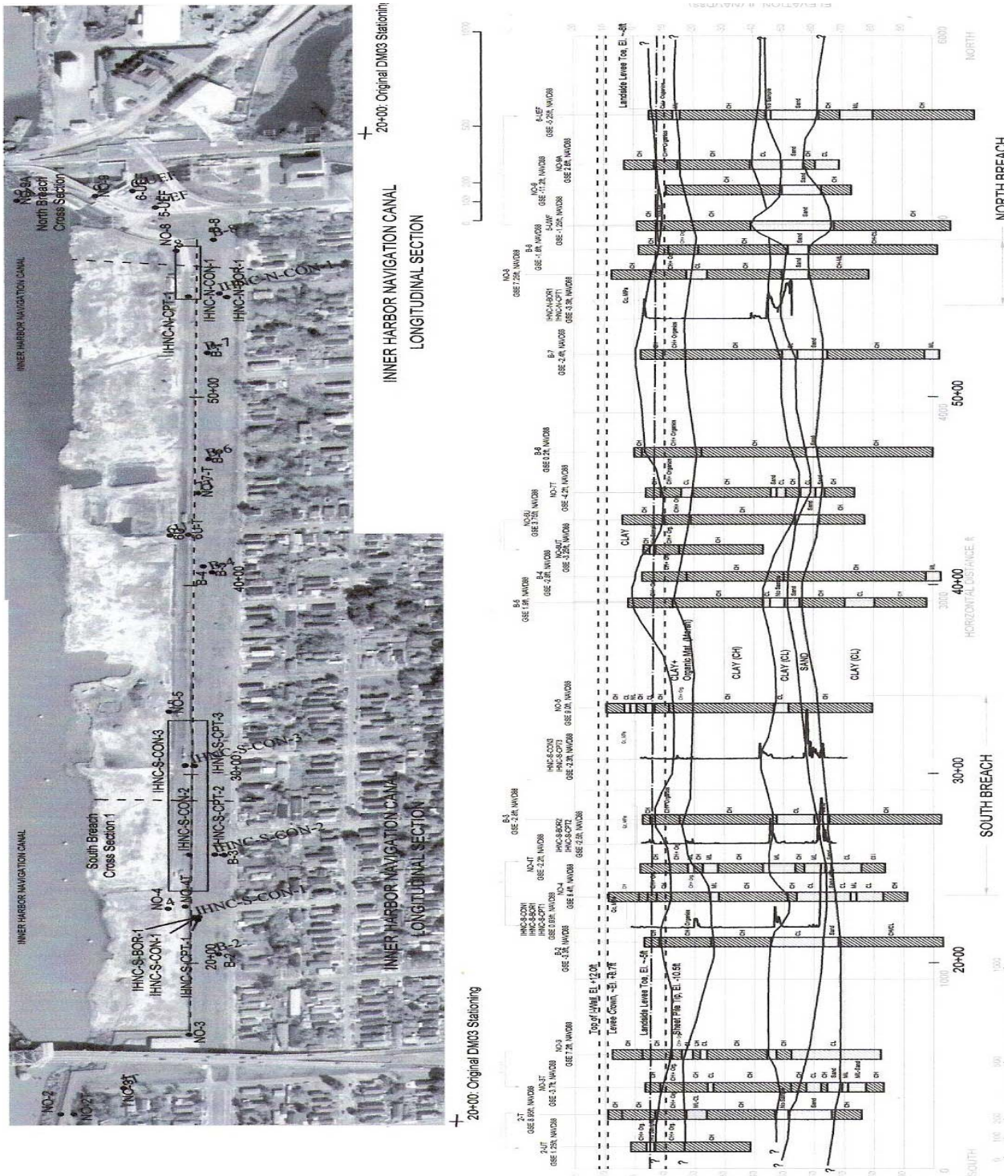


Figure 4-1. Longitudinal Profile along IHNC.

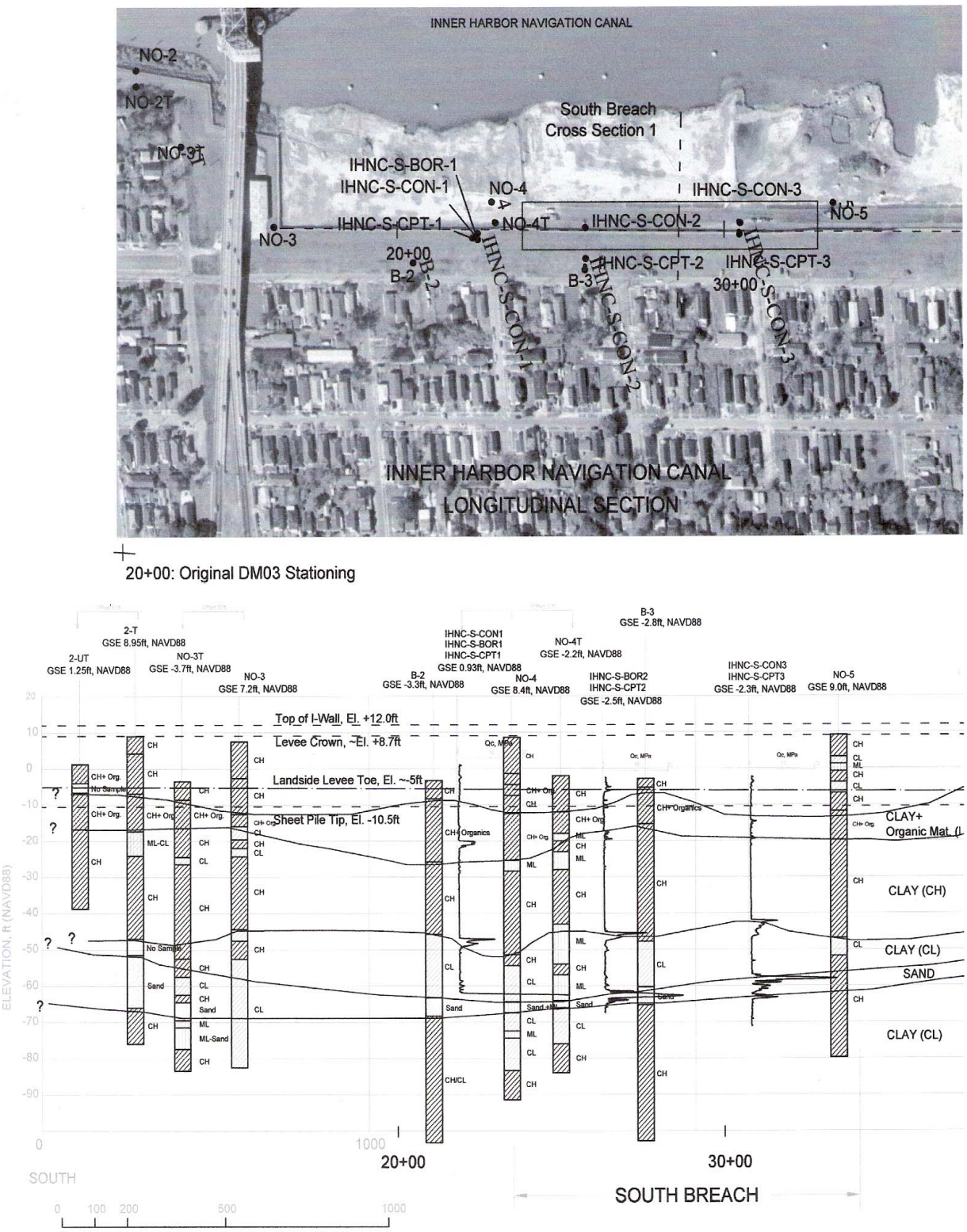


Figure 4-2. Longitudinal Profile along IHNC, South Breach.

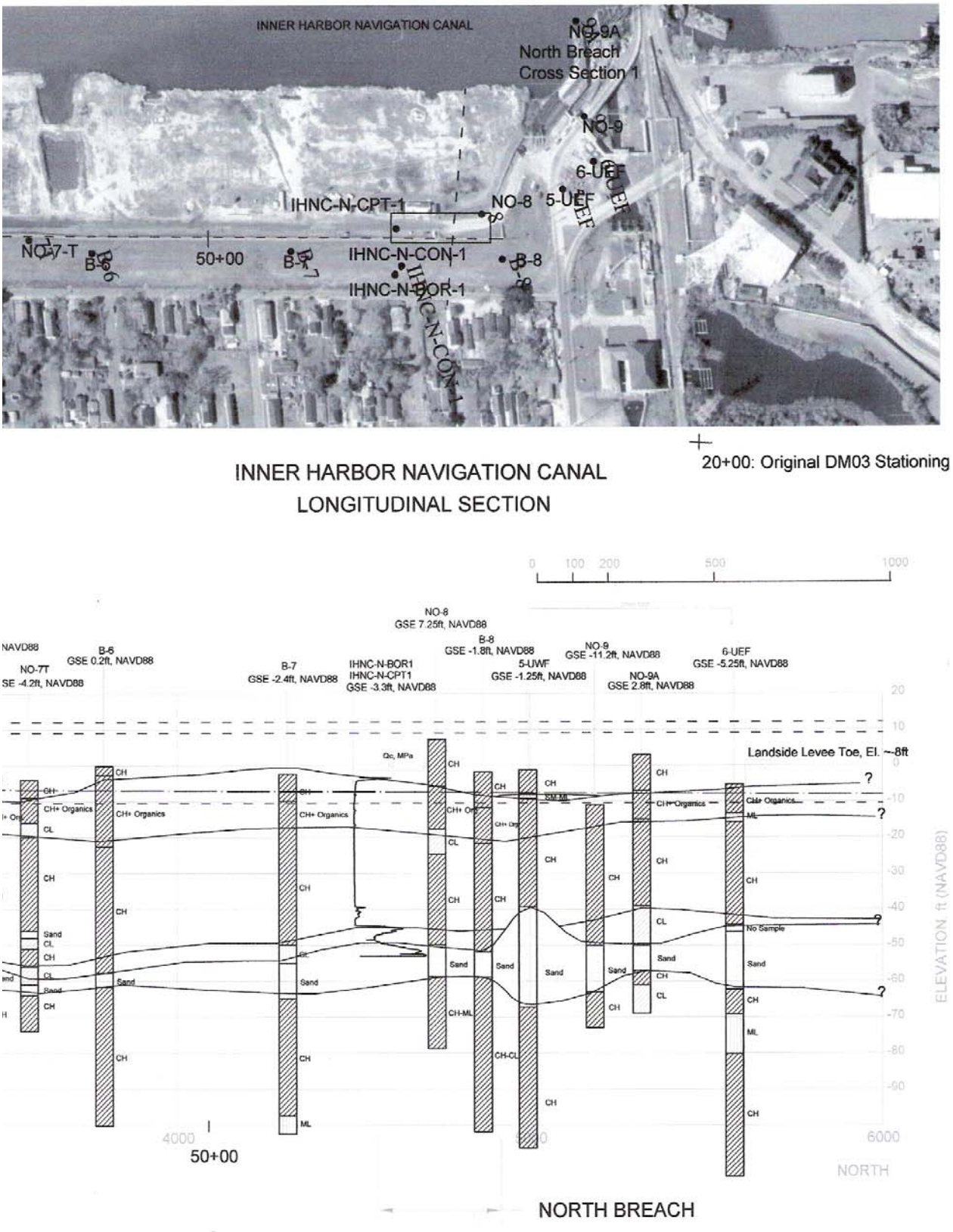


Figure 4-3. Longitudinal Profile along IHNC, North Breach.

4.1 North Breach Section and Failed Configuration

From Figure 4-1 (profile/plan figure), the North Breach is located approximately between stations 55+00 and 58+00 of the original DM03 levee stationing. Figure 4-4 shows the interpreted cross section along the North Breach. Note in this section the elevation of the landside toe, which is located between elevations -7 and –8 feet; being approximately 10 feet lower than the waterside ground elevation.

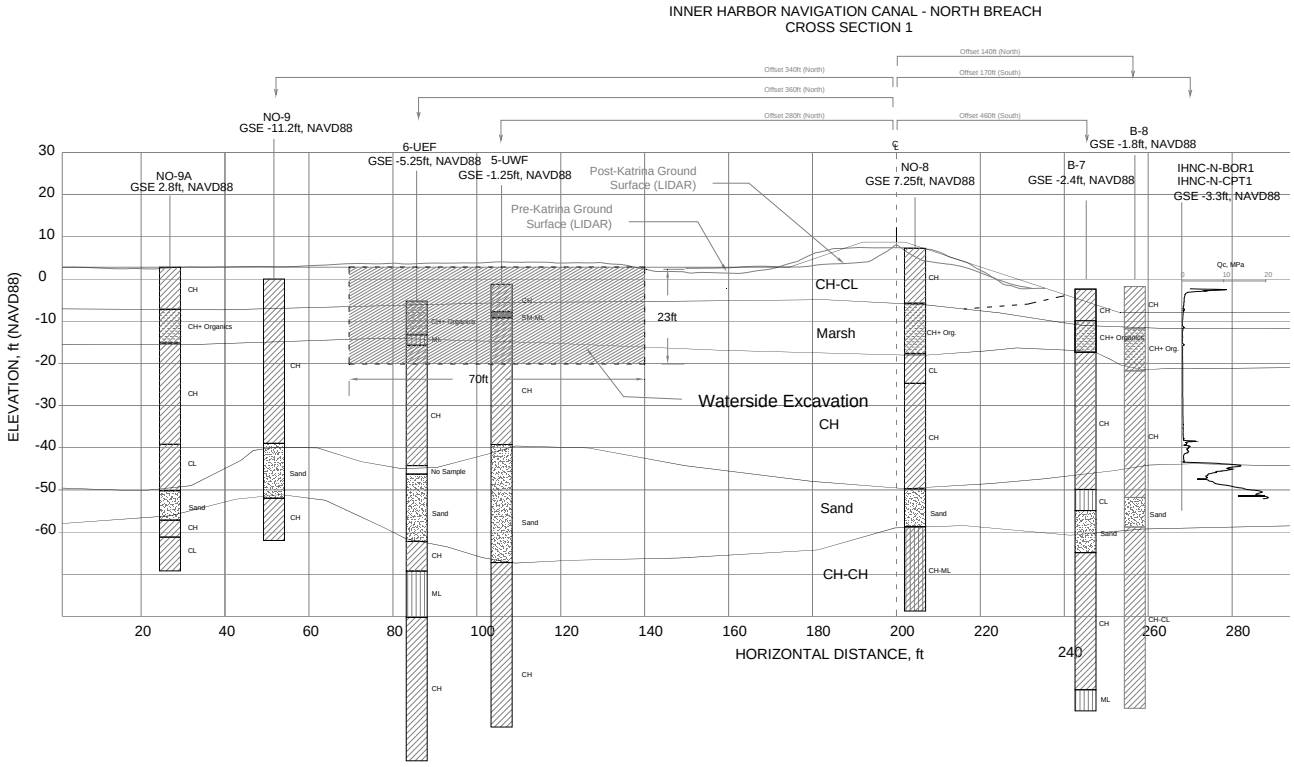


Figure 4-4. Cross section through North Breach.

The stratigraphic interpretation was based on borings NO-8 (1966), 6UEF and 5UWF (1971), B-7, B-8 IHNC-N-CPT-1 and IHNC-N-BOR-1 (2006). The levee embankment is composed mainly by compacted clays, underlain by a Marsh deposit, described as organic matter, organic clay, wood, roots and saturated-very low density material. A thin clay blanket seems to be located at the toe of the levee and towards the waterside surface. Given the poor descriptions presented in the borings from DM03 and the IPET (2006) report, samples that contained organic

materials with high water contents, low density and low strengths were classified as Marsh samples.

Underlying the marsh deposit, a thick "fat" clay deposit occurs from elevation –20 feet to approximately –50 feet, located atop a sand deposit. The sands are in turn underlain by another clay and silt deposit, probably associated with Pleistocene age deposits.

The excavated hole appears to be located less than 70 feet away from the centerline of the levee, as seen on Figure 2-4. Based on this map and WGI photographs taken during the EBIA engineering and site clearing operations, the hole was determined to be approximately 23 feet deep and about 70 feet wide. The walls of the excavation were assumed vertical since they do not have any influence on the analyses performed. Based on the available information on the WGI backfilling operations for these excavations, the material used as backfill was coarse-grained material (sand). Based on the USACE LiDAR survey performed during 2000, the top of the floodwall - sheet pile extends from elevation +12.0 feet down to elevation -10.5 feet.

The observed movement on the North Breach was a short-narrow movement that possibly started under the landside toe and progressed towards the flood side. The concrete I-wall failed and the sheet pile was elongated landward. The movement and resting place of the sheet pile leads to think that levee and foundation materials were washed away beneath the sheet pile and the water force pushed away the steel sheets and rotated them until a section of the pile rotated vertically 180 degrees. Figure 4-5a shows the failed levee - floodwall at the North Breach. Figure 4-5b shows an aerial view of the North Breach.



Figure 4-5a. North Breach. Note the sheet pile – concrete I-wall connection after rotating


Figure 4-5b. North Breach. Note excavation on IHNC side of floodwall. This excavation was associated with the EBIA site clearing operations.

4.2 South Breach Section & Failed Configuration

The South Breach extends from station 24+00 to 33+00 of the original DM03 (USACE, 1966). Figure 4-1 shows a thick Marsh layer, bottomed in an irregular fashion around elevation –25 feet. As the north section, a thin clay layer "covers" the surface and is apparently related to embankment fill. The top of the Marsh deposit is located at about elevation –5 feet, but a thin clay layer appears to cut the marsh layer in half.

The sheet pile extends from +12.0 feet to -10.5 feet, and again, it fails to cut through the Marsh deposit. The cross section in Figure 4-6 shows another waterside excavation; this time narrower than the one found in the North section, but assumed the same depth to the bottom and backfill material.

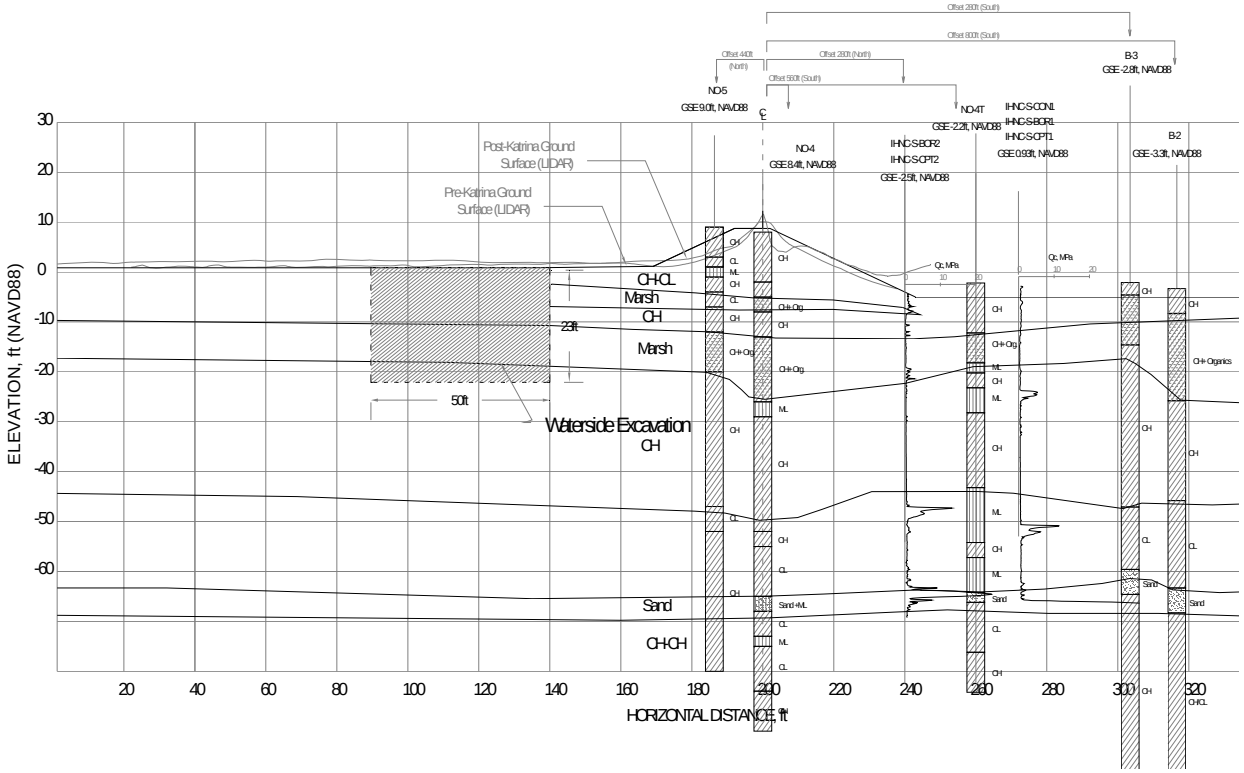


Figure 4-6. Cross section through South Breach.

The ILIT field investigations indicated that the South Breach was a translational-relatively deep stability failure. It is longer than the one located to the north, with approximately 900 feet of failed embankment - floodwall, whereas the North Breach was approximately 250 feet long. The evidence from available reports and photographs shows that the I-wall lost lateral support when a scour trench opened on the landside crown and subsequently a gap opened on the waterside, allowing water pressures to load the sheet pile and trigger a non-circular failure. Figure 4-7a shows the post-failure configuration of the South Breach. Figure 4-7b shows an aerial view of this breach.



Figure 4.7a. South Breach. Note the sheet pile displaced landward without flipping as at the North Breach.



Figure 4.7b. South Breach. Note large excavation on IHNC side of floodwall. This excavation was associated with the EBIA site clearing operations.

5. IHNC SOILS DATA REVIEW

The information available for the interpretation and analysis process of the breaches along IHNC was divided into two categories:

- Reports
    - DM03, Chalmette Area Plan (1966)
    - IPET (2006) report, Volumes II and V (and appendices)
    - Final Draft Analysis of Performance of the IHNC, IPET 2006
    - ILIT (2006) report, Chapter 6 (and appendices)
- Historic information
    - WGI EBIA site clearing work pictures.

The boring and CPT data was classified by year and performing agency, as shown in Table 5-1. This table summarizes the available exploration near the two breaches, and gives information on location, coordinates, approximate elevation and type of boring. Table 5-2 shows the same list of borings after the pre and post Katrina elevations from the LIDAR surveys were compared to the "design" top of boring elevation (what was shown on the boring log). The right column shows the final elevation chosen for each boring incorporated in the models.

This section briefs the reader on the available exploration information and the construction activities on the waterside of the IHNC levee and I-wall. A total of 31 borings and CPTs were used in the interpretation and analyses.

Document	Boring Year	Datum	Boring ID	Boring Type	Top Elevation	Bottom Elevation	Boring Length	TOP EL. in NAVD88	Latitude	Longitude	Notes
Lake Pontchartrain, LA. And Vicinity Chalmette Area Plan, DM03	1965	MSL	**NO-2-U**	n/a	9.2	-75	84.2	8.95			
Lake Pontchartrain, LA. And Vicinity Chalmette Area Plan, DM03	1965	MSL	**NO-2-UT**	n/a	1.5	-37	38.5	1.25			
Lake Pontchartrain, LA. And Vicinity Chalmette Area Plan, DM03	1965	MSL	NO-3	n/a	7.2	-82.5	89.7	6.95			
Lake Pontchartrain, LA. And Vicinity Chalmette Area Plan, DM03	1965	MSL	NO-3T	n/a	-3.5	-85	81.5	-3.75	29.968265	-90.024531	
Lake Pontchartrain, LA. And Vicinity Chalmette Area Plan, DM03	1965	MSL	NO-4	n/a	8.6	-55	63.6	8.35	29.970578	-90.023351	
Lake Pontchartrain, LA. And Vicinity Chalmette Area Plan, DM03	1965	MSL	NO-4T	n/a	-2	-83	81	-2.25	29.970554	-90.023198	
Lake Pontchartrain, LA. And Vicinity Chalmette Area Plan, DM03	1965	MSL	NO-5	n/a	9.2	-88	97.2	8.95	29.973277	-90.02246	
Lake Pontchartrain, LA. And Vicinity Chalmette Area Plan, DM03	1965	MSL	**NO-6U**	n/a	4	-76	80	3.75	29.97567	-90.021664	
Lake Pontchartrain, LA. And Vicinity Chalmette Area Plan, DM03	1965	MSL	**NO-6UT**	n/a	-3	-42	39	-3.25	29.97563	-90.02512	
Lake Pontchartrain, LA. And Vicinity Chalmette Area Plan, DM03	1965	MSL	NO-7T	n/a	-4	-78	74	-4.25	29.976152	-90.021239	
Lake Pontchartrain, LA. And Vicinity Chalmette Area Plan, DM03	1965	MSL	NO-8	n/a	7.5	-79	86.5	7.25	29.979321	-90.023398	
Lake Pontchartrain, LA. And Vicinity Chalmette Area Plan, DM03	1965	MSL	NO-9	n/a	-11	-71	60	-11.25	29.980242	-90.02827	
Lake Pontchartrain, LA. And Vicinity Chalmette Area Plan, DM03	1965	MSL	NO-9A	n/a	3	-70	73	2.75	29.980392	-90.02149	
Lake Pontchartrain LA and Vicinity, Lake Pontchartrain Area, 1971	1971	MSL	**5EF**	5" Undist.	-1	-80	79	-1.25	29.979932	-90.020376	
Lake Pontchartrain LA and Vicinity, Lake Pontchartrain Area, 1971	1971	MSL	**6UEF**	5" Undist.	-5	-108	103	-5.25	29.980211	-90.020504	
IPET webpage	2005	NAVD88	**B-2**	3" Undist.	0	-98	98	0	29 58 11.4	90 01 23.22	Datum Uncertain
IPET webpage	2005	NAVD88	**B-3**	3" Undist.	0	-98	98	0	29 58 16.2	90 01 21.54	Datum Uncertain
IPET webpage	2005	NAVD88	**B-4**	3" Undist.	0	-98	98	0	29 58 30.18	90 01 38.58	Datum Uncertain
IPET webpage	2005	NAVD88	**B-5**	3" Undist.	0	-98	98	0	29 58 30.54	90 01 17.46	Datum Uncertain
IPET webpage	2005	NAVD88	**B-6**	3" Undist.	0	-98	98	0	29 58 35.58	90 01 15.66	Datum Uncertain
IPET webpage	2005	NAVD88	**B-7**	3" Undist.	0	-98	98	0	29 58 40.56	90 01 14.1	Datum Uncertain
IPET webpage	2005	NAVD88	**B-8**	3" Undist.	0	-98	98	0	29 58 45.72	90 01 12.18	Datum Uncertain
IPET webpage	2005	NAVD88	IHBR-10CON	CPT	0	-80	80	0	29 58 30.7	90 01 17.9	Datum Uncertain
IPET webpage	2005	NAVD88	IHBR-11CON	CPT	0	-80	80	0	29 58 36.3	90 01 16.1	Datum Uncertain
IPET webpage	2005	NAVD88	IHBR-12CON	CPT	0	-80	80	0	29 58 24.1	90 01 20.1	Datum Uncertain
IPET webpage	2005	NAVD88	IHBR-14CON	CPT	0	-80	80	0	29 58 22.9	90 01 19.9	Datum Uncertain
IPET webpage	2005	NAVD88	IHBR-15CON	CPT	0	-80	80	0	29 58 16.8	90 01 21.1	Datum Uncertain
IPET webpage	2005	NAVD88	IHBR-16CON	CPT	0	-80	80	0	29 58 14.4	90 01 22.7	Datum Uncertain
IPET webpage	2005	NAVD88	IHBR-1CON	CPT	0	-80	80	0	29 58 45.8	90 01 13.7	Datum Uncertain
IPET webpage	2005	NAVD88	IHBR-2CON	CPT	0	-80	80	0	29 58 43.5	90 01 12.8	Datum Uncertain
IPET webpage	2005	NAVD88	IHBR-3CON	CPT	0	-80	80	0	29 58 14.0	90 01 14.1	Datum Uncertain
IPET webpage	2005	NAVD88	IHBR-5CON	CPT	0	-80	80	0	29 58 14.0	90 01 23.6	Datum Uncertain
IPET webpage	2005	NAVD88	IHBR-6CON	CPT	0	-80	80	0	29 58 15.2	90 01 23.8	Datum Uncertain
IPET webpage	2005	NAVD88	IHBR-7CON	CPT	0	-80	80	0	29 58 16.7	90 01 23.4	Datum Uncertain
IPET webpage	2005	NAVD88	IHBR-8CON	CPT	0	-80	80	0	29 58 18.7	90 01 22.6	Datum Uncertain
IPET webpage	2005	NAVD88	IHBR-9CON	CPT	0	-80	80	0	29 58 20.4	90 01 22.1	Datum Uncertain
ILIT Final Report, Appendix B and C	2006	NAVD88	**IHNC-S-BOR1**	3" Undist.	0.93		0.93	0.93	29.9786	90.0202	
ILIT Final Report, Appendix B and C	2006	NAVD88	IHNC-S-CON-1	Continuous	-3.4		-3.4	-3.4	29.97038	90.02313	
ILIT Final Report, Appendix B and C	2006	NAVD88	IHNC-S-CON-2	Continuous	-2.7		-2.7	-2.7	29.97118	90.0227	
ILIT Final Report, Appendix B and C	2006	NAVD88	IHCN-S-CON-3	Continuous	-2.3		-2.3	-2.3	29.97246	90.0225	
ILIT Final Report, Appendix B and C	2006	NAVD88	**IHNC-N-BOR-1**	3" Undist.	-3.4		-3.4	-3.4	29.97039	90.02315	
ILIT Final Report, Appendix B and C	2006	NAVD88	IHNC-S-CPT-1	CPT	-0.9	-62	61.1	-0.9	29.97035	90.02314	
ILIT Final Report, Appendix B and C	2006	NAVD88	IHNC-S-CPT-2	CPT	-2.7	-67	64.3	-2.7	29.97126	90.02292	
ILIT Final Report, Appendix B and C	2006	NAVD88	IHNC-S-CPT-3	CPT	-2.3	-71	68.7	-2.3	29.97248	90.02257	
ILIT Final Report, Appendix B and C	2006	NAVD88	IHNC-N-CPT-1	CPT	-3.38	-54	50.62	-3.38	29.9787	90.02049	

Table 5-1. Available Borings and CPTs in the vicinity of the breaches along IHNC.

Document	Boring Year	Datum	Boring ID	Top Elevation	Bottom Elevation	TOP EL. in NAVD88	PRE-BREACH LIDAR ELEV.	POST-BREACH LIDAR ELEV.	FINAL BORING ELEVATION, NAVD88
Lake Pontchartrain, LA. And Vicinity Chalmette Area Plan, DM0	1965	MSL	NO-2-U	9.2	-74	8.95	-	-	8.95
Lake Pontchartrain, LA. And Vicinity Chalmette Area Plan, DM0	1965	MSL	NO-2-UT	1.5	-37	1.25	-	-	1.25
Lake Pontchartrain, LA. And Vicinity Chalmette Area Plan, DM0	1965	MSL	NO-3T	-3.5	-85	-3.75	-	-1.4	-3.75
Lake Pontchartrain, LA. And Vicinity Chalmette Area Plan, DM0	1965	MSL	NO-4	8.6	-55	8.35	1.8	1.1	8.35
Lake Pontchartrain, LA. And Vicinity Chalmette Area Plan, DM0	1965	MSL	NO-4T	-2	-83	-2.25	1.2	2.4	-2.25
Lake Pontchartrain, LA. And Vicinity Chalmette Area Plan, DM0	1965	MSL	NO-5	9.2	-88	8.95	1.6	2.9	8.95
Lake Pontchartrain, LA. And Vicinity Chalmette Area Plan, DM0	1965	MSL	NO-6U	4	-76	3.75	2	1.2	3.75
Lake Pontchartrain, LA. And Vicinity Chalmette Area Plan, DM0	1965	MSL	NO-6UT	-3	-42	-3.25	2.9	3.3	-3.25
Lake Pontchartrain, LA. And Vicinity Chalmette Area Plan, DM0	1965	MSL	NO-7T	-4	-78	-4.25	5.5	5.3	-4.25
Lake Pontchartrain, LA. And Vicinity Chalmette Area Plan, DM0	1965	MSL	NO-8	7.5	-79	7.25	5.9	0.8	7.25
Lake Pontchartrain, LA. And Vicinity Chalmette Area Plan, DM0	1965	MSL	NO-9	-11	-71	-11.25	1	1.4	-11.25
Lake Pontchartrain, LA. And Vicinity Chalmette Area Plan, DM0	1965	MSL	NO-9A	3	-70	2.75	-0.9	1.2	2.75
Lake Pontchartrain LA and Vicinity, Lake Pontchartrain Area, 19	1971	MSL	5EF	-1	-80	-1.25	-2.1	-1.2	-1.25
Lake Pontchartrain LA and Vicinity, Lake Pontchartrain Area, 19	1971	MSL	6UEF	-5	-108	-5.25	-3.5	-2.4	-5.25
IPET webpage	2005		B-2	0	-98	0	-5	-3.3	-3.3
IPET webpage	2005		B-3	0	-98	0	-5.5	-2.8	-2.8
IPET webpage	2005		B-4	0	-98	0	-4.3	-2.8	-2.8
IPET webpage	2005		B-5	0	-98	0	1.3	1.9	1.9
IPET webpage	2005		B-6	0	-98	0	-1.9	0.2	0.2
IPET webpage	2005		B-7	0	-98	0	-1.4	-2.4	-2.4
IPET webpage	2005		B-8	0	-98	0	-3.2	-1.8	-1.8
IPET webpage	2005		IHBR-10CON	0	-80	0			
IPET webpage	2005		IHBR-11CON	0	-80	0			
IPET webpage	2005		IHBR-12CON	0	-80	0			
IPET webpage	2005		IHBR-14CON	0	-80	0			
IPET webpage	2005		IHBR-15CON	0	-80	0			
IPET webpage	2005		IHBR-16CON	0	-80	0			
IPET webpage	2005		IHBR-1CON	0	-80	0			
IPET webpage	2005		IHBR-2CON	0	-80	0			
IPET webpage	2005		IHBR-3CON	0	-80	0			
IPET webpage	2005		IHBR-5CON	0	-80	0			
IPET webpage	2005		IHBR-6CON	0	-80	0			
IPET webpage	2005		IHBR-7CON	0	-80	0			
IPET webpage	2005		IHBR-8CON	0	-80	0			
IPET webpage	2005		IHBR-9CON	0	-80	0			
ILIT Final Report, Appendix B and C	2006	NAVD88	IHNC-S-BOR1	0.93	0	0.93	5.3	5.7	0.93
ILIT Final Report, Appendix B and C	2006	NAVD88	IHNC-S-CON-1	-3.4	0	-3.4	3.7	4.7	-3.4
ILIT Final Report, Appendix B and C	2006	NAVD88	IHNC-S-CON-2	-2.7	0	-2.7	-4.4	-2.7	-2.7
ILIT Final Report, Appendix B and C	2006	NAVD88	IHCN-S-CON-3	-2.3	0	-2.3	4	1.4	-2.3
ILIT Final Report, Appendix B and C	2006	NAVD88	IHNC-N-CON-1	-3.4	0	-3.4	-5.7	-3.2	-3.4
ILIT Final Report, Appendix B and C	2006	NAVD88	IHNC-N-BOR-1	-3.4	0	-3.4	-6.8	-3.2	-3.4
ILIT Final Report, Appendix B and C	2006	NAVD88	IHNC-S-CPT-1	-0.9	-62	-0.9	3.6	4.8	-0.9
ILIT Final Report, Appendix B and C	2006	NAVD88	IHNC-S-CPT-2	-2.7	-67	-2.7	3	2.9	-2.7
ILIT Final Report, Appendix B and C	2006	NAVD88	IHNC-S-CPT-3	-2.3	-71	-2.3	2	6.7	-2.3
ILIT Final Report, Appendix B and C	2006	NAVD88	IHNC-N-CPT-1	-3.38	-54	-3.38	3	8.5	-3.38

Table 5-2. Interpreted elevations for borings and CPTs.

6. MATERIAL PROPERTIES

Material properties were determined from available laboratory and field testing. Section 13.1 contains all laboratory testing extracted from the borings. Since the 2006 investigations (IPET, ILIT) were performed after Katrina, no new samples could be obtained from soils below the embankment. Available crest borings are exclusively the 1966 DM03 soil borings.

6.1 South Breach Section

Figure 6-1 shows the available undrained shear strength (Su) for the soils beneath the embankment load. Figure 6-2 shows the same properties for the conditions away from the levee toe. The difference in values is evident, as the shear strengths are significantly lower for the values away from the toe.

To confirm the test values performed on the toe of the levee, the ILIT (2006) CPTs were correlated to undrained shear strengths using common relationships between tip resistance (q) and Su. Figures 6-3 and 6-4 show the correlated CPT tip resistance values to Su and overconsolidation ratio (OCR). The correlated values from CPTs IHNC-S-CPT-1 and IHNC-S-CPT-2 show evidence of slight overconsolidation, probably due to desiccation crusts in the early stages of deposition. Undrained shear strength to effective vertical pressure ratio (Su/p') values were calculated on the same CPT probes. It was found that for the soft Gray Clays – underneath the overconsolidated crust - a value of Su/p' of 0.3 to 0.31 is representative of the nearly normally consolidated behavior of the fine grained deposit.

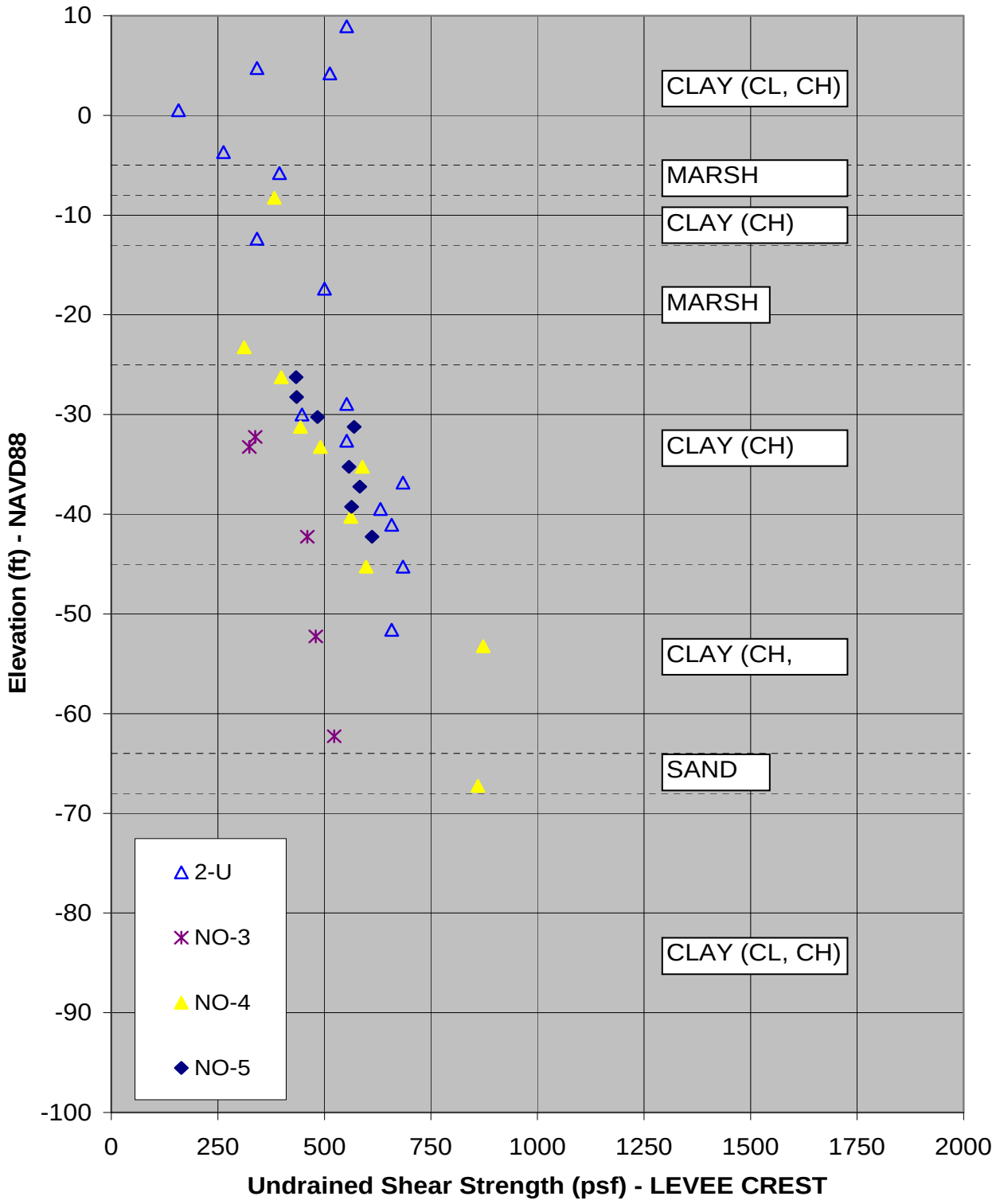


Figure 6-1. Soil shear strength values for South Breach, under the levee crest.

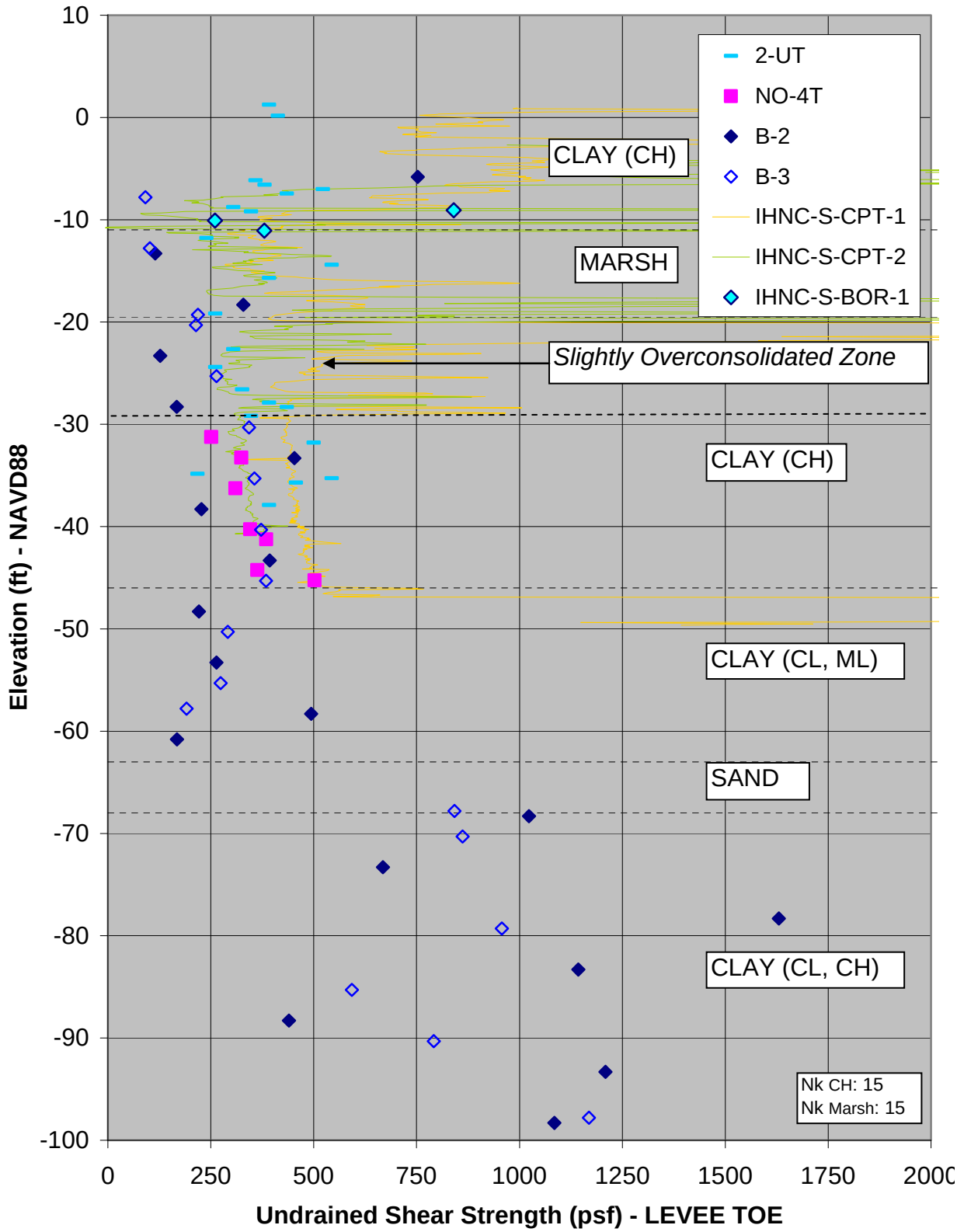


Figure 6-2. Su values for South Breach, away from the levee toe.

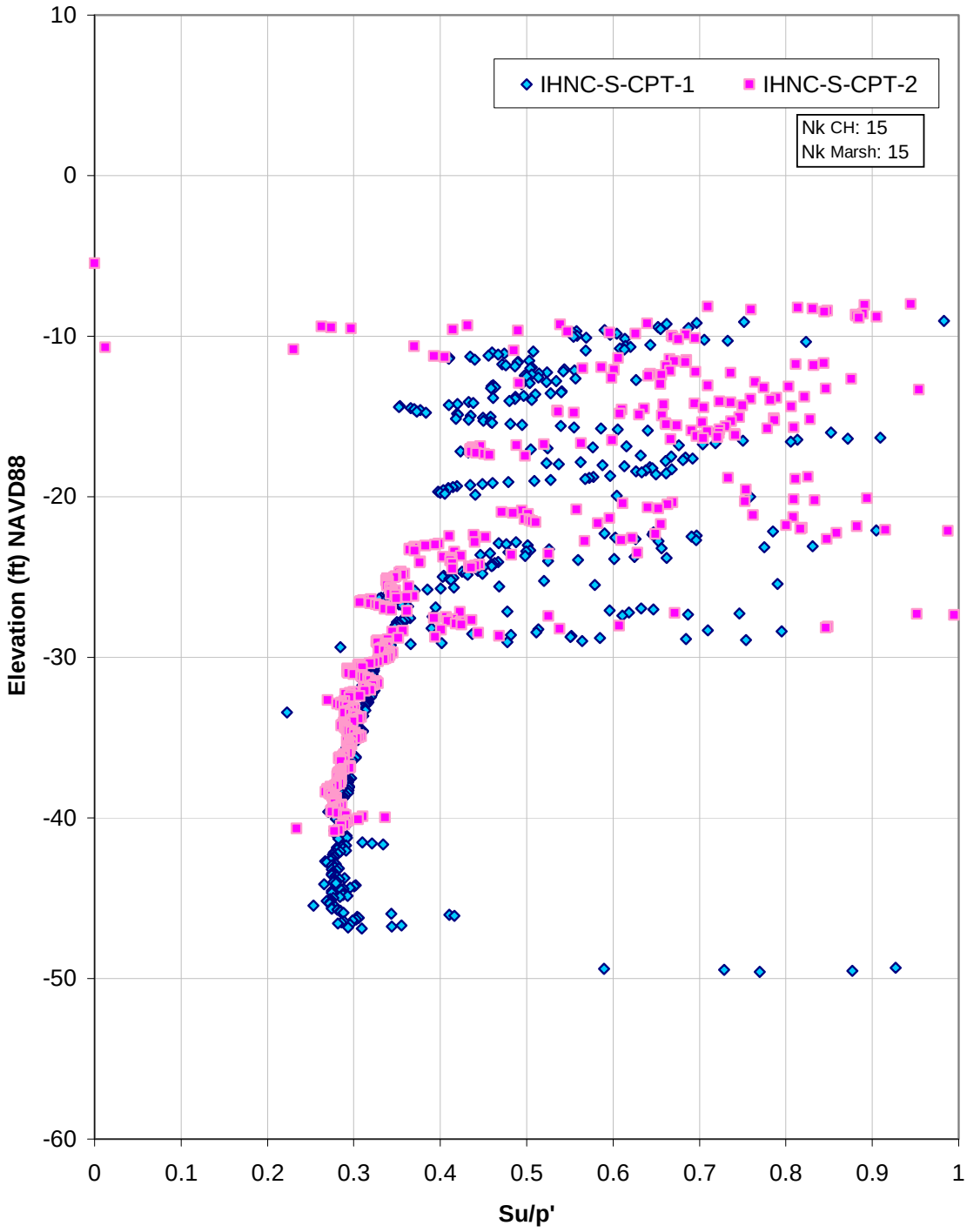


Figure 6-3. Su/p' values for South Breach, away from the levee toe.



Figure 6-4. OCR values for South Breach, away from the levee toe.

Based on the data processing by ILIT (2006), tip factors (Nk) between 12 and 20 were assigned to the Marsh and underlying CH deposit. The correlated values were then plotted against the available laboratory testing, and the "best estimate" for the Nk parameter was determined. The correlated OCRs show the same area corresponding to an Su/p' value of 0.3 to be nearly normally consolidated. However, overconsolidated crusts are present in the upper 5 to 7 feet of the deposit. The Su/p value of 0.3 was reduced in the stability analyses to account for mode and rate of shearing. Based on the available information regarding these effects, a reduction of 15 % was applied (ILIT 2006)

Tables 6-1 and 6-2 show the summary of depths obtained from the cross sections for the South Breach section, under the levee fill and away from the toe. Based on these depth intervals, the available laboratory testing was grouped (undrained shear strengths, index tests) and statistical properties were developed for each soil unit (i.e. median, coefficient of variation) to describe the uncertainties associated with the soil parameters.

Material	Elevation Interval, ft (NAVD88)	
	From	To
Clays (CL, CH)	+9	-5
Upper Marsh (Peat)	-5	-8
Gray Clay (CH)	-8	-13
Lower Marsh (Peat)	-13	-25
Clays (CH)	-25	-45
Lean Clays (CL)	-45	-64
Sand	-64	-68
Deep Clays (CH)	-68	n/a

Table 6-1. Profile for South Breach. Under Centerline of Levee

Material	Elevation Interval, ft (NAVD88)	
	From	To
Clays (CL, CH)	-4	-11
Lower Marsh (Peat)	-11	-19.5
Gray Clay (CH)	-19.5	-43
Lean Clay and Silt	-43	-63
Sand	-63	-68
Deep Clays (CH)	-68	n/a

Table 6-2. Profile for South Breach. Under Toe of Levee

6.2 North Breach Section

For the North Breach section, the same procedure described in Section 6.1 for the CPT characterization, laboratory testing grouping and statistical parameter calculations were followed. The results are shown in Figures 6-5 through 6-8 and Tables 6-3 and 6-4.

Tables 6-3 and 6-4 show the summary of depths obtained from the cross sections for the North Breach, under the levee fill and away from the toe. Based on these depth intervals, the available laboratory testing was grouped (undrained shear strengths, index tests) and statistical properties were developed for each soil unit (i.e. median, coefficient of variation) to describe the uncertainties associated with the soil parameters.

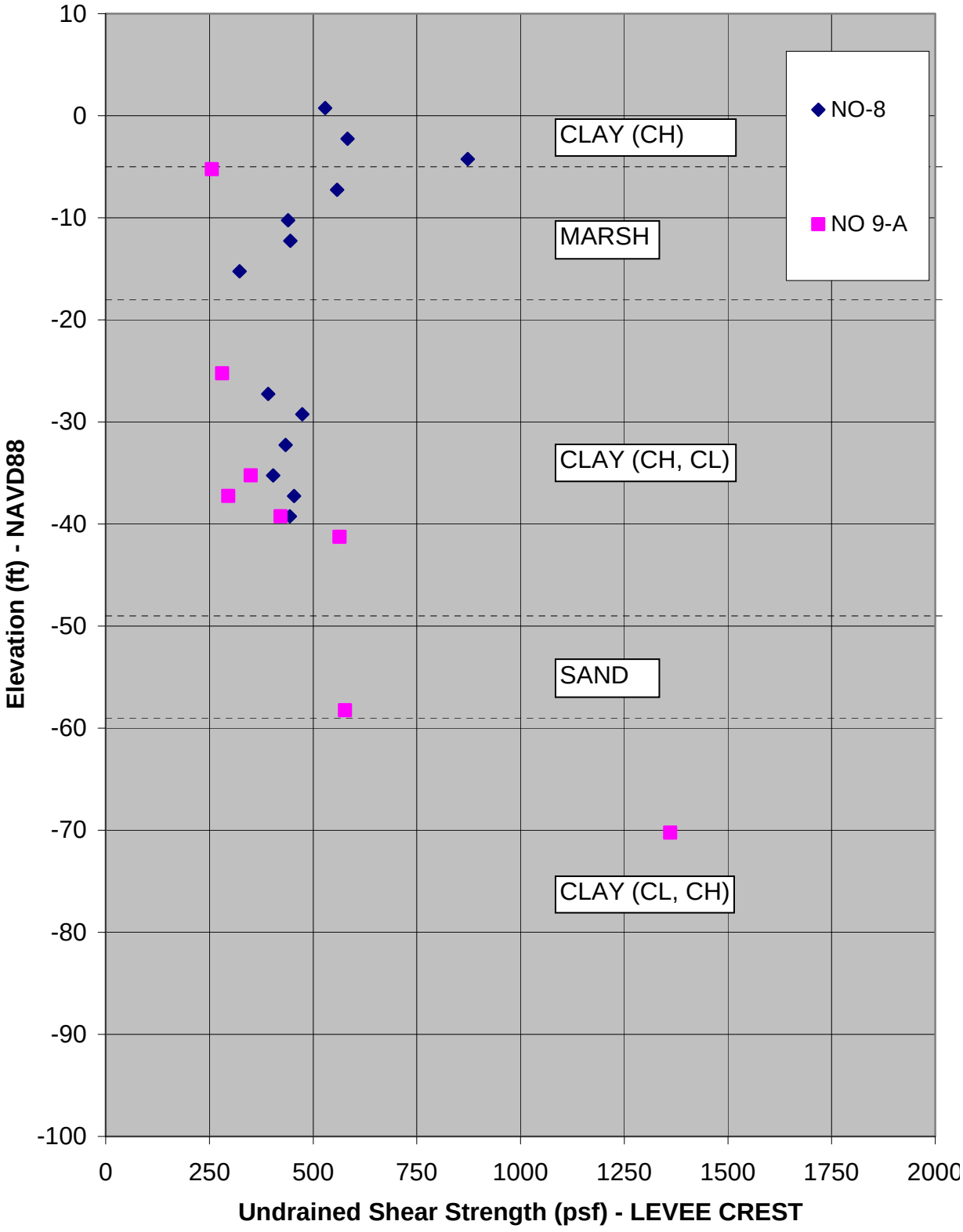


Figure 6-5. Soil shear strength data for North Breach; under the levee fill.

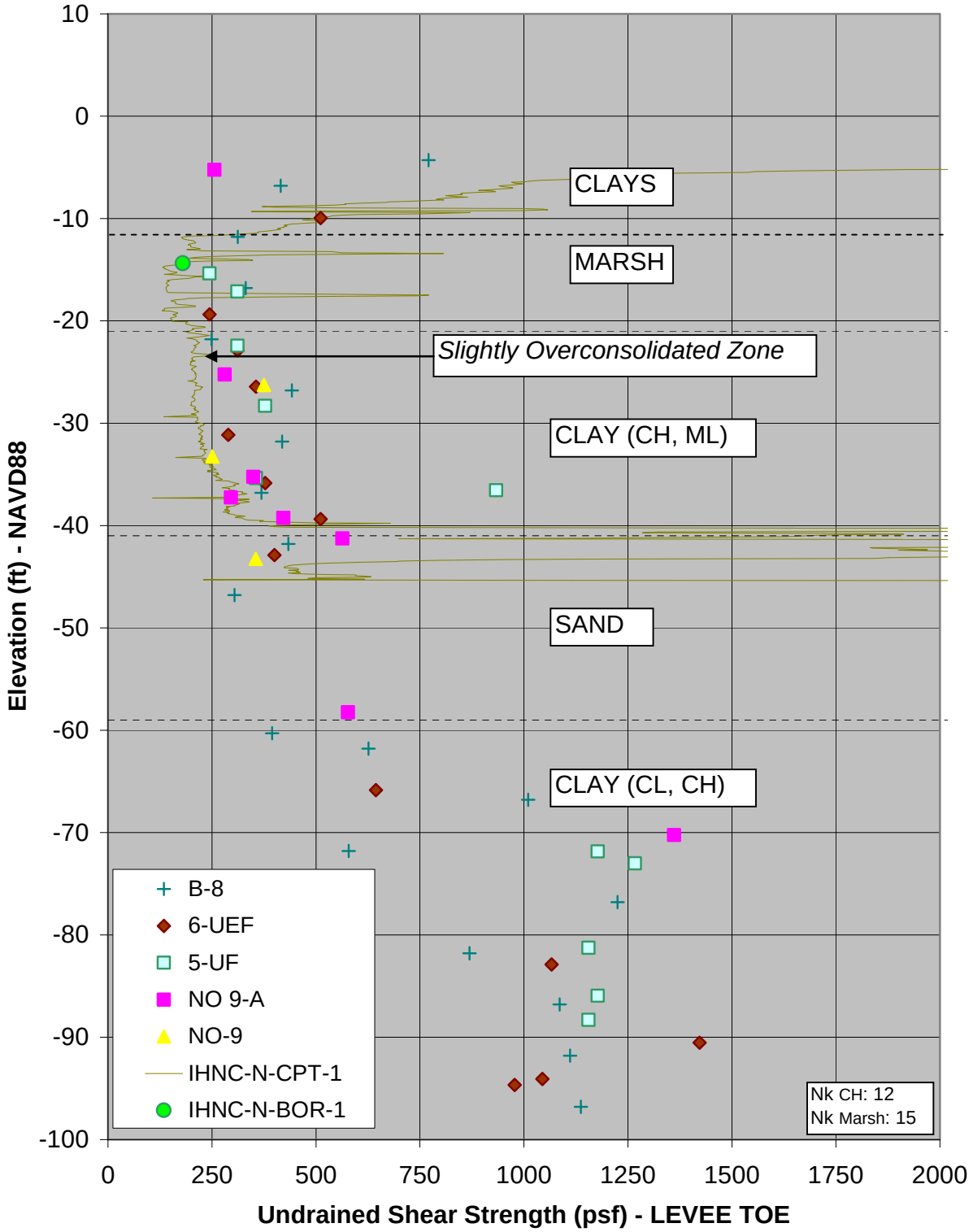


Figure 6-6. Su data for North Breach; away from the levee toe.

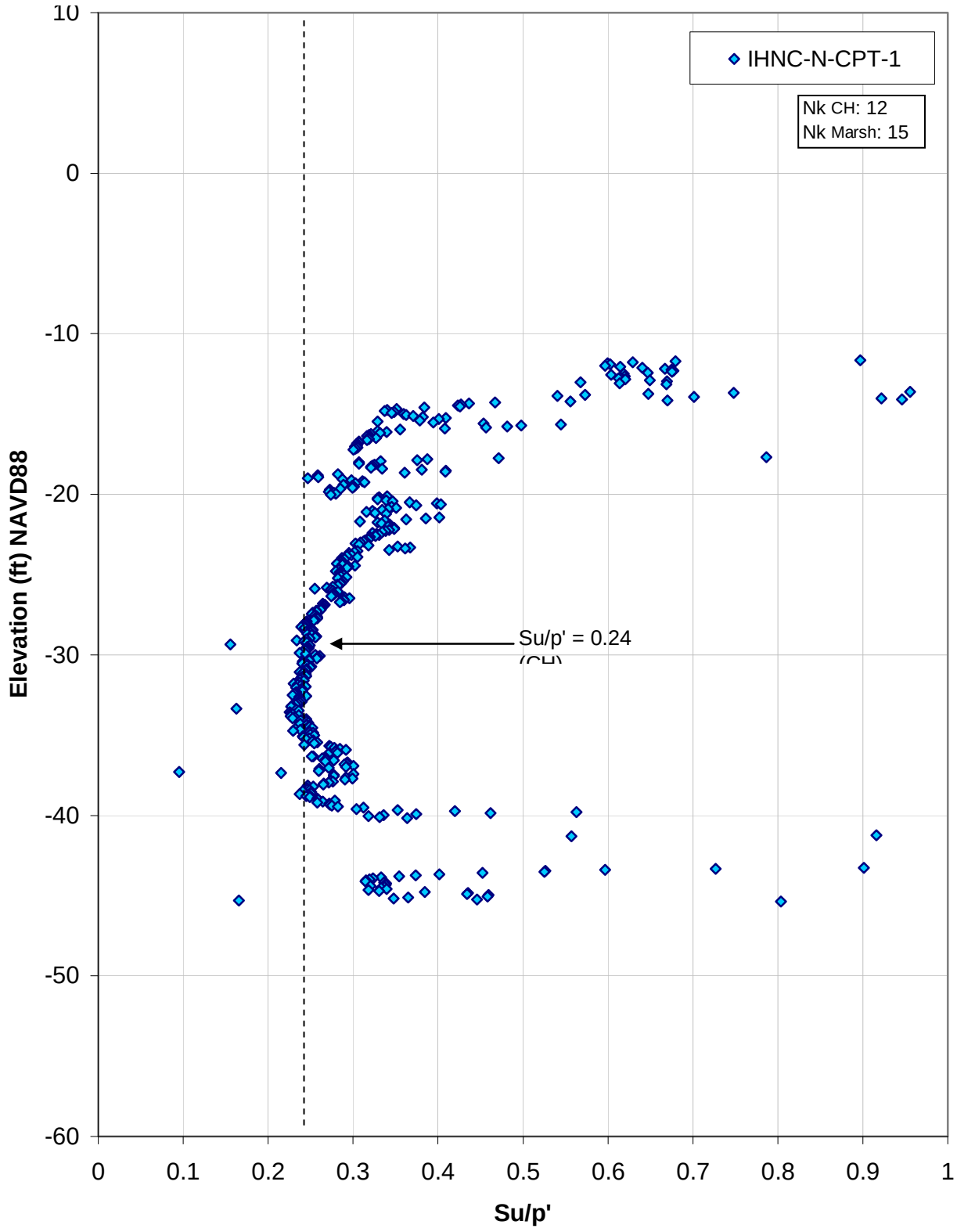


Figure 6-7. Su/p' values for North Breach, away from the levee toe.

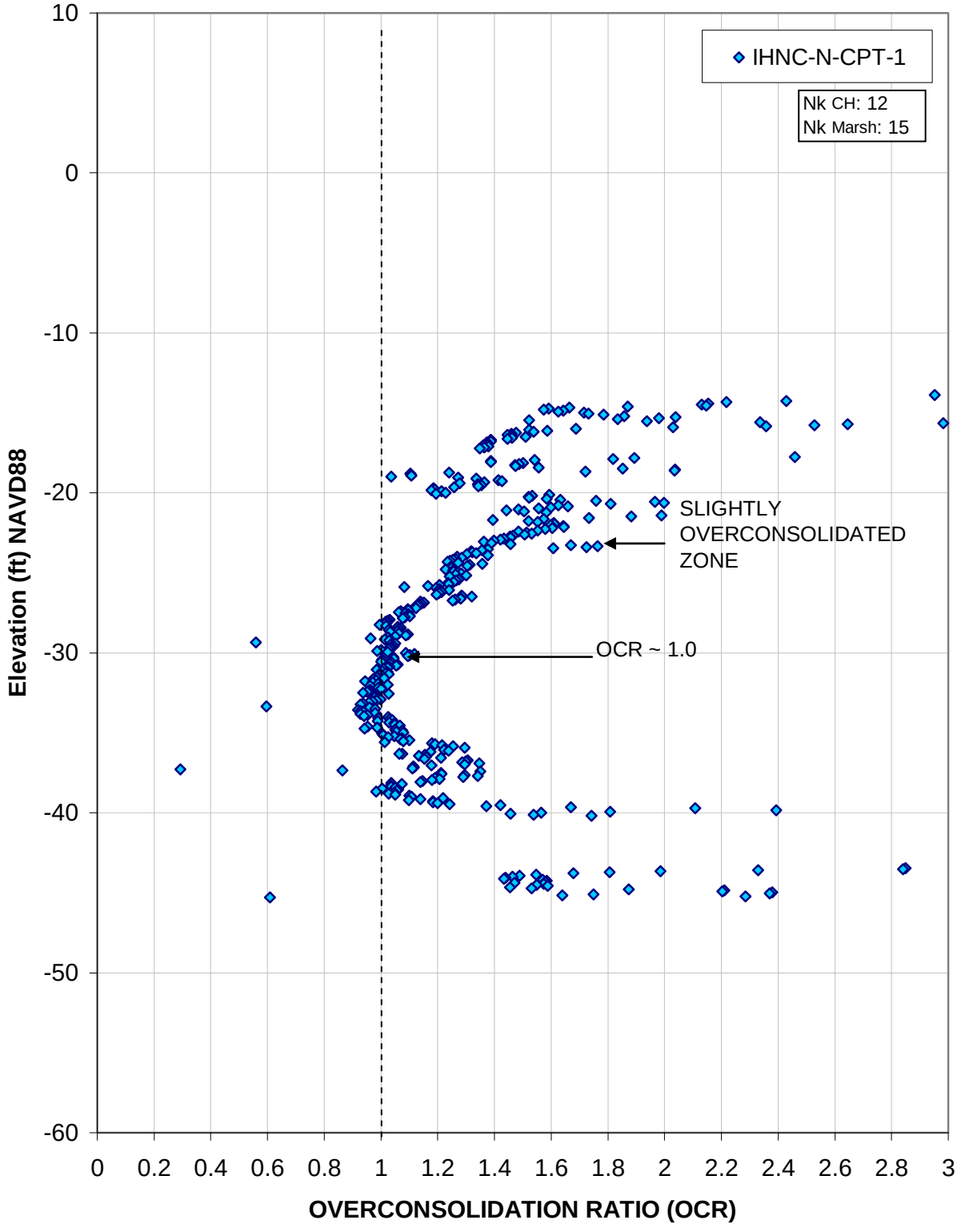


Figure 6-8. OCR values for North Breach, away from the levee toe.

Material	Elevation Interval, ft (NAVD88)	
	From	To
Clays (CL, CH)	+9	-11
Marsh (Peat)	-11	-18
Gray Clay (CH)	-18	-49
Sands	-49	-59
Deep Clays (CH)	-59	n/a

Table 6-3. Profile for North Breach. Under Centerline of levee.

Material	Elevation Interval, ft (NAVD88)	
	From	To
Marsh (Peat)	-8	-21
Gray Clay (CH)	-21	-49
Sands	-49	-59
Deep Clays (CH)	-59	n/a

Table 6-4. Profile for North Breach. Away from levee toe.

7. MARSH PERMEABILITY

Marsh (swamp, wetland, peat, humus) deposits are highly compressible materials that exhibit rapid decrease of hydraulic conductivity (permeability, K) as stresses increase and void spaces decrease (Mesri, 2007). The factors influencing the behavior of such soils depend not only on stresses, but on depositional mechanics, aging and decomposition, amount, type and orientation of fibers and saturation.

Hogan et al, (2006) shows field tests performed on a peat-bog fen deposit. Using pumping and slug tests the investigators were able to determine widely scattered permeability values, ranging from 10^{-3} to 10^{-4} centimeters per second (cm/s), but with values as high as 10^{-2} cm/s. The results of the test program showed that permeability decreases with depth.

An important result from Hogan (2006) is that by using a load test, the time of dissipation of excess piezometric head occurred in just 2.5 hours, indicating high permeability values.

According to Egglesmann (1975), Phragmites peats have the highest permeability values, and these will decrease with time of drainage to a nearly constant value. His statistical investigation of more than 2000 permeability measurements on different peats, concluding that when large water discharges flow through peat, the macropores spaces are transformed into smaller spaces, leading to decreases in hydraulic conductivity and soil deformation (consolidation).

Beckwith et al (2003) have developed a new mechanism for extraction of "undisturbed" peat samples for permeability testing. Strong emphasis is made on the need to incorporate several samples at different depths inside a single deposit to capture the anisotropy (ratio of vertical to horizontal permeability, Kv/Kh) and variation of permeability with depth (and consequently

stresses). A summary of the results developed by Beckwith et al (2003) is given in Figure 7-1. The plots show the permeability (K, cm/s, $\log_{10}$ K = -1 and K = 0.1 cm/s), the ratio of the horizontal to vertical permeability (Kh/Kv, $\log_{10}$ Kh/Kv = 1 and Kh/Kv = 10). The results show very high horizontal permeabilities (Kh) close to the ground surface (dark circles, Kh = 0.1 cm/s) and these values decrease steadly with depth to values of about Kh = 10^{-4} cm/s. The anisotropy reflected in the ratio of Kv/Kh ranges from 1 to more than 1000. It is obvious that results from standard consolidation testing of conventional samples in which the primary drainage paths are vertical can not be relied upon to give valid indications of horizontal permeability in most Marsh deposits.

Laboratory methods tend to overestimate values of hydraulic conductivity (Ronkanen et al, 2005), compared with in-situ measurements. The large variation on the permeability values imposes the need for in-situ testing coupled with laboratory testing in order to assess a more realistic value of permeability for the Marsh near the breach site, and analyze the controlling aspects of the hydraulic behavior of this member.

Mesri et al (2007) indicate that initial permeability for Marsh deposits can be equal to 1000 times the initial permeability value for soft clay or silt deposits when subject to a fill load of about 10 feet.

Permeability tests such as piezometer slug test and cube methods have suggested by some of the above mentioned authors; however, there is no absolute value of the K values used in this report in order to generate a “best estimate” value for this permeability.

Future work on the breach site (and non-failure sites) should be carried out to assess the permeability of this complex deposit. Surridge et al (2005) and Clymo (2004) evaluated and compared results from laboratory and field tests, acknowledging the pronounced uncertainties and the fact that different organic deposits (swamp, marsh, peat, humus) have very different hydraulic properties, and at the moment, a generalization is not possible.

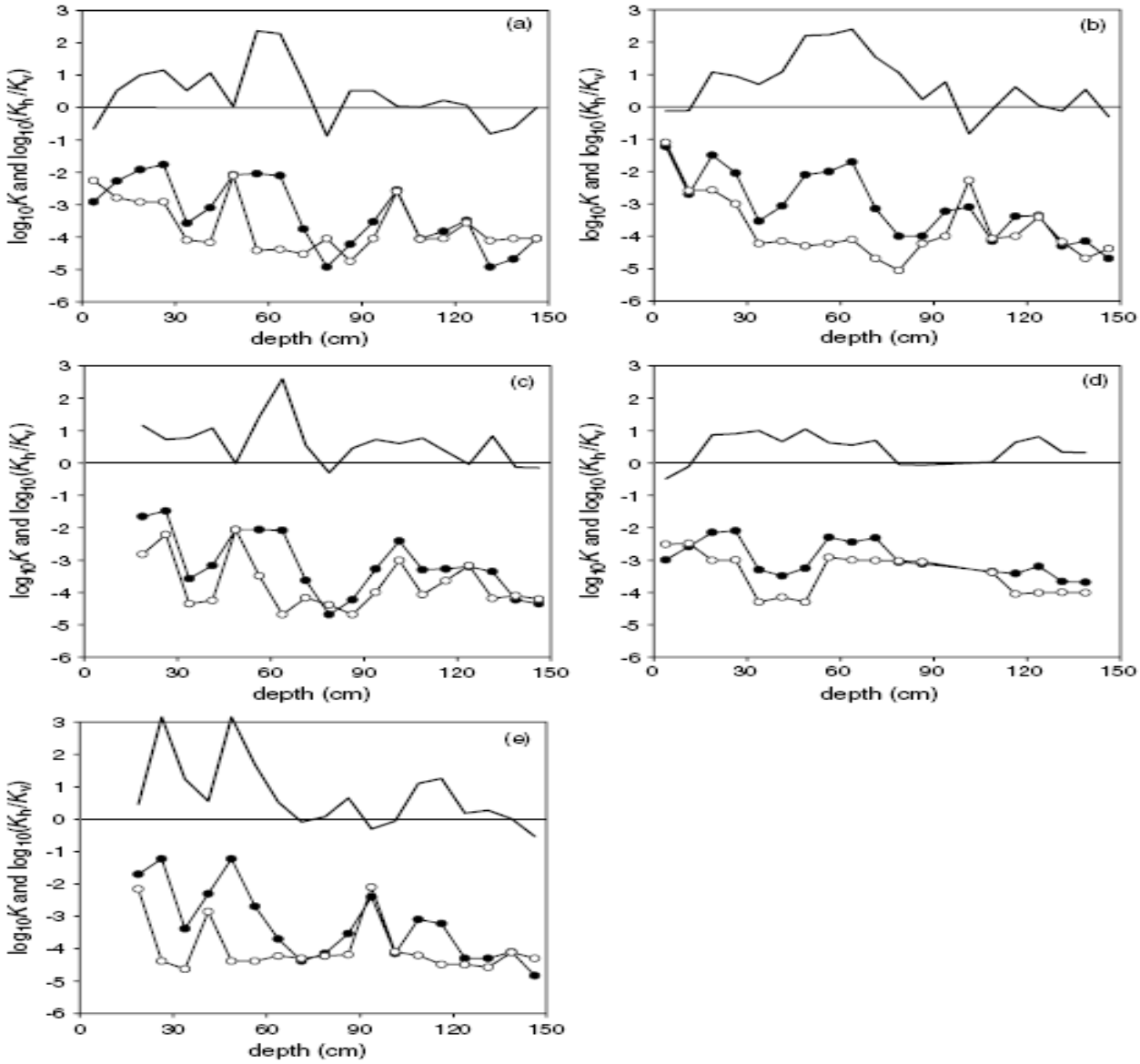


Figure 7-1. Summary of permeability tests performed on Marsh deposits (Beckwith et al 2002).

Table 7-1 summarizes the permeability values computed and/or tested by field and laboratory methods found in the researched publications.

Author	K-range (cm/s)		Observations
	Minimum	Maximum	
Hogan et al (2006)	10^{-4}	10^{-2}	K Varies with depth and peat type
Egglesmann (1975)	10^{-4}	$8x10^{-3}$	Highly dependant on drainage time
Beckwith et al (2003)	$2x10^{-3}$	$2x10^{-2}$	Calculated high anisotropy ratios and variations with depth
Clymo (2004)	10^{-6}	$2x10^{-5}$	Used falling head piezometers
Ronkanen et al (2005)	10^{-5}	0.30	Vertical conductivity was usually higher than horizontal

Table 7-1. Summary of permeability values.

When selecting high permeability values for the Marsh deposit (e.g. 10^{-3} cm/s), this unit acts as a draining layer, conducting pore water pressures much faster beneath the levee. The effect of these values does not significantly increase the calculated hydraulic gradients on the levee toe, but it allows the potential for underseepage and water exiting at the levee toe.

If the Marsh is considered to have low permeabilities (10^{-5} cm/s and lower), the system now behaves as a blanket as described by the USACE EM 1110-2-1913 (2000). The principle of the blanket theory is that pore water pressures underneath an embankment carried by an underlying aquifer will impose pressures in excess of hydrostatic conditions that can cause uplift and potential for blowout failures and sand boils.

Modeling the Marsh deposit as a "draining" layer or as a "blanket" has different impacts on the performance of the system. Both can be negative. First, if the Marsh is considered a permeable

layer, pore water pressures will develop faster beneath the levee toe and can accelerate the material softening and/or produce internal erosion.

Second, when modeled as a low permeability material, the deposit generates excess pore water pressures by being recharged from below by the aquifer, and might experience uplift pressures that can lead to failure. For the two breach sites at IHNC, this turned out not be the critical condition, since the marsh is underlain by a thick clay deposit which would also become part of the blanket if the Marsh were to be modeled as a fine grained material, thus the calculated hydraulic gradients would be small.

The models incorporated all these conditions by performing transient seepage analyses for a range of permeabilities. The results show the that pore water pressures rise inside the Marsh deposit to values close to those of a steady-state condition (more than 80%).

Analyzing the seepage analyses performed by IPET, on Appendix 17 of their Final Report, the best estimate for the permeability of the Marsh deposit is 10^{-4} cm/s. According to the plot on Figure V-17-15 (Figure 7-2), this permeability occurs when the soils are subject to overburden effective stresses from 0 to 500psf. This is a likely range for the shallow layer located at the toe of the levee, but the deeper Marsh underneath the levee is probably subject to effective stresses in the order of 0 to 1000 pounds per square foot (psf), with permeability of 10^{-5} to 10^{-7} cm/s.

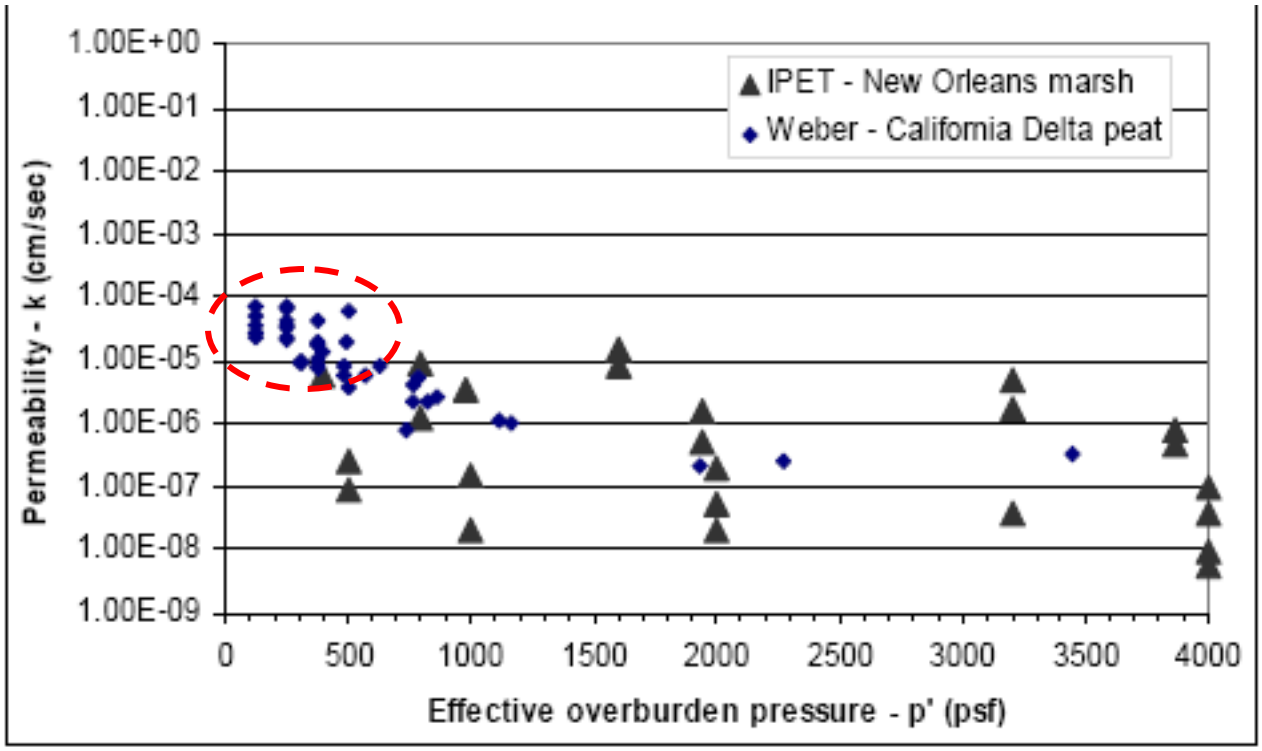


Figure 7-2. Hydraulic conductivity values for Peat. The range of effective stresses for the shallow (toe) peats ranges from 0 to 1000psf (red circle). Source: USACE IPET.

This graph shows a trend that stabilizes somewhere between 10^{-6} and 10^{-7} cm/s as effective stresses increase; but the values reported by Weber (1969) in the California Delta peat seem higher with low stress levels; this might be due to the fact that Weber performed field tests (piezometers) and this type of test captures the "macro" effects of large particles and irregularities of the layer, such as vegetal matter, wood and roots. The laboratory consolidation testing performed by IPET was on smaller scale samples which are not able to account for these heterogeneities; and -obviously-, the “macro” permeability of the deposit is what controls the hydraulic behavior of the member.

Recently, as part of an assessment of levee vulnerability in the Sacramento Delta area, URS (2007) have performed a review of available data and information on the permeabilities of Marsh / Peat layers that underlie the levees in this region. This evaluation included the work cited by the USACE (Weber 1969). This work resulted in the following conclusions (URS 2007, p. 44):

"*Consistent with its depositional history, the team believes that the horizontal permeability (kh) of peat/organic soils will generally be higher than the vertical permeability (kv), especially if the peat is in a 'free-field' condition , away from the consolidating loads of a constructed levee. Therefore, for the initial evaluations, the Levee Vulnerability Team recommended using an anisotropy (kh/kv) of 10 with a kh of* $1x10^{-4}$ *and a kv of* $1x10^{-5}$ *cm/s, for 'free-field peat/organic soil."*

"As expected, due to the consolidating impact of the weight of a constructed levee, peat/organic materials lying beneath the levee showed lower permeability than the free field peat. Therefore, for the initial analyses, the levee vulnerability *evaluation team recommended using horizontal and vertical permeability values of* $1x10^{-5}$ *and* $1x10^{-6}$ *cm/s respectively. This is one order of magnitude lower than the permeability of the free field peat/organic soils."*

Based on available information on the buried Marsh deposits under the Lower 9th Ward levees and floodwalls, it is not possible to define a single value for the intrinsic hydraulic conductivity – permeability. For this reason, the effects of a wide range of plausible permeabilities on seepage and hydraulic effects and horizontal stability of the levee – floodwall were assessed in the analyses that will be discussed in the subsequent sections of this report.

8. SEEPAGE & HYDRAULIC EFFECTS ANALYSES

8.1 Analytical Model Description

The Finite Element Analysis (FEA) software SEEP\W, part of the package GEOSTUDIO 2004 was used for seepage and hydraulic effects analyses. The program uses a finite element code to route the boundary conditions imposed as hydraulic heads on the boundaries of the problem through a porous media, calculating heads and pressures along the nodes of the FEA mesh.

The software requires the generation of permeability functions that include the decrease of permeability depending upon increases in negative pore water pressures (suction).

Figure 8-1 shows a typical mesh used in SEEP\W (this case the section for South Breach).

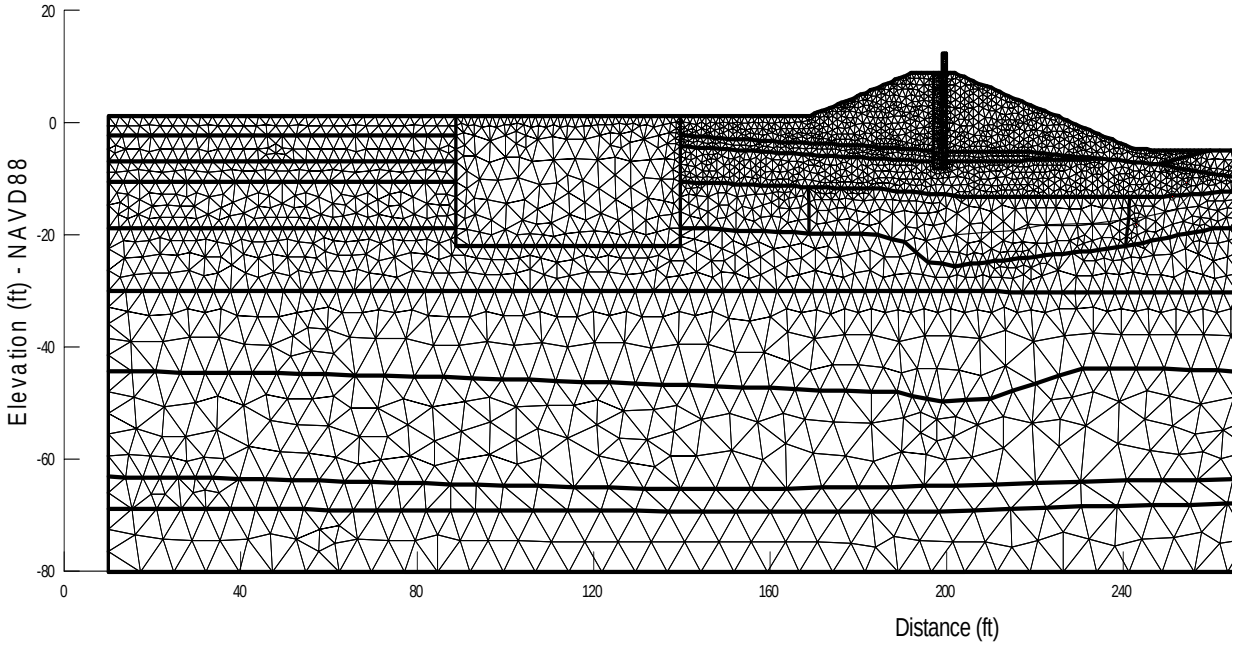


Figure 8-1. Typical FEA mesh used for seepage calculations.

Table 8-1 summarize the hydraulic properties of the soil layers, including conductivity at saturation and anisotropy ratio. The last row on Table 8-1 gives the permeability value used for gap formed between the levee and sheet-pile. This element was not modeled in the IPET (2006) seepage computations.

Material	K at saturation (cm/s)	Anisotropy Ratio (ky/kx)
Clays	10^{-6}	0.3
Sands	10^{-2}	0.25
Marsh (upper bound)	10^{-2}	0.10
Marsh (lower bound)	10^{-6}	0.10
Gap	100	1.0
Waterside Excavation Fills	10^{-1}	1.0

Table 8-1. Input values for seepage models.

Figure 8-2 is the idealized hydrograph as it was introduced into the model.

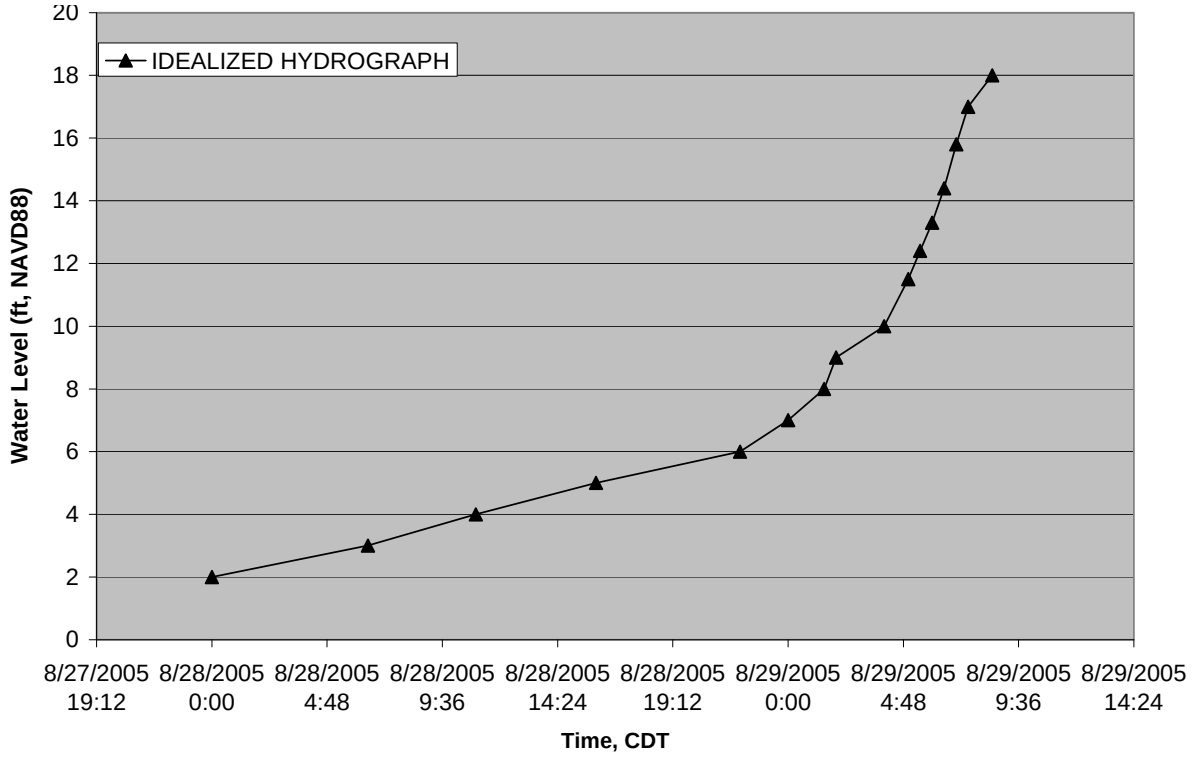


Figure 8-2. Idealized hydrograph – hydraulic head for the transient seepage analyses. (H: total head in ft), time in seconds.

Boundary conditions for the FEA model include prescribing no-flow boundaries (or zero pressure) along the bottom, canal side edge, and landside levee slope and ground surface (the latter ones have the option of allowing water to flow out of the mesh, called review nodes). Total heads equal to different values of storm surge were applied to the waterside levee slope and canal bottom; and total heads with elevation equal to the ground surface elevation were applied at the nodes on the "far field" vertical edge of the model (landside).

8.2 South Breach Section

8.2.1 Steady State

A baseline steady state analysis was performed using a water elevation of +14.0 feet for the South Breach, and +12.0 feet for the North Breach. These elevations were taken as reference of maximum development of pore water pressures. The elevation of 1 4feet was used for the South Breach, since field evidence suggested at least a couple of feet of overtopping at the time of full development of the breach, and the information from the hydrograph shows 14 feet to be a good estimate for this elevation. The elevation of +12 feet was used for the North Breach for the maximum height since the field investigations and eyewitness reports (IPET 2006, ILIT 2006) indicate that failure occurred before overtopping, therefore the maximum I-wall elevation would be the maximum elevation for development of pore water pressures.

Steady state implies that water has had enough time to flow through the media and a constant pressure regime has developed, therefore no flow is occurring. This does not mean that the pressures are hydrostatic. Often times, when less permeable deposits are at or near the surface, they act as "blankets" that do not permit the pore water pressures to alleviate, creating excess heads and pore water pressures that can cause uplift or blowout failures. This can be particularly critical on levees and embankments subject to relatively rapid hydraulic loading with thin fine

grained soil layers located at or near the toe of the levee. Substantial differences in pore water pressures can be seen when a steady state regime of pressures is calculated, compared with a simpler "sketched" phreatic surface that assumes hydrostatic pressures are developed underneath it. Figure 8-3 shows the difference on calculated pore water pressures for a simplified case of seepage analysis.

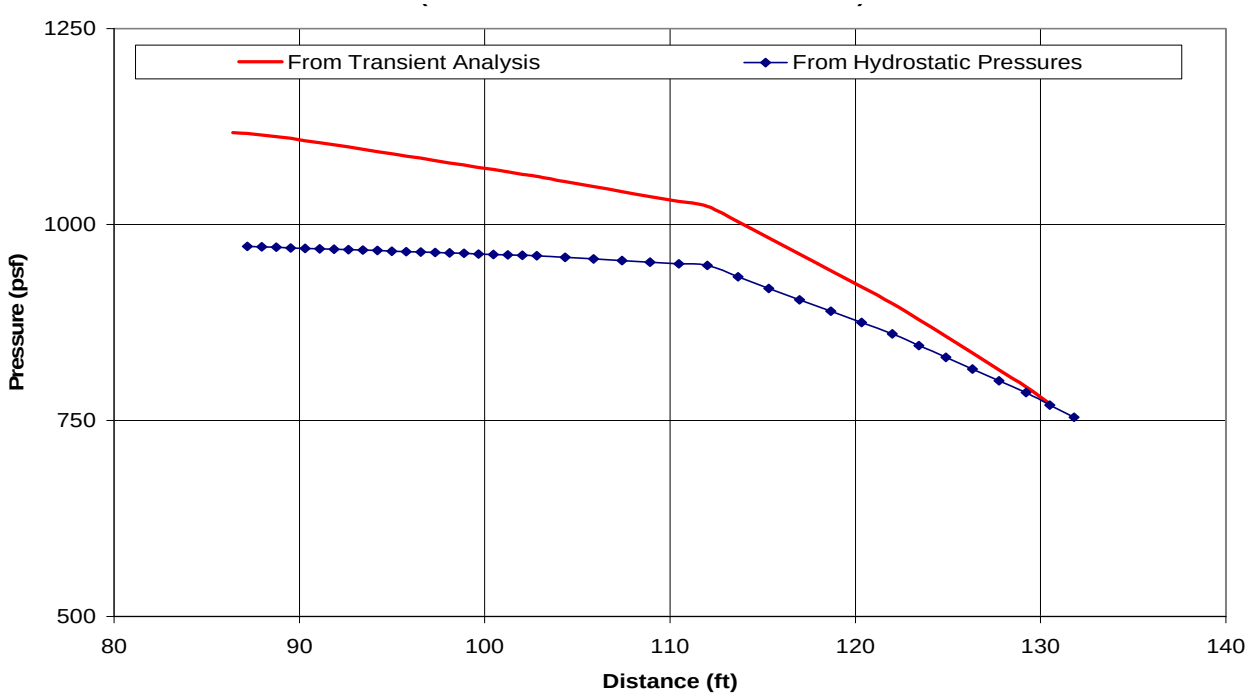


Figure 8-3. Difference between steady-state generated pore water pressures and hydrostatic pressures (general case, Marsh permeability 10^{-4} cm/s).

A 5 % to 15 % increase in pore water pressures is generated by running a seepage analysis, with the highest differences near the centerline of the levee. This is a factor that will contribute to slope instability, as soft materials are greatly affected by this condition (stress dependant behavior). This will have a significant impact on the calculated factors of safety, as the effective stresses for soft materials with stress-dependant shear strengths will be lower, and consequently will be their shear strengths.

It is seen from the plots on Figure 8-4 that the pore water pressures along the bottom of the Marsh vary about 10 % when the hydraulic conductivity decreases from 10^{-3} to 10^{-6} cm/s. The same plot prepared for the section on the North Breach shows significantly larger differences between the generated pore water pressures, mainly due to the fact that the gap in this South section ends on a clay deposit, whereas in the North Breach, the gap (and sheet pile) end directly on the marsh deposit.

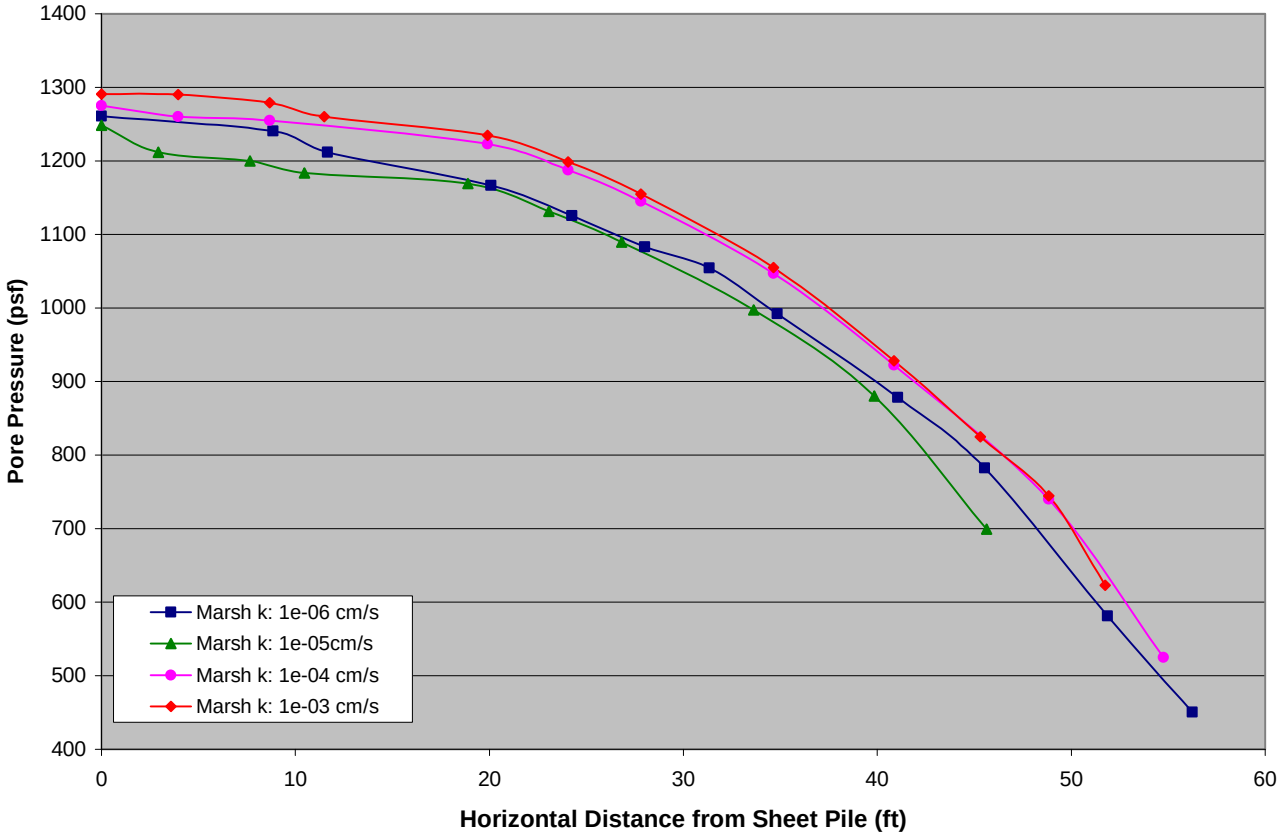


Figure 8-4. Steady State pore water pressures along Marsh layer. Storm surge at +12.0 feet with floodwall – sheet pile – soil gap on water side.

8.2.2 Transient Analyses

Transient analyses were performed for the rising water level on the Canal according to the hydrograph from Figure 2-5. Figure 8-2 shows the idealized hydraulic head versus time acting on the canal side of the IHNC levee.

This curve was input into the seepage models, which generated calculation steps beginning at a water elevation +2ft, believed to have been established before the storm surge occurred, thus having developed a steady state regime prior to the relatively rapid water rise.

To account for the effects of increased stresses beneath the levee on Marsh permeability, the Marsh was divided into "free field marsh", and "marsh beneath embankment". The latter case was always 10 times lower than the free field case. The values shown in the property tables correspond to the free field case.

The results of the analysis show that after 33 hours of modeled time (August 28, 2005 12:00am to August 29, 2005, 9:00am), high pore water pressures near Steady State condition developed along the Marsh deposit for the previously mentioned permeabilities. The transient models start from the "low" pre-storm generated steady state at 2ft, generated by August 28, 2005 06:00 hours, and in 11 time increments, +12.0ft (NAVD88) are reached on August 29, 2005 7:00am. Results for every hour are plotted in these figures.

Figure 8-5 shows the evolution of pore water pressure at three different locations on the toe of the levee: 1) Center of surficial clay layer, 2(Bottom of surficial clay layer, and 3) Center of Marsh layer.

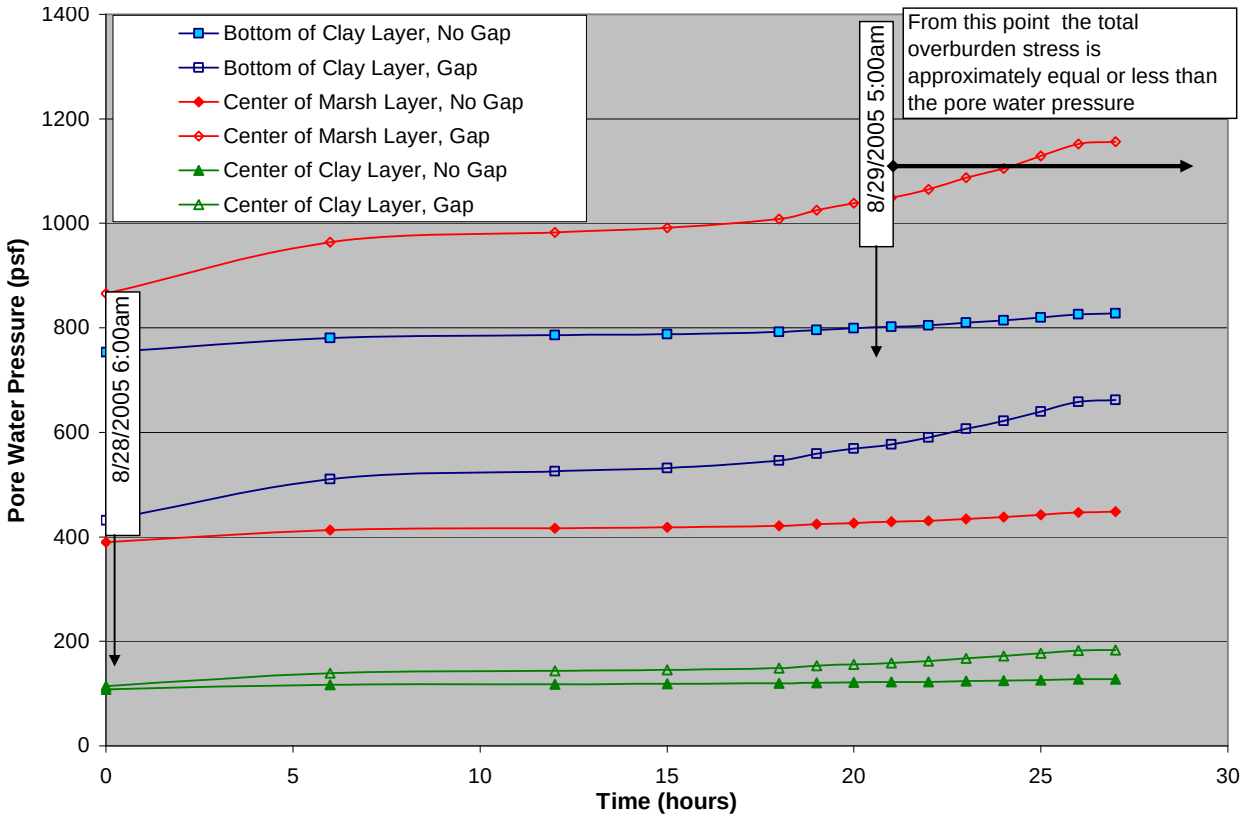


Figure 8-5. Transient model results. Pore pressure versus time on three points near the toe of the levee (Marsh permeability 10-3 cm/s).

The "Center of Marsh" series is deeper, and consequently exhibits larger pore water pressures than the other two shallower points. To note from this plot is the difference between the cases where a gap was considered in the analyses and when it was not. The increase in pore water pressures by considering the gap is more than 10 % near the toe of the levee.

Figures 8-6 through 8-8 show the output of the computer program, in terms of total heads (feet of water) and hydraulic gradients at 7:00 am on August 29, 2005. It can be seen to the left of the sheet pile, that the canal-side portion of the levee is not fully saturated, but to the protected side, the phreatic surface has risen enough to exit on the levee slope.

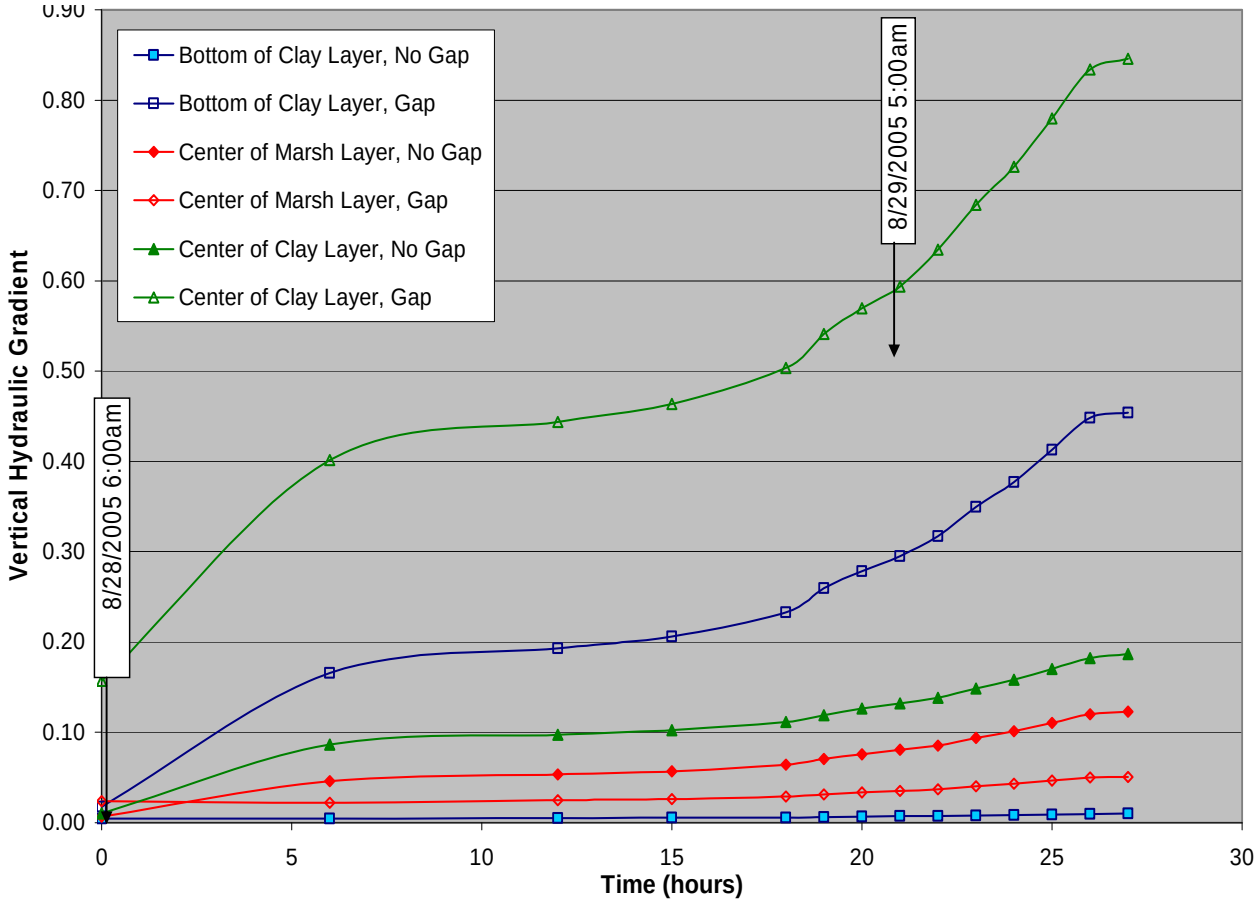


Figure 8-6. Transient model results. Hydraulic gradients versus time on three points near the toe of the levee (Marsh permeability 10^{-3} cm/s)

It is evident from Figures 8-4 and 8-5 that the differences in pore pressure are important when the gap is introduced into the model; because the full head of the storm surge can be applied along the back of the sheet pile and to the foundation soils. As mentioned before, the south section shows a clay layer just beneath the sheet pile tip, therefore the differences between gap and no gap are not as pronounced as the North Breach model shows, which has the sheet pile bottomed in the middle of the Marsh deposit. When the gap was not considered, the degree of saturation and advance of the wetting front was completely different from the result shown in Figure 8-4.

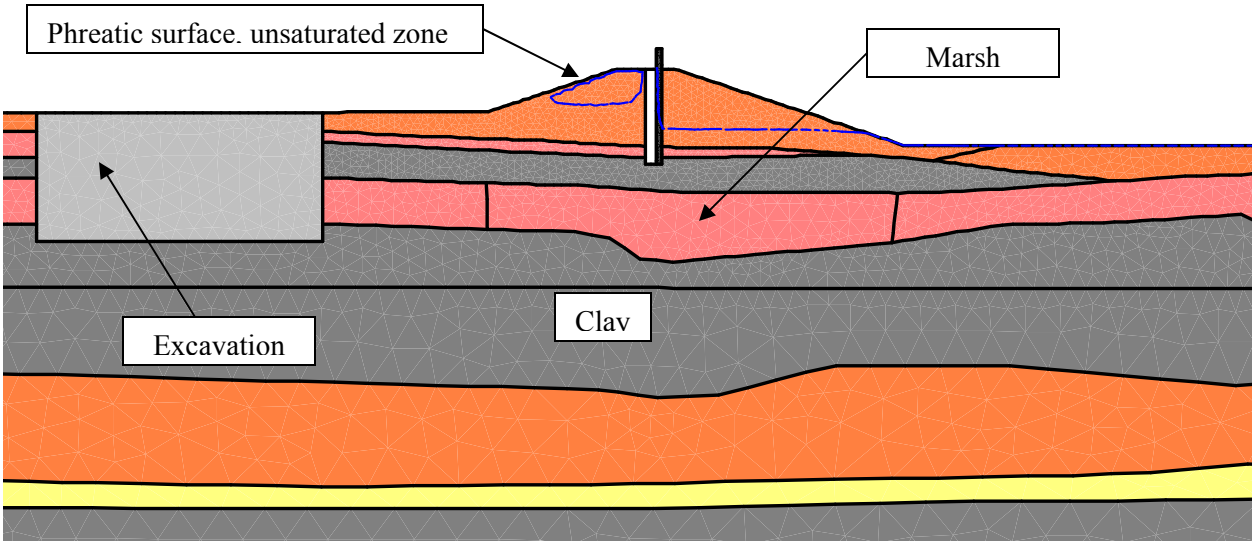


Figure 8-7. Transient model result. Time: between 7:00 and 8:00 am on August 29, 2005. The blue line represents the calculated phreatic surface.

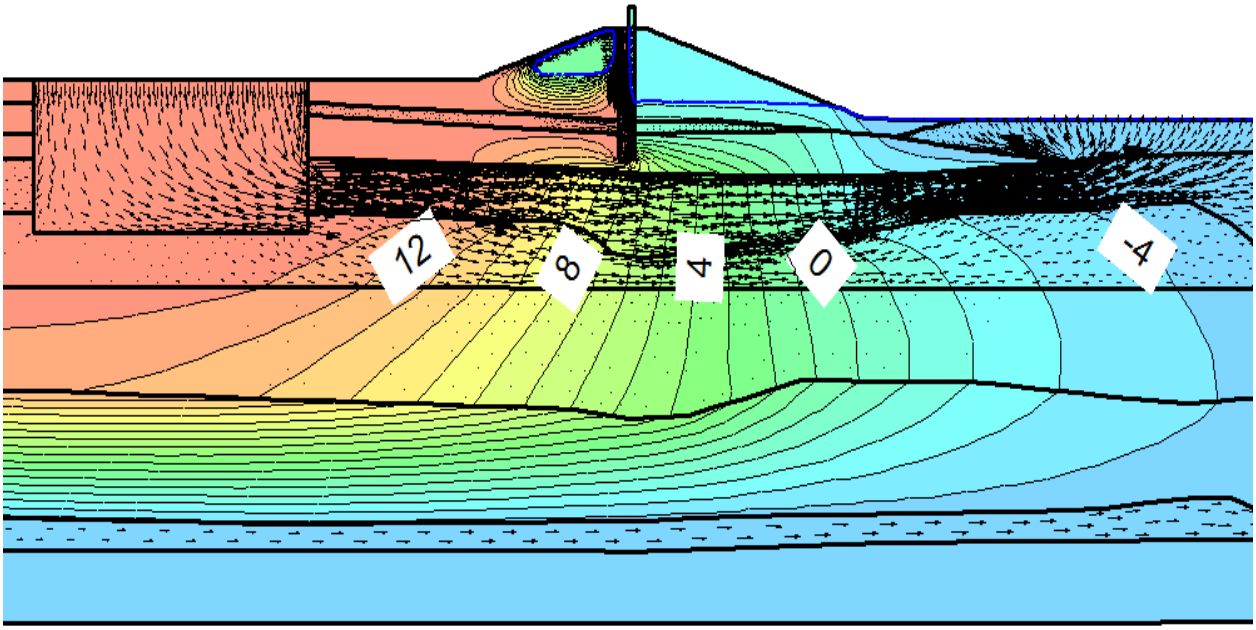


Figure 8-8. Transient model result, total Heads (ft). Time: between 7:00 and 8:00 am on August 29, 2005. The blue line represents the calculated phreatic surface. Note that there is virtually no head loss on the levee until the sheet pile is reached (zone with no head contours extending from the waterside towards the right).

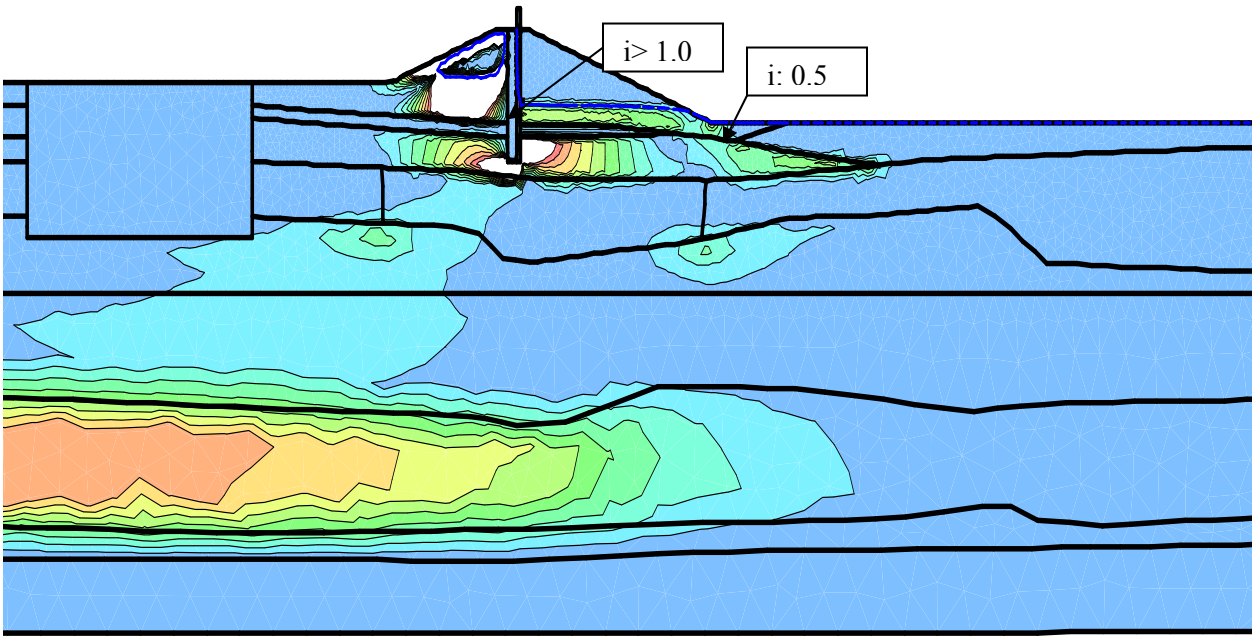


Figure 8-9. Transient model result, Hydraulic gradients. Time: between 7:00 and 8:00 am on August 29, 2005. Maximum Gradient through the clay layer above the marsh

From the plot in Figure 8-9 it can be seen that the model predicts hydraulic gradients of approximately 0.5 at the clay layer near the toe of the levee. Values higher than 0.5 are considered unacceptable by current practice. Figures 8-10 through 8-13 show the variation of pore pressure for the different permeability values utilized for the Marsh deposit.

It can be seen that as the permeability of the marsh deposit increases, the percent of steady state pore pressure (thick black line) is closer to the calculated transient steps (color lines). For the highest permeability, the pore water pressures at 7:00am on August 29, 2005 are more than 90% of the steady state, and for the lowest permeability they are more than 75%. This explains the importance of the inclusion of the gap in the seepage analyses. If disregarded, the calculated pore water pressures would have been 20 to 25 % lower.

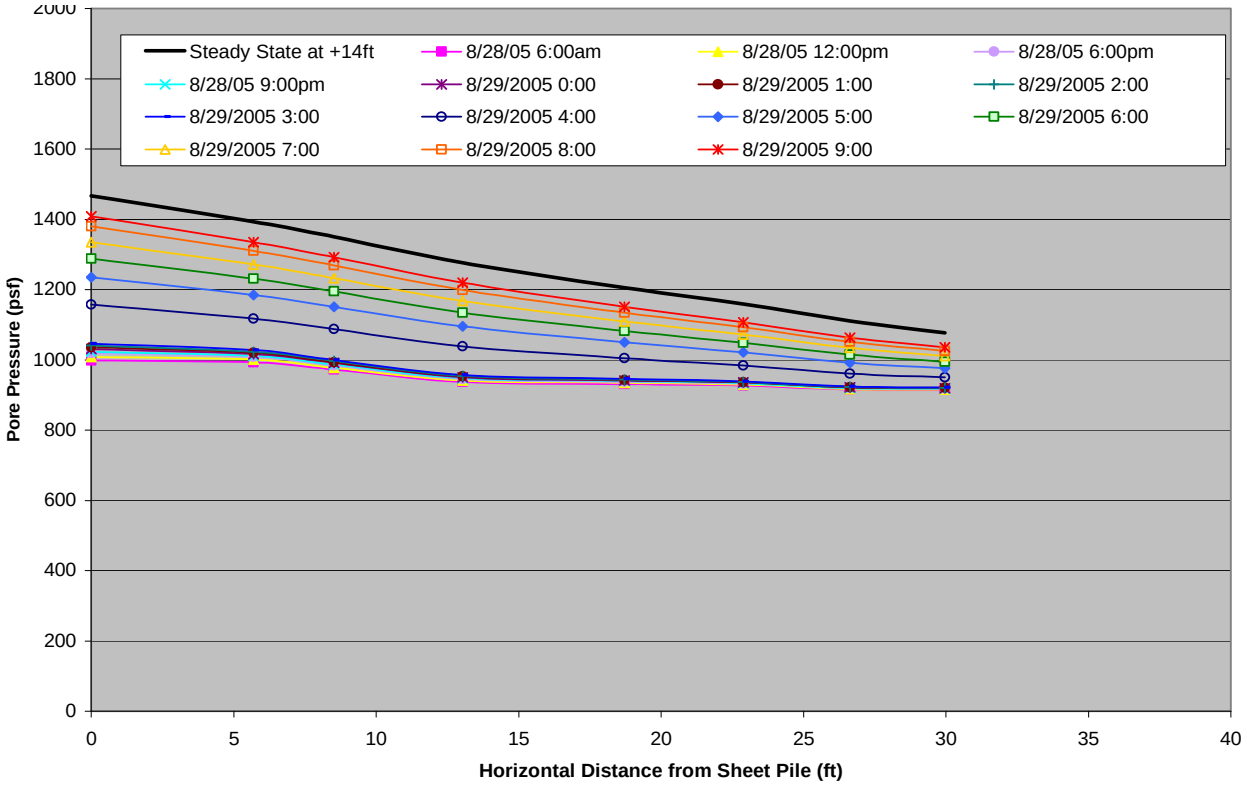


Figure 8-10. Transient model result, Pore pressures along Marsh layer. Marsh k: 10^{-6}cm/s.

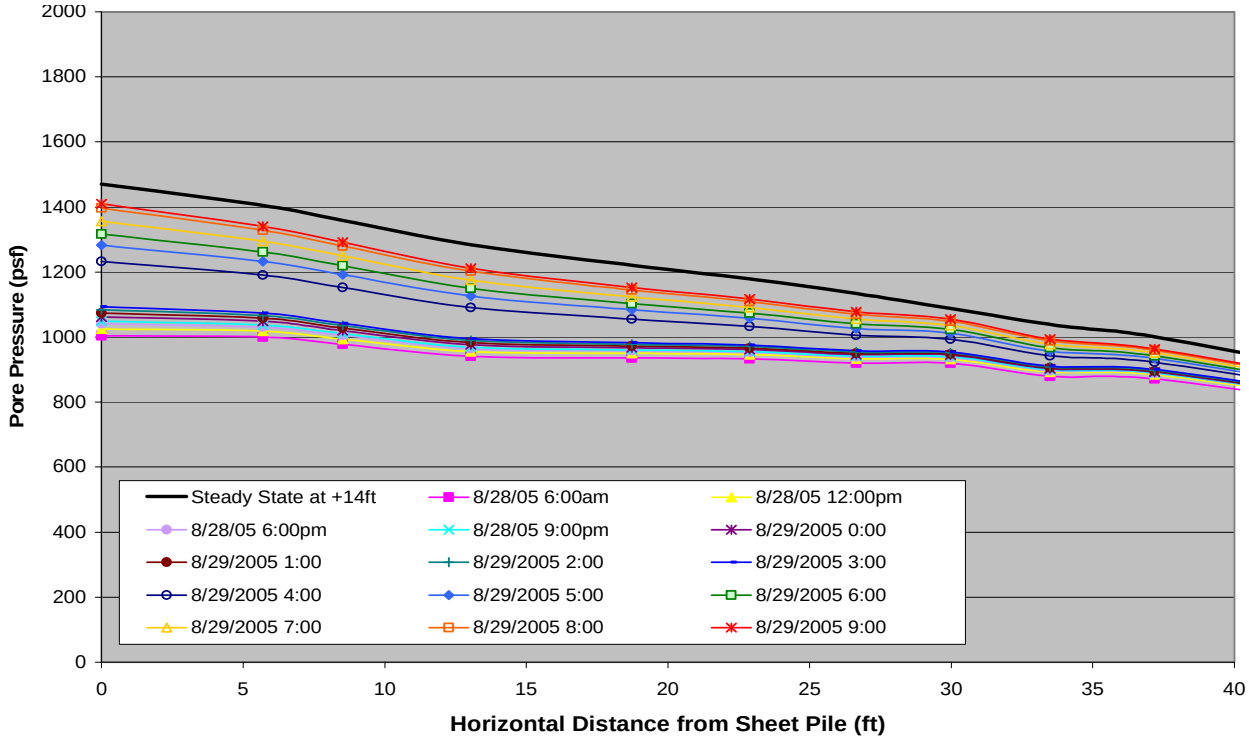


Figure 8-11. Transient model result, Pore pressures along Marsh layer. Marsh k: 10^{-5} cm/s.

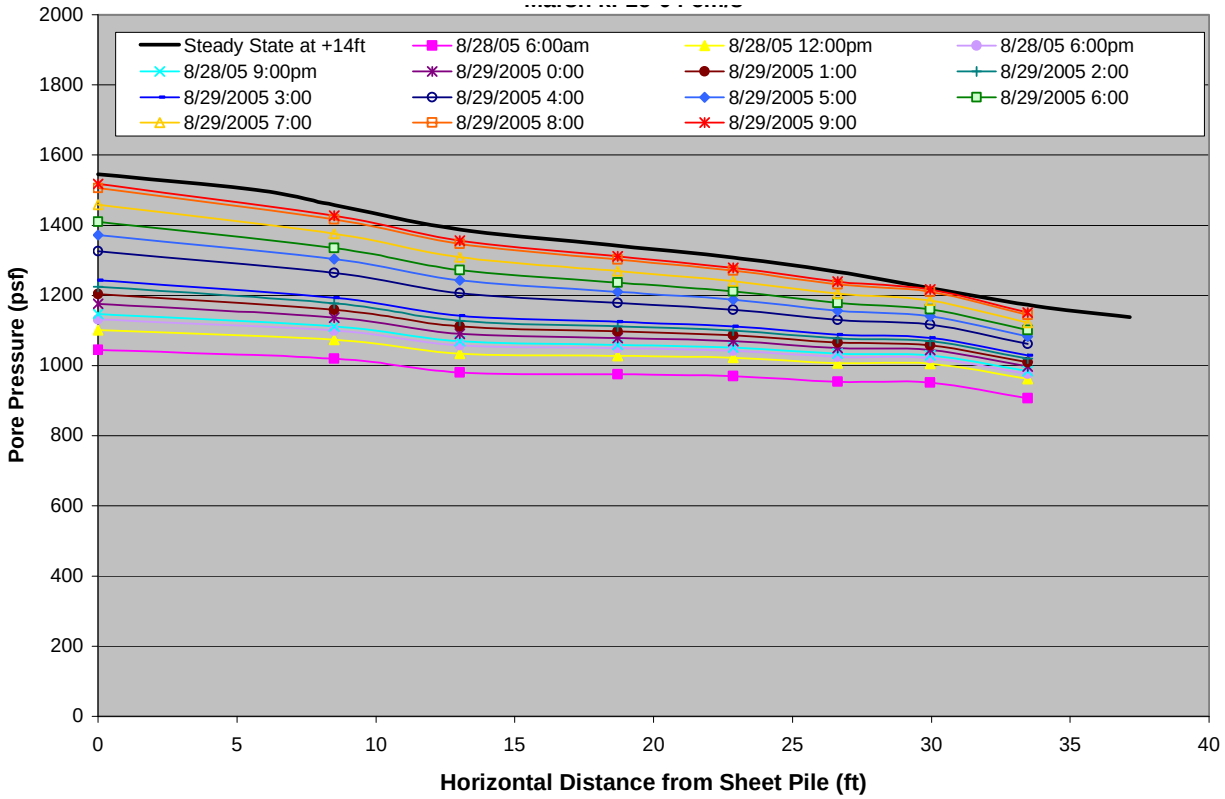


Figure 8-12. Transient model result, Pore pressures along Marsh layer. Marsh k: 10^{-4}cm/s.

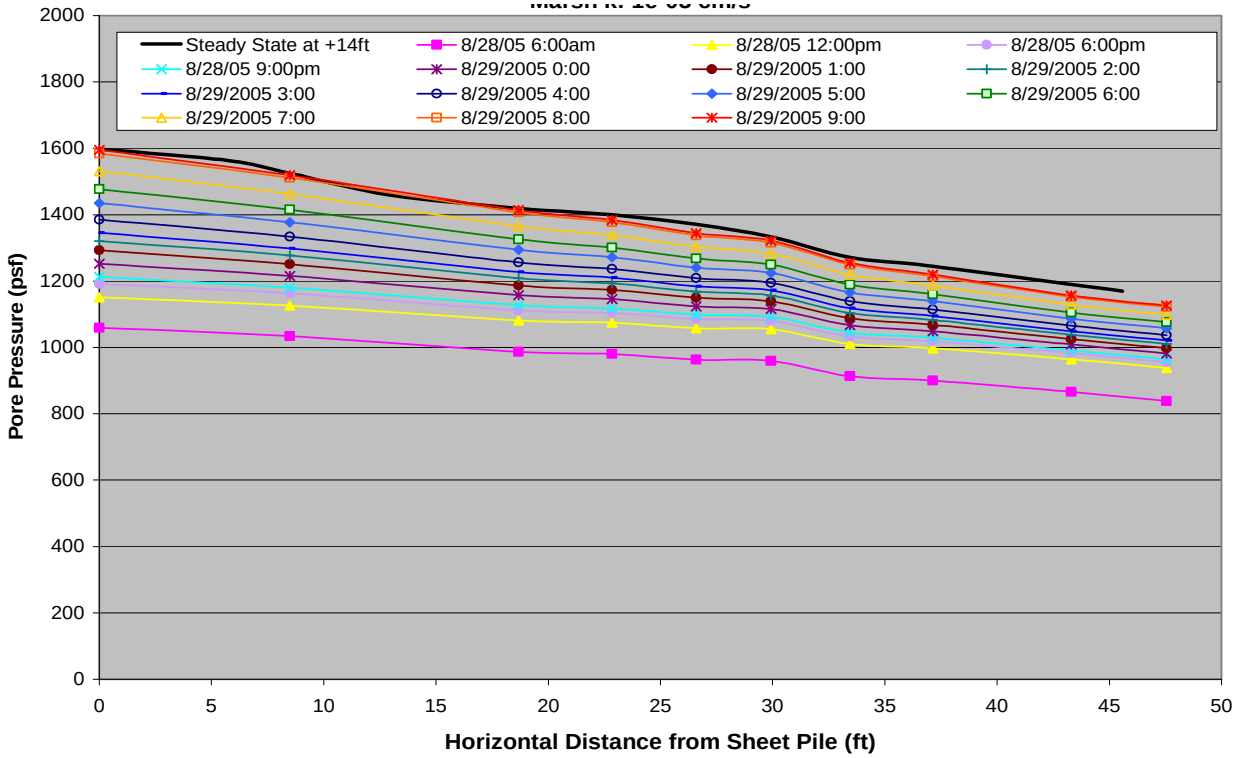


Figure 8-13. Transient model result, Pore pressures along Marsh layer. Marsh k: 10^{-3}cm/s.

8.2.3 Effects of Excavations

The effects of the EBIA waterside excavations were analyzed by modeling the permeable backfill 60 feet away from the levee waterside toe and at the levee waterside toe. A clay-filled excavation was also modeled in order to capture the effect of the placement of low permeability material on the excavations. Figures 8-14 and 8-15 show calculated pore water pressures for different excavation configurations and presence of gap on the center of the clay layer and center of the marsh layer, respectively.

The calculated pore water pressures vary significantly depending on the case of analysis. When the gap is "turned off" and the excavation is assumed to have low permeability materials as backfill, the pore water pressures inside the marsh deposit are about 10 times lower when compared to the case of fully developed gap and permeable excavation backfill at the waterside toe.

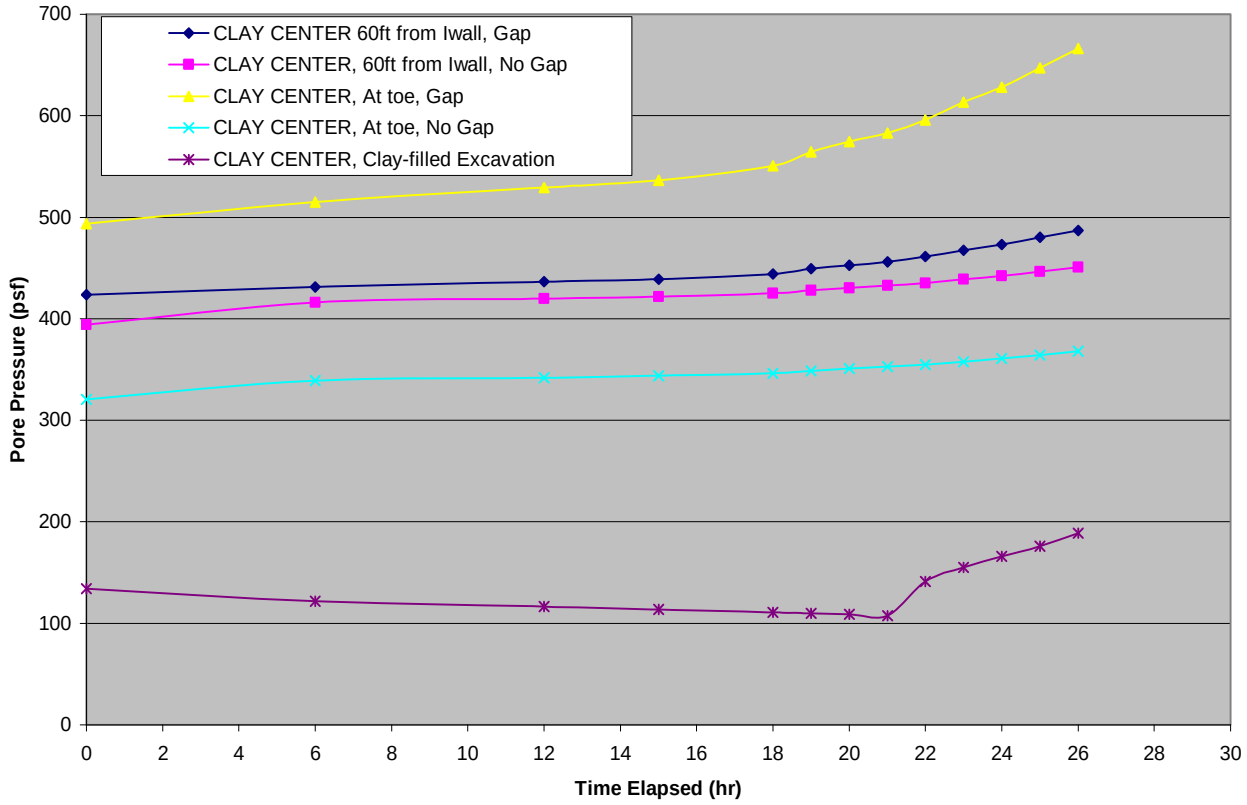


Figure 8-14. Transient model results. Pore pressures along center of clay layer. Marsh k: 10^{-3} cm/s.

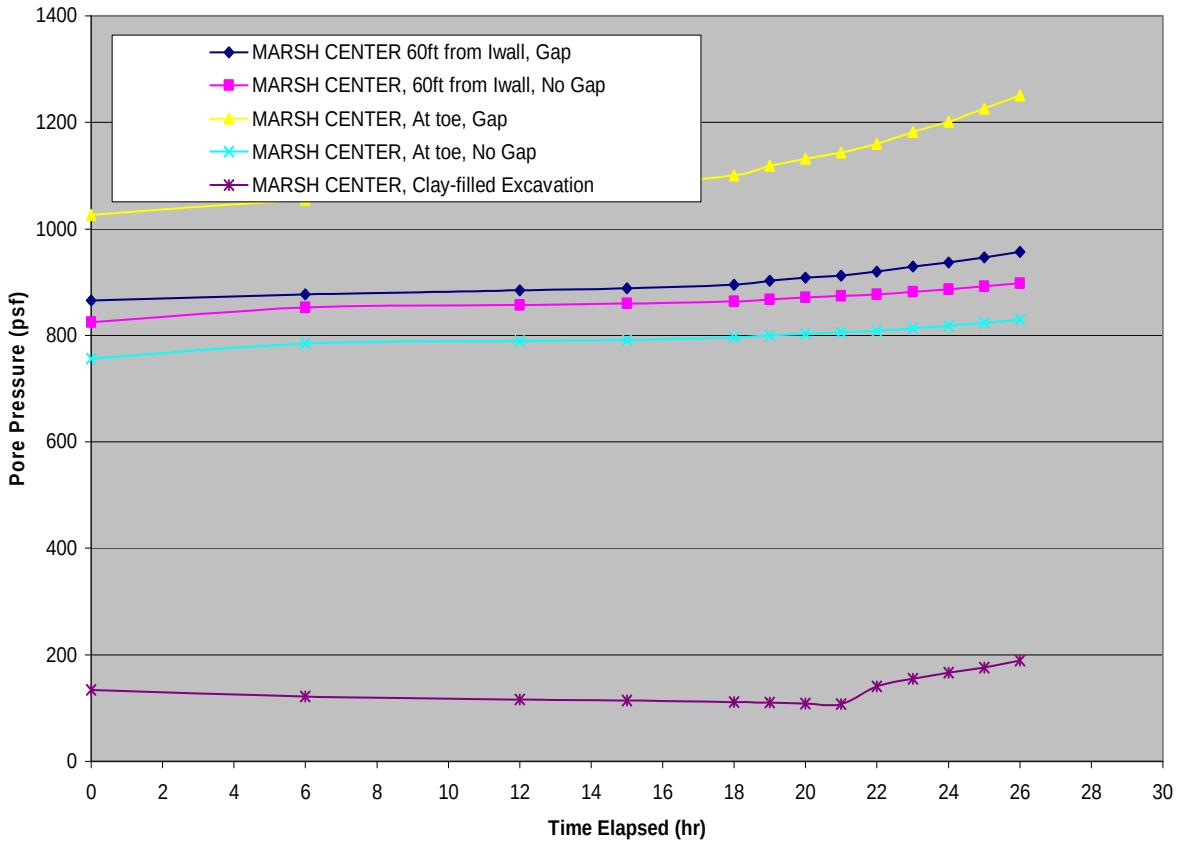


Figure 8-15. Transient model results. Pore pressures along center of Marsh layer. Marsh k: 10^{-3} cm/s.

A factor of safety for hydraulic uplift was calculated as the relation between the effective stress acting at the bottom of the clay blanket and the pore pressure at the same point. Results from these analyses are given in Figure 8-16. For the case of a clay filled excavation, the computed factors of safety against uplift are well above two. This indicates that if the excavations had been backfilled with proper materials that there would not have been a high potential for levee blowout failure. Whereas for the cases considering excavations filled with permeable materials, the factors of safety range from 1.2 to 0.8 after about 6:00 am on August 29, 2005. This indicates a high potential for levee blowout failure.

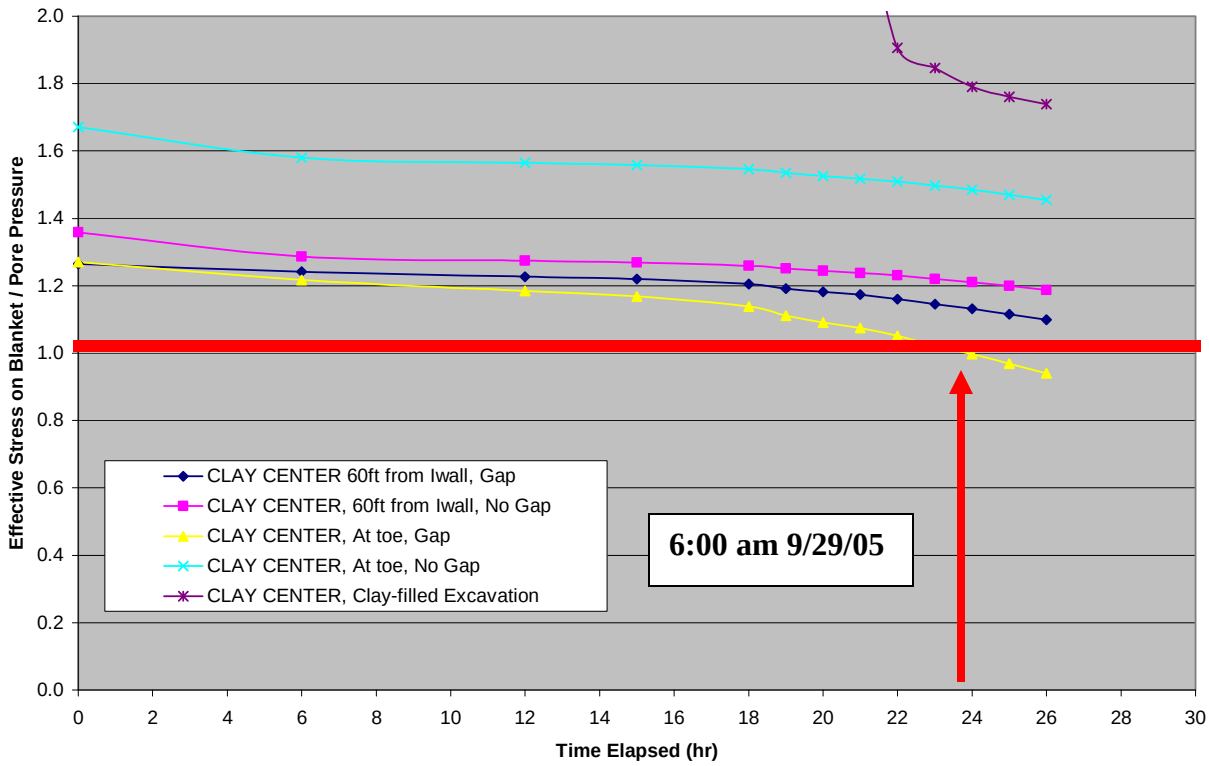


Figure 8-16. Factor of Safety against hydraulic uplift. South breach. Marsh k: 10^{-3} cm/s.

8.3 North Breach

8.3.1 Steady State

As discussed earlier, the sheet pile in the North Breach section is tipped inside the Marsh deposit making it much easier for water to be transported from the waterside gap and excavations to the foundation soils near the toe of the levee.

Figures 8-17 through 8-26 correspond to the same parameters as the previous section on the South Breach, but using the North Breach analytical models.

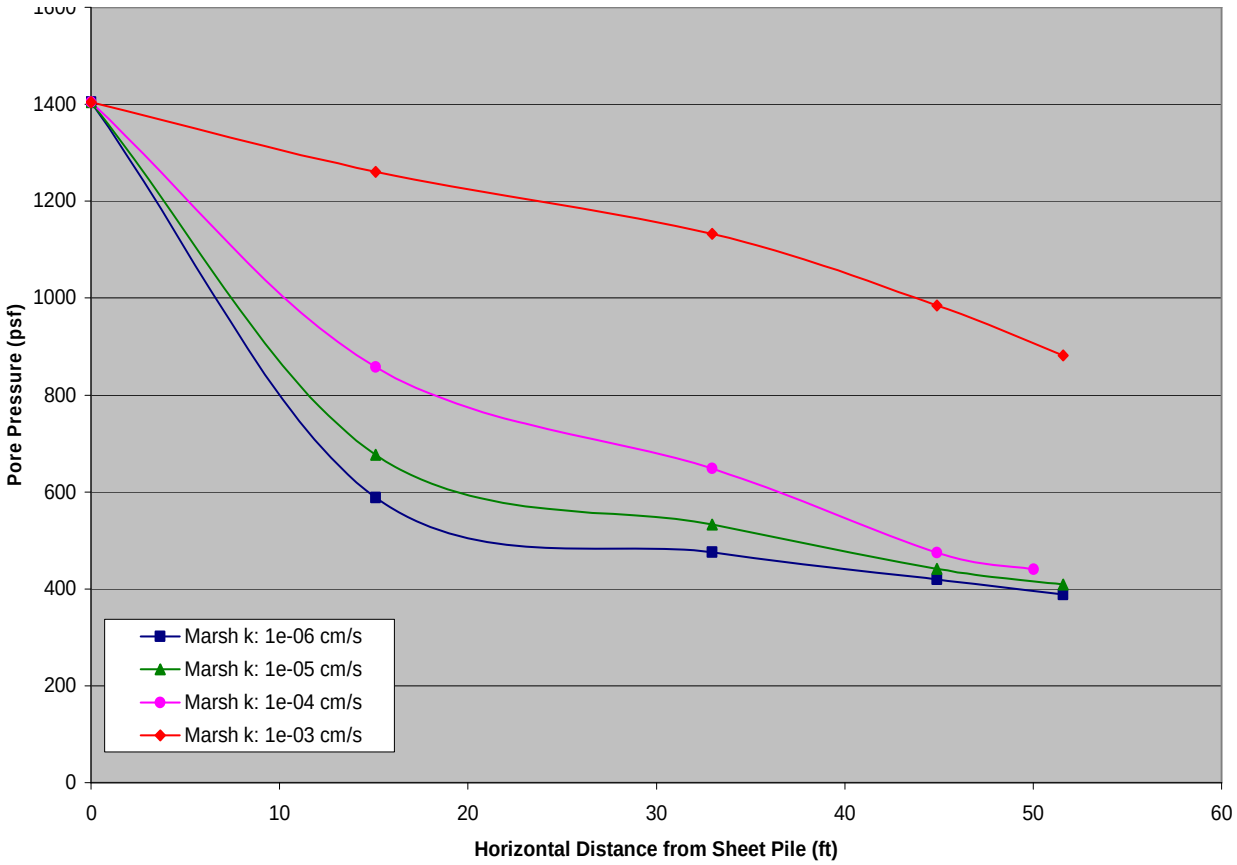


Figure 8-17. Steady State pore pressures along Marsh layer. Storm surge at +12.0 feet, North Breach.

The calculated pore water pressures shown in Figure 8-17 exhibit a very large variation when 10^{-3} and 10^{-6} cm/s are used. As stated before, this condition is probably worsened by the fact that the Marsh layer is being fed the entire head of the surge.

8.3.2 Transient Models

Using the same hydrograph as the South Breach (Figure 8-2), slightly more critical conditions are shown by the transient seepage analyses for the North Breach.

Figure 8-18 shows the evolution of pore water pressure at three different locations on the toe of the levee: 1) Center of surficial clay layer, 2) Bottom of surficial clay layer, 3) Center of Marsh layer.

Based on the analytical results summarized in Figure 8-17, the steady state generated pore water pressures vary about 100 % when the hydraulic conductivity decreases from 10^{-3} to 10^{-6} cm/s. This is due to the fact that in the North Breach the waterside gap that opens between the sheet pile and soils transmits the heads from the storm surge directly to the underlying Marsh deposit. This does not occur in the South Breach where the sheet pile tip is located inside a low permeability layer and therefore there is a significant head loss before the pressure pulse reaches the Marsh layer. After about 5:00 am on August 29, 2005, the calculated pore water pressures are almost equal to the values of overburden stress acting on the surficial clay layer. This would lead to the initiation of uplift deformation (or failure) near the toe of the levee (Figure 8-18).

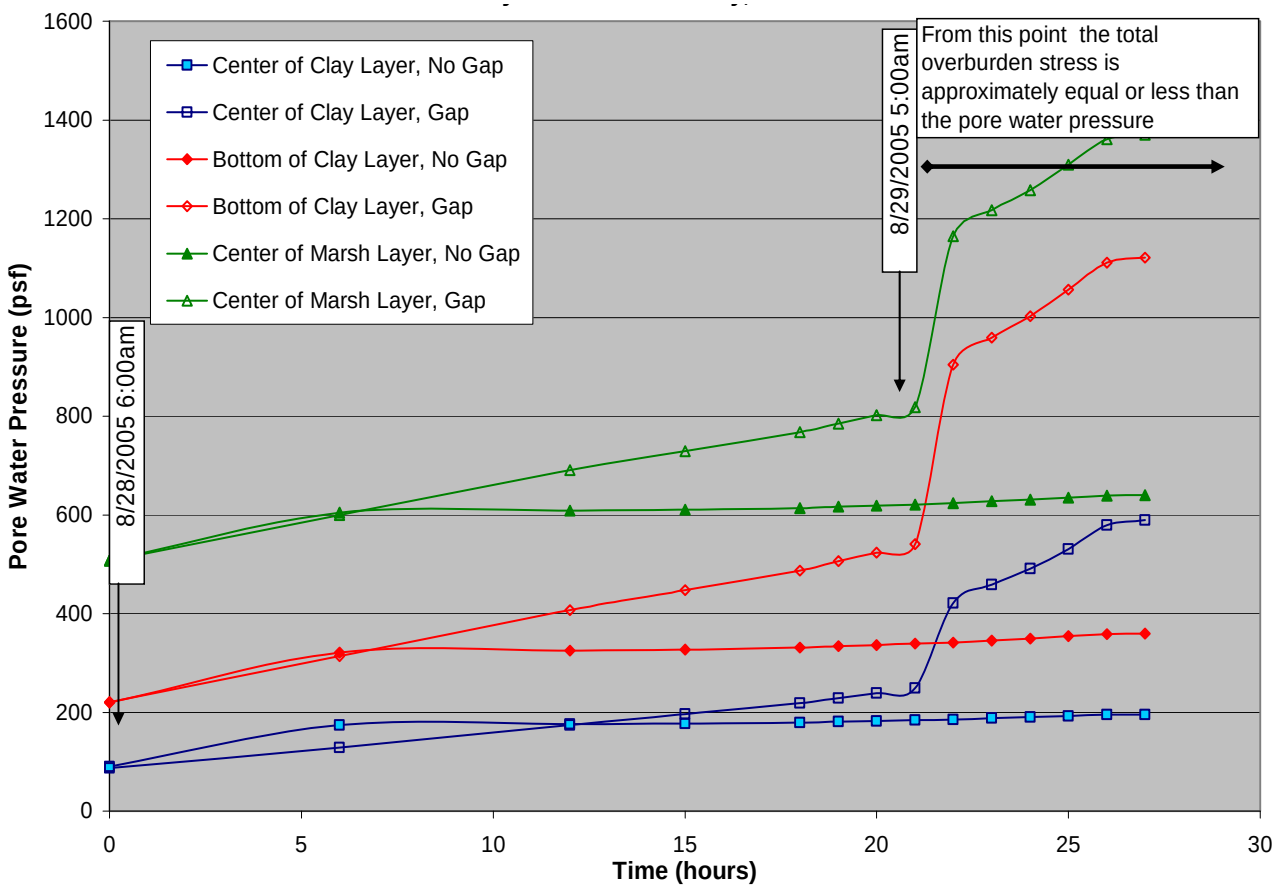


Figure 8-18. Transient model results. Pore pressure versus time on three points near the toe of the levee.

An arrow points to the approximate location of 5:00 am on August 29, 2005. The data shows a rapid increase in pore water pressures and hydraulic gradients (Figure 8-19) after this time. This would have led to the beginning of softening of soil materials (loss of shear strength) at the levee toe that would have progressed into a slope failure.

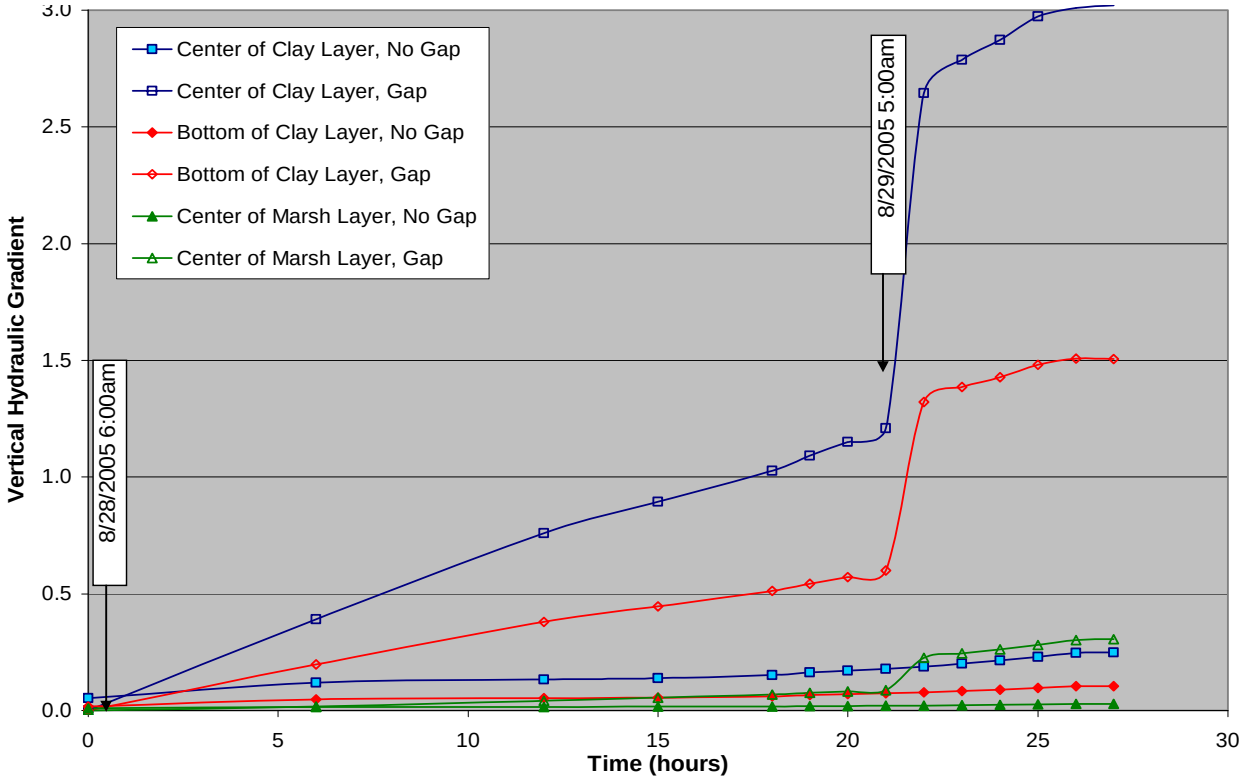


Figure 8-19. Transient seepage analyses results. Hydraulic gradients are shown versus time on three points near the toe of the levee.

Comparing the analytical results summarized in Figure 8-20 with its equivalent for the South Breach (Figure 8-7), a significant head loss is experienced by the surficial clay on the landside of the North Breach as evidenced by the closely spaced head contours near the toe. These hydraulic effects results in the high water pressure gradients summarized in Figure 8-22. These analytical results indicate hydraulic pressure - flow gradients in excess of 1.0 between the landside toe and the infilled drainage canal which acts as a high hydraulic conductivity material. Such gradients are sufficient to develop blowout conditions at the toe of the levee.

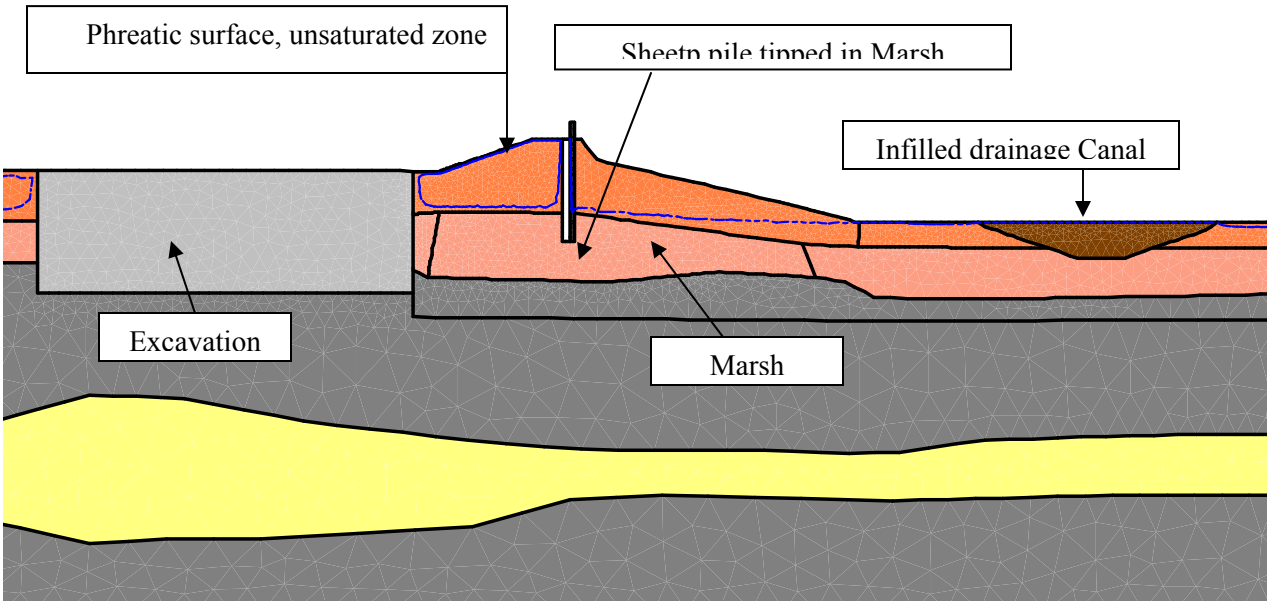


Figure 8-20. Transient model result. Time: between 7:00 and 8:00 am on August 29,2005. The blue line represents the calculated phreatic surface.

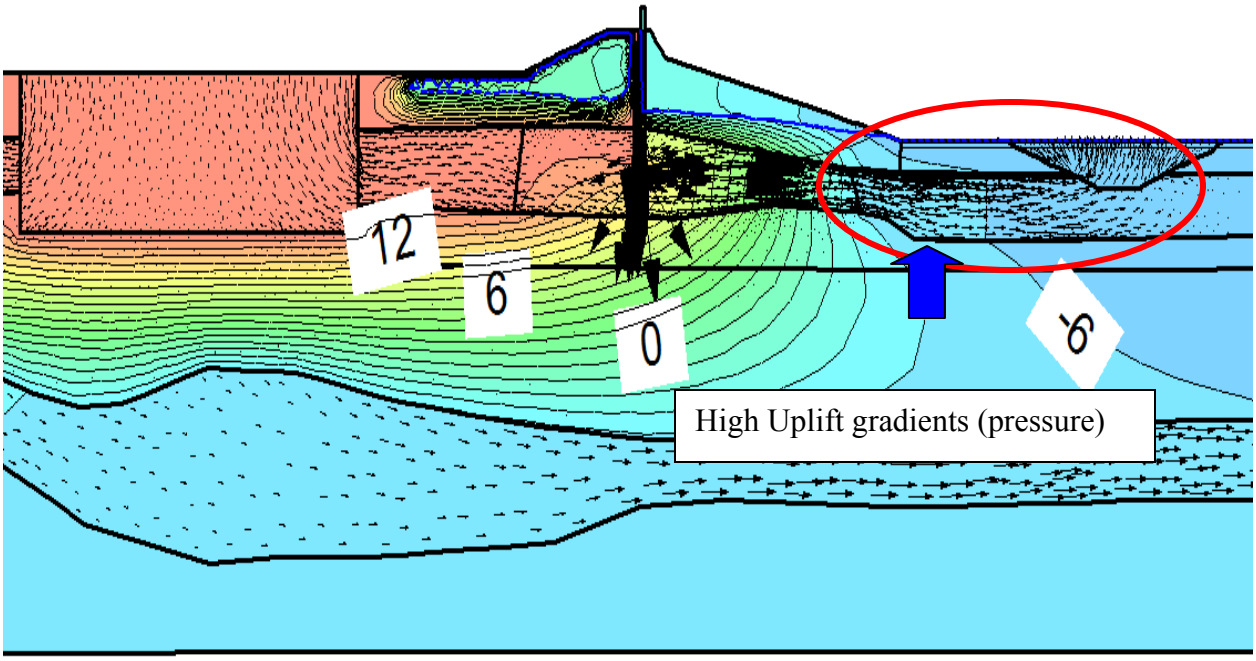


Figure 8-21. Transient seepage analysis results, Total Heads (feet of water). Time: between 7:00 and 8:00 am on August 29, 2005.

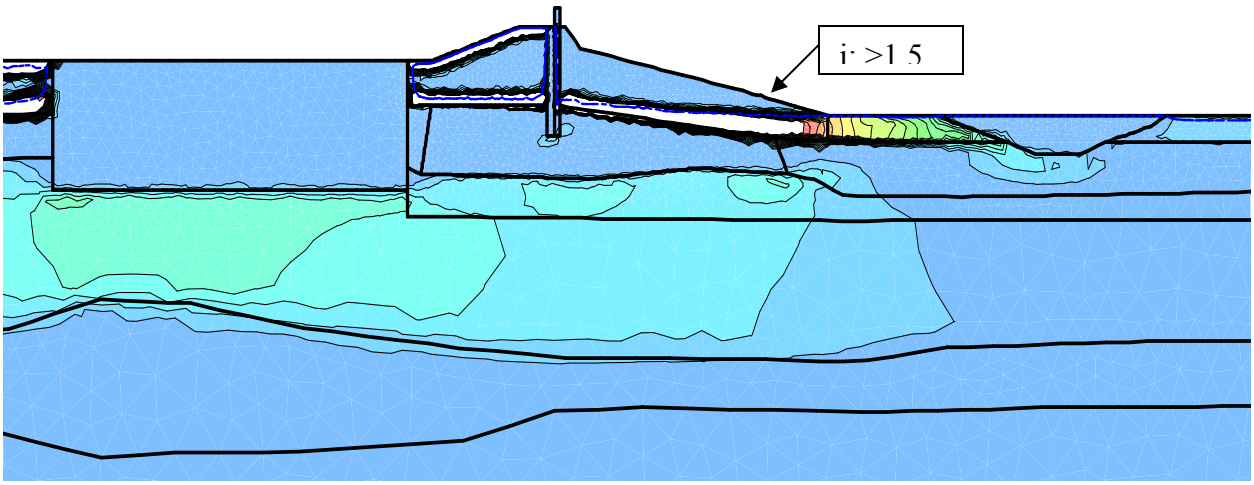


Figure 8-22. Transient model results. Hydraulic gradients. Time: 7:00 am on August 29, 2005. Gradient through the clay layer above the marsh deposit: >1.5 indicating blowout at the levee toe.

Figures 8-23 through 8-26 show the variation of pore pressure for the different permeability values utilized for the Marsh deposit.

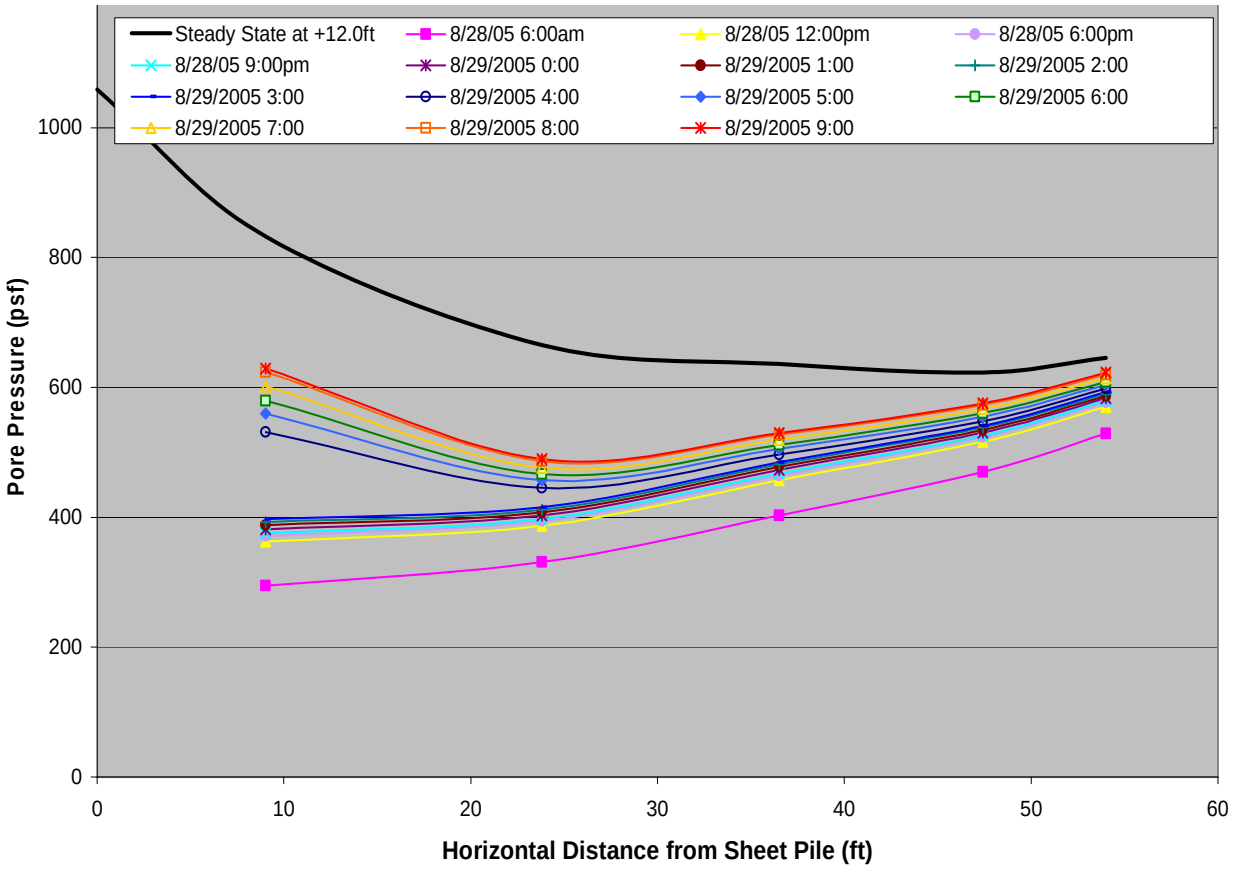


Figure 8-23. Transient model results. Pore pressures along Marsh layer. Marsh k: 10^{-6} cm/s.

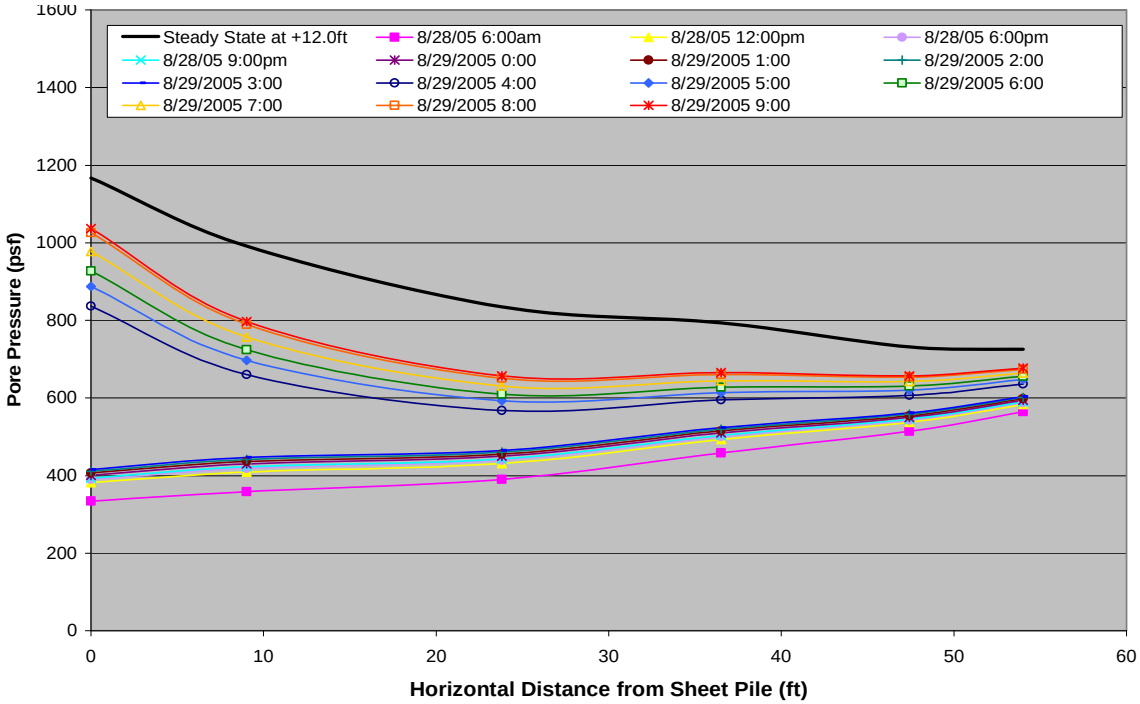


Figure 8-24. Transient model results. Pore pressures along Marsh layer. Marsh k: 10^{-5} cm/s.

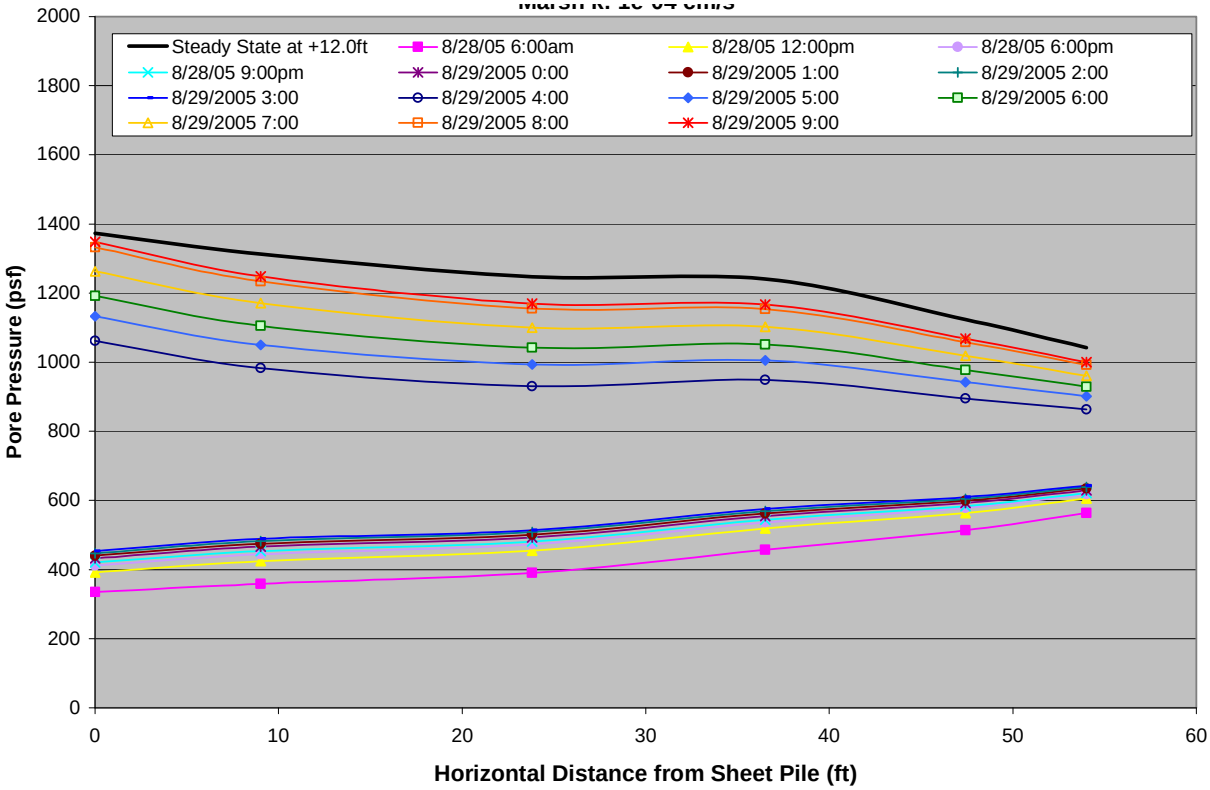


Figure 8-25. Transient model results. Pore pressures along Marsh layer. Marsh k:10^{-4} cm/s.

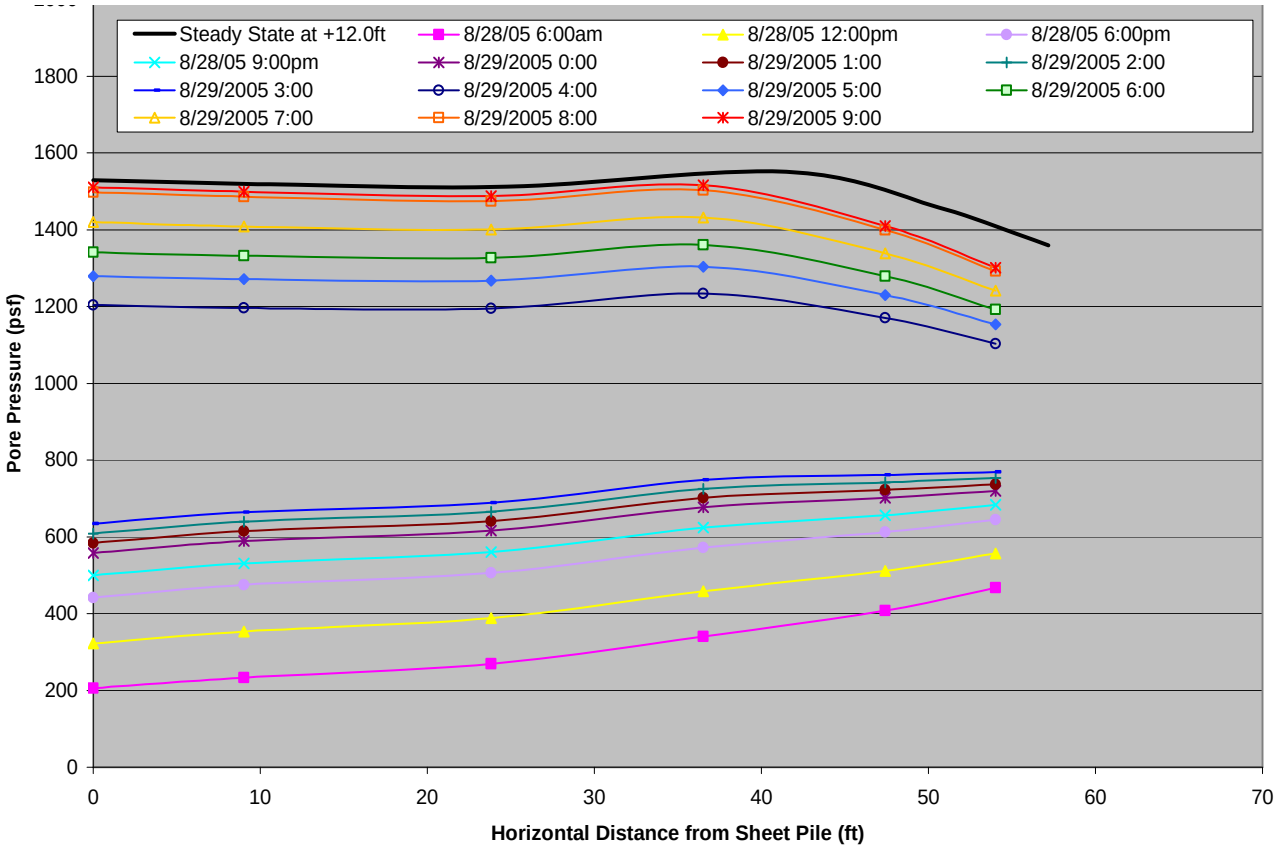


Figure 8-26. Transient model results. Pore pressures along Marsh layer. Marsh k: 10^{-3} cm/s.

It can be seen that as the permeability of the marsh deposit increases, the percent of steady state pore pressure (thick black line) is closer to the calculated transient steps (colored lines). For the highest permeability, the pore water pressures at 7:00 am on August 29, 2005 are 80% of the steady state, and for the lowest permeability they are 70 % of the steady state pressures.

8.3.3 Effects of Waterside Excavations

The effects of the waterside excavations were analyzed by modeling the permeable backfill 60ft away from the waterside toe and at the waterside toe. A clay-filled excavation was also modeled in order to capture the effect of the placement of low permeability material on the excavations. Figures 8-27 and 8-28 show calculated pore water pressures for different excavation configurations and presence of gap on the center of the clay layer and center of the marsh layer, respectively.

The calculated pore water pressures vary significantly depending on the case of analysis. When the gap is "turned off" and the excavation is assumed to have low permeability materials as backfill, the pore water pressures inside the marsh deposit are about 10 times lower when compared to the case of fully developed gap and permeable excavation backfill at the waterside toe.

Figure 8-29 shows transient pore water pressures for the case of Marsh k: 10^{-3} cm/s, with a coarse-grained backfilled excavation. A second trend was added by calculating pressures along the same line, this time using a fine-grained filled excavation. A second analysis was performed, changing only the properties of the backfill to a fine-grained material. Approximately 30 feet away from the sheet pile, a 30% reduction on pore water pressures is achieved by this permeability change. The calculated hydraulic gradients exhibit a smaller decrease due to the presence of the gap between the sheet pile and levee soils.

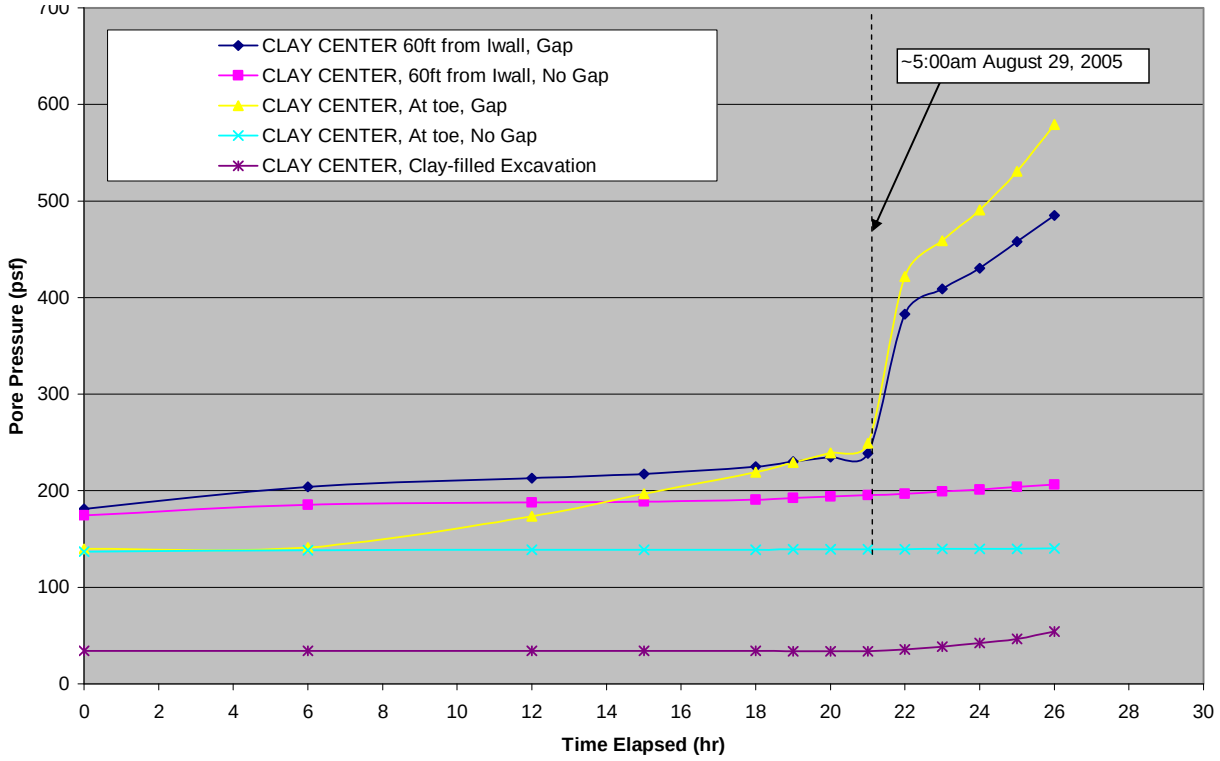


Figure 8-27. Transient model results. Pore pressures along center of clay layer. Marsh K: 10^{-3} cm/s.

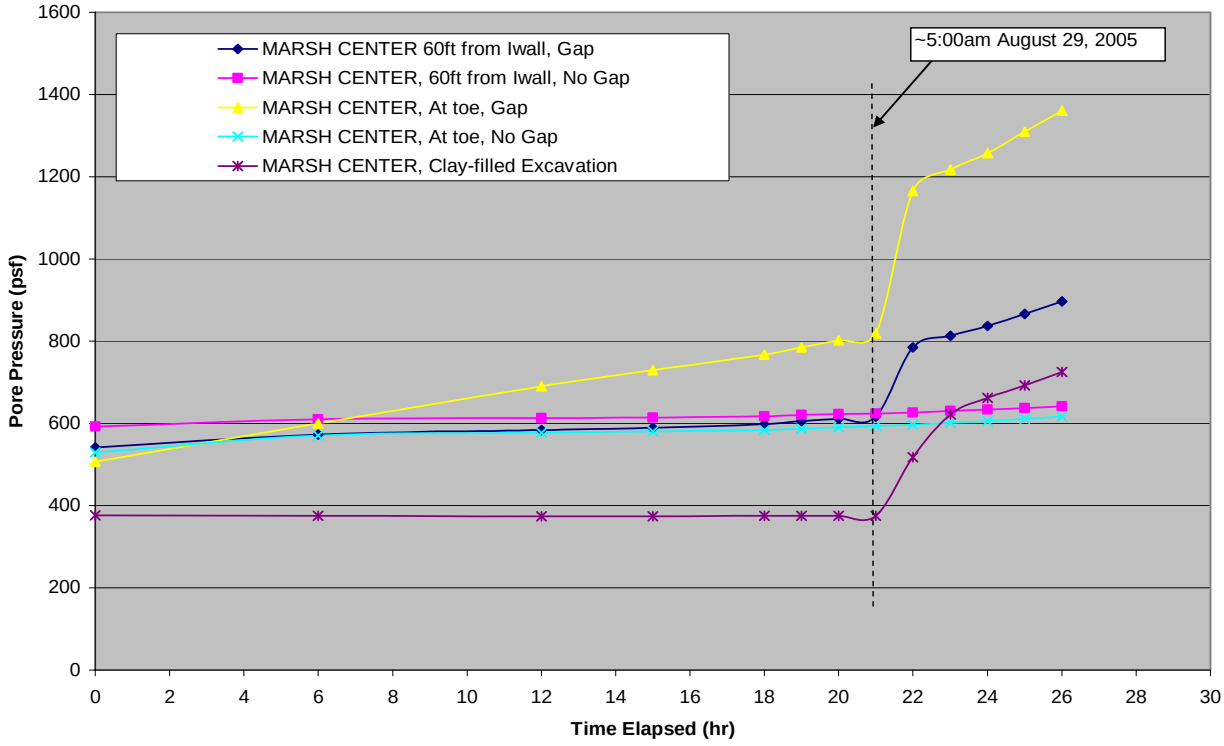


Figure 8-28. Transient model results. Pore pressures along center of Marsh layer. Marsh K: 10^{-3} cm/s.

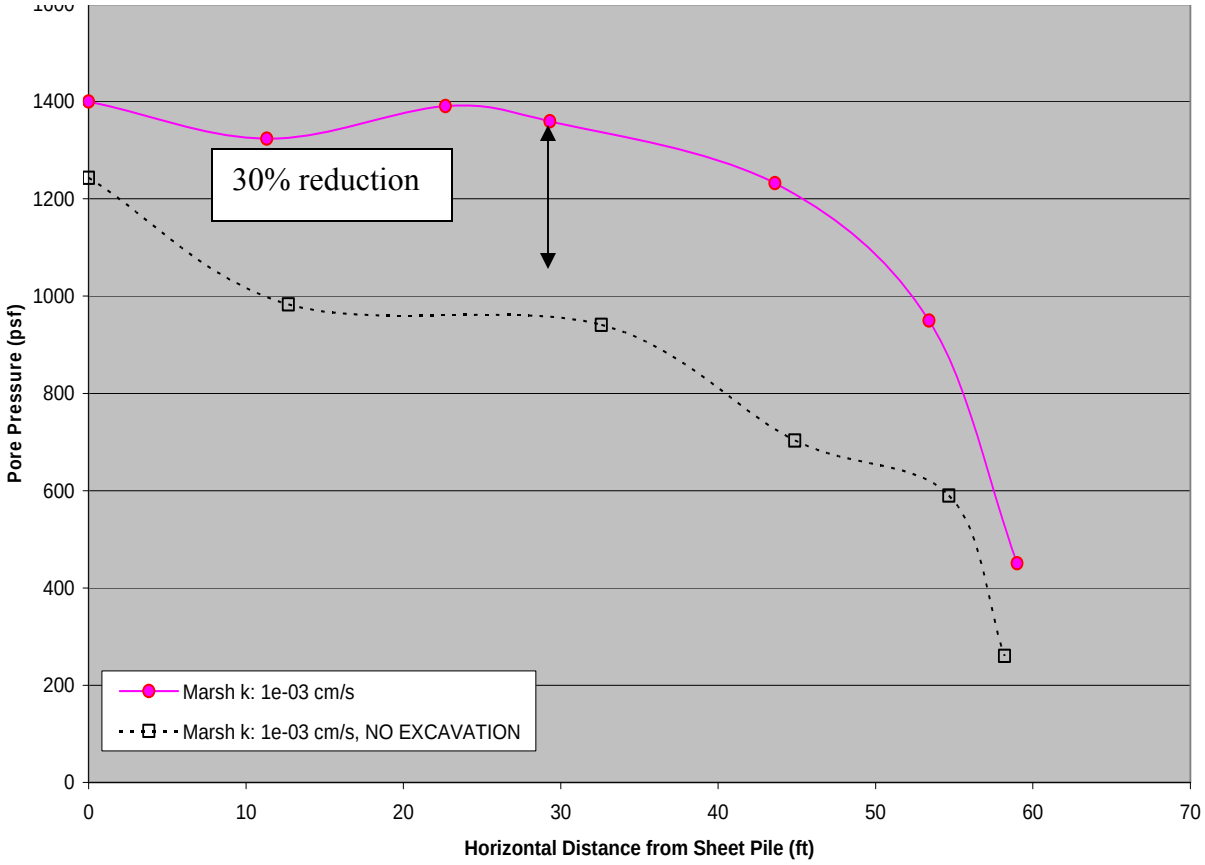


Figure 8-29. Transient model result, Pore pressures along Marsh layer. Marsh k: 1e-03 cm/s. Comparison between excavation filled with permeable material (magenta line) and fine grained material (dashed black line).

A factor of safety against hydraulic uplift was determined as the relation between the effective stress acting at the bottom of the blanket and the pore pressure at the same point. For the case of no-gap and clay filled excavations, the computed factors of safety against uplift are well above two, whereas for the cases considering a gap and excavation filled with permeable material, the factors of safety range from 1.2 to 0.8 after 3:00 am on August 29, 2005. Figure 8-30 shows the results of these analyses.

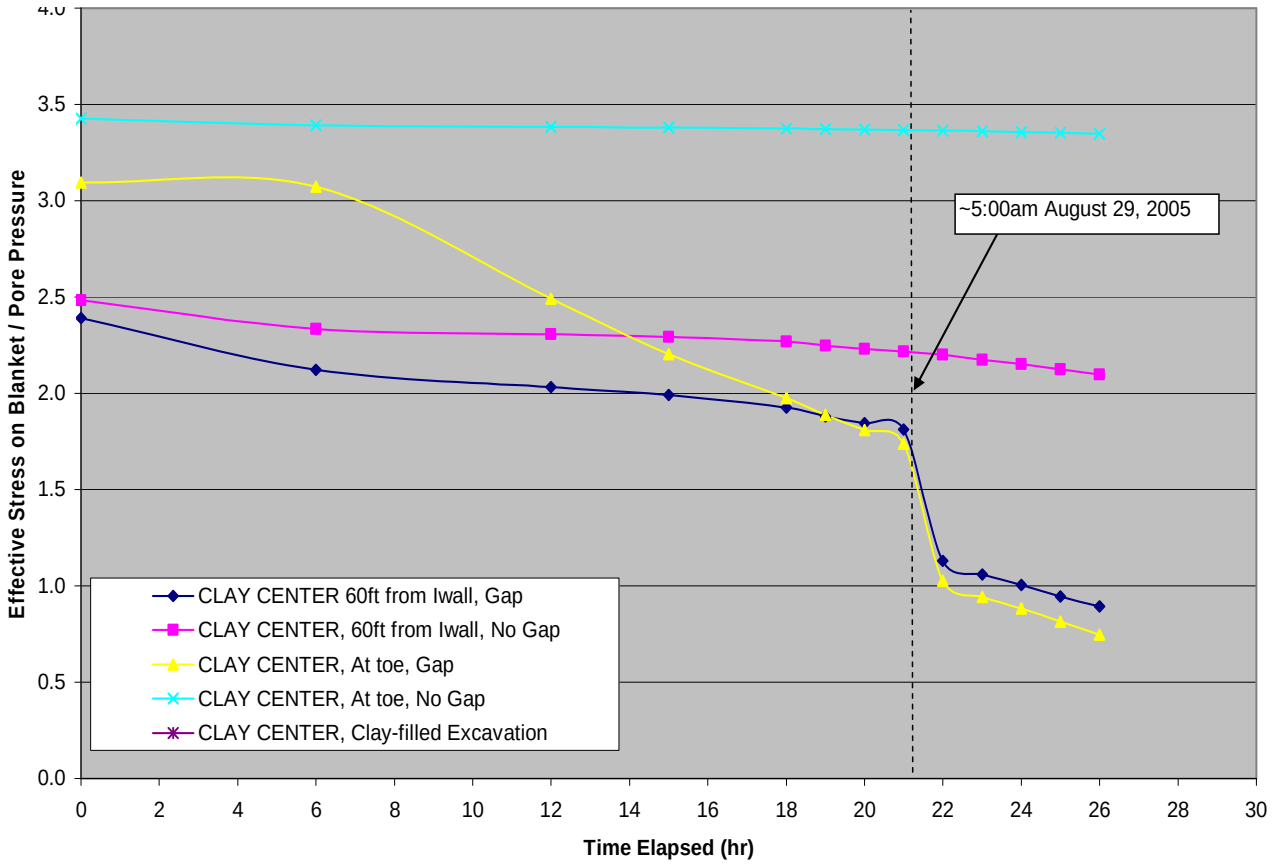


Figure 8-30. Factor of Safety against hydraulic uplift for South Breach. Marsh K: 10^{-3} cm/s.

8.4 Summary of Results from Seepage Analyses

Results from the hydraulic conductivity – seepage FEA analyses show that both breaches are very sensitive to the presence of the gap and proximity of coarse-grained backfilled excavations. Calculated pore water pressures and hydraulic gradients increase when the storm surge rises above the landside crown elevation and the heads are fed to the sheet pile – soil gap and the underlying foundation soils.

8.4.1 South Breach

The South Breach exhibits slightly less critical hydraulic conditions than the North Breach. An important head loss occurs from the tip of the sheet pile since it is found in fine grained soils, therefore decreasing the total heads that charge the foundation layers.

The computations indicate that after about 7:00 am on August 29, 2005, the hydraulic gradients rise above 1.0, and pore water pressures on the bottom of the clay layer become larger than the in-situ stresses. These results indicate a high potential for blowout of the soils at and near the toe of the levee – floodwall.

These hydraulic processes (water flow, pore water pressures, uplift pressures) are major contributors to the instability processes that resulted in the levee breach.

8.4.2 North Breach

The North Breach has a thinner clay blanket, and the sheet pile (and gap) is directly connected to the Marsh deposit – and consequently - the full storm surge. Pore pressure generation and hydraulic gradient rise to critical values occurred earlier than the South Breach, two hours before, approximately at 5:00 am.

This section is more sensitive to the effects of the presence, distance and materials of the excavation, since the Marsh is now fed the hydraulic load from two sources: the gap behind the sheet pile and the waterside excavation. The calculated pore water pressures show an alarming jump in values when the surge rises above the waterside crown of the levee, (approximately twice the values without a gap) and as a result the computed hydraulic gradients rise above 2.0.

9. SLOPE STABILITY ANALYSES

9.1 Analytical Model Description

The next part of this study was to perform slope stability analyses that incorporate the hydraulic response of the levee – floodwall system. The software SLOPE\W was employed for this task. The pore water pressures generated by the SEEP\W finite element analyses are used by SLOPE\W when calculating Factors of Safety.

The software uses Limit Equilibrium Analysis (sum of forces and moments equal to zero) to calculate Factors of Safety by a number of methods used to determine the shape of the failure surface. The results included in these analyses were based on the Spencer method.

The critical failure surface search resulted in a non-circular (translational) surface, starting from the tip of the sheet pile and extending landward and exiting the toe. Both south and north sections show similar types of failure; with the north surface shorter and deeper than the south.

For the Slope Stability models developed at this stage, the determination of the gap formation and extent as a function of storm surge rise is not known. To account for the range of possible results, factors of safety were calculated for the cases where no gap was developed (therefore a failure surface extending to the waterside slope was used), and a second set of analyses assuming that a gap had formed throughout the length of the sheet pile. The cases of failure through the Sensitive Layer and the underlying intermixing zone were analyzed for the following values of permeability within the Marsh deposit: $1x10^{-3}$ cm/s, $1x10^{-4}$ cm/s, $1x10^{-5}$ cm/s, and $1x10^{-6}$ cm/s.

Consequently, the pore pressure field generated from the seepage analyses for each of the permeability and storm surge elevation values were used to calculate the Factor of Safety at different water elevations.

9.2 South Breach Results

The soil properties determined in Section 6 (median values) for unit weight, undrained shear strengths and friction angles were assigned to the different layers according to the stratigraphic interpretation on Section 4. Table 9-1 shows the material properties used in the slope stability calculations. Figure 9-1 shows the input geometry used for the stability analyses of the South Breach.

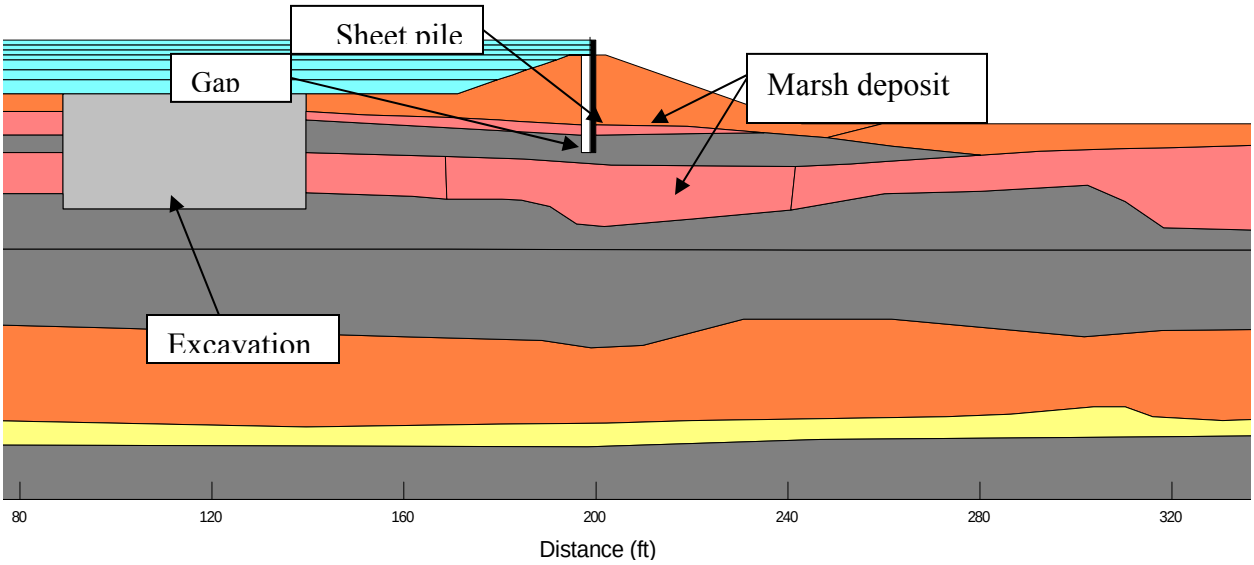


Figure 9-1. Analysis cross section for South breach.

Material	Shear Strength Parameter			
	Su (psf)	ϕ (deg)	Su/p'	γ (pcf)
Clays (Fill)	342			104
Marsh (under levee)	400			86
Marsh (free field)	250			86
Sands		30		110
Overconsolidated "Crust"	300			104
Deep Clays (CH)			0.26	104

Table 9-1. Material properties used for the slope stability models, South Breach.

Figure 9-2 shows the "median values" of results for factor of safety for the South Breach, for the cases of no gap formed, and the gap fully formed. Results from the analyses show that factors of safety drop below unity for all cases between surge water elevations +12 feet and +14 feet between 7:00 am and 8:00 am on August 29, 2005. The excavations backfilled with high permeability materials played a critical role in development of the lateral stability failure.

These results are in agreement with the reported and observed response of this levee - floodwall during hurricane Katrina. The forensic engineering observations indicate that overtopping occurred along this stretch of the floodwall (an overtopping scour trench was present). With the top of the floodwall at elevation +12 feet, overtopping would have been taking place during the last stage of the failure leading to breaching.

The case of no-gap and clay-filled excavation is stable even with a storm surge elevation of +14 feet. These results indicate if the excavations has been filled with proper backfill materials and the development of a gap between the waterside soils and the sheet piling had been inhibited, the floodwall and levee section would have been able to withstand overtopping. If splash-pads had

been provided on the protected side, this would have prevented soil erosion behind the supporting sheet piling and loss of support. With these additional measures, it is likely that the levee and floodwall section would have survived hurricane Katrina without failure.

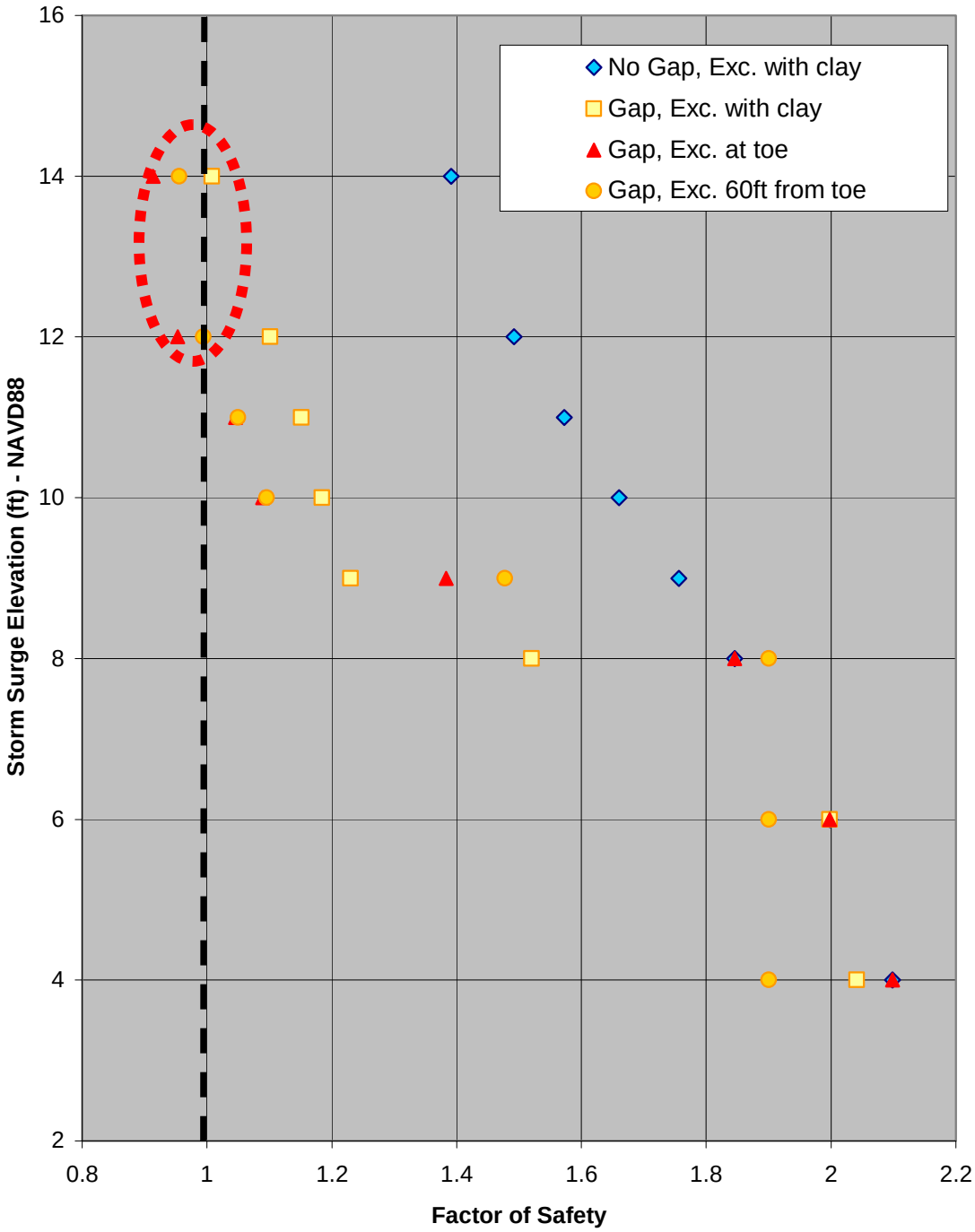


Figure 9-2. Factors of Safety versus storm surge elevations for the South Breach section.

Critical failure surfaces were determined to be non-circular surfaces starting at the tip of the sheet pile and progressing towards the landside toe along the Marsh deposit. Figure 9-3 shows the critical surface for a storm surge of +14 feet. The black arrows represent hydrostatic pressures acting against the sheet pile.

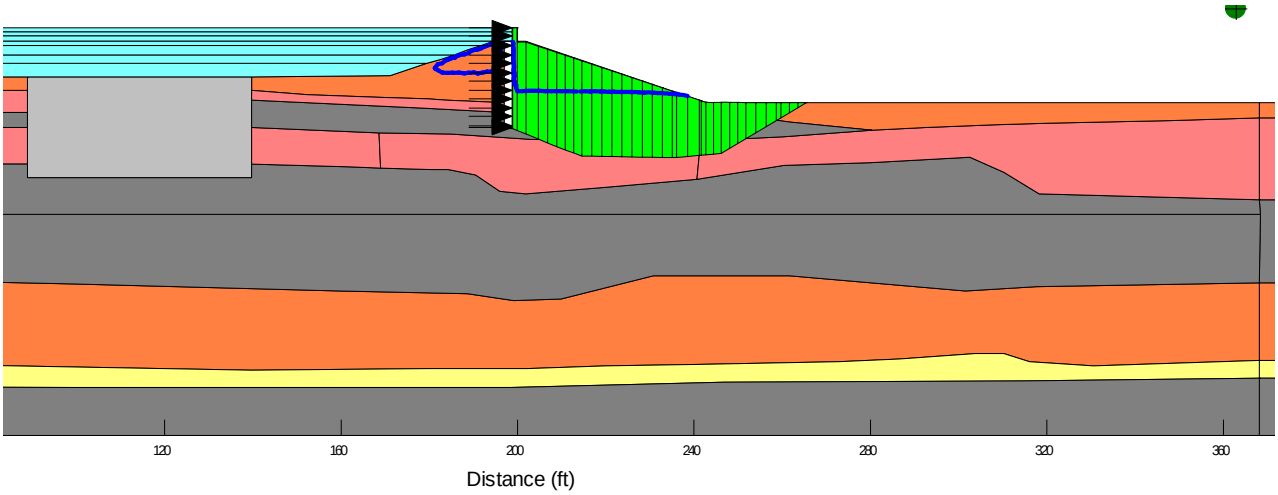


Figure 9-3. Critical shear surface for South Breach, storm surge +14 feet, Factor of Safety = 0.94.

9.3 North Breach Results

The soil properties determined in Section 5 (median values) for unit weight, undrained shear strengths and friction angles were assigned to the different layers according to the stratigraphic interpretation on Section 3. Table 9-2 shows the material properties used in the slope stability calculations. Figure 9-4 shows the input geometry used for the stability analyses of the South Breach.

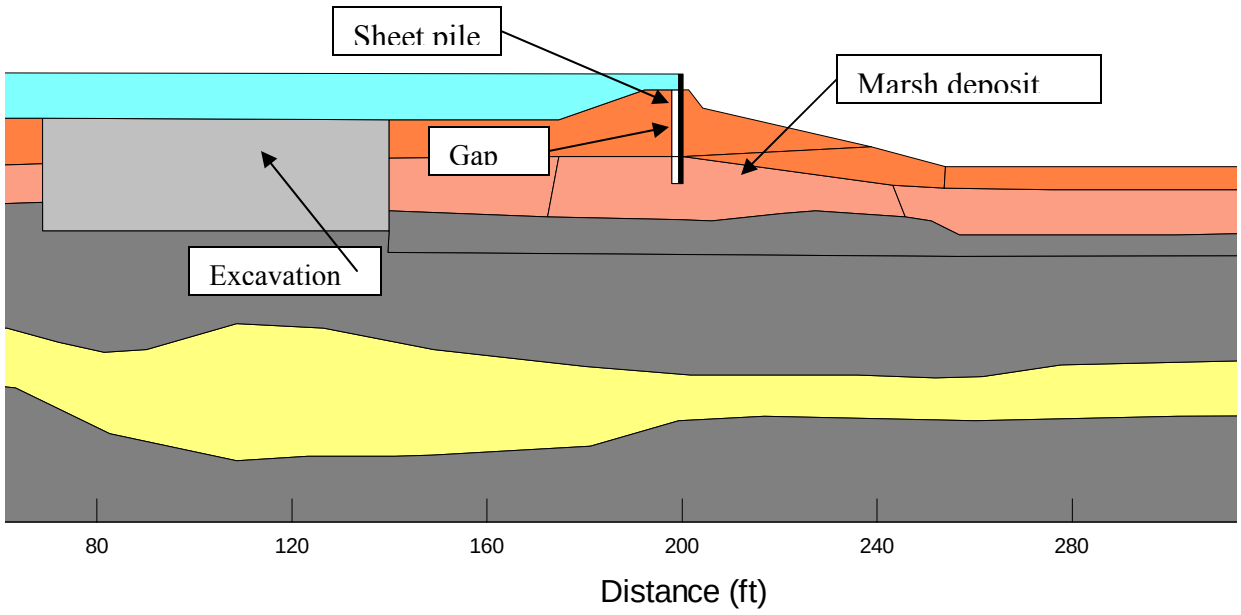


Figure 9-4. Analysis cross section for South breach.

Material	Shear Strength Parameter			
	Su (psf)	ϕ (deg)	Su/p'	γ (pcf)
Clays (Fill)	555			105
Marsh (under levee)	442			86
Marsh (free field)	250			86
Sands		30		110
Overconsolidated "Crust"	300			100
Deep Clays (CH)			0.26	110

Table 9-2. Material properties used for the slope stability models, North Breach.

Figure 9-5 shows the "median value" results of factor of safety for the North Breach, for the cases of no gap formed, and the waterside gap fully formed. Factors of safety are slightly lower than for the South Breach, dropping below unity between a surge water elevation of + 9 feet and +10 feet. These surge elevations developed at approximately 4:00 am to 5:00 am on August 29, 2005.

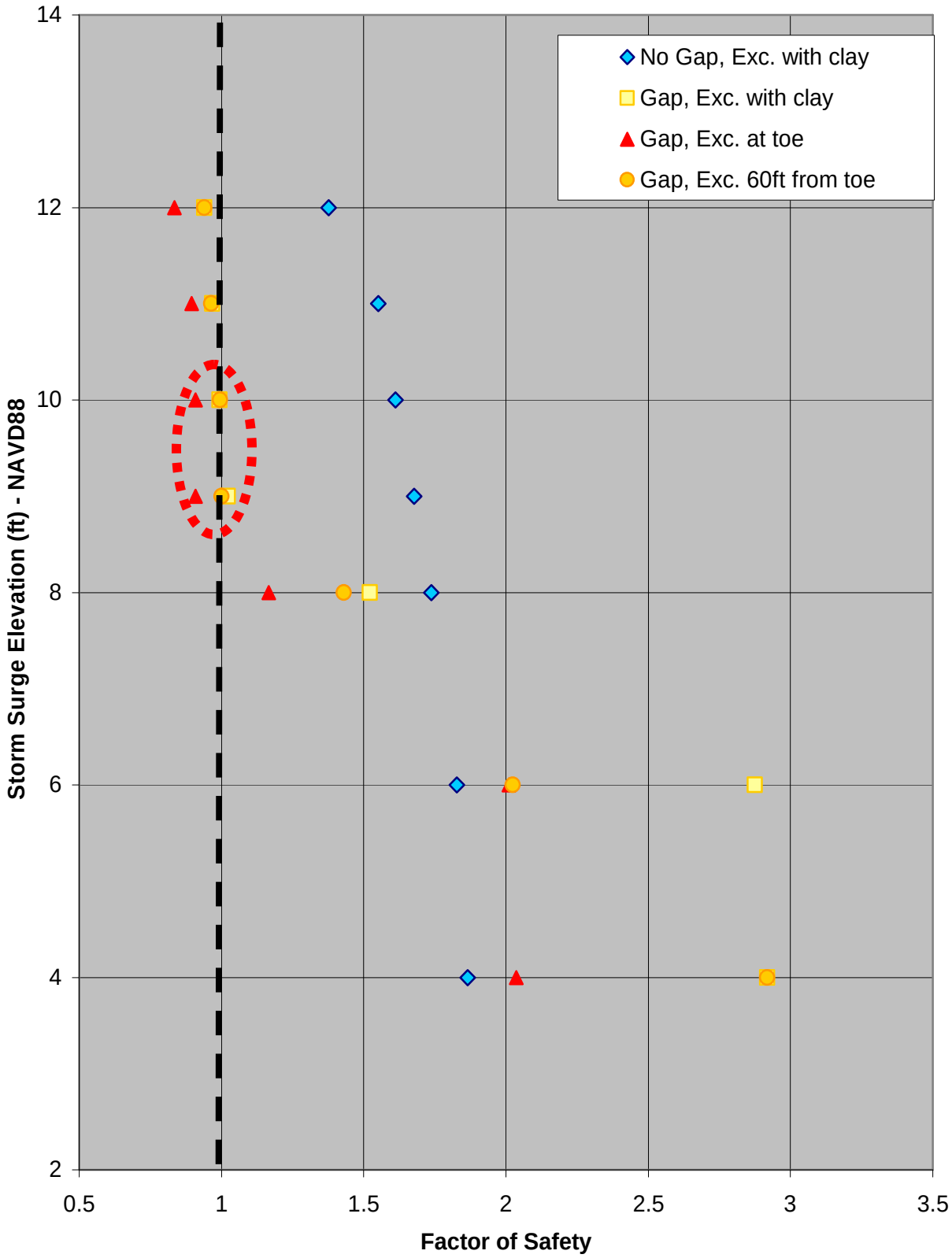


Figure 9-5. FOS versus storm surge elevation for the North Breach.

Figure 9-6 shows the critical shear surface for a storm surge of 12 feet, approximately at 7:00 am on August 29, 2005.

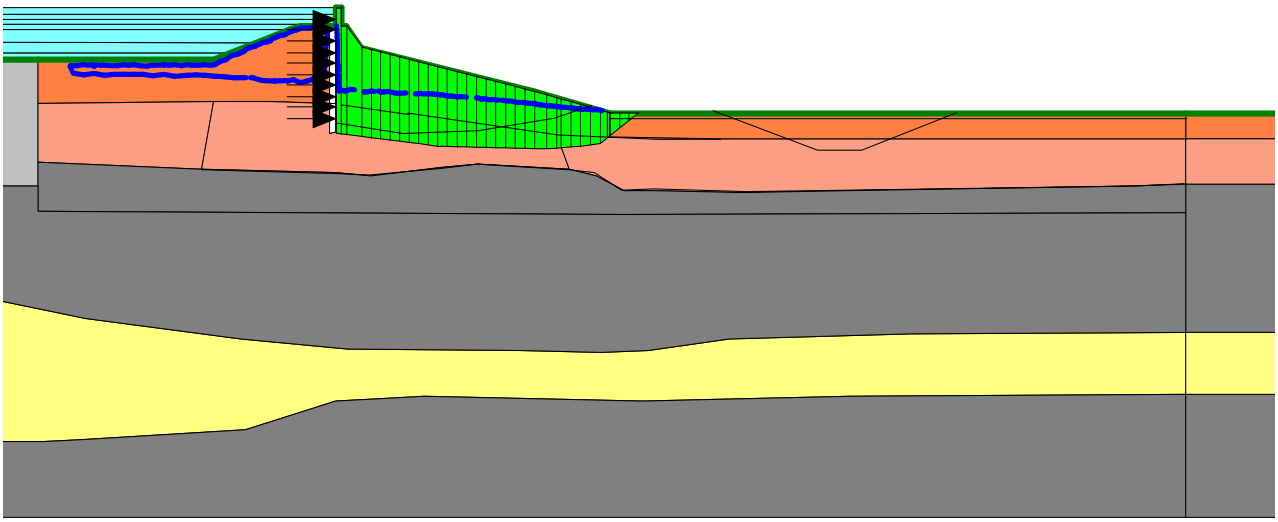


Figure 9-6. Critical shear surface for North breach, storm surge elevation + 12 feet, Factor of Safety = 0.80.

10. PROBABILILISTIC ANALYSES

Monte-Carlo simulations were performed using the statistical parameters summarized in Section 5 for unit weight and shear resistance of the soils involved in the breaches.

10.1 Statistical Analysis of Undrained Shear Strengths for South Breach

Statistical characteristics were calculated for the strength parameters, using the mean value as the expected value (E[X]), and determining standard deviation and coefficient of variation (ETL 1110-2-561, 2005). The strength parameters were assumed to be distributed in log-normal behavior, and probability density functions were generated for unit weights and undrained shear strengths of surficial clay, marsh deposits and deeper high-plasticity clays (CH). Appendix 13.2 details the available data and probability density functions obtained for each material from the laboratory testing.

The probability density functions (pdf) were created using the following formula:

Log-Normal Distribution:

$$f(x) = \frac{e^{-((\ln(x)/E[x])^2/2*\sigma_x^2)}}{x*\sigma_x*\sqrt{2*\pi}}$$

Where:
f(x): Probability value of (x)
σx: Standard deviation of x
E[x]: Expected value (mean) of x
The Log-normal distributions were created by Probabilistic package of SLOPE-W.

The statistical parameters are calculated as follows:

Standard deviation of lognormal variable X,

$$\sigma x = X_{50}\left[\exp(\sigma^2{}_{\ln X}) - 1\right]^{0.5}$$

Coefficient of Variation,

$$Vx = \left[\exp(\sigma^2_{\ln X}) - 1\right]^{0.5}$$

and

$$\sigma \ln X = \left[\ln(1 + Vx^2)\right]^{0.5}$$

Where not enough data for the calculation of COV's was available, a COV of 30% was assumed for clays, silts and sands; and 40% for Marsh soils. This 40% was obtained from published values (Duncan, 2000; Bea, 2005).

Sands are believed to have little influence on the breaches along the IHNC. No laboratory data is available; therefore strength (friction angles) values will be assumed for these materials.

Tables 10-1 and 10-2 summarize the results of the statistical calculations for the area under the levee fill and away from the toe, respectively.

Material	Elevation Interval, ft		Median Su	VX	Median γ	VX
	From	To	(psf)		(pcf)	
Clays	+9	-5	342	0.55	104	0.05
Upper Marsh	-5	-8	400	*0.4*	*86*	*0.4*
Gray Clay	-8	-13	362	*0.08*	*95*	*0.3*
Lower Marsh	-13	-25	395	*0.34*	*86*	*0.4*
Clays	-25	-45	Su/p': 0.26	0.3	104	0.03
Lean Clays	-45	-64	627	0.21	113	0.06
Sand	-64	-68	ϕ: 30	--	110	--
Deep Clays	-68	n/a	800	--	110	--

Table 10-1. Distribution of Su and total unit weight for South Breach. Under Centerline of Levee.

Material	Elevation Interval, ft (NAVD88)		Mean Su	VX	Median γ	VX
	From	To	(psf)		(pcf)	
Clays	-4	-11	380	0.58	91	0.05
Lower Marsh	-11	-19.5	250	0.62	86	0.13
Gray Clay	-19.5	-43	Su/p': 0.26	0.3	104	0.03
Lean Clay and Silt	-43	-63	291	0.38	115	0.1
Sand	-63	-68	ϕ: 30	--	110	--
Deep Clays	-68	n/a	800	--	110	--

Table 10-2. Distribution of Su for South Breach. Away from toe of levee.

10.2 Statistical Analysis of Undrained Shear Strengths for North Breach

Tables 10-3 and 10-4 summarize the results of the statistical calculations for the area under the levee fill and away from the toe, respectively.

Material	Elevation Interval, ft (NAVD88)		Median Su	VX	Median γ	VX
	From	To	(psf)		(pcf)	
Clays (CL, CH)	+9	-5	555	0.36	*105*	*0.3*
Marsh (Peat)	-5	-18	442	0.23	86	0.13
Gray Clay (CH) – OC zone	-18	-25	300	0.3	100	0.3
Clays (CH)	-25	-50	Su/p': 0.26	0.3	110	0.3
Sand	-50	-59	□□30	--	110	--
Deep Clays (CH)	-59	n/a	800	--	104	--

Table 10-3. Distribution of undrained shear strength and unit weight for North Breach. Under Centerline of Levee.

Material	Elevation Interval, ft (NAVD88)		Median Su	VX	Median □	VX
	From	To	(psf)		(pcf)	
Clays (CL, CH)	-7	-11	338	0.3	95	0.3
Marsh (Peat)	-11	-21	250	0.22	86	0.13
Gray Clay (CH) – OC zone	-21	-26	300	0.3	100	0.3
Clays (CH)	-26	-50	Su/p': 0.26	0.3	110	0.3
Sand	-50	-59	□□30	--	110	--
Deep Clays (CH)	-59	n/a	800	--	104	--

Table 10-4. Distribution of undrained shear strength and unit weight for North Breach. Away from toe of levee.

The foregoing statistical parameters were added as input to the stability analyses and new analyses were performed assigning the probability density functions for every material. The individual probability density functions for each material are documented in Appendix 13.2.

10.3 Results of Probability of Failure Analyses

Figures 10-1 and 10-2 show plots of probability of failure (POF, Pf) for the several failure mechanisms involved in the South Breach and North Breach, respectively.

The probabilistic assessment performed for the stability models show that for the conditions with excavations backfilled with permeable backfill the probabilities of failure are larger than 60% for the North Breach when the storm surge elevation rises above elevation 12 to 13 feet. This is the point at which surge overtopping would have initiated leading to backside erosion of the levee. These results indicate that it is very likely this section of the levee-floodwall failed after overtopping. The results also show that the probabilities of failure would have been negligible (less than 2 to 3 %) for the condition of the EBIA excavations backfilled with impermeable materials.

The probabilistic assessment performed for the stability models show that the probabilities of failure are larger than 60% for the North Breach when the storm surge elevation rises above elevation 9 to 11 feet. This indicates that it is very likely this section of the levee – floodwall failed before overtopping. The results also show that the probabilities of failure would have been very small (less than 10 to 11 %) for the condition of the EBIA excavations backfilled with impermeable materials.

Tables 10-5 and 10-6 summarize the results of the Monte Carlo simulations for the South Breach and North Breach, respectively.

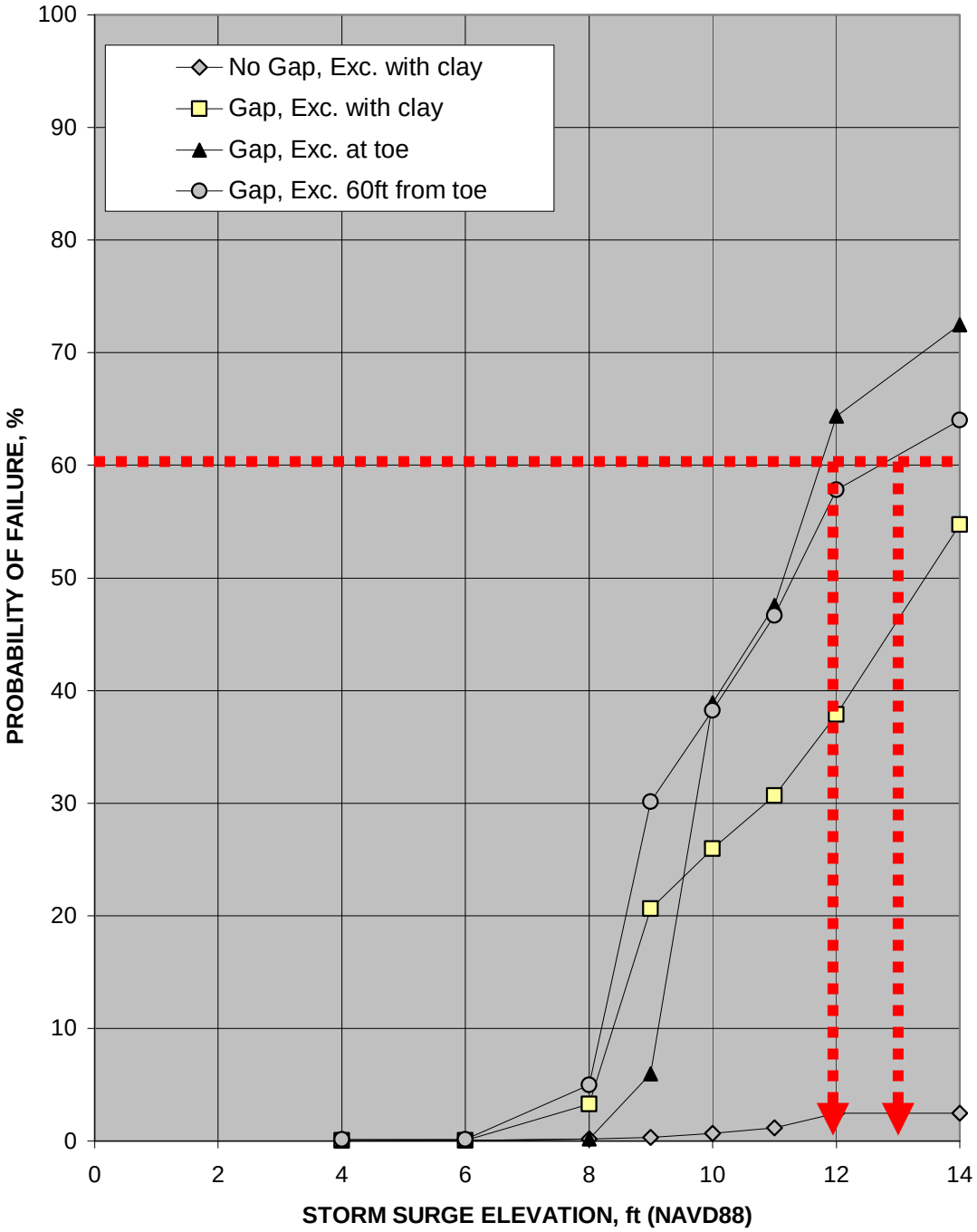


Figure 10-1. Probability of Failure for South Breach.

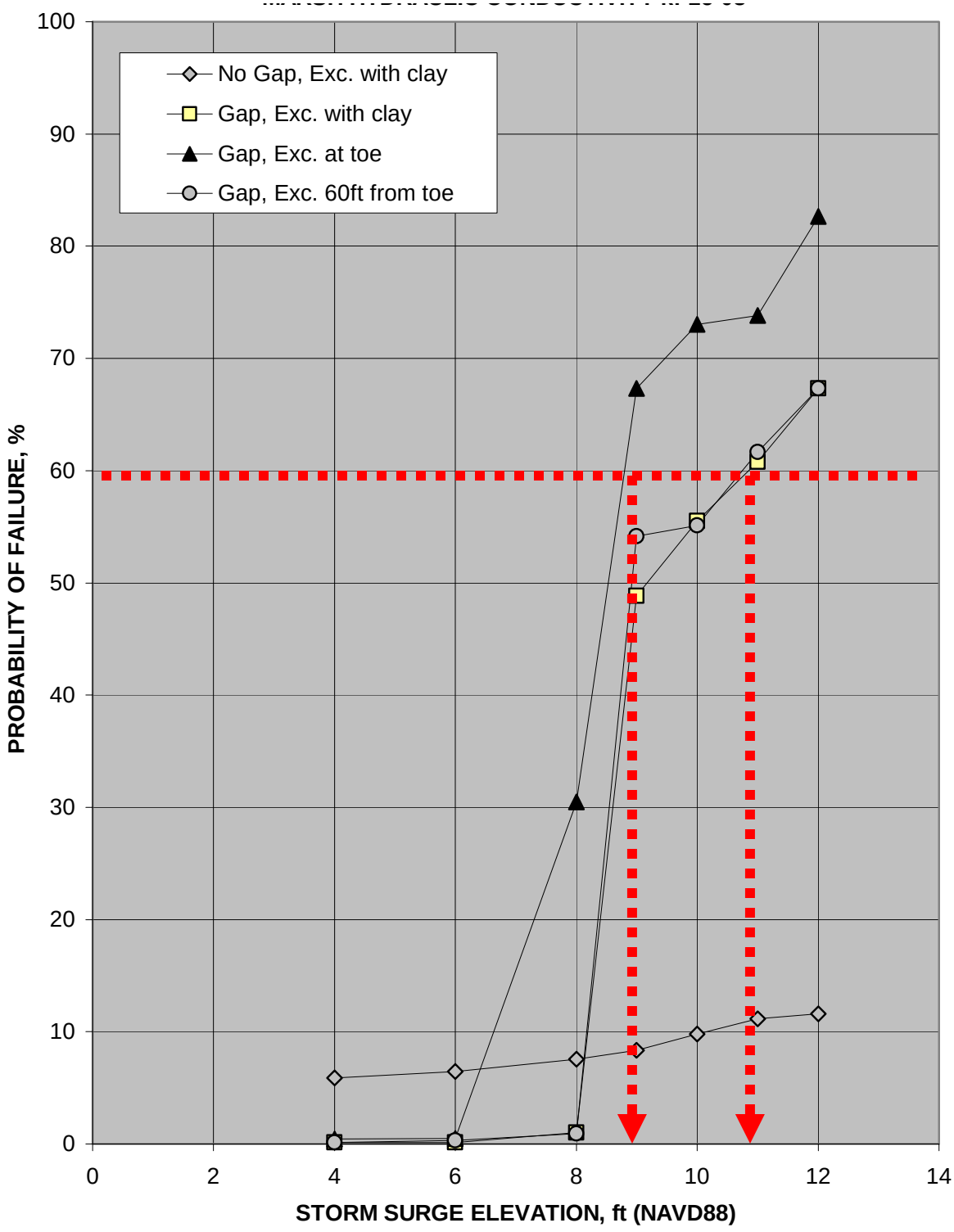


Figure 10-2. Probability of Failure for North Breach.

Storm Surge (ft)	Failure Mode	Median FOS	Min. FOS	Max. FOS	σ FOS	Pf (%)
14	Excavation at toe + Gap	0.91	0.48	2.15	0.20	72.5
	Excavation 60ft from toe + Gap	0.96	0.50	2.25	0.21	64.0
	Clay filled excavation + Gap	1.01	0.49	2.35	0.23	54.7
	Clay filled excavation + No Gap	1.49	0.66	3.44	0.32	2.5
12	Excavation at toe + Gap	0.95	0.50	2.24	0.21	64.3
	Excavation 60ft from toe + Gap	1.0	0.52	2.34	0.22	57.8
	Clay filled excavation + Gap	1.10	0.53	2.57	0.25	37.9
	Clay filled excavation + No Gap	1.49	0.66	3.4	0.32	2.5
11	Excavation at toe + Gap	1.05	0.55	2.5	0.23	47.5
	Excavation 60ft from toe + Gap	1.06	0.55	2.47	0.23	46.6
	Clay filled excavation + Gap	1.15	0.56	2.68	0.27	30.6
	Clay filled excavation + No Gap	1.57	0.70	3.62	0.34	1.15
10ft	Excavation at toe + Gap	1.09	0.57	2.5	0.24	38.9
	Excavation 60ft from toe + Gap	1.1	0.57	2.6	0.24	38.2
	Clay filled excavation + Gap	1.18	0.44	2.71	0.27	25.9

	Clay filled excavation + No Gap	1.66	0.74	3.8	0.36	0.6
9ft	Excavation at toe + Gap	1.38	0.62	3.17	0.29	6.0
	Excavation 60ft from toe + Gap	1.48	0.66	3.4	0.31	2.6
	Clay filled excavation + Gap	1.23	0.5	2.8	0.28	20.6
	Clay filled excavation + No Gap	1.75	0.79	4.0	0.38	0.30
8ft	Excavation at toe + Gap	1.84	0.83	4.25	0.40	0.20
	Excavation 60ft from toe + Gap	1.90	0.85	4.38	0.41	0.15
	Clay filled excavation + Gap	1.52	0.57	3.48	0.35	3.3
	Clay filled excavation + No Gap	1.85	0.83	4.25	0.40	0.20
6ft	Excavation at toe + Gap	1.99	0.96	5.7	0.43	0.05
	Excavation 60ft from toe + Gap	1.90	0.85	4.38	0.41	0.15
	Clay filled excavation + Gap	2.0	0.96	5.7	0.43	0.05
	Clay filled excavation + No Gap	2.0	0.96	5.7	0.43	0.05

Table 10-5. Results of the Monte Carlo simulations for South Breach.

Storm Surge (ft)	Failure Mode	Median FOS	Min. FOS	Max. FOS	σ FOS	Pf (%)
12	Excavation at toe + Gap	0.84	0.36	3.13	0.21	82.6
	Excavation 60ft from toe + Gap	0.94	0.53	2.96	0.17	67.3
	Clay filled excavation + Gap	0.94	0.53	2.96	0.17	67.3
	Clay filled excavation + No Gap	1.37	0.65	8.40	0.39	11.6
11	Excavation at toe + Gap	0.90	0.37	3.3	0.22	73.8
	Excavation 60ft from toe + Gap	0.95	0.55	3.04	0.18	61.7
	Clay filled excavation + Gap	0.97	0.56	3.05	0.18	60.7
	Clay filled excavation + No Gap	1.55	0.49	6.01	0.54	11.15
10	Excavation at toe + Gap	0.91	0.42	3.3	0.22	73.0
	Excavation 60ft from toe + Gap	1.0	0.57	3.14	0.18	55.1
	Clay filled excavation + Gap	1.0	0.57	3.14	0.18	55.0
	Clay filled excavation + No Gap	1.61	0.50	6.5	0.59	9.8
9ft	Excavation at toe + Gap	0.94	0.38	3.48	0.23	67.3
	Excavation 60ft from toe + Gap	1.00	0.58	3.15	0.18	54.2
	Clay filled excavation + Gap	1.02	0.59	3.22	0.19	48.8

	Clay filled excavation + No Gap	1.68	0.50	7.4	0.63	8.35
8ft	Excavation at toe + Gap	1.17	0.47	4.33	0.29	30.5
	Excavation 60ft from toe + Gap	1.43	0.88	4.8	0.29	0.9
	Clay filled excavation + Gap	1.52	0.87	4.8	0.28	1.0
	Clay filled excavation + No Gap	1.74	0.51	8.4	0.68	7.5
6ft	Excavation at toe + Gap	2.01	0.79	6.9	0.54	0.5
	Excavation 60ft from toe + Gap	2.91	0.78	11.2	0.91	0.15
	Clay filled excavation + Gap	2.92	0.87	11.2	0.92	0.2
	Clay filled excavation + No Gap	1.82	0.52	11.3	0.78	5.9

Table 10-6. Results of the Monte Carlo simulations for North Breach.

11. SUMMARY OF RESULTS AND CONCLUSIONS

Marsh permeability is a key player in the hydraulic behavior and instability of the breaches along the East levee of the IHNC-Lower Ninth Ward. The evident uncertainties that the proper assessment of hydraulic conductivity carries have led to the parametric study performed in this report. A wide range of permeabilities (10^{-3} to 10^{-6} cm/s) were used to characterize the Marsh deposit and compute the response of the levee and underlying materials.

The South and North Breaches were modeled using finite element and limit equilibrium analyses and incorporated two main differences with published analyses (ILIT 2006, IPET 2007):

- **Presence of excavations on the waterside of the levee.** Previous models did not include the effect of the very deep excavations that took place during the 1990s; their influence on the levee response to the storm surge is that it brings the IHNC right to the waterside toe of the levee. The 100 to 200ft between the levee and the shore of the canal are now reduced to a couple of tens of feet, meaning that the full hydraulic load of the surge on IHNC will be directly applied below the toe of the levee to the Marsh deposits, known for their high horizontal permeability.
- **Generation of pore pressure through the gap** formed between the sheet pile and the embankment on the canal side to allow direct communication of the rising surge water with the soils supporting the levee - floodwall.

The seepage analyses show that pore water pressures develop quickly and near-steady state conditions are reached within less than 30 hours of the initiation of the surge, starting on August 28, 2005. Calculated pore water pressures and hydraulic gradients are within less than 20 to 30 % of those

computed for a hypothetical steady state at the water elevation at time of failure (between +9 and 11ft for the North Breach, and +12 and +14ft for the South Breach).

The different relative permeabilities considered between Marsh and surrounding soils yield differences of pore pressure on soft layers that control stability (Marsh). Higher permeabilities on the Marsh deposit give slightly larger pore water pressures, and consequently reduce the effective stresses that control shear strengths.

Another factor influenced by increased pore water pressures is the potential for "blowout" failures. This type of failure can be produced by uplift pressures that are equal or larger than the in-situ overburden stresses; the case was evidenced more critically at the North Breach, at the thin clay layer located on the landside toe of the levee.

Sudden water loads on embankments impose pore water pressures inside the levee and its foundation soils, generating excess pressures along fine grained blankets and deposits with relatively low permeability. A slope stability analysis using an assumed phreatic surface (even if it were drawn correctly) would underestimate the pore water pressures acting on levee and underlying soils. It is clear that a seepage analyses (steady state or transient) are needed to capture a more realistic behavior of the development of pore water pressures and consequently slope stability.

It was observed that the calculations here differ from the ILIT and IPET reports. The main difference is that the transient model considered the gap being opened and transporting the water heads directly to the back of the sheet-pile, thus applying "instant" pressures to the model at the tip of the sheet-pile. This is why more than 80% of the steady state pressures are developed within the system, compared with the 60 to 70% calculated by IPET on their seepage modeling section. Seepage modeling

performed by ILIT did not consider the formation of the gap in the pressure calculations (it was only considered for stability calculations).

It can be concluded that the breaches along the East side of the IHNC-Lower Ninth Ward during hurricane Katrina were influenced significantly by the excavations present on the waterside. The formation of the gap between the sheet pile and levee soils also played an important role. These two factors are as influential as the levee and subsoil internal geometry and strength characteristics.

The critical failure surface was determined to be a translational surface through the Marsh deposit. Slightly higher factors of safety were found to occur through the underlying soft gray clay deposits. The fact that a slightly overconsolidated crust was present in the interface Marsh-Clay might have contributed for the movement to occur through the Marsh layer.

The calculated Factors of Safety drop below unity at a storm surge elevation of approximately +9 feet for the North Breach, and between +12 and +13 feet for the South Breach.

12. REFERENCES

Bea, R. G., (2006), *Connecting the Lower Ninth Ward "Dots",* Center for Catastrophic Risk Management, University of California, Berkeley.

Beckwith, C. W., Baird, A. J., and Heathwaite, A. L., (2003), *Anisotropy and Depth-related Heterogeneity of Hydraulic Conductivity in a Bog Peat. I: Laboratory Measurements*, Hydrological Processes, 17, pp. 89-101. Published online 13 November 2002 in Wiley InterScience (www.interscience.wiley.com) DOI: 10.1002/hyp.1116.

Clymo, R. S., (2004), *Hydraulic Conductivity of Peat at Ellergower Moss, Scotland*, Hydrological Processes, 18, pp. 261-274. Published online in Wiley InterScience (www.interscience.wiley.com) DOI: 10.1002/hyp.1374.

Dr. Robert G. Bea, personal communications on September through December, 2007.

Egglesmann, R., (1975), *Physical Effects of Drainage in Peat Soils of the Temperate Zone and their Forecasting*, pp. 69-76.

Gagliano, S., (2005), *Effects of Geological Faults on Levee Failures in South Louisiana,* Prepared for presentation and discussion, U.S. Senate Committee on Environment and Public Works, Washington D.C.

Hemond, H. F., and Fifield, J. L., (1982), *Subsurface Flow in Salt Marsh Peat: A Model and Field Study*, Limnol Oceanography, 27(1), pp. 126-136.

Hogan, J. M., Van der Kamp, G. Barbour, S. L., Scmidth, R. (2006), *Field Methods for Measuring Hydraulic Properties of Peat Deposits*, Hydrological Processes, 20. pp. 3635-3649. Published online in Wiley InterScience (www.interscience.wiley.com) DOI: 10.1002/hyp.6379.

GEOSLOPE (2004), *Complete set of Manuals,* John Kran (Edit.), Calgary, Alberta, Canada.

IPET – Interagency Performance Evaluation Task Force (2007), *Final Report on the Interagency Performance Evaluation Task Force, Volume V, The Performance – Internal Drainage and Pumping*.

IPET – Interagency Performance Evaluation Task Force (2007), *Final Report on the Interagency Performance Evaluation Task Force, Volume II, Geodetic Vertical and Water Elevation Datums.*

Mesri, G. and Ajlouni, M., (2007), *Engineering Properties of Fibrous Peats*, ASCE Publication, available online at: www.pubs.asce.org, DOI: 10.1061/(ASCE) 1090-0241 (2007).

Ronkanen, A. and Kløve, B., (2005), *Hydraulic Soil Properties of Peatlands Treating Municipal Wastewater and Peat Harvesting Runoff*, Finnish Peatland Society, Helsinki 2005.

Seed, R. B., Bea, R. G., Abdelmalak, R. I., Athanasopoulos, A. G., Boutwell, G. P., Bray, J. D., Briaud, J. L., Cheung, C., Cobos-Roa, D., Cohen-Waeber, J., Collins, B. D., Ehrensing, L., Farber, D., Hanemann, M., Harder, L. F., Inkabi, K. S., Kammerer, A. M., Karadeniz, D., Kayen, R.E., Moss, R. E. S., Nicks, J., Nimmala, S., Pestana, J. M., Porter, J., Rhee, K., Riemer, M. F., Roberts, K., Rogers, J. D., Storesund, R., Govindasamy, A. V., Vera-Grunauer, X., Wartman, J. E., Watkins, C. M., Wenk Jr., E., and Yim, S. C. (2006), *Investigation of the Performance of the New Orleans Flood Protection Systems in Hurricane Katrina on August 29, 2005*, Final Report to the National Science Foundation, under Grants CMS-0413327 and CMS-0611632, July 31, 2006, 742 p.

Surridge, B. W., Baird, A. J., and Heathwaite, A. L., (2005), *Evaluating the Quality of Hydraulic Conductivity Estimates from Piezometer Slug Tests in Peat*, Hydrological Processes, 19, pp. 1227-1244. Published online in Wiley InterScience (www.interscience.wiley.com) DOI: 10.1002/hyp.5653.

Van der Schaaf, S., (2003), *A Single Well Pumping and Recovery Test to Measure In Situ Acrotelm Transmissivity in Raised Bogs*, Journal of Hydrology 290 (2004) pp. 152-160, Available online at www.sciencedirect.com

USACE (1969), *Design Memorandum DM03, Chalmette Area Plan, Lake Pontchartrain and Vicinity.*

USACE (2000), *Engineer Memorandum 1110-2-1913 Design and Construction of Levees, Appendix B.*

USACE (2001), *4025 Approval of the: Sampling and Analysis Plan Project Ste Development and Remedial Action of East Bank Industrial Area Inner Harbor Navigation Canal Lock Replacement Project*, New Orleans, Louisiana, February.

USACE (2002), *4025 Approval of the RECAP Work Plan Amendment – Bank Material Remediation Inner Harbor Navigational Canal – East Bank Industrial Area*, August.

Washington Group International (2005), Technical Completion Report and Record Drawings Inner Harbor Navigation Canal – East Bank Industrial Area, Report to USACE, WGI079460, July.

13. APPENDICES

13.1 Available soil boring and laboratory tests utilized in analyses

Document	Boring Year	Datum	Boring ID	Boring Type	Top Elevation	Bottom Elevation	Boring Length	TOP EL. in NAVD88	Latitude	Longitude	Notes
Lake Pontchartrain, LA. And Vicinity Chalmette Area Plan, DM03	1965	MSL	NO-2-U	n/a	9.2	-75	84.2	8.95			
Lake Pontchartrain, LA. And Vicinity Chalmette Area Plan, DM03	1965	MSL	NO-2-UT	n/a	1.5	-37	38.5	1.25			
Lake Pontchartrain, LA. And Vicinity Chalmette Area Plan, DM03	1965	MSL	NO-3	n/a	7.2	-82.5	89.7	6.95			
Lake Pontchartrain, LA. And Vicinity Chalmette Area Plan, DM03	1965	MSL	NO-3T	n/a	-3.5	-85	81.5	-3.75	29.968265	-90.024531	
Lake Pontchartrain, LA. And Vicinity Chalmette Area Plan, DM03	1965	MSL	NO-4	n/a	8.6	-55	63.6	8.35	29.970578	-90.023351	
Lake Pontchartrain, LA. And Vicinity Chalmette Area Plan, DM03	1965	MSL	NO-4T	n/a	-2	-83	81	-2.25	29.970554	-90.023198	
Lake Pontchartrain, LA. And Vicinity Chalmette Area Plan, DM03	1965	MSL	NO-5	n/a	9.2	-88	97.2	8.95	29.973277	-90.02246	
Lake Pontchartrain, LA. And Vicinity Chalmette Area Plan, DM03	1965	MSL	NO-6U	n/a	4	-76	80	3.75	29.97567	-90.021664	
Lake Pontchartrain, LA. And Vicinity Chalmette Area Plan, DM03	1965	MSL	NO-6UT	n/a	-3	-42	39	-3.25	29.97563	-90.02512	
Lake Pontchartrain, LA. And Vicinity Chalmette Area Plan, DM03	1965	MSL	NO-7T	n/a	-4	-78	74	-4.25	29.976152	-90.021239	
Lake Pontchartrain, LA. And Vicinity Chalmette Area Plan, DM03	1965	MSL	NO-8	n/a	7.5	-79	86.5	7.25	29.979321	-90.023398	
Lake Pontchartrain, LA. And Vicinity Chalmette Area Plan, DM03	1965	MSL	NO-9	n/a	-11	-71	60	-11.25	29.980242	-90.02827	
Lake Pontchartrain, LA. And Vicinity Chalmette Area Plan, DM03	1965	MSL	NO-9A	n/a	3	-70	73	2.75	29.980392	-90.02149	
Lake Pontchartrain LA and Vicinity, Lake Pontchartrain Area, 1971	1971	MSL	5EF	5" Undist.	-1	-80	79	-1.25	29.979932	-90.020376	
Lake Pontchartrain LA and Vicinity, Lake Pontchartrain Area, 1971	1971	MSL	6UEF	5" Undist.	-5	-108	103	-5.25	29.980211	-90.020504	
IPET webpage	2005	NAVD88	B-2	3" Undist.	0	-98	98	0	29 58 11.4	90 01 23.22	Datum Uncertain
IPET webpage	2005	NAVD88	B-3	3" Undist.	0	-98	98	0	29 58 16.2	90 01 21.54	Datum Uncertain
IPET webpage	2005	NAVD88	B-4	3" Undist.	0	-98	98	0	29 58 30.18	90 01 38.58	Datum Uncertain
IPET webpage	2005	NAVD88	B-5	3" Undist.	0	-98	98	0	29 58 30.54	90 01 17.46	Datum Uncertain
IPET webpage	2005	NAVD88	B-6	3" Undist.	0	-98	98	0	29 58 35.58	90 01 15.66	Datum Uncertain
IPET webpage	2005	NAVD88	B-7	3" Undist.	0	-98	98	0	29 58 40.56	90 01 14.1	Datum Uncertain
IPET webpage	2005	NAVD88	B-8	3" Undist.	0	-98	98	0	29 58 45.72	90 01 12.18	Datum Uncertain
IPET webpage	2005	NAVD88	IHBR-10CON	CPT	0	-80	80	0	29 58 30.7	90 01 17.9	Datum Uncertain
IPET webpage	2005	NAVD88	IHBR-11CON	CPT	0	-80	80	0	29 58 36.3	90 01 16.1	Datum Uncertain
IPET webpage	2005	NAVD88	IHBR-12CON	CPT	0	-80	80	0	29 58 24.1	90 01 20.1	Datum Uncertain
IPET webpage	2005	NAVD88	IHBR-14CON	CPT	0	-80	80	0	29 58 22.9	90 01 19.9	Datum Uncertain
IPET webpage	2005	NAVD88	IHBR-15CON	CPT	0	-80	80	0	29 58 16.8	90 01 21.1	Datum Uncertain
IPET webpage	2005	NAVD88	IHBR-16CON	CPT	0	-80	80	0	29 58 14.4	90 01 22.7	Datum Uncertain
IPET webpage	2005	NAVD88	IHBR-1CON	CPT	0	-80	80	0	29 58 45.8	90 01 13.7	Datum Uncertain
IPET webpage	2005	NAVD88	IHBR-2CON	CPT	0	-80	80	0	29 58 43.5	90 01 12.8	Datum Uncertain
IPET webpage	2005	NAVD88	IHBR-3CON	CPT	0	-80	80	0	29 58 14.0	90 01 14.1	Datum Uncertain
IPET webpage	2005	NAVD88	IHBR-5CON	CPT	0	-80	80	0	29 58 14.0	90 01 23.6	Datum Uncertain
IPET webpage	2005	NAVD88	IHBR-6CON	CPT	0	-80	80	0	29 58 15.2	90 01 23.8	Datum Uncertain
IPET webpage	2005	NAVD88	IHBR-7CON	CPT	0	-80	80	0	29 58 16.7	90 01 23.4	Datum Uncertain
IPET webpage	2005	NAVD88	IHBR-8CON	CPT	0	-80	80	0	29 58 18.7	90 01 22.6	Datum Uncertain
IPET webpage	2005	NAVD88	IHBR-9CON	CPT	0	-80	80	0	29 58 20.4	90 01 22.1	Datum Uncertain
ILIT Final Report, Appendix B and C	2006	NAVD88	IHNC-S-BOR1	3" Undist.	0.93		0.93	0.93	29.9786	90.0202	
ILIT Final Report, Appendix B and C	2006	NAVD88	IHNC-S-CON-1	Continuous	-3.4		-3.4	-3.4	29.97038	90.02313	
ILIT Final Report, Appendix B and C	2006	NAVD88	IHNC-S-CON-2	Continuous	-2.7		-2.7	-2.7	29.97118	90.0227	
ILIT Final Report, Appendix B and C	2006	NAVD88	IHCN-S-CON-3	Continuous	-2.3		-2.3	-2.3	29.97246	90.0225	
ILIT Final Report, Appendix B and C	2006	NAVD88	IHNC-N-BOR-1	3" Undist.	-3.4		-3.4	-3.4	29.97039	90.02315	
ILIT Final Report, Appendix B and C	2006	NAVD88	IHNC-S-CPT-1	CPT	-0.9	-62	61.1	-0.9	29.97035	90.02314	
ILIT Final Report, Appendix B and C	2006	NAVD88	IHNC-S-CPT-2	CPT	-2.7	-67	64.3	-2.7	29.97126	90.02292	
ILIT Final Report, Appendix B and C	2006	NAVD88	IHNC-S-CPT-3	CPT	-2.3	-71	68.7	-2.3	29.97248	90.02257	
ILIT Final Report, Appendix B and C	2006	NAVD88	IHNC-N-CPT-1	CPT	-3.38	-54	50.62	-3.38	29.9787	90.02049	

Document	Boring Year	Datum	Boring ID	Boring Type	Top Elevation	Bottom Elevation	Boring Length	TOP EL. in NAVD88	Latitude	Longitude	Notes
Lake Pontchartrain, LA. And Vicinity Chalmette Area Plan, DM03	1965	MSL	NO-2-U	n/a	9.2	-75	84.2	8.95			
Lake Pontchartrain, LA. And Vicinity Chalmette Area Plan, DM03	1965	MSL	NO-2-UT	n/a	1.5	-37	38.5	1.25			
Lake Pontchartrain, LA. And Vicinity Chalmette Area Plan, DM03	1965	MSL	NO-3	n/a	7.2	-82.5	89.7	6.95			
Lake Pontchartrain, LA. And Vicinity Chalmette Area Plan, DM03	1965	MSL	NO-3T	n/a	-3.5	-85	81.5	-3.75	29.968265	-90.024531	
Lake Pontchartrain, LA. And Vicinity Chalmette Area Plan, DM03	1965	MSL	NO-4	n/a	8.6	-55	63.6	8.35	29.970578	-90.023351	
Lake Pontchartrain, LA. And Vicinity Chalmette Area Plan, DM03	1965	MSL	NO-4T	n/a	-2	-83	81	-2.25	29.970554	-90.023198	
Lake Pontchartrain, LA. And Vicinity Chalmette Area Plan, DM03	1965	MSL	NO-5	n/a	9.2	-88	97.2	8.95	29.973277	-90.02246	
Lake Pontchartrain, LA. And Vicinity Chalmette Area Plan, DM03	1965	MSL	NO-6U	n/a	4	-76	80	3.75	29.97567	-90.021664	
Lake Pontchartrain, LA. And Vicinity Chalmette Area Plan, DM03	1965	MSL	NO-6UT	n/a	-3	-42	39	-3.25	29.97563	-90.02512	
Lake Pontchartrain, LA. And Vicinity Chalmette Area Plan, DM03	1965	MSL	NO-7T	n/a	-4	-78	74	-4.25	29.976152	-90.021239	
Lake Pontchartrain, LA. And Vicinity Chalmette Area Plan, DM03	1965	MSL	NO-8	n/a	7.5	-79	86.5	7.25	29.979321	-90.023398	
Lake Pontchartrain, LA. And Vicinity Chalmette Area Plan, DM03	1965	MSL	NO-9	n/a	-11	-71	60	-11.25	29.980242	-90.02827	
Lake Pontchartrain, LA. And Vicinity Chalmette Area Plan, DM03	1965	MSL	NO-9A	n/a	3	-70	73	2.75	29.980392	-90.02149	
Lake Pontchartrain LA and Vicinity, Lake Pontchartrain Area, 1971	1971	MSL	5EF	5" Undist.	-1	-80	79	-1.25	29.979932	-90.020376	
Lake Pontchartrain LA and Vicinity, Lake Pontchartrain Area, 1971	1971	MSL	6UEF	5" Undist.	-5	-108	103	-5.25	29.980211	-90.020504	
IPET webpage	2005	NAVD88	B-2	3" Undist.	0	-98	98	0	29 58 11.4	90 01 23.22	Datum Uncertain
IPET webpage	2005	NAVD88	B-3	3" Undist.	0	-98	98	0	29 58 16.2	90 01 21.54	Datum Uncertain
IPET webpage	2005	NAVD88	B-4	3" Undist.	0	-98	98	0	29 58 30.18	90 01 38.58	Datum Uncertain
IPET webpage	2005	NAVD88	B-5	3" Undist.	0	-98	98	0	29 58 30.54	90 01 17.46	Datum Uncertain
IPET webpage	2005	NAVD88	B-6	3" Undist.	0	-98	98	0	29 58 35.58	90 01 15.66	Datum Uncertain
IPET webpage	2005	NAVD88	B-7	3" Undist.	0	-98	98	0	29 58 40.56	90 01 14.1	Datum Uncertain
IPET webpage	2005	NAVD88	B-8	3" Undist.	0	-98	98	0	29 58 45.72	90 01 12.18	Datum Uncertain
IPET webpage	2005	NAVD88	IHBR-10CON	CPT	0	-80	80	0	29 58 30.7	90 01 17.9	Datum Uncertain
IPET webpage	2005	NAVD88	IHBR-11CON	CPT	0	-80	80	0	29 58 36.3	90 01 16.1	Datum Uncertain
IPET webpage	2005	NAVD88	IHBR-12CON	CPT	0	-80	80	0	29 58 24.1	90 01 20.1	Datum Uncertain
IPET webpage	2005	NAVD88	IHBR-14CON	CPT	0	-80	80	0	29 58 22.9	90 01 19.9	Datum Uncertain
IPET webpage	2005	NAVD88	IHBR-15CON	CPT	0	-80	80	0	29 58 16.8	90 01 21.1	Datum Uncertain
IPET webpage	2005	NAVD88	IHBR-16CON	CPT	0	-80	80	0	29 58 14.4	90 01 22.7	Datum Uncertain
IPET webpage	2005	NAVD88	IHBR-1CON	CPT	0	-80	80	0	29 58 45.8	90 01 13.7	Datum Uncertain
IPET webpage	2005	NAVD88	IHBR-2CON	CPT	0	-80	80	0	29 58 43.5	90 01 12.8	Datum Uncertain
IPET webpage	2005	NAVD88	IHBR-3CON	CPT	0	-80	80	0	29 58 14.0	90 01 14.1	Datum Uncertain
IPET webpage	2005	NAVD88	IHBR-5CON	CPT	0	-80	80	0	29 58 14.0	90 01 23.6	Datum Uncertain
IPET webpage	2005	NAVD88	IHBR-6CON	CPT	0	-80	80	0	29 58 15.2	90 01 23.8	Datum Uncertain
IPET webpage	2005	NAVD88	IHBR-7CON	CPT	0	-80	80	0	29 58 16.7	90 01 23.4	Datum Uncertain
IPET webpage	2005	NAVD88	IHBR-8CON	CPT	0	-80	80	0	29 58 18.7	90 01 22.6	Datum Uncertain
IPET webpage	2005	NAVD88	IHBR-9CON	CPT	0	-80	80	0	29 58 20.4	90 01 22.1	Datum Uncertain
ILIT Final Report, Appendix B and C	2006	NAVD88	IHNC-S-BOR1	3" Undist.	0.93		0.93	0.93	29.9786	90.0202	
ILIT Final Report, Appendix B and C	2006	NAVD88	IHNC-S-CON-1	Continuous	-3.4		-3.4	-3.4	29.97038	90.02313	
ILIT Final Report, Appendix B and C	2006	NAVD88	IHNC-S-CON-2	Continuous	-2.7		-2.7	-2.7	29.97118	90.0227	
ILIT Final Report, Appendix B and C	2006	NAVD88	IHCN-S-CON-3	Continuous	-2.3		-2.3	-2.3	29.97246	90.0225	
ILIT Final Report, Appendix B and C	2006	NAVD88	IHNC-N-BOR-1	3" Undist.	-3.4		-3.4	-3.4	29.97039	90.02315	
ILIT Final Report, Appendix B and C	2006	NAVD88	IHNC-S-CPT-1	CPT	-0.9	-62	61.1	-0.9	29.97035	90.02314	
ILIT Final Report, Appendix B and C	2006	NAVD88	IHNC-S-CPT-2	CPT	-2.7	-67	64.3	-2.7	29.97126	90.02292	
ILIT Final Report, Appendix B and C	2006	NAVD88	IHNC-S-CPT-3	CPT	-2.3	-71	68.7	-2.3	29.97248	90.02257	
ILIT Final Report, Appendix B and C	2006	NAVD88	IHNC-N-CPT-1	CPT	-3.38	-54	50.62	-3.38	29.9787	90.02049	

BORING	Depth	Test El.	TEST					
	ft	NAVD88	W (%)	LL (%)	PL (%)	Su (psf)	γ (pcf)	USCS
Top El.	-3.3	NAVD88						
B-2	0	-3.3	35			0	0	
	2.5	-5.8	49			753	104	CH
	5	-8.3	66			0	0	CH
	7.5	-10.8	126					CH
	10	-13.3	129			115	82	CH+ORG
	12.5	-15.8	90					CH+ORG
	15	-18.3	32			329	114	CH
	17.5	-20.8	36					CL
	20	-23.3	62			127	101	CH
	22.5	-25.8	51					CH
	25	-28.3	58			167	102	CH
	27.5	-30.8	70					CH
	30	-33.3	57			453	102	CH
	32.5	-35.8	54					CH
	35	-38.3	69			227	97	CH
	37.5	-40.8	68					CH
	40	-43.3	70			393	97	CH
	42.5	-45.8	61					CH
	45	-48.3	23			221	125	CH
	47.5	-50.8	24					CL
	50	-53.3	30			264	115	CL
	52.5	-55.8	23					CL
	55	-58.3	60			494	100	CL
	57.5	-60.8	26			168	118	CH
	60	-63.3	29					CL
	62.5	-65.8	24					SM
	65	-68.3	59			1023	100	SM
	67.5	-70.8	22					CH
	70	-73.3	23			668	123	CL
	72.5	-75.8	20					CL
	75	-78.3	37			1630	116	CL
	77.5	-80.8	35					CH
	80	-83.3	52			1143	104	CH
	82.5	-85.8	48					CH
	85	-88.3	30			440	118	CH
	87.5	-90.8	23					CL
	90	-93.3	43			1209	110	CL
	92.5	-95.8	45					CH
	95	-98.3	45			1085	109	CH
	97.5	-100.8	42					CH

BORING	Depth	Test El.	TEST					
	ft	NAVD88	W (%)	LL (%)	PL (%)	Su (psf)	γ (pcf)	USCS
Top El.	-2.8	NAVD88						
B-3	0	-2.8	32					CH
	2.5	-5.3	129					CH+ORG
	5	-7.8	70			91	93	CH
	7.5	-10.3	76					CH
	10	-12.8	91			102	84	CH+ORG
	12.5	-15.3	72					CH
	15	-17.8	44					CH
	16.5	-19.3	59			219	100	CH
	17.5	-20.3	51			214	104	CH
	20	-22.8	41					CH
	22.5	-25.3	45			264	107	CH
	25	-27.8	68					CH
	27.5	-30.3	51			343	104	CH
	30	-32.8	54					CH
	32.5	-35.3	67			356	96	CH
	35	-37.8	69					CH
	37.5	-40.3	63			372	97	CH
	40	-42.8	50					CH
	42.5	-45.3	68			384	96	CH
	45	-47.8	27					CL
	47.5	-50.3	43			291	104	CH
	50	-52.8	48					CH
	52.5	-55.3	28			274	115	CL
	55	-57.8	23			191	120	CL
	57.5	-60.3	21					SM
	60	-62.8	22					SM
	62.5	-65.3	41					CH
	65	-67.8	23			842	124	CL
	67.5	-70.3	21			862	127	CL
	70	-72.8	21					SM
	72.5	-75.3	19					SM
	75	-77.8	35					CH
	76.5	-79.3	39			957	112	CH
	77.5	-80.3	43					CH
	80	-82.8	48					CH
	82.5	-85.3	57			593	104	CH
	85	-87.8	51					CH
	87.5	-90.3	26			792	120	CH
	90	-92.8	52					CH
	92.5	-95.3	42					CH
	95	-97.8	37			1169	114	CH
	97.5	-100.3	43			898	110	CH

BORING	Depth	Test El.	TEST					
	ft	NAVD88	W (%)	LL (%)	PL (%)	Su (psf)	γ (pcf)	USCS
Top El.	-2.8	NAVD88						
B-4	0	-2.8	28			1577.5	119	CH
	2.5	-5.3	43			755.8	105	CH
	5	-7.8	59			560.6	102	CH
	7.5	-10.3	78			408.3	94	CH
	10	-12.8	80			337.7	92	CH
	12.5	-15.3	155			75.8	80	CH+ORG
	15	-17.8	64					CL
	17.5	-20.3	63			76.3	100	CH
	20	-22.8	42					CH
	22.5	-25.3	63			257.3	98	CH
	25	-27.8	62					CH
	27.5	-30.3	73			301.8	94	CH
	30	-32.8	71					CH
	32.5	-35.3	50			319.8	106	CH
	35	-37.8	67					CH
	37.5	-40.3	61			394.4	102	CH
	40	-42.8	66					CH
	42.5	-45.3	58			461.6	102	CH
	45	-47.8	71			329.7	97	CH
	47.5	-50.3	57					CL
	50	-52.8	40			361.6	110	CH
	52.5	-55.3	45			389	104	CH
	55	-57.8	52					CH
	57.5	-60.3	44			379.5	112	CH
	60	-62.8	53					CH
	62.5	-65.3	25			508.5	124	CL
	65	-67.8	45					CH
	67.5	-70.3	38			905.1	114	CH
	70	-72.8	45					CH
	72.5	-75.3	26			601.3	121	CH
	75	-77.8	66					CH
	77.5	-80.3	23			737.1	126	CL
	80	-82.8	30					CH
	82.5	-85.3	32			2607.3	116	CH
	85	-87.8	38					CH
	87.5	-90.3	42			877	110	CH
	90	-92.8	48					CH
	92.5	-95.3	24			1298	122	CL
	95	-97.8	24					ML
	97.5	-100.3	25					ML

BORING	Depth	Test El.	TEST					
	ft	NAVD88	W (%)	LL (%)	PL (%)	Su (psf)	γ (pcf)	USCS
Top El.	1.9	NAVD88						
B-5	0	1.9	28			770.6	108	CH
	2.5	-0.6	52					CH
	5	-3.1	60			420.3	100	CH
	7.5	-5.6	164			64.6	79	CH+ORG
	10	-8.1	131			72.9	83	CH+ORG
	12.5	-10.6	442			250.6	63	PT
	15	-13.1	70					CH
	17.5	-15.6	35			225.2	112	CH
	20	-18.1	75					CH
	22.5	-20.6	54			156	110	CH
	25	-23.1	79					CH
	27.5	-25.6	74			362.8	97	CH
	30	-28.1	66					CH
	32.5	-30.6	72			136.1	96	CH
	35	-33.1	62					CH
	37.5	-35.6	62			309.7	99	CH
	40	-38.1	72					CH
	42.5	-40.6	72			347.3	95	CH
	45	-43.1	25					CL
	47.5	-45.6	36			241.6	112	NS
	50	-48.1						SM
	52.5	-50.6	21					SM
	55	-53.1	22					CH
	57.5	-55.6	42					CH
	60	-58.1	48			459.9	107	CH
	62.5	-60.6	38					CH
	65	-63.1	39			588.9	113	CL
	67.5	-65.6	24					CH
	70	-68.1	26			923.1	122	CL
	72.5	-70.6	20					CL
	75	-73.1	22			601.4	125	CL
	77.5	-75.6	22					CL
	80	-78.1	26			185.5	123	CH
	82.5	-80.6	38					CH
	85	-83.1	40			1042.9	111	CH
	87.5	-85.6	40					CH
	90	-88.1	38			809.7	116	CH
	92.5	-90.6	46					CH
	95	-93.1	54			1110	103	CH
	97.5	-95.6	48					CH

BORING	Depth	Test El.	TEST					
	ft	NAVD88	W (%)	LL (%)	PL (%)	Su (psf)	γ (pcf)	USCS
Top El.	0.2	NAVD88						
B-6	0	0.2	22			1192.3	121	CL
	2.5	-2.3	42			676.7	101	CH
	5	-4.8	51			499.9	102	CH+ORG
	7.5	-7.3	245					CH+ORG
	12.5	-12.3	246			327.4	69	CH+ORG
	15	-14.8	123					CH+ORG
	17.5	-17.3	101			262.3	87	CH+ORG
	20	-19.8	120					CH
	22.5	-22.3	74					CH
	25	-24.8	58					CH
	27.5	-27.3	68			260.5	97	CH
	30	-29.8	67					CH
	32.5	-32.3	60			241.5	100	CH
	35	-34.8	70					CH
	37.5	-37.3	63			345	98	CH
	40	-39.8	67					CH
	42.5	-42.3	58			1032	101	CH
	45	-44.8	27					CL
	47.5	-47.3	34					CL
	50	-49.8	54			665.4	102	CH
	52.5	-52.3	74					CH
	55	-54.8	19					CL
	57.5	-57.3	25					SM
	59	-58.8	22					SM
	61.5	-61.3	38					CL
	63	-62.8	50			159.7	104	CH
	65	-64.8	56					CH
	67.5	-67.3	25					CH
	70	-69.8	42					CH
	72.5	-72.3	35			342.6	116	CH
	75	-74.8	40					CH
	77.5	-77.3	43			579.6	108	CH
	80	-79.8	55					CH
	82.5	-82.3	51			757.7	104	CH
	85	-84.8	40					CH
	87.5	-87.3	36			672.8	113	CH
	90	-89.8	45					CH
	92.5	-92.3	51			691.2	105	CH
	95	-94.8	47					CH
	97.5	-97.3	37			642.8	113	CH

BORING	Depth	Test El.	TEST					
	ft	NAVD88	W (%)	LL (%)	PL (%)	Su (psf)	γ (pcf)	USCS
Top El.	2.4	NAVD88						
B-7	0	2.4	30			3195.5	116	CH
	2.5	-0.1	37					CH
	5	-2.6	45			782.8	106	CH
	7.5	-5.1	215			336.4	73	CH+ORG
	10	-7.6	407					PT
	12.5	-10.1	73			137.3	97	CH
	15	-12.6	40					CL
	17.5	-15.1	36			134.2	114	CL
	20	-17.6	62					CH
	22.5	-20.1	49			215.2	105	CH
	25	-22.6	64					CH
	27.5	-25.1	65			398.4	100	CH
	30	-27.6	70					CH
	32.5	-30.1	71			391	98	CH
	35	-32.6	68					CH
	37.5	-35.1	67			393.7	98	CH
	40	-37.6	62					CH
	42.5	-40.1	67			468.3	96	CH
	45	-42.6	26					CL
	47.5	-45.1	49			248.3	105	CH
	50	-47.6	26					CL
	52.5	-50.1	25					SM
	55	-52.6	20					SM
	57.5	-55.1	19					SP
	60	-57.6	20					SM
	62.5	-60.1	44					CH
	65	-62.6	27			3264.6	118	CH
	67.5	-65.1	36			2414.3	110	CH
	70	-67.6	28					CL
	72.5	-70.1	28			2222.5	123	CL
	75	-72.6	38					CH
	77.5	-75.1	48			3836.5	107	CH
	80	-77.6	29					CL
	82.5	-80.1	53			541.5	102	CH
	85	-82.6	43					CH
	87.5	-85.1	37			2407.4	114	CH
	90	-87.6	43					CH
	92.5	-90.1	59			573.4	101	CH
	95	-92.6	26					ML
	97.5	-95.1	24					ML

BORING	Depth	Test El.	TEST					
	ft	NAVD88	W (%)	LL (%)	PL (%)	Su (psf)	γ (pcf)	USCS
Top El.	-1.8	NAVD88						
B-8	0	-1.8	29					CH
	0.5	-2.3	31					CH
	2.5	-4.3	40			771	109	CH
	5	-6.8	54			415	104	CH
	7.5	-9.3	65					CH
	10	-11.8	111			312	85	CH+ORG
	12.5	-14.3	187					CH+ORG
	15	-16.8	187			331	74	CH+ORG
	17.5	-19.3	36					CL
	20	-21.8	70			249	98	CH
	22.5	-24.3	72					CH
	25	-26.8	62			442	100	CH
	27.5	-29.3	62					CH
	30	-31.8	69			419	97	CH
	32.5	-34.3	65					CH
	35	-36.8	67			369	98	CH
	37.5	-39.3	68					CH
	40	-41.8	63			434	98	CH
	42.5	-44.3	57					CH
	45	-46.8	24			304	120	CL
	47.5	-49.3	27					CL
	50	-51.8	23					SP
	52.5	-54.3	24					SP
	55	-56.8	22					SP
	57	-58.8	30					CL
	58.5	-60.3	32			395	114	CH
	60	-61.8	33			626	114	CH
	62.5	-64.3	27					CH
	65	-66.8	28			1010	119	CH
	67.5	-69.3	27					CL
	70	-71.8	27			579	121	CL
	72.5	-74.3	26					CL
	75	-76.8	32			1225	118	CH
	77.5	-79.3	41					CH
	80	-81.8	30			869	118	CL
	82.5	-84.3	26					CL
	85	-86.8	54			1086	104	CH
	87.5	-89.3	38					CH
	90	-91.8	33			1111	116	CH
	92.5	-94.3	33					CH
	95	-96.8	37			1137	114	CH
	97.5	-99.3	41					CH

BORING	Depth	Test El.	TEST					
	ft	NAVD88	W (%)	LL (%)	PL (%)	Su (psf)	γ (pcf)	USCS
Top El.	8.95	NAVD88						
2-U	0.0	9.0	44.2	94.7	27.4	552.6	113.7	
	4.2	4.7	48.4	69.5	29.5	342.1	104.7	
	4.7	4.2	52.6	63.2	23.2	513.2	104.2	
	8.4	0.5	62.1	71.6	27.4	157.9	103.2	
	9.2	-0.3	56.8	84.2	31.6			
	12.6	-3.7	58.9	82.1	21.1	263.2	101.1	
	14.7	-5.8	50.5	84.2	33.7	394.7	110.0	
	16.8	-7.9	69.5	101.1	27.4		98.4	
	21.3	-12.4	75.8	113.7	35.8	342.1		
	22.1	-13.2	192.0					
	23.4	-14.5	155.0					
	25.5	-16.6	255.0					
	25.7	-16.7	186.0					
	25.8	-16.8	275.0					
	26.1	-17.1	125.0					
	26.3	-17.4	125.0	245.0	119.0	500.0		
	36.8	-27.9	46.3	54.7	25.3			
	37.9	-28.9	48.4	58.9	26.3	552.6	110.0	
	38.9	-30.0	56.8	77.9	23.2	447.4	104.2	
	41.6	-32.6	56.8	71.6	27.4	552.6		
	45.8	-36.8	54.7	88.4	29.5	684.2	105.3	
	46.8	-37.9	46.3	77.9	23.2			
	48.4	-39.5	58.9	77.9	21.1	631.6	101.1	
	50.0	-41.1	67.4	92.6	31.6	657.9	104.7	
	54.2	-45.3	73.7	86.3	31.6	684.2	104.7	
	60.5	-51.6	71.6	84.2	25.3	657.9	102.1	

BORING	Depth	Test El.	TEST					
	ft	NAVD88	W (%)	LL (%)	PL (%)	Su (psf)	γ (pcf)	USCS
Top El.	1.25	NAVD88						
2-UT	0.0	1.3	53.9	85.2	22.6	391.3	92.2	
	1.1	0.2	55.7			413.0	91.7	
	7.4	-6.1	80.0			358.7	90.0	
	7.8	-6.6	69.6			380.4	90.4	
	8.3	-7.0	69.6			521.7	92.0	
	8.7	-7.4	71.3	116.5	29.6	434.8	90.0	
	10.0	-8.8	88.7			304.3	87.4	
	10.4	-9.2	87.0			347.8	87.4	
	11.7	-10.5	124.0					
	13.0	-11.8	141.0	201.0	59.1	239.1	80.4	
	13.9	-12.7	432.0					
	15.7	-14.4	270.0			543.5	77.0	
	17.0	-15.7	81.7	97.4	24.3	391.3	89.1	
	20.4	-19.2	50.4			260.9	93.5	
	23.9	-22.7	67.8			304.3	90.0	
	25.7	-24.4	45.2			260.9	94.8	
	27.8	-26.6	66.1			326.1	91.3	
	29.1	-27.9	62.6	71.3	19.1	391.3	91.7	
	29.6	-28.3	47.0			434.8	95.2	
	30.4	-29.2	67.8			347.8	91.7	
	33.0	-31.8	59.1	80.0	19.1	500.0	94.8	
	36.1	-34.8	53.9			217.4	90.4	
	36.5	-35.3	64.3			543.5	91.1	
	37.0	-35.7	62.6	83.5	24.3	456.5	90.4	
	39.1	-37.9	69.6			391.3	90.0	

BORING	Depth	Test El.	TEST					
	ft	NAVD88	W (%)	LL (%)	PL (%)	Su (psf)	γ (pcf)	
Top El.	-5.25	NAVD88						
	4.7	-10.0	46.7	75.6	28.9	511.1	86.7	
	14.1	-19.4	60.0	80.0	26.7	244.4	97.8	
	15.3	-20.5	68.9	82.2	24.4			
	17.6	-22.9	51.1			311.1	97.8	
	21.2	-26.4	73.3			355.6	100.0	
	22.4	-27.6	75.6				97.8	
	23.5	-28.8	73.3	93.3	28.9			
	25.9	-31.1	66.7	88.9	26.7	288.9	95.6	
	30.6	-35.8	68.9			377.8	95.6	
	34.1	-39.4	60.0			511.1	100.0	
	37.6	-42.9	75.6	93.3	26.7	400.0	95.6	
6-UEF	44.7	-50.0					126.7	
	60.6	-65.8	35.6	53.3	22.2	644.4	120.0	
	61.2	-66.4	28.9	35.6	15.6			
	68.2	-73.5	57.8				104.4	
	77.6	-82.9	66.7	117.8	35.6	1066.7	97.8	
	78.8	-84.1	40.0	73.3	22.2			
	85.3	-90.5	35.6			1422.2	115.6	
	88.8	-94.1	44.4	75.6	22.2	1044.4	108.9	
	89.4	-94.7	48.9	57.8	28.9	977.8	111.1	
	95.3	-100.5	35.6			1688.9	120.0	
	103.5	-108.8	40.0			1377.8	113.3	
	108.2	-113.5	48.9			1600.0	111.1	

BORING	Depth	Test El.	TEST					
	ft	NAVD88	W (%)	LL (%)	PL (%)	Su (psf)	γ (pcf)	
Top El.	-1.25	NAVD88						
	14.1	-15.4	73.3	68.9	20.0	244.4	93.3	
	14.7	-16.0	53.3	73.3	22.2		0.0	
	15.9	-17.1	46.7	53.3	17.8	311.1	106.7	
	21.2	-22.4	75.6	93.3	26.7	311.1	95.6	
	22.4	-23.6	57.8	66.7	22.2		0.0	
	25.9	-27.1	62.2	77.8	20.0		0.0	
	27.1	-28.3	64.4	86.7	24.4	377.8	97.8	
	30.0	-31.3	66.7	80.0	26.7		97.8	
	33.5	-34.8	64.4	82.2	22.2		0.0	
5-UF	34.1	-35.4	73.3	91.1	26.7	355.6	93.3	
	35.3	-36.5	42.2	51.1	11.1	933.3	108.9	
	67.1	-68.3	35.6	53.3	13.3			
	70.6	-71.8	37.8	60.0	15.6	1177.8	108.9	
	71.8	-73.0	28.9	46.7	11.1	1266.7	120.0	
	75.3	-76.5	37.8	48.9	17.8			
	80.0	-81.3	35.6	53.3	15.6	1155.6	111.1	
	84.7	-86.0	40.0	62.2	17.8	1177.8	113.3	
	87.1	-88.3	35.6	48.9	13.3	1155.6	106.7	
	100.0	-101.3	44.4	68.9	22.2		108.9	

BORING	Depth	Test El.	TEST					
	ft	NAVD88	W (%)	LL (%)	PL (%)	Su (psf)	γ (pcf)	
Top El.	-3.25	NAVD88						
6-UT	1.3	-4.6	66.1	243.5	47.0	804.3	100.9	
	4.3	-7.6	184.0					
	4.8	-8.0	243.0					
	5.2	-8.5	173.0					
	5.7	-8.9	127.0					
	7.4	-10.6	114.8	127.0	29.6	108.7	87.0	
	9.1	-12.4	385.0					
	9.6	-12.8	417.0	395.0	154.0	130.4	66.0	
	10.0	-13.3	363.0			130.4	67.0	
	10.9	-14.1	205.0			195.7	81.7	
	13.9	-17.2	64.3			239.1	103.5	
	15.7	-18.9	76.5			195.7	96.5	
	17.8	-21.1	76.5	80.0	26.1	304.3	100.0	
	18.7	-21.9	64.3			326.1	99.1	
	19.1	-22.4	81.7			260.9	97.4	
	19.6	-22.8	80.0			173.9	96.5	
	20.0	-23.3	73.0			369.6	100.0	
	20.4	-23.7	81.7			413.0	98.3	
	23.0	-26.3	80.0	92.2	19.1	239.1	98.3	
	24.3	-27.6	67.8			282.6	101.7	
	25.7	-28.9	71.3			347.8	100.9	
	27.0	-30.2	57.4	74.8	22.6	347.8	106.1	
	27.8	-31.1	55.7			304.3	107.0	
	28.7	-31.9	60.9			326.1	104.3	
	30.0	-33.3	55.7			413.0	106.1	
	30.9	-34.1	55.7	74.8	19.1	347.8	106.1	
	33.0	-36.3	71.3			413.0	102.6	
	33.9	-37.2	74.8			434.8	99.1	
	34.8	-38.0	67.8	85.2	20.9	478.3	100.0	
	35.7	-38.9	66.1			347.8	102.6	
	37.0	-40.2	66.1			260.9	98.3	
	37.4	-40.6	64.3			413.0	100.9	
	38.3	-41.5	66.1	81.7	26.1	478.3	100.9	
	39.6	-42.8	73.0			391.3	100.9	

BORING	Depth	Test El.	TEST					
	ft	NAVD88	W (%)	LL (%)	PL (%)	Su (psf)	γ (pcf)	
Top El.	3.75	NAVD88						
	2.5	1.3	42.5	60	27.5	468.75	115	
	9.4	-5.6	72.5	92.5	32.5			
	10.3	-6.6	77.5	90	35	281.25	98.75	
	11.3	-7.5	147	97.5	40	500	88.75	
	13.1	-9.4	62.5	95	35	531.25	105	
	14.4	-10.6	160					
	15.0	-11.3	130					
	15.6	-11.9	179					
	16.9	-13.1	191					
	17.5	-13.8	282					
	18.8	-15.0	115	125	50	187.5	83.75	
6-U	20.6	-16.9	233	337	135	625	81.25	
	21.9	-18.1	165			468.75	102.5	
	23.1	-19.4	203			406.25	98.75	
	25.6	-21.9	70	77.5	32.5		100	
	30.0	-26.3	65	95	27.5		107.5	
	31.3	-27.5	75	92.5	35	437.5		
	35.0	-31.3	62.5	75	25	875		
	38.1	-34.4	62.5	80	25	468.75	106.25	
	41.9	-38.1	67.5	87.5	30	656.25	105	
	55.6	-51.9	50	67.5	22.5	656.25	112.5	
	56.9	-53.1	52.5	60	20	687.5	108.75	
	70.6	-66.9	52.5	62.5	25	937.5	112.5	

13.2 STATISTICAL CALCULATIONS OF SHEAR STRENGTH AND UNIT WEIGHT– SOUTH BREACH

a. Above -5ft, data under crest

STRENGTH DATA
SOUTH 1- CREST
Above -5ft, CL

Su (psf)	ln Su
552.6	6.3
342.1	5.8
513.2	6.2
157.9	5.1
263.2	5.6

5.8	X50
6.7	X
0.5	sln(x)
188.1	s(x)
0.5	Vx
342.1	MEDIAN

UNIT WEIGHT DATA
SOUTH 1- CREST
Above -5ft, CL

γ (pcf)	ln γ
113.7	4.733425
104.7	4.651451
104.2	4.646413
103.2	4.636261
101.1	4.615641

4.6464131	X50
4.6511337	X
0.0450654	sln(x)
4.6986767	s(x)
0.0450883	Vx
104.21053	MEDIAN

b. Between -5ft and -13, data under crest. No data for unit weight.

STRENGTH DATA
SOUTH 1- CREST
-8 to -13, CH

Su (psf)	ln Su
342.1	5.835118
383	5.948035
5.8915767	X50
5.9103863	X
0.079844	sln(x)
28.947713	s(x)
0.0799715	Vx
361.97557	MEDIAN

UNIT WEIGHT DATA
SOUTH 1- CREST
-8 to -13, CH

γ (pcf)	ln γ
	X50
	X
	sln(x)
	s(x)
	Vx
	MEDIAN

c. Between -13ft and -25, data under crest. No data for Unit Weight

STRENGTH DATA
SOUTH 1- CREST
-13 to -25, MARSH

Su (psf)	ln Su
500	6.214608
312	5.743003

5.9788056	X50
6.3206599	X
0.333475	sln(x)
135.46013	s(x)
0.3429645	Vx
394.96835	MEDIAN

UNIT WEIGHT DATA
SOUTH 1- CREST
-13 to -25, MARSH

γ (pcf)	ln γ

	X50
	X
	sln(x)
	s(x)
	Vx
	MEDIAN

d. Between -25ft and -45, data under crest

STRENGTH DATA
SOUTH 1- CREST
-25 to -45, CH

Su (psf)	ln Su
552.63158	6.314692
447.36842	6.103382
552.63158	6.314692
684.21053	6.528266
631.57895	6.448223
657.89474	6.489045
684.21053	6.528266
338	5.823046
324	5.780744
460	6.131226
399	5.988961
444	6.095825
491	6.196444
589	6.378426
562	6.331502
598	6.393591

6.3146916	X50
6.4928806	X
0.2359126	sln(x)
132.20793	s(x)
0.2392334	Vx
552.63158	MEDIAN

UNIT WEIGHT DATA
SOUTH 1- CREST
-25 to -45, CH

γ (pcf)	ln γ
110	4.70048
104.21053	4.646413
105.26316	4.656463
101.05263	4.644391
104.73684	4.651451
104.73684	4.651451
4.6514509	X50
4.6531759	X
0.0272312	sln(x)
2.8526381	s(x)
0.0272362	Vx
104.73684	MEDIAN

e. Between -45ft and -64, data under crest

STRENGTH DATA
SOUTH 1- CREST
-45 to -64, CH

Su (psf)	ln Su
684.21053	6.528266
657.89474	6.489045
480	6.173786
523	6.259581
598	6.393591
873	6.771936

6.4413178	X50
6.5884552	X
0.2125359	sln(x)
134.82922	s(x)
0.2149588	Vx
627.23285	MEDIAN

UNIT WEIGHT DATA
SOUTH 1- CREST
-45 to -64, CH

γ (pcf)	ln γ
104.73684	4.651451
102.10526	4.626004
4.6387276	X50
4.6394786	X
0.0179935	sln(x)
1.8609077	s(x)
0.017995	Vx
103.41268	MEDIAN

f. Below -68ft, data under crest.

STRENGTH DATA
SOUTH 1- CREST
below -68, CH

Su (psf)	ln Su
1023	6.930495
668	6.504288
1630	7.396335
1143	7.041412
440	6.086775
1209	7.097549
1085	6.989335
842	6.73578
862	6.759255
957	6.863803
593	6.385194
792	6.674561

6.8115293	X50
7.2418015	X
0.3500095	sln(x)
327.88853	s(x)
0.3610078	Vx
908.25877	MEDIAN

UNIT WEIGHT DATA
SOUTH 1- CREST
below -68, CH

γ (pcf)	ln γ
100	4.60517
123	4.812184
116	4.75359
104	4.644391
118	4.770685
110	4.70048
109	4.691348
124	4.820282
127	4.844187
112	4.718499
104	4.644391
120	4.787492

4.7360445	X50
4.7502977	X
0.077524	sln(x)
8.849667	s(x)
0.0776406	Vx
113.98245	MEDIAN

g. Above -11ft, data under toe

STRENGTH DATA
SOUTH 1- TOE
Above -11ft, CL

Su (psf)	ln Su
391	5.969486
413	6.023553
359	5.882474
380	5.941315
522	6.257168
435	6.074846
304	5.718171
348	5.851703
753	6.624065
91	4.51086
840	6.733402
260	5.560682
380	5.940171

5.941315	X50
6.86535	X
0.537693	sln(x)
220.2724	s(x)
0.579002	Vx
380.4348	MEDIAN

UNIT WEIGHT DATA
SOUTH 1- TOE
Above -11ft, CL

γ (pcf)	ln γ
92	4.523677
92	4.518949
90	4.49981
90	4.504629
92	4.521316
90	4.49981
87	4.470396
87	4.470396
104	4.644391
93	4.532599

4.511789	X50
4.517207	X
0.048991	sln(x)
4.465025	s(x)
0.049021	Vx
91.08462	MEDIAN

h. Between -11ft and -19.5, data under toe

STRENGTH DATA
SOUTH 1- TOE
-11 to -19.5ft, MARSH

Su (psf)	ln Su
239.1304	5.477009
543.4783	6.29799
391.3043	5.969486
260.8696	5.564021
115	4.744932
329	5.796058
102	4.624973
219	5.389072

5.520515	X50
6.504005	X
0.57262	sln(x)
155.5853	s(x)
0.62293	Vx
249.7636	MEDIAN

UNIT WEIGHT DATA
SOUTH 1- TOE
-11 to -19.5ft, MARSH

γ (pcf)	ln γ
80.43478	4.387447
77	4.343805
89.13043	4.490101
93.47826	4.537729
82	4.406719
114	4.736198
84	4.430817
100	4.60517

4.460459	X50
4.498356	X
0.130079	sln(x)
11.30315	s(x)
0.130631	Vx
86.5272	MEDIAN

i. Between -19.5ft and -43, data under toe

STRENGTH DATA
SOUTH 1- TOE
-19.5 to -43ft, CH

Su (psf)	ln Su
304.3478	5.718171
260.8696	5.564021
326.087	5.787164
391.3043	5.969486
434.7826	6.074846
347.8261	5.851703
500	6.214608
217.3913	5.381699
543.4783	6.29799
456.5217	6.123636
391.3043	5.969486
251	5.525453
324	5.780744
310	5.736572
346	5.846439
385	5.953243
127	4.844187
167	5.117994
453	6.115892
227	5.42495
214	5.365976
264	5.575949
343	5.83773
356	5.874931
372	5.918894

5.83773	X50
6.19242	X
0.343464	sln(x)
121.3696	s(x)
0.353847	Vx
343	MEDIAN

UNIT WEIGHT DATA
SOUTH 1- TOE
-19.5 to -43ft, CH

γ (pcf)	ln γ
90	4.49981
94.78261	4.551586
91.30435	4.514198
91.73913	4.518949
95.21739	4.556163
91.73913	4.518949
94.78261	4.551586
90.43478	4.504629
91.08696	4.511815
90.43478	4.504629
90	4.49981
101	4.615121
102	4.624973
102	4.624973
97	4.574711
104	4.644391
107	4.672829
104	4.644391
96	4.564348
97	4.574711

4.553874	X50
4.561066	X
0.05618	sln(x)
5.341296	s(x)
0.056224	Vx
94.99975	MEDIAN

j. Between -43ft and -63, data under toe

STRENGTH DATA
SOUTH 1- TOE
-43 to -63ft, CH

Su (psf)	ln Su
363	5.894403
502	6.2186
393	5.97381
221	5.398163
264	5.575949
494	6.202536
168	5.123964
384	5.950643
291	5.673323
274	5.613128
191	5.252273

5.673323	X50
6.066842	X
0.366232	sln(x)
110.2491	s(x)
0.378863	Vx
291	MEDIAN

UNIT WEIGHT DATA
SOUTH 1- TOE
-43 to -63ft, CH

γ (pcf)	ln γ
97	4.574711
125	4.828314
115	4.744932
100	4.60517
118	4.770685
96	4.564348
104	4.644391
115	4.744932
120	4.787492

4.744932	X50
4.768478	X
0.099499	sln(x)
11.47079	s(x)
0.099746	Vx
115	MEDIAN

13.3 STATISTICAL CALCULATIONS OF SHEAR STRENGTH AND UNIT WEIGHT – NORTH BREACH

a. Above -5ft, data under crest. No data for unit weight.

STRENGTH DATA
NORTH- CREST
Above -5ft, CH

Su (psf)	ln Su
529	6.270988
583	6.368187
873	6.771936
375	5.926926

6.319588	X50
6.713317	X
0.347676	sln(x)
199.064	s(x)
0.358452	Vx
555.344	MEDIAN

UNIT WEIGHT DATA
NORTH- CREST
Above -5ft, CH

γ (pcf)	ln γ

	X50
	X
	sln(x)
	s(x)
	Vx
	MEDIAN

b. Between -5ft and -18, data under crest. No data for unit weight.

STRENGTH DATA
NORTH- CREST
-5 to -18ft, MARSH

Su (psf)	ln Su
558	6.324359
440	6.086775
445	6.098074
323	5.777652

6.092425	X50
6.247929	X
0.224517	sln(x)
100.6123	s(x)
0.227376	Vx
442.4929	MEDIAN

UNIT WEIGHT DATA
NORTH- CREST
-5 to -18ft, MARSH

γ (pcf)	ln γ

	X50
	X
	sln(x)
	s(x)
	Vx
	MEDIAN

c. Between -18ft and -49, data under crest. No data for unit weight.

STRENGTH DATA
NORTH- CREST
-18 to -49ft, CH

Su (psf)	ln Su
392	5.971262
474	6.161207
434	6.073045
404	6.001415
454	6.118097
444	6.095825
281	5.638355
296	5.690359
350	5.857933
422	6.045005
564	6.335054

6.045005	X50
6.172182	X
0.204059	sln(x)
87.01717	s(x)
0.206202	Vx
422	MEDIAN

UNIT WEIGHT DATA
NORTH- CREST
-18 to -49ft, CH

γ (pcf)	ln γ

	X50
	X
	sln(x)
	s(x)
	Vx
	MEDIAN

d. Above -21, data under toe

STRENGTH DATA
NORTH- TOE
Above -21ft, MARSH

Su (psf)	ln Su
180	5.192957
331	5.802118
244.4444	5.498988
244.4444	5.498988
311.1111	5.74015
256	5.545177

5.522083	X50
5.651891	X
0.215569	sln(x)
54.55841	s(x)
0.218098	Vx
250.1555	MEDIAN

UNIT WEIGHT DATA
NORTH- TOE
Above -21ft, MARSH

γ (pcf)	ln γ

	X50
	X
	sln(x)
	s(x)
	Vx
	MEDIAN

e. Between -21ft and -49, data under toe. No data for unit weight.

STRENGTH DATA
NORTH- TOE
-21 to -49ft, CH

Su (psf)	ln Su
180	5.192957
249	5.517453
442	6.09131
419	6.037871
369	5.910797
434	6.073045
304	5.717028
311.1111	5.74015
355.5556	5.873682
288.8889	5.666042
377.7778	5.934306
511.1111	6.236587
400	5.991465
311.1111	5.74015
377.7778	5.934306
355.5556	5.873682
933.3333	6.838762
281	5.638355
296	5.690359
350	5.857933
422	6.045005
564	6.335054

5.892239	X50
6.209335	X
0.323783	sln(x)
120.4211	s(x)
0.332457	Vx
362.2154	MEDIAN

UNIT WEIGHT DATA
NORTH- TOE
-21 to -49ft, CH

γ (pcf)	ln γ

	X50
	X
	sln(x)
	s(x)
	Vx
	MEDIAN

f. Below -59, data under toe. No data for unit weight.

STRENGTH DATA
NORTH- TOE
below -59ft, CH

Su (psf)	ln Su
564	6.335054
395	5.978886
626	6.43935
1010	6.917706
579	6.361302
1225	7.110696
869	6.767343
1086	6.990257
1111	7.013016
1137	7.036148
644.4444	6.468389
1066.667	6.972294
1422.222	7.259976
1044.444	6.95124
977.7778	6.885282
1688.889	7.431826
1377.778	7.228227
1600	7.377759
1177.778	7.071385
1266.667	7.144144
1155.556	7.052337
1177.778	7.071385
1155.556	7.052337
1361	7.215975

7.024582	X50
7.492653	X
0.359186	sln(x)
417.0753	s(x)
0.371088	Vx
1123.925	MEDIAN

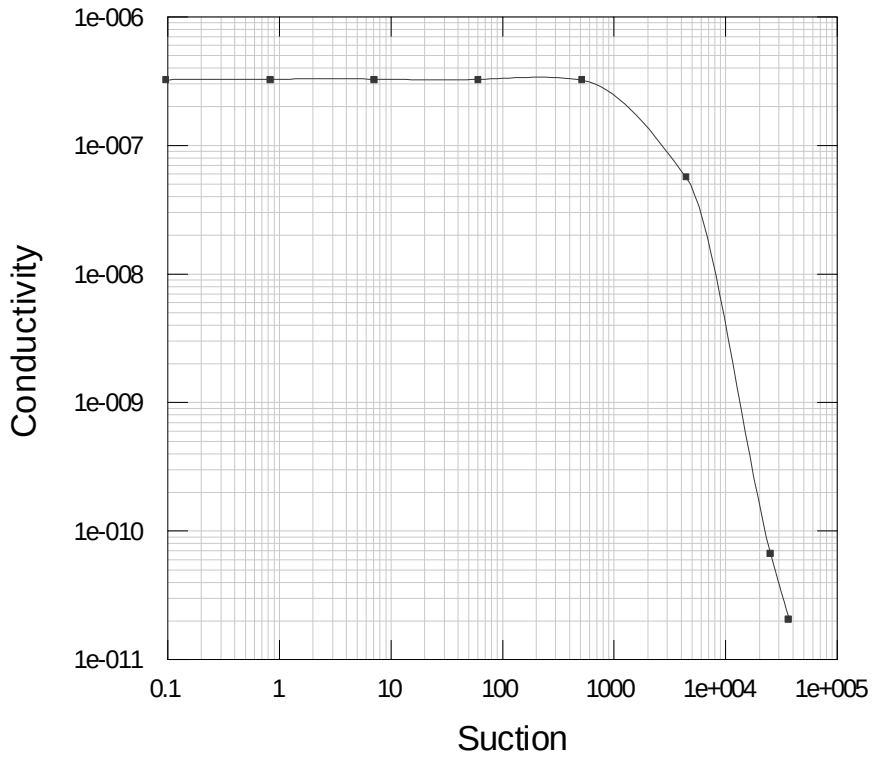
UNIT WEIGHT DATA
NORTH- TOE
below -59ft, CH

γ (pcf)	ln γ

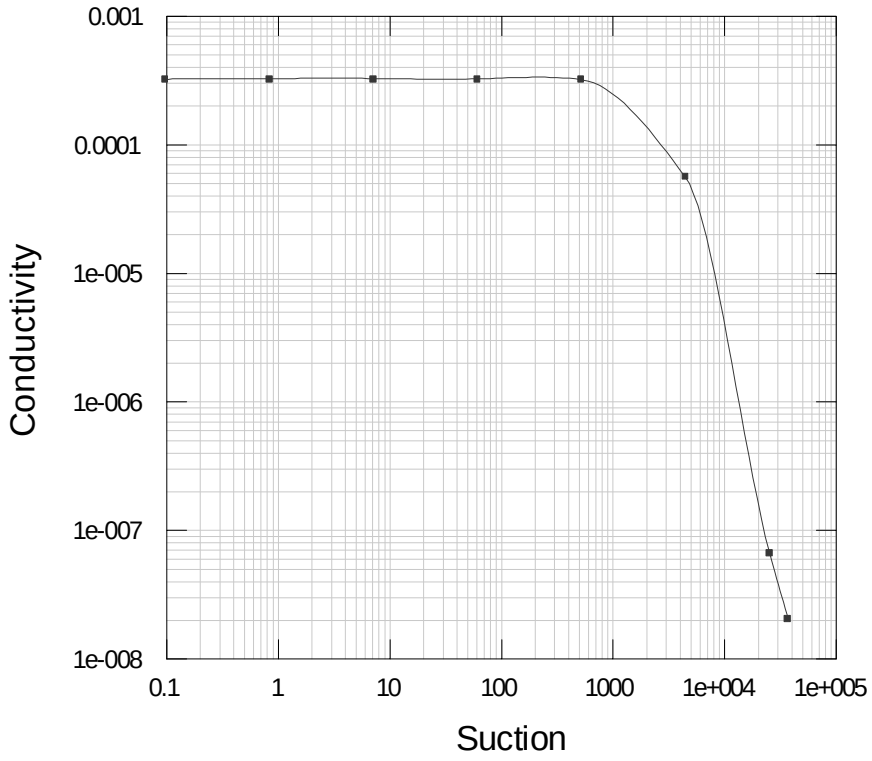
	X50
	X
	sln(x)
	s(x)
	Vx
	MEDIAN

13.4 HYDRAULIC CONDUCTIVITY FUNCTIONS USED FOR SEEPAGE ANALYSES (ALL SECTIONS)

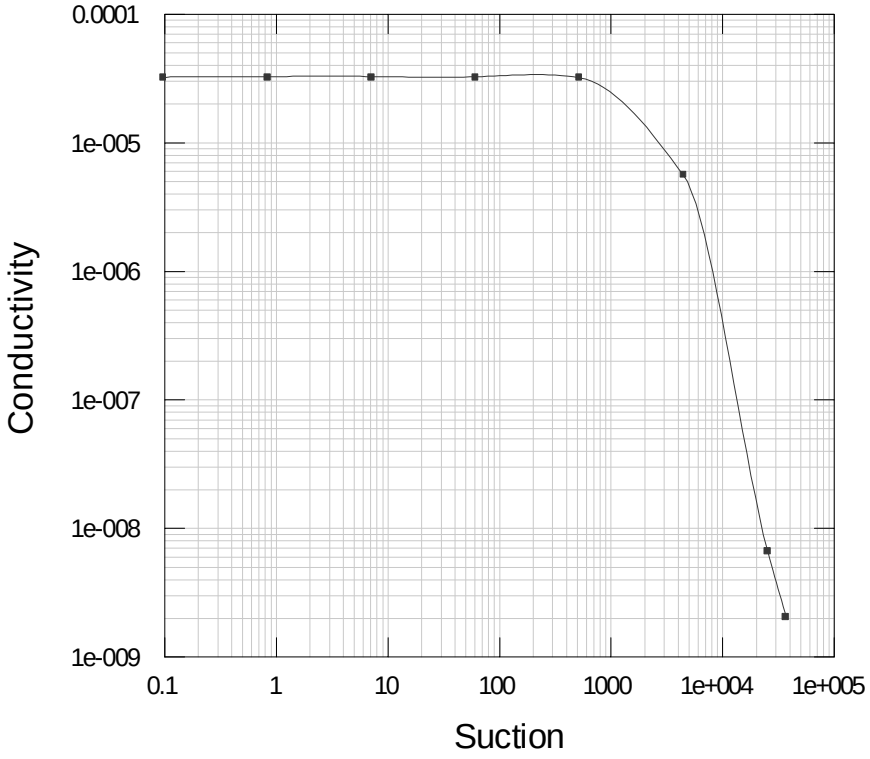
13.4.1 CLAY MATERIALS



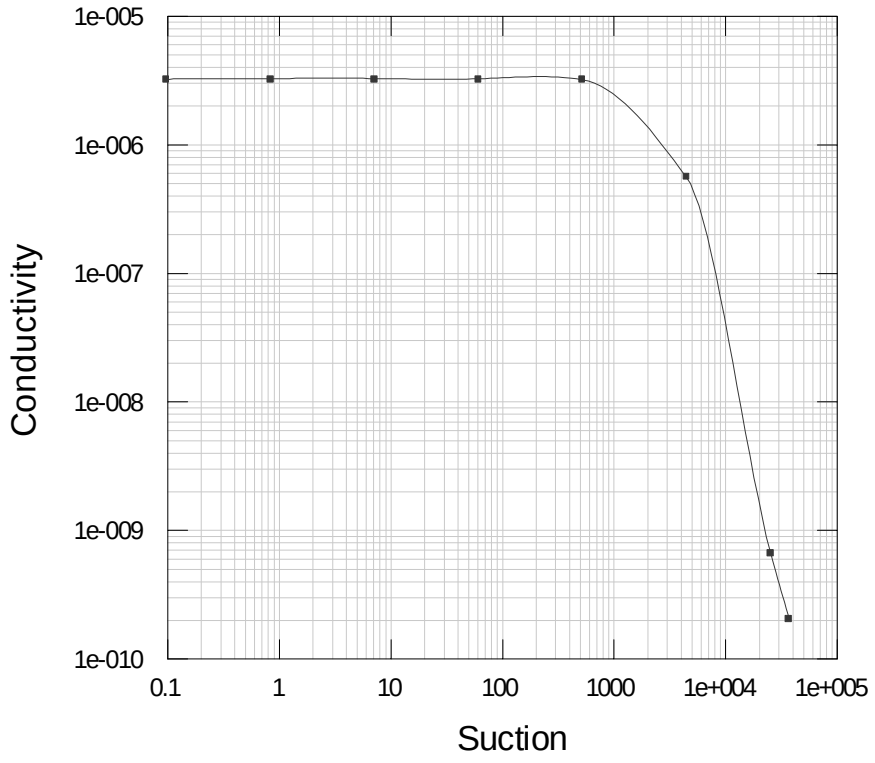
13.4.2 SANDS


0.001
0.0001
1e-005
1e-006
1e-007
1e-008
Conductivity
0.1
1
10
100
1000
1e+004
1e+005
Suction

13.4.3 MARSH, K: 1e-03 cm/s



13.4.4 MARSH, K: 1e-04 cm/s (under levee).

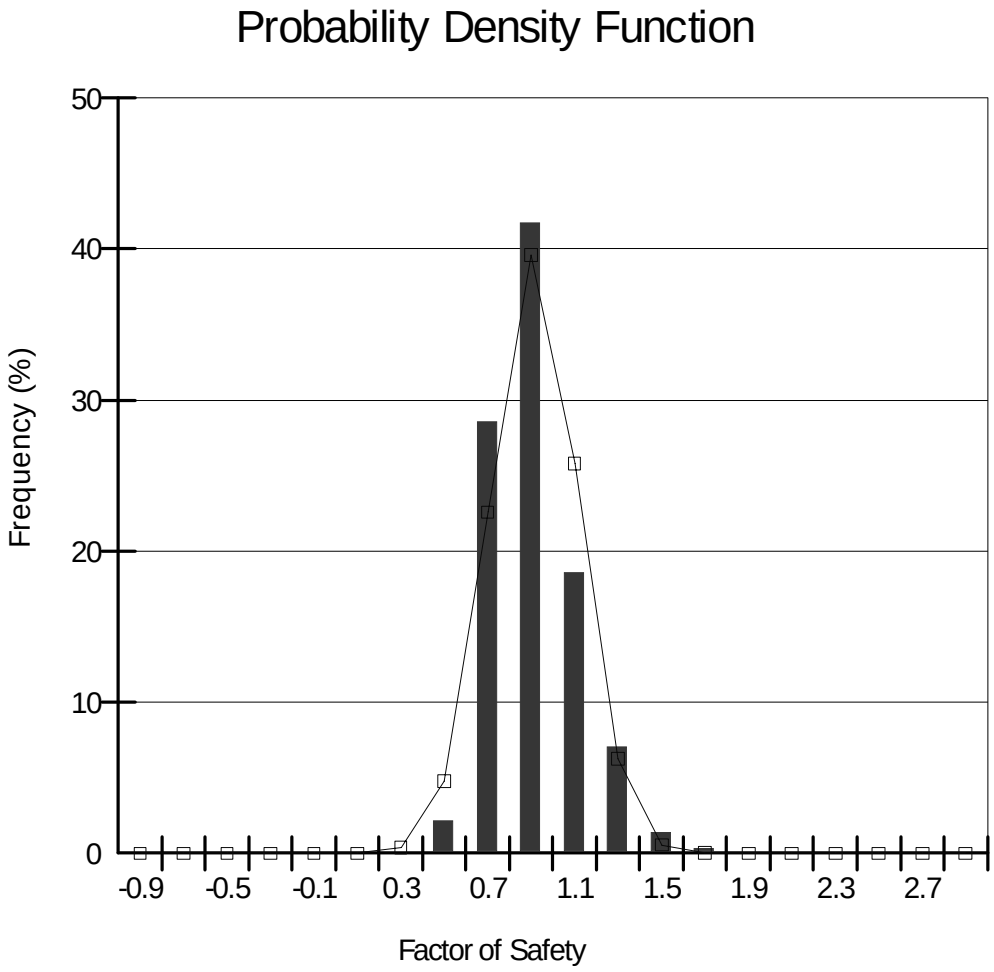


Note: When used lower permeabilities for the Marsh soils, the curve simply "shifts up" to the new value (i.e. 10^{-6} cm/s), maintaining the shape of the above curve.

13.5 RESULTS FROM THE MONTE CARLO SIMULATIONS

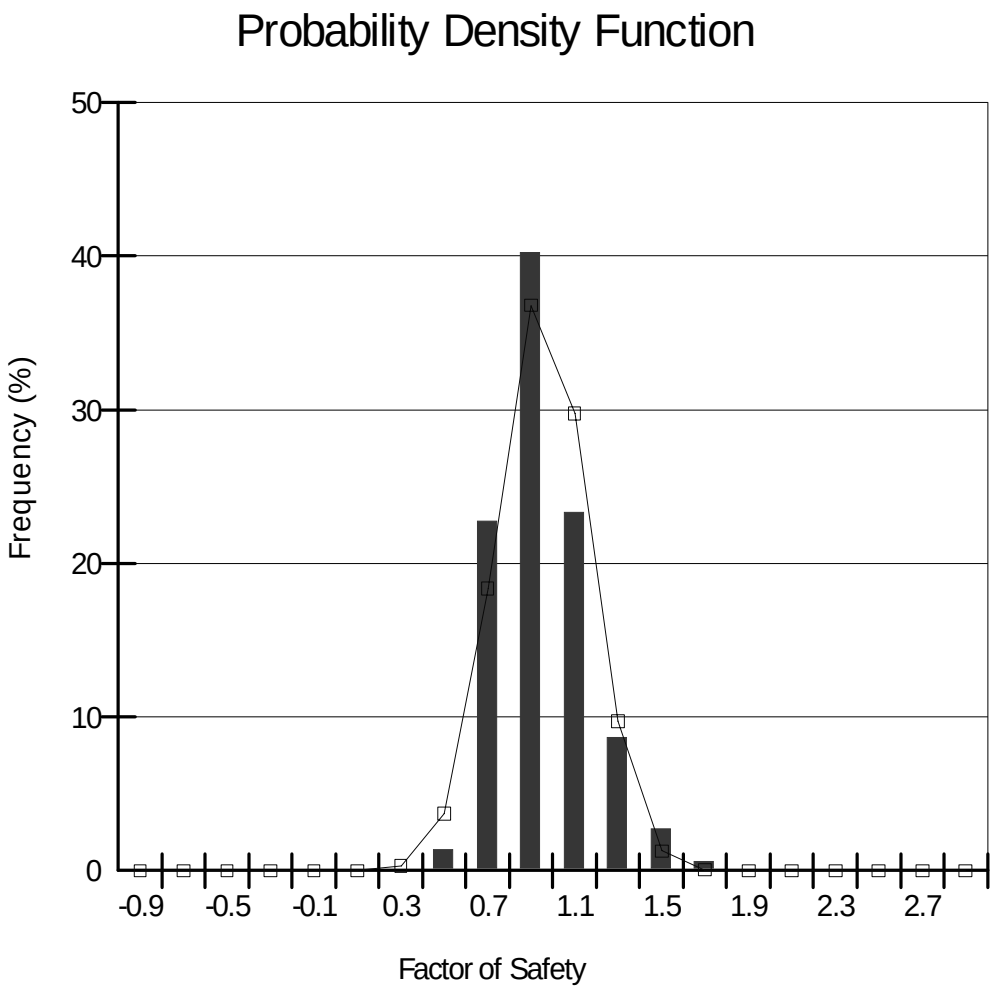
13.5.1 SOUTH BREACH – EXCAVATION AT TOE OF LEVEE

STORM SURGE AT 14ft



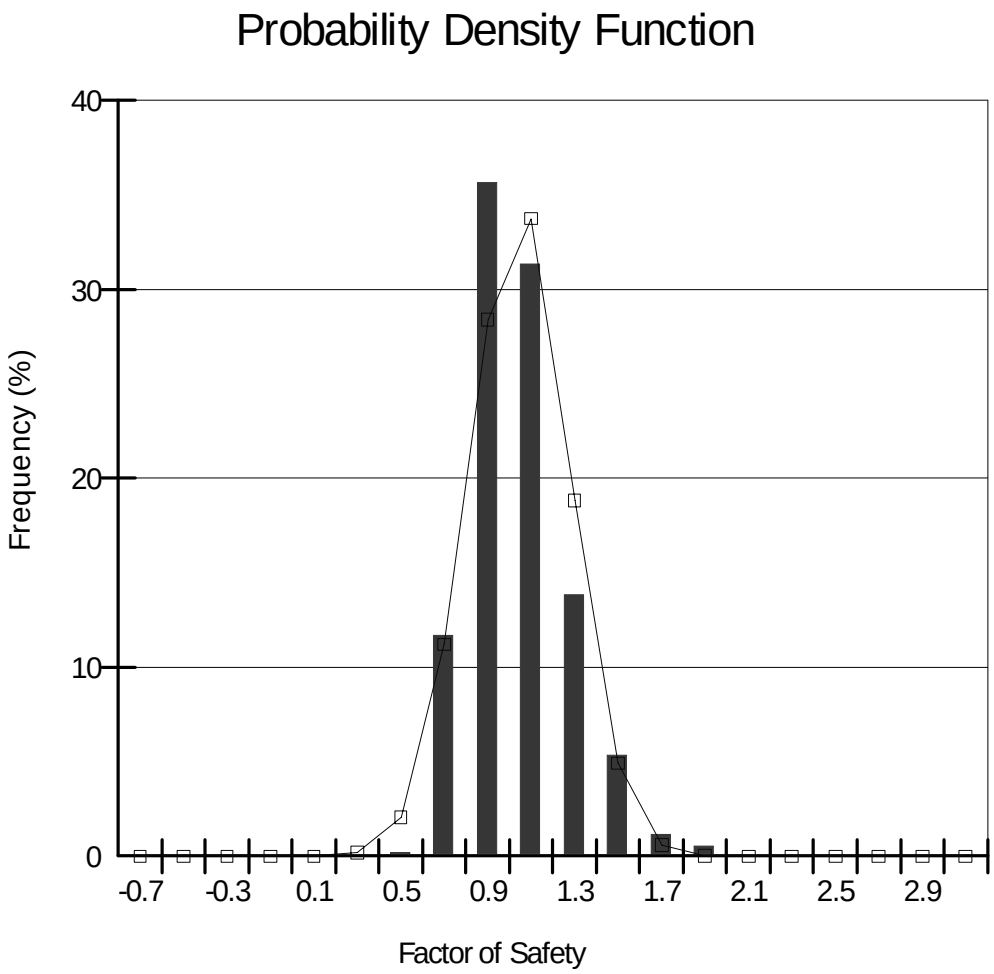
Mean F of S 0.91346
Reliability Index -0.431
P (Failure) (%) 72.466810
Standard Dev. 0.201
Min F of S 0.47869
Max F of S 2.1505
# of Trials 2000

STORM SURGE AT 12ft



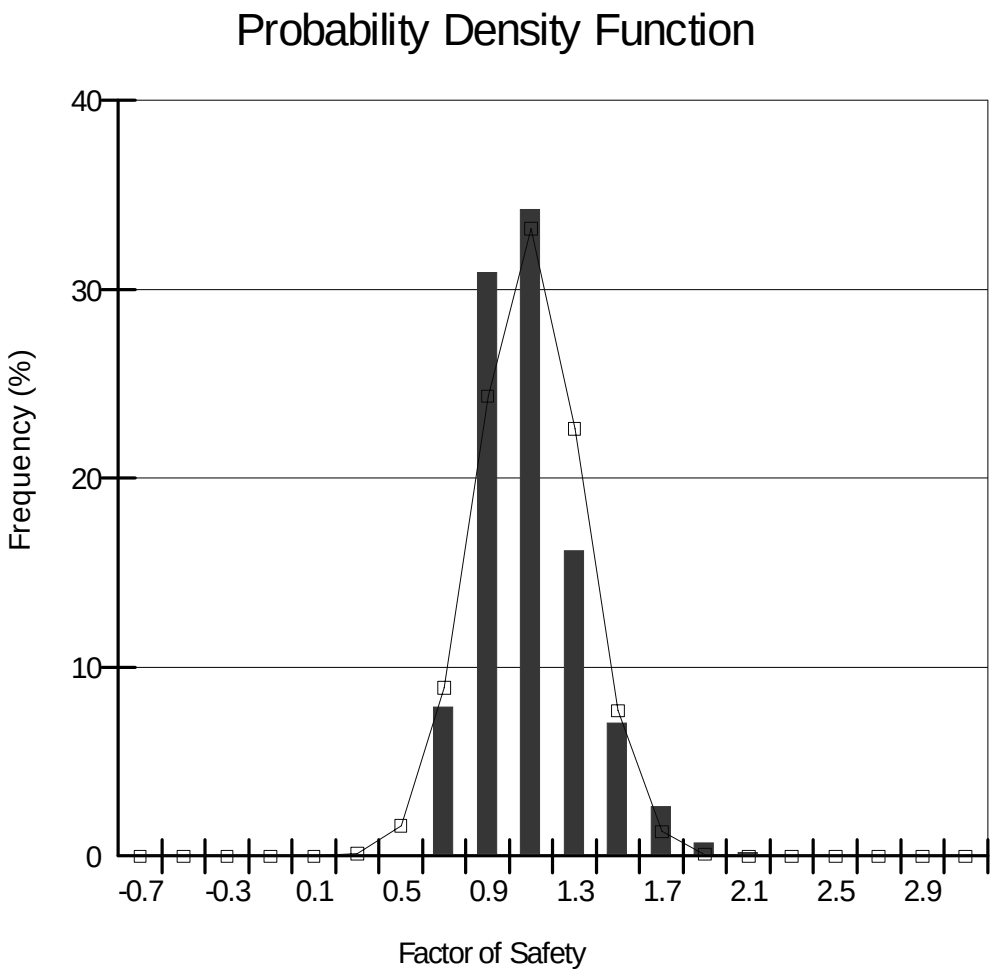
Mean F of S 0.95331
Reliability Index -0.223
P (Failure) (%) 64.350240
Standard Dev. 0.21
Min F of S 0.49978
Max F of S 2.247
# of Trials 2000

STORM SURGE AT 11ft



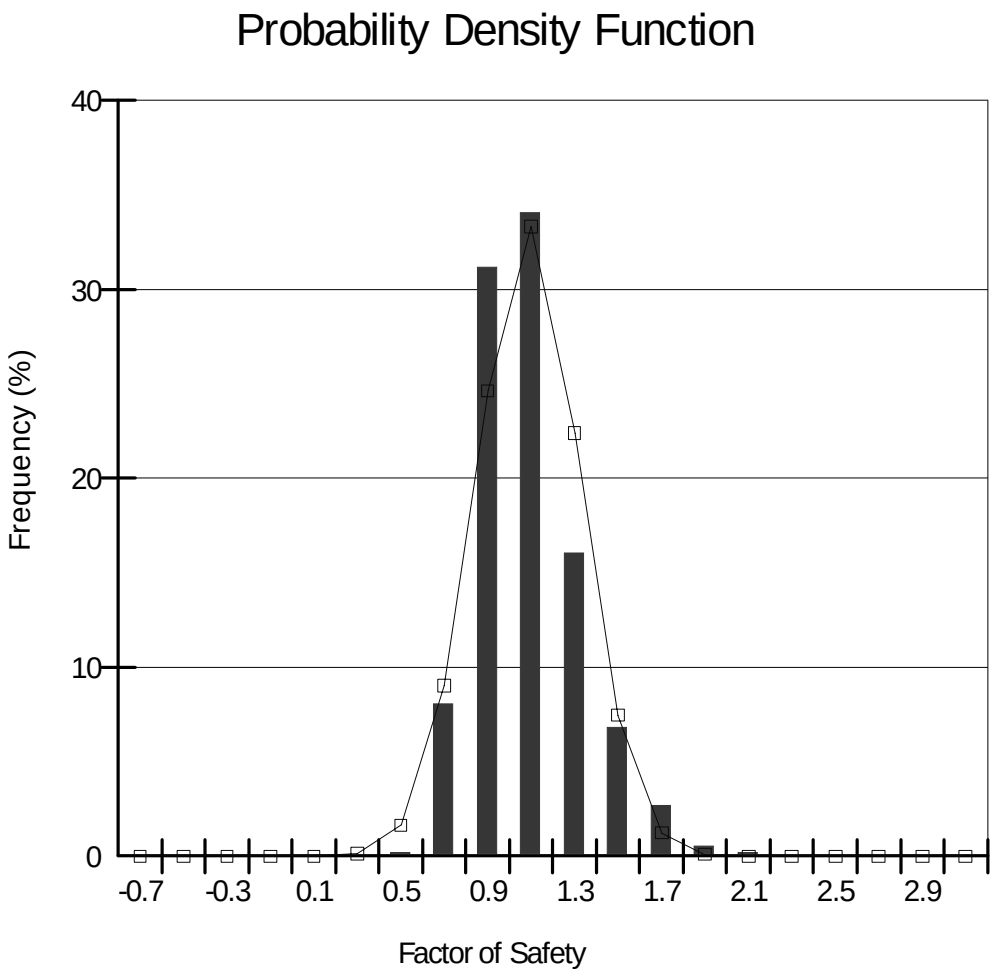
Mean F of S 1.0456
Reliability Index 0.198
P (Failure) (%) 47.539850
Standard Dev. 0.23
Min F of S 0.54816
Max F of S 2.4656
# of Trials 2000

STORM SURGE AT 10ft



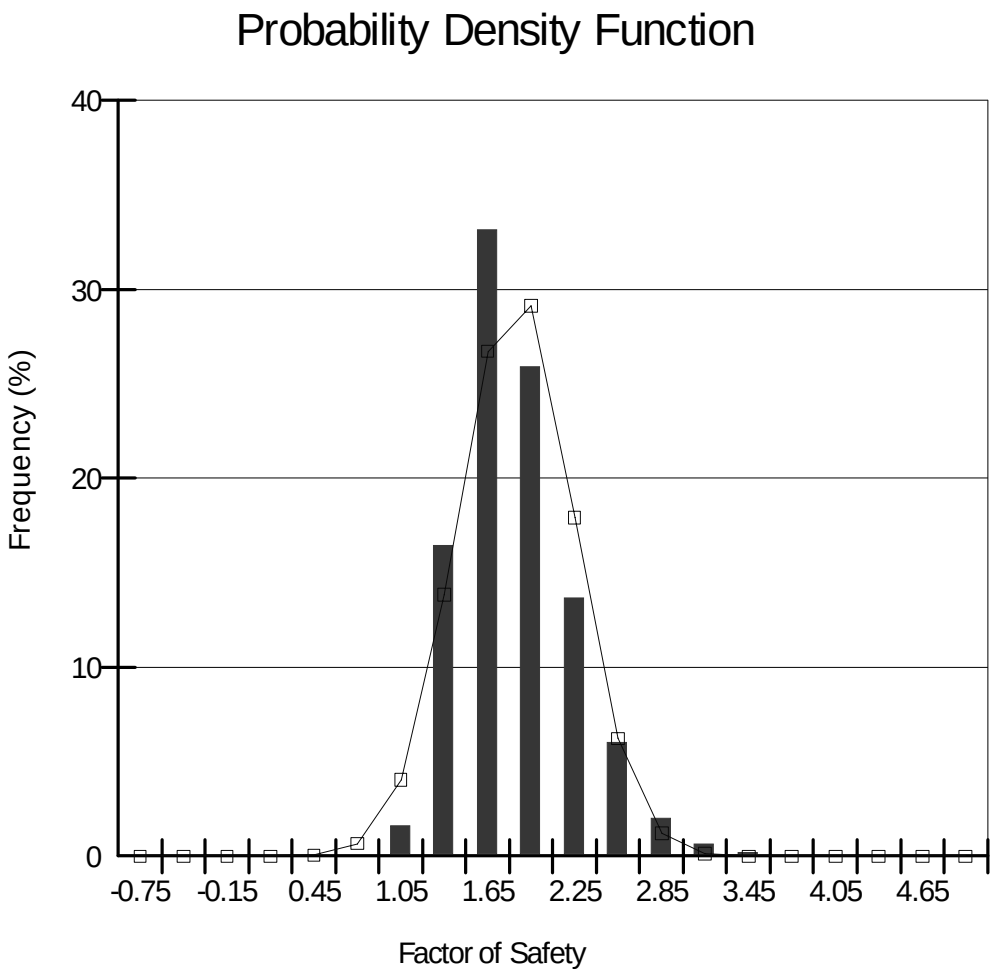
Mean F of S 1.0895
Reliability Index 0.373
P (Failure) (%) 38.908090
Standard Dev. 0.24
Min F of S 0.57105
Max F of S 2.5696
# of Trials 2000

STORM SURGE AT 9ft



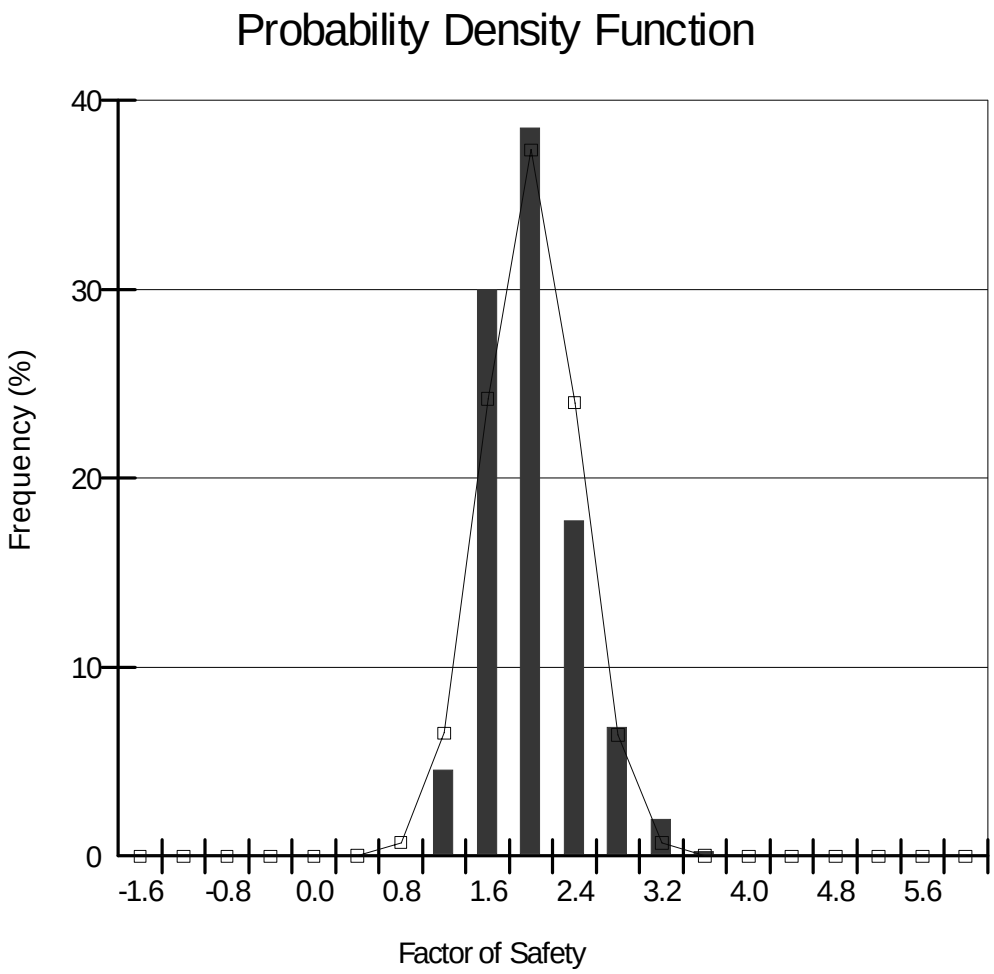
Mean F of S 1.0864
Reliability Index 0.361
P (Failure) (%) 39.448280
Standard Dev. 0.239
Min F of S 0.56918
Max F of S 2.5621
# of Trials 2000

STORM SURGE AT 8ft



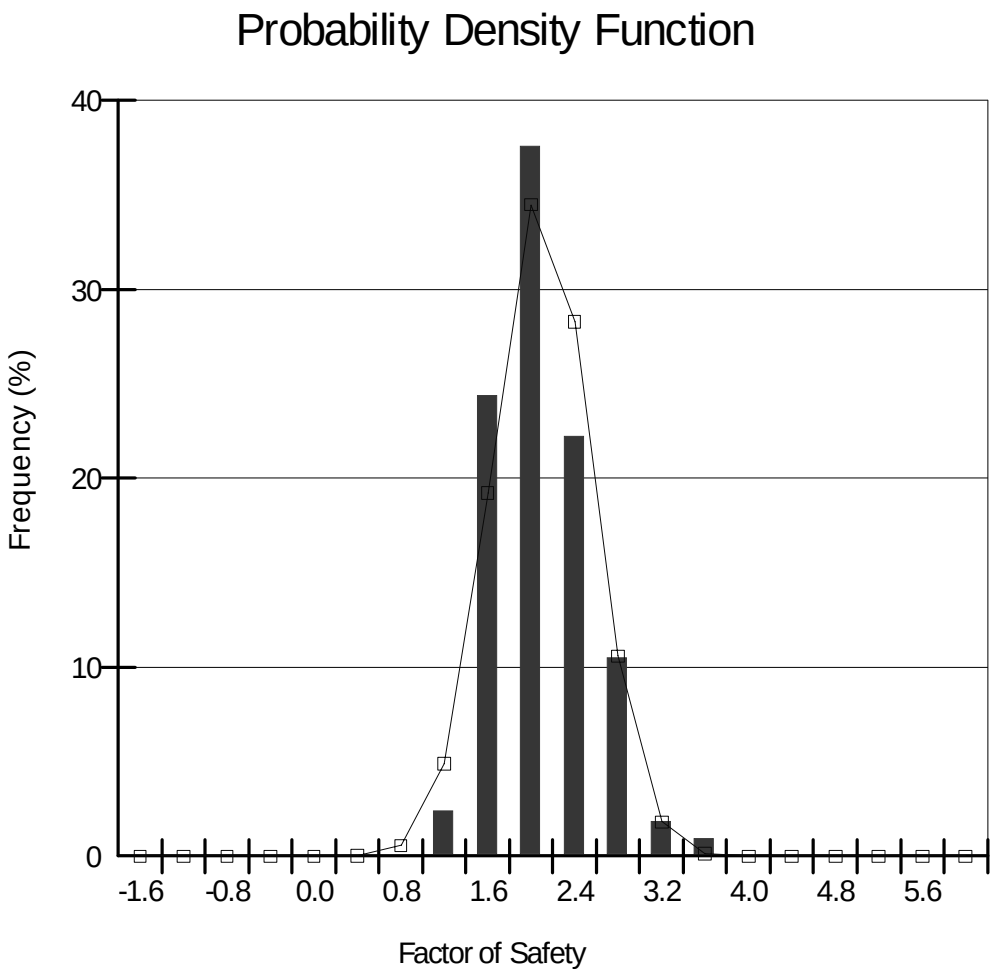
Mean F of S 1.8453
Reliability Index 2.131
P (Failure) (%) 0.201110
Standard Dev. 0.397
Min F of S 0.82776
Max F of S 4.255
# of Trials 2000

STORM SURGE AT 6ft



Mean F of S 1.9982
Reliability Index 2.335
P (Failure) (%) 0.050810
Standard Dev. 0.427
Min F of S 0.96482
Max F of S 5.705
# of Trials 2000

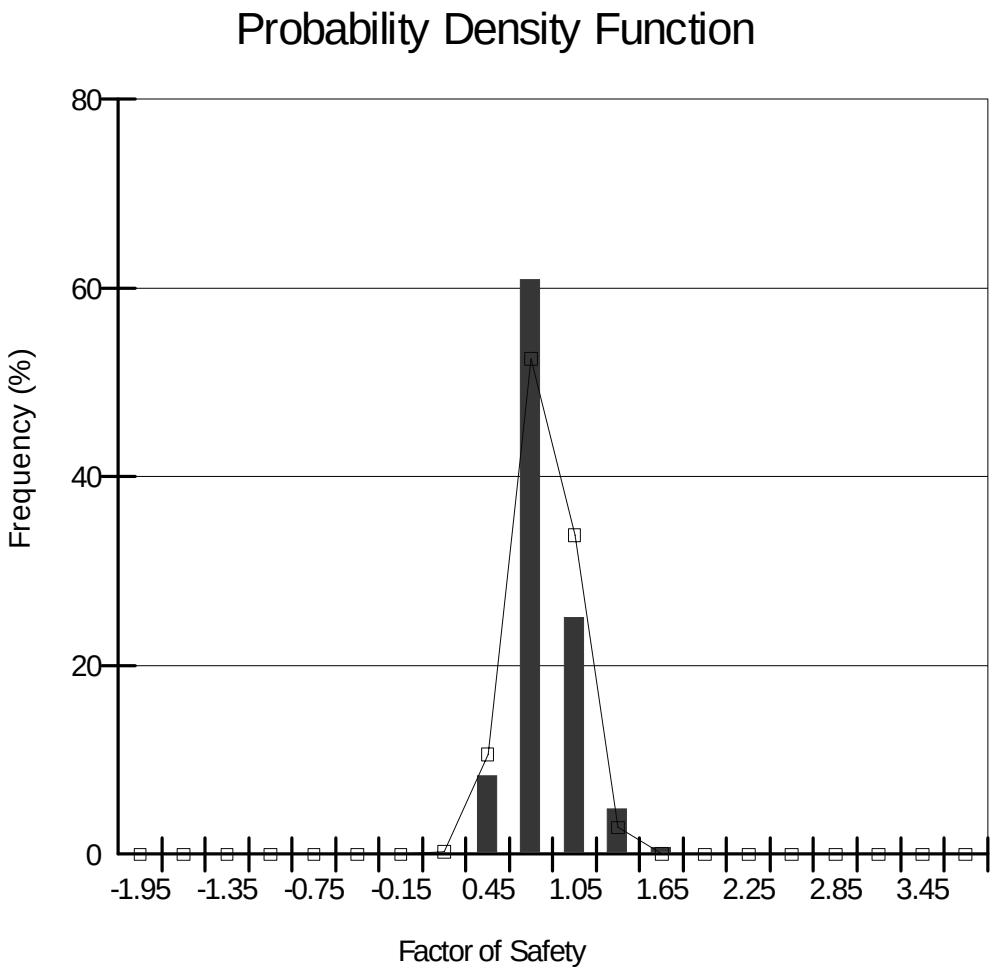
STORM SURGE AT 4ft



Mean F of S	2.0985
Reliability Index	2.431
P (Failure) (%)	0.000000
Standard Dev.	0.452
Min F of S	1.0093
Max F of S	5.9878
# of Trials	2000

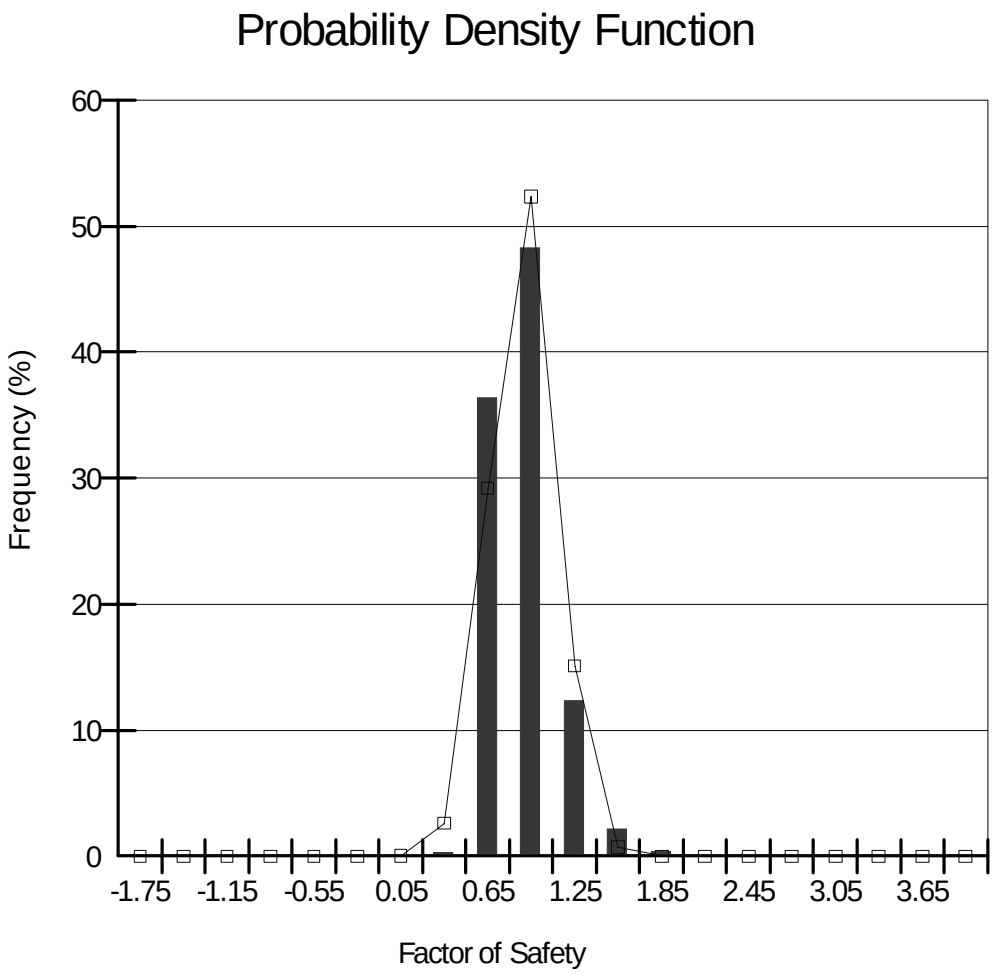
13.5.2 NORTH BREACH – EXCAVATION AT TOE OF LEVEE

STORM SURGE AT 12ft



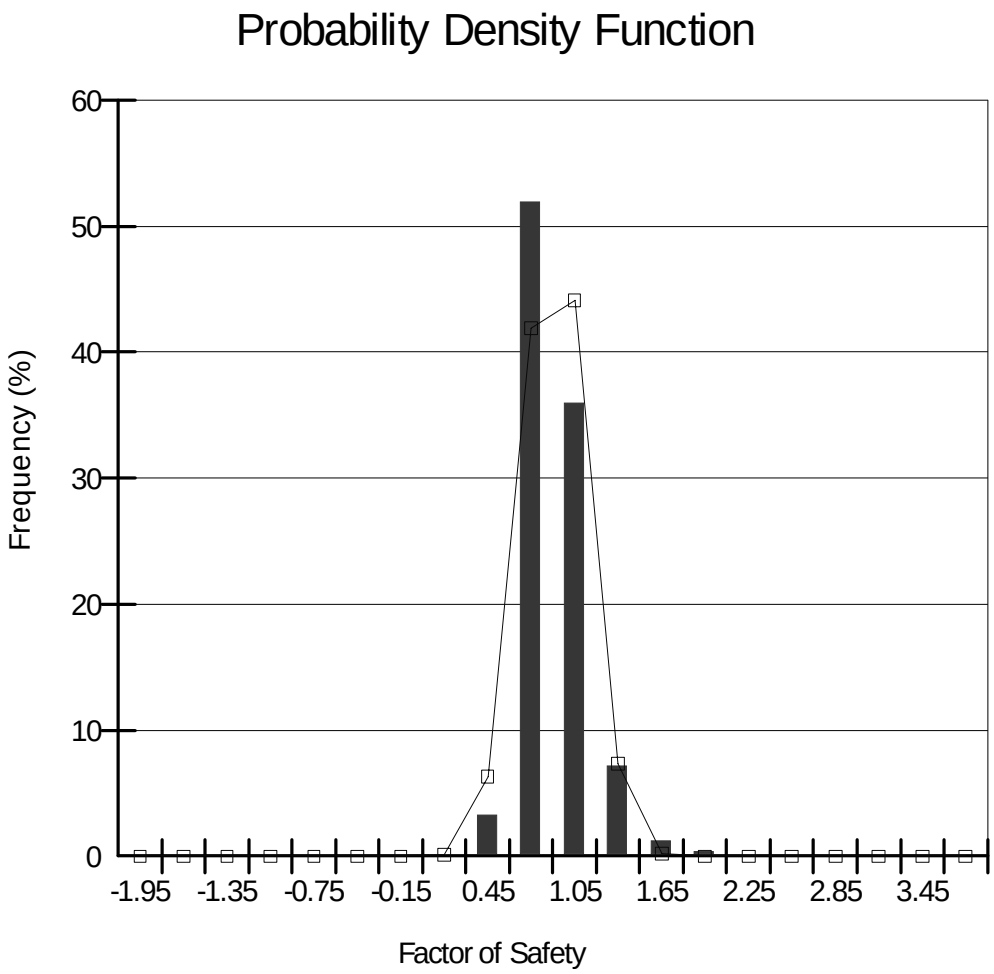
Mean F of S 0.83546
Reliability Index -0.783
P (Failure) (%) 82.640450
Standard Dev. 0.21
Min F of S 0.35911
Max F of S 3.1326
# of Trials 2000

STORM SURGE AT 11ft



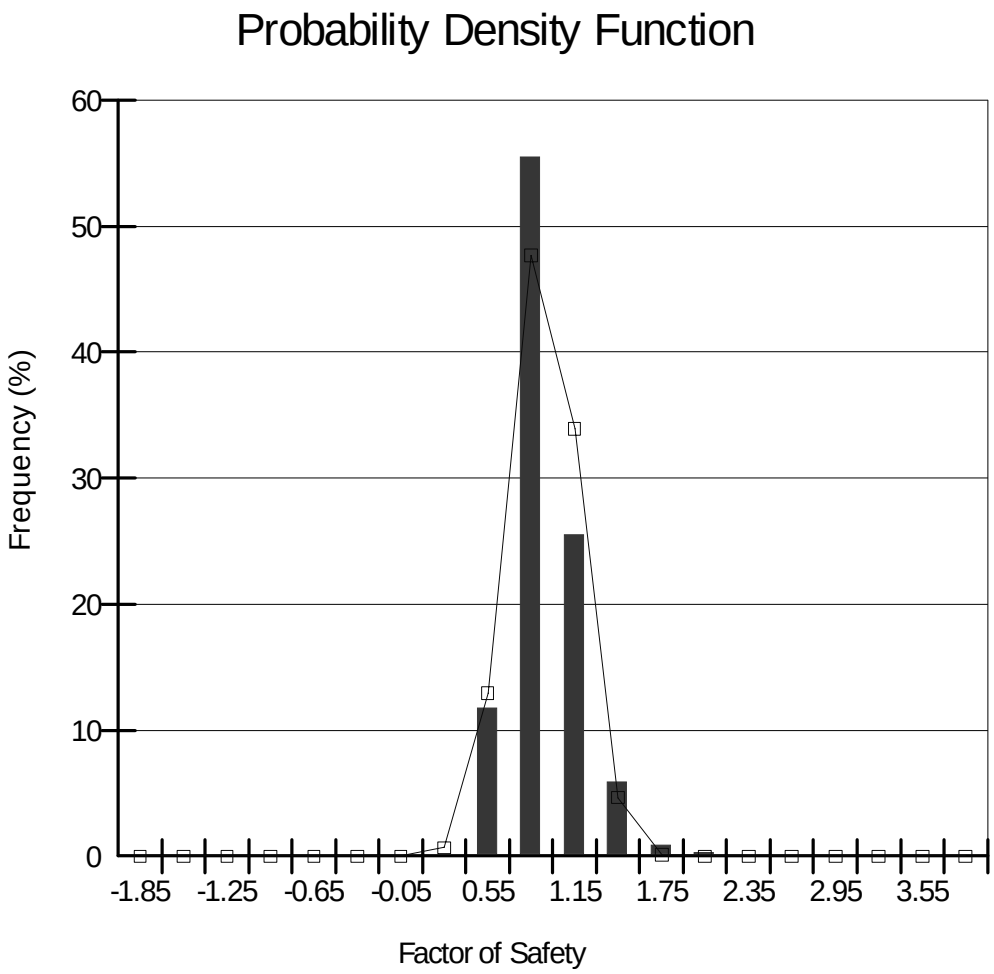
Mean F of S 0.89583
Reliability Index -0.469
P (Failure) (%) 73.815590
Standard Dev. 0.222
Min F of S 0.37337
Max F of S 3.3038
# of Trials 2000

STORM SURGE AT 10ft



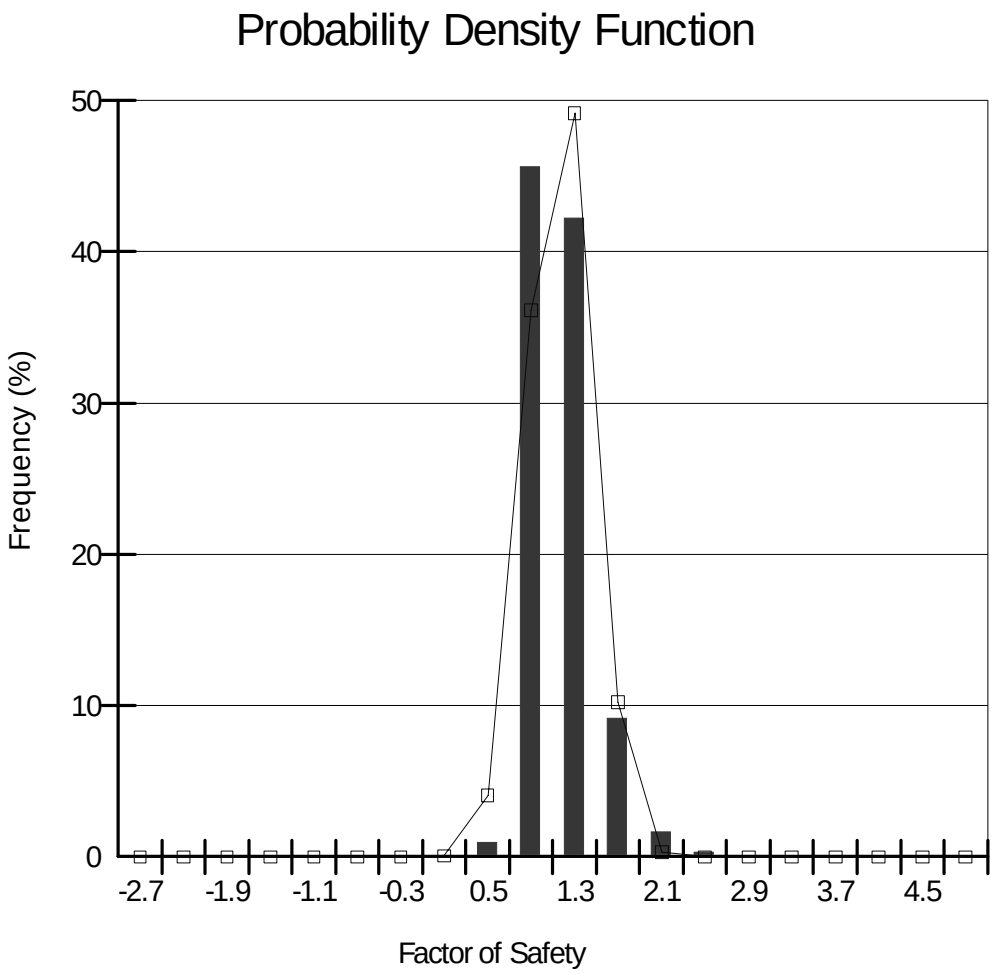
Mean F of S 0.90829
Reliability Index -0.415
P (Failure) (%) 73.047380
Standard Dev. 0.221
Min F of S 0.42081
Max F of S 3.2759
# of Trials 2000

STORM SURGE AT 9ft



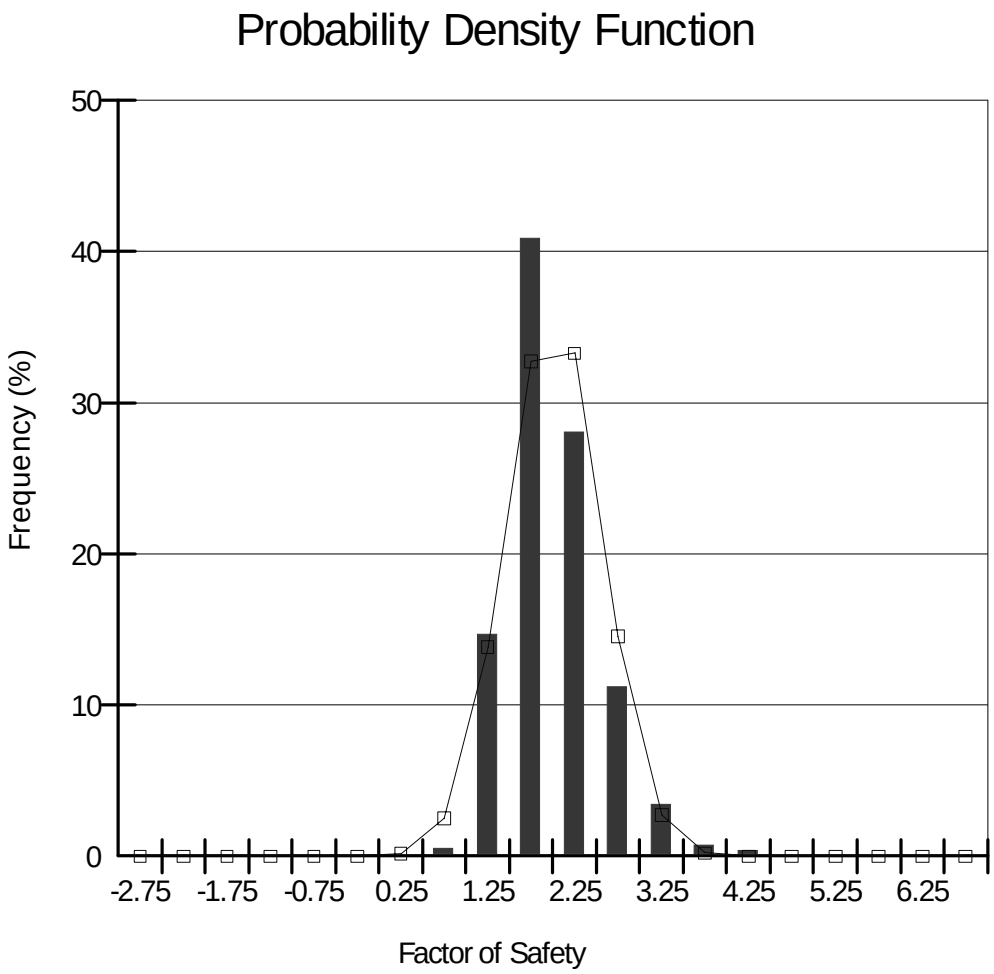
Mean F of S 0.93793
Reliability Index -0.265
P (Failure) (%) 67.318580
Standard Dev. 0.234
Min F of S 0.38218
Max F of S 3.4839
# of Trials 2000

STORM SURGE AT 8ft



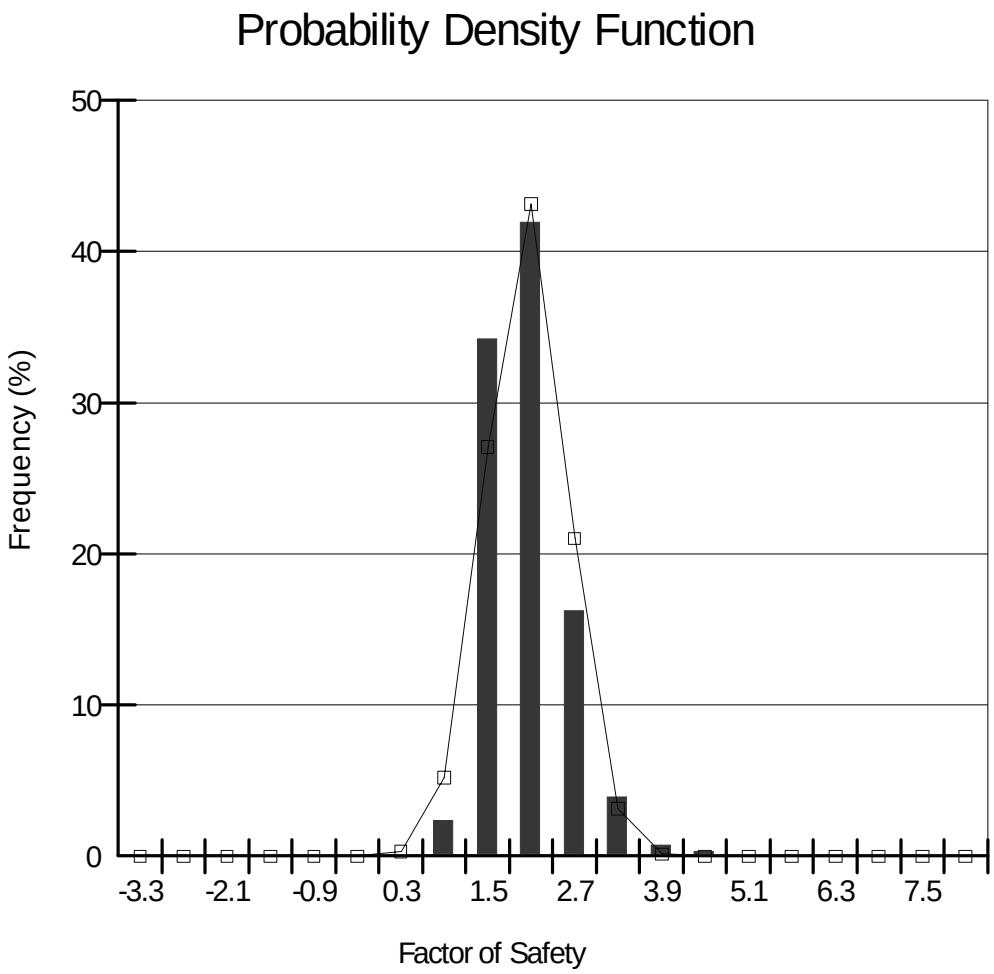
Mean F of S 1.1656
Reliability Index 0.568
P (Failure) (%) 30.499740
Standard Dev. 0.292
Min F of S 0.47759
Max F of S 4.3371
# of Trials 2000

STORM SURGE AT 6ft



Mean F of S	2.0098
Reliability Index	1.858
P (Failure) (%)	0.500000
Standard Dev.	0.544
Min F of S	0.79031
Max F of S	6.9442
# of Trials	2000

STORM SURGE AT 4ft



Mean F of S 2.0362
Reliability Index 1.881
P (Failure) (%) 0.450000
Standard Dev. 0.551
Min F of S 0.80057
Max F of S 7.04
# of Trials 2000